Connectivity and Function of the Primate Insula

Thesis by

Soyoung Park

In Partial Fulfillment of the Requirements

for the Degree of

Doctor of Philosophy

California Institute of Technology

Pasadena, California

2016

(Defended July 20th, 2015)

With thanks to my parents, for trust and freedom,

and to all my teachers, for encouraging me to transcend fear.

Acknowledgments

Counting the time I have spent as an undergraduate and a research technician, this marks the end of my 10th year at California Institute of Technology. As I conclude this significant, so far the most challenging stage of my life, it is with the sincerest gratitude that I recognize the wonderful set of people who have given so much meaning to the experience that, without knowing them, would have only been a series of difficult moments.

My parents, Yong Taek Park and Mi Hwa Kim, have been the most dedicated supporters of my academic career. Owing to their strong will to maximize my potential, for my entire life I have never wanted for anything when it came to fulfilling intellectual curiosity. And more importantly, my parents have given me the most incredible level of freedom, which allowed me to learn at my own pace and enjoy the process, without experiencing the extreme pressure and control that my peers often dealt with. My parents also exercised extreme courage and trust 13 years ago, when I became disappointed in the Korean education system and asked to study abroad. In a situation where many parents would doubt the child's ability to stay on track without direct parental supervision, they agreed without much hesitation, and 8 months later I was dropped off at a New York boarding school 6,700 miles away from home. Going away to school at an early age and growing up in the American system is easily one of the best things that have ever happened to me, and I am tremendously grateful to my parents for their trust in me and for the freedom that I was so fortunate to enjoy, both of which they have never ceased to provide.

Besides my advisors and committee members, there are many teachers who have made this thesis possible. My excellent teachers at Millbrook School played especially important roles in forming the basis for my higher education, and they deserve my boundless appreciation. I thank Dr. Alan Tousignant and the late Dr. Sylvia Roberts, who enabled my first foray into behavioral science through their advanced biology/animal behavior curriculum. Although my project (observing the black and white ruffed lemurs at the school zoo, and their reaction to various types of noise; for me, mostly an excuse to play my violin in front of their cage every afternoon) did not prove to be very fruitful, it was through this wonderful course that I learned for the first time the challenges of finding a good research topic, interpreting the existing literature, designing an experiment in an organized manner, and keeping track of the data. I consider this experience a truly crucial part of my research career, and I cherish the memories of spending my afternoons performing manual labor at the zoo with Dr. Tousignant and staying at Dr. Roberts' lake house during a very lovely long weekend. I would also like to thank Mr. Walker Zeiser and Mrs. Cathy Zeiser for being splendid parental figures during my formative years, and helping me build the reading and writing skills required for making this dissertation happen. I never imagined, as a 15-year-old ESL student quietly struggling her way through Frankenstein, that I would some day produce in English a large body of work 80 times the length of the writing assignment due the next day. I am also very grateful to Mr. Somerset Waters, Mr. Todd Feitelson, and Mr. Walter Manny for re-kindling my interest in physics and math when I thought that the memorization-based Korean math and science curriculum had ruined the subjects for me forever. In addition, I thank Mr. Steve Siktberg for helping me discover music as a wonderful emotional outlet — without which I could not have survived Caltech — and Ms. Julia Martin for her incredible support as my advisor.

I am deeply indebted to my extremely intelligent and kind colleagues in the Allman and Adolphs Laboratories. In the Allman Lab, I found great mentors in Dr. Atiya Hakeem and Dr. Nicole Tetreault, who guided me through every stressful research

moment during my undergraduate and early graduate student days. In the Adolphs Lab, Dr. Mike Tyszka has provided an incredible amount of technical help throughout my time at Caltech, so much so that at this point he probably qualifies as my 3rd thesis advisor. I'm also grateful to Dr. Bob Spunt, Dr. Julien Dubois, Ms. Marisol Espino, Ms. Remya Nair, and Dr. Shuo Wang for their help in making the olfactory fMRI study possible. Dr. Anita Tusche, Dr. Alma Gharib, and Dr. Damian Stanley have taken time to help improve my defense talk, for which I am so thankful. I would also like to express gratitude to the administrative staff in the department — Ms. Tanya Owen, Ms. Mary Martin, Ms. Sheryl Cobb and Ms. Barbara Estrada — for their patience and help. In addition, I am thankful to Dr. Ralph Lee for the MRI scanner superuser training.

Finally, I feel vastly fortunate to have received kind support of the following fantastic friends: Lori Spalsbury, Tatjana Kanashiro, Tiffany Kim, Shuo Wang, Daniel Mc-Namee, Yong-Jun Lin, Bo Chen, Tamara Bevard, Weslee Glenn, Andrej Svorenčik, Stephanie Coronel, Melanie Stefan, Kana Takematsu, Renee Arias, Keith Beadle, Yong Wu, Xi Xi, Jinglin Huang, Sue Jiang, Alice Lin, Michael Inadomi, Diana Inadomi, and Nathaniel Tiberius Inadomi. Words cannot describe how impossibly lovely these individuals are.

Abstract

The insula is a mammalian cortical structure that has been implicated in a wide range of low- and high-level functions governing one's sensory, emotional, and cognitive experiences. One particular role of this region is considered to be processing of olfactory stimuli. The ability to detect and evaluate odors has significant effects on an organism's eating behavior and survival and, in case of humans, on complex decision making. Despite such importance of this function, the mechanism in which olfactory information is processed in the insula has not been thoroughly studied. Moreover, due to the structure's close spatial relationship with the neighboring claustrum, it is not entirely clear whether the connectivity and olfactory functions attributed to the insula are truly those of the insula, rather than of the claustrum. My graduate work, consisting of two studies, seeks to help fill these gaps. In the first, the structural connectivity patterns of the insula and the claustrum in a non-human primate brain is assayed using an ultra-high-quality diffusion magnetic resonance image, and the results suggest dissociation of connectivity — and hence function — between the two structures. In the second study, a functional neuroimaging experiment investigates the insular activity during odor evaluation tasks in humans, and uncovers a potential spatial organization within the anterior portion of the insula for processing different aspects of odor characteristics.

Published Content

Chapter 2 of this thesis has been published as:

Park, S., Tyszka, J. M., and Allman, J. M. (2012). The claustrum and insula in *Microcebus murinus*: a high resolution diffusion imaging study. Front. Neuroanat. 6(21), doi: 10.3389/fnana.2012.00021

Contents

List of Figures

List of Tables

Chapter 1

Introduction

1.1   Overview

The insula is a cortical region found in mammalian species. It can be anatomically and functionally divided into three major parts. The anterior portion of the insula, on which the second portion of this thesis focuses, seems to serve olfactory and gustatory functions in non-human species, while the human anterior insula, and the specialized frontoinsular cortex included in the ventral part of the anterior insula, appear involved in social, emotional, and cognitive domains as well as olfactory and gustatory. The insula, and especially the frontoinsular cortex, is a fascinating structure in which much of important sensory information is processed and integrated to create rich, detailed emotional and cognitive experiences, and hence greatly influences our day-to-day life. While the currently available literature on the human insula's connectivity with other regions seem to support this, there is only limited data on this topic due to technical limitations, and further studies must be conducted to elucidate the functions and connections of the human frontoinsular cortex and anterior insula in more detail. It is also worth noting that the additional – social, emotional, and cognitive – functions found almost exclusively in the human anterior insula may be largely a consequence of the ease of testing human subjects and the large number of studies done in them, rather than reflecting a fundamental difference between humans and other primates.

My thesis aims to contribute to our understanding of these structures through two studies. The first study demonstrates the efficacy of a noninvasive, computational approach of modeling structural connectivity, through exploring the insular connections of the gray mouse lemur. The outcome of this work demonstrates that the insula has a connectivity pattern that is distinct from that of the closely neighboring claustrum, which has been rather difficult to confirm in the past due to the difficulty in studying claustral connectivity. The second study seeks to clarify the role of the frontoinsular cortex and anterior insula in olfactory hedonic value computation through a functional neuroimaging experiment, and provides a possibility that the function of the FI is spatially organized.

In this chapter, I will begin the discussion by describing the anatomical structure, connections, and functions of the insula. Then I will focus on the insular cortex in the human brain, describing its structural complexity. The following section will be dedicated to the discussion of von Economo neurons and the generally speculated functions of the frontoinsular cortex, one of the main cortical areas that contain von Economo neurons. Subsequently, the role that the frontoinsular cortex and the anterior insula serve in the olfactory, gustatory, social, emotional, and cognitive modalities will be discussed, followed by a description of the structural and functional connectivity patterns of the frontoinsular cortex and the anterior insula that have been observed in past studies. I will close this chapter by describing the general outline of this thesis.

1.2 Insula: General Anatomy and Function

1.2.1 General Structure of the Insula

The insula is a mammalian cortical structure. In many small-brained mammals it is located on the ventrolateral surface of the brain, while in monkeys, apes, humans,

and other large-brained species such as the African elephant (Hakeem et al. 2009), the region lies hidden under the operculum and inside the lateral sulcus (Bamiou et al. 2003).

The insular anatomy has been extensively studied in rodents and macaques, and the results have established the anatomical and functional division of the insula into three distinct portions. The anteroventral division, due to its lack of the granular layer IV, is called the agranular insular cortex, whereas the layer-IV-containing posterodorsal part is dubbed the granular insular cortex. The area between these two regions, which represents the transition from the agranular to the granular cortex in terms of cytoarchitecture and structural connections, is called the dysgranular insular cortex (Brodmann 1909, Rose 1928, Mesulam and Mufson 1982a, Shi and Cassell 1998, Van De Werd et al. 2010).

These three portions of the insula exhibit different structural connectivity patterns, and hence different functions. According to conventional tract tracing studies in the macaque, the agranular insula appears to be involved mainly in olfactory, gustatory, and emotional processes, as evidenced by its connections with the amygdala, anterior cingulate cortex (ACC), and the prorhinal-entorhinal cortex. In contrast, the granular insula, based on its association with the auditory, somatosensory, and visual cortical areas, seems to integrate the sensory inputs from the external environment (Mesulam and Mufson 1982b, Mufson and Mesulam 1982, Mufson and Mesulam 1984). The somesthetic pathway in non-human primates from lamina I neurons of the spinal cord, to the ventromedial nucleus of the thalamus, and in turn to the granular insular indicates that that the granular insula is also involved in representing the interoceptive state of the animal (Craig 2002). And as to be expected from the transitional nature of its cytoarchitecture, the dysgranular insula exhibits a mixture of the two types of connections, with the agranular-like connections in the anterior portion and the granular-like ones in the posterior portion (Mesulam and Mufson 1982b, Mufson and Mesulam 1982, Musfson and Mesulam 1984). A similar division of the insular cortex seems to hold in rodents (Allen et al. 1991).

1.2.2   The Human Insula

The morphology of the human insula is considerably more complicated than that of rodents or non-human primates (Afif and Mertens 2010, Menon and Uddin 2010). Moreover, the gross anatomical features of the human insula – namely, the total number of insular gyri – can vary significantly among individuals, and even between hemispheres from the same individual (Naidich et al. 2004). Also, a recent study, using an observer-independent approach in which the cortical cytoarchitecture was analyzed objectively, further parcellated the posterior granular and dysgranular human insular cortex into distinct subregions, suggesting that the human insula may be more detailed than originally thought to be (Kurth et al. 2010), though this may be mainly due to the fact that observer-dependent methods at relatively low resolutions – an approach that renders itself vulnerable to human error – have been employed to divide the insula in the past. In fact, a more recent study employing an observer-dependent segmentation but using very high-resolution photomicrographs has categorized the macaque insula into 15 different architectonic regions (Evrard et al. 2014). However, it is worth noting that while Kurth et al. 2010 has relied only on cytoarchitecture for segmentation, Evrard et al. 2014 utilized both cyto- and myeloarchitecture, which might have enabled the authors to categorize the region a bit further than any other studies on the macaque insula. Hence Kurth et al. might have found a larger number of subregions, had myeloarchitectonic divisions been also taken into account. In addition, Kurth et al. only examined the posterior portion of the human insula, while the most significant volumetric difference between humans and non-human primate insular cortices appear to occur in the agranular portion (Bauernfeind et al. 2013), and hence the comparison of architectonic organization of the agranular insula between humans and macaques might illustrate more complexity (Evrard et al. 2014).

In addition to the above evidence of increased complexity in the human insula, functional imaging studies suggest that the primary gustatory cortex, which is located in the anterior insula in non-human brains (Mesulam and Mufson 1982b, Shi and

Cassell 1998), is located more caudally in humans, starting in the posterior part of the anterior dorsal insula, and extending into the mid-insular area (Small 2010).

Despite the above differences, studies so far indicate that the overall distinction between the anterior and posterior insular divisions is similar to the patterns found in non-human primates and rodents. One study utilized diffusion imaging data from human subjects, and ran probabilistic fiber tractography using every voxel in the insular region of interest (ROI) as seeds. Then the degrees of cross-correlation among the connectivity patterns of these seeds were computed, and based on this information, the seeds were categorized using 1,000 repetitions of the k-means clustering algorithm. The authors identified two major clusters in the ROI, roughly corresponding to the anteroventral and the posterodorsal portions of the insula. The method was unsuccessful in categorizing the area in between the two clusters (corresponding to the dysgranular cortex), however, perhaps due to its transitional nature of this region, which made it correlate highly with both clusters (Nanetti et al. 2009).

The functional distribution of the human insula reflects the anterior-posterior segregation described above, and is consistent with the results of non-human studies. A relatively recent meta-study of 1,768 functional neuroimaging experiments has shown that the insula can be functionally divided largely into four different portions: the sensorimotor portion, located in the mid-posterior section of the insula; the portion processing social emotions such as empathy, located in the anteroventral insula; the portion activated by olfactory and gustatory stimuli, situated in the central part of the insula; and the part responsive during cognitive tasks related to attention, memory, and language, in the anterodorsal insula. In addition, a small overlap region where all of these functional categories (except for parts of the sensorimotor category) appear to be computed was observed in the anterodorsal insula. Taken together, these data suggest that the human insula participates in high-level processing of these different types of systems, and integrating the results into a clear representation of the internal and external experiences (Kurth et al. 2010). In section 1.5, further discussion on the connectivity of the human insula, with a focus on that of the anterior insula (AI),

will be presented.

1.3 Frontoinsular Cortex and von Economo Neurons

In a small number of mammalian species, the anterior portion of the agranular insula – the inferior portion of the AI (Allman et al. 2010) – contains a specialized region called the frontoinsular cortex (FI). First characterized by Constantin von Economo and Georg Koskinas in 1925, the FI is defined by its agranular nature and the presence of a specialized group of large bipolar neurons in the layer V (von Economo and Koskinas 1925, Kennedy et al. 2007).

These neurons, although now usually called von Economo neurons (VENs), are often labeled "spindle cells" due to their distinctive morphology (Nimchinsky et al. 1999): while the pyramidal neurons in layer V tend to have basal dendrites that are richly arborized, VENs exhibit a roughly bipolar arrangement with basal dendrites that are quite sparse in comparison with those of the nearby pyramidal cells (Watson et al. 2006a). This simple computational structure, combined with the evidence that VENs are large projection neurons (Nimchinsky et al. 1995, Nimchinsky et al. 1999) that are likely to possess large and rapidly conducting axons (Nimchinsky et al. 1995, Sherwood et al. 2003) and sample information from small cortical columns, suggests that VENs' main function might be fast relay of information from VEN-containing regions to other areas of the brain (Watson et al. 2006a). Besides the FI, VENs can also be found in the limbic anterior (LA), which is a cortical structure contained within the ACC (Allman et al. 2010). Other regions, such as the dorsolateral prefrontal cortex of the human brain (Fajardo et al. 2008) and the frontal polar cortex of the humpback whale (Hof and Van der Gucht 2007) and the African elephant (Hakeem et al. 2009), have also been reported to contain VENs.

VENs, hence the FI or its non-primate homolog, are found in only a small number of mammalian species, including humans, gorillas, chimpanzees, bonobos, orangutans,

elephants, and cetaceans (Hof and Van der Gucht 2007, Butti et al. 2009, Hakeem et al. 2009, Allman et al. 2010), and in small numbers in macaques (Evrard et al. 2012). It is unlikely that the presence of VENs is a function of the degree of encephalization or the brain size relative to body size, as some primate species with large relative brain sizes or high degrees of encephalization, such as gibbons and some New World monkeys, do not exhibit VENs. It has also doubtful that VEN occurrence is related to social behavior, as many of the small-brained animals without VENs are highly social, and there appears to be no correlation between the size of the insular cortex's subdivisions and the species' social group size (Bauernfeind et al. 2013). Instead, it appears that the absolute brain size is highly correlated with VEN incidence, as the species that possess VENs have rather large adult brain sizes (around 300g or over in primates, and massively larger in elephants and cetaceans), and exhibit sophisticated social structures in most cases. Given the relatively slow processing in larger brains (action potentials must be transported over greater distances), demand for fast responses in complex social behaviors, and the probable role of VENs as projection neurons with large axons, it seems plausible that VENs have evolved to manage social interactions among big-brained organisms (Allman et al. 2010).

The symptoms of a number of neuropsychiatric disorders to which VENs are linked are consistent with the possible role of VENs postulated above. Individuals affected by the behavioral variant of frontotemporal dementia (bvFTD) exhibit significant impairments in perceiving their own self as well as the emotions of others, and these deficits manifest as reduced embarrassment, self-control, empathy, and theory of mind (Seeley et al. 2007). VENs in the LA and FI are selectively destroyed in the early stages of bvFTD, with most of the remaining VENs appearing dysmorphic. This presents a sharp contrast to the Alzheimer's disease (AD), in which VENs are not reduced selectively or significantly, and individuals affected do not show severe reduction in the ability to process social emotions or mentalize about others' thoughts (Seeley et al. 2006, Seeley et al. 2007, Seeley 2008). VENs also appear selectively reduced in the agenesis of corpus callosum (AgCC), in which the corpus callosum fails

to emerge during development (Kaufman et al. 2008). This supports the possible role of VENs in complex social behavior, as individuals affected by AgCC often experience social isolation and reduced interpersonal skills (Paul et al. 2007). In addition, a post-mortem study of chronically alcoholic individuals showed noticeable reduction in the number of VENs, suggesting that these neurons may contribute to regulating impulsive behavior (Senatorov et al. 2014).

There is also, albeit not very compelling, evidence that VENs are implicated in autism. An early stereological study of individuals with autism of varying ages showed no significant reduction or increase of FI VENs (Kennedy et al. 2007). A later study in the adult human ACC, however, has found that some autistic individuals possess higher numbers of VENs compared to controls, while other autistic individuals exhibit very low numbers of VENs (Simms et al. 2009). Another study indicated higher VEN-to-pyramidal-neuron ratios in the FIs of a small number of children with autism (Santos et al. 2011). This indicates that the VEN population might be somehow affected in autism, and suggests that the behavioral impairment in autistic individuals might originate from this disturbance. This hypothesis is consistent with a meta-analysis of functional neuroimaging studies which found that, in participants with autism, the perigenual ACC and the AI tend to be hypoactive during social tasks, and the rostral ACC tend to be hyperactive during non-social, attention-related tasks, when compared to healthy controls (Di Martino et al. 2009). A number of structural and functional connectivity imaging studies also associate the FI and AI with autism, and will be discussed in Section 1.5.

1.4 Known Functions of the Frontoinsular Cortex and Anterior Insula in Humans

1.4.1 Olfactory and Gustatory Functions

As discussed above, many animal studies suggest that the AI is involved in higher-level processing of olfactory and gustatory information. In this section, these aspects of the human FI and AI's functions, elucidated from functional neuroimaging and lesion studies, are described in detail.

A growing number of human neuroimaging studies have implicated the FI and the AI in olfactory processing. They all seem to converge on the opinion that the AI, including the inferior portion that makes up the FI, is involved in the neural network that processes olfactory information: experiments using positron emission tomography (PET) (Zatorre et al. 1992; Bengtsson et al. 2001; Ciumas et al. 2008), as well as those utilizing functional magnetic resonance imaging (fMRI) (Francis et al. 1999; Sobel et al. 2000; Suzuki et al. 2001; de Araujo et al. 2003), have suggested that the region becomes active when human participants are exposed to odor stimuli, even including subliminal stimuli as estrogen-like compounds (Savic et al. 2001). Further, the activation pattern in the AI exhibited habituation in response to prolonged (60-second) olfactory stimuli, and this was observed to be similar to the activations of the primary olfactory cortex and the hippocampus in reaction to the same type of stimuli. This result suggests that these three regions may interact with one another to cause one to be desensitized when exposed an odor for an extended period of time (Poellinger et al. 2001).

The past olfactory neuroimaging studies do not agree, however, on the role of the FI and the AI (from now collectively referred to as the AI, as the FI is included in the AI) in computation of hedonic values – pleasantness – of odors. While the authors of some studies have observed activation of the AI regardless of the valence of odor

stimuli when participants were judging their pleasantness (Savic et al. 2000), some have only found correlation between the AI activity and perceived pleasantness of odors (de Araujo et al. 2005), and others linked AI activity with perceived olfactory unpleasantness (Rolls 2003; Royet et al. 2003; Wicker et al. 2003; Grabenhorst and Rolls 2009). Meanwhile, others have argued that the AI has relatively little to do with olfactory hedonic value signals, and that other regions, such as the orbitofrontal cortex (OFC), are better candidates for investigating hedonic value computation (Kringel-bach 2005; Katata et al. 2009; Kühn and Gallinat 2012). Hence, it appears that it is an important task to sort out this lack of consensus with a more extensive and systematic experiment. In Chapter 3, I describe an fMRI study with olfactory stimuli that attempts to address this issue.

Many neuroimaging studies have shown a strong link between gustation and the AI: the region has exhibited activity in response to sucrose (de Araujo et al. 2003a), glucose (Francis et al. 1999) and mineral water (de Araujo et al. 2003b), and the dorsal AI appears to be involved in tracking the fat content and viscosity of food in the mouth (de Araujo et al. 2004). Furthermore, various portions of the FI and the dorsal AI have been shown to process different tastes (sour, bitter, salty, sweet, and umami), further strengthening this link. In addition, it appears that mere imagery of gustatory sensation, in the absence of actual taste stimuli, can also activate the AI (Kobayashi et al. 2004).

The relationship between the AI and hedonic value computation seems complicated in the gustatory modality as well. Some neuroimaging studies reported activation of the region in response to taste stimuli of either valence (O'Doherty et al. 2001; Zald et al. 2002; Haase et al. 2007), while others have observed preferential activation in response to unpleasant (bitter or salty) tastes (Zald et al. 1998; Small et al. 2003). There is also some evidence of greater AI response toward taste stimuli that are preferred by participant, compared to non-preferred ones (Berns et al. 2001). Hence, again, it seems that these conflicting findings should be addressed with further research, although gustation is unfortunately not in the scope of this thesis.

Given the above information, one may begin to wonder whether or not the same portions of the AI are responsive to both olfactory and gustatory experiences. Indeed, a number of studies have shown that these two categories of activations do occur in overlapping regions. For instance, an imaging study that presented both olfactory and gustatory stimuli to the same individuals have found that a small set of areas such as the amygdala, frontal operculum, OFC, and a small region in the lateral FI exhibited convergence of the activations elicited by odors and sucrose solution (de Araujo et al. 2003a). In addition, a neuroimaging meta-study that utilized the activation likelihood estimation (ALE) technique to investigate the neural signals associated with intranasal trigeminal stimulation found that the FI also plays a role in processing trigeminal signals (Albrecht et al. 2010). These results, along with other neuroimaging data, suggest that the lateral portion of the FI is the only area in the human brain that becomes active in response to all three types of stimuli that together form a flavor — olfactory, gustatory, and trigeminal (Lundström et al. 2011). Therefore, it appears that the FI may play the principal role in integrating these different categories of signals to create the experience of flavor.

In addition to the neuroimaging studies discussed above, a small number of lesion studies support the link between AI and olfactory and gustatory functions. For example, a patient with an extensive bilateral lesion in the insula (as well as other regions adjacent to it) exhibited reduced ability to recognize disgust in other people's dynamic facial expressions, even though his performance in identifying other basic emotions fell in the normal range. The patient was also unable to feel or recognize disgust when presented with stories of people experiencing disgust (Adolphs et al 2003). While one cannot entirely exclude the possibility that other regions and the fiber tracts damaged in this patient's brain have contributed to this effect, given the association between the insula and the olfactory/gustatory functions discussed above, and the selective nature of the patient's impairment, it appears plausible that the insular damage is the main cause of this phenomenon. Similarly, a patient with damage in the insula and putamen showed impairment in recognizing disgust from facial and

vocal expressions (Calder et al. 2000).

The eating behavior exhibited by some patients diagnosed with FTD is also consistent with the suggested link between the AI and olfactory/gustatory function. A clinical study that measured the degree of binge eating and brain degeneration in subjects with various types of dementia found that, unlike those who had been diagnosed with non-FTD dementia, the patients with FTD engaged in binge eating, even when they were feeling satiated. Analyzing these patients' brain atrophy patterns using voxel-based morphometry (VBM) has revealed that all of the binge eaters had much greater damage in the right lateral FI, as well as the striatum and OFC, compared to non-binge-eating individuals (Wooley et al. 2007). This outcome suggests that the atrophy of the FI, along with degeneration of the striatum and the OFC, may have affected these patients' motivation to eat, and is consistent with the proposed role of the FI in gustatory behavior.

1.4.2   Social, Emotional, and Cognitive Functions

A growing number of studies in humans suggest that the AI and the FI are crucial in facilitating social emotions and some cognitive functions, as well as olfactory and gustatory experiences. In this section, I describe recent neuroimaging studies that reflect this.

AI appears to be involved in processing generalized emotional responses to stimuli. For example, the lateral FI was active when participants were recalling personal experiences that elicited happiness, sadness, anger, or fear (Damasio et al. 2000), and more active while participants viewed pictures containing emotionally charged contents compared to when viewing neutral ones (Bermpohl et al. 2006). Moreover, the degree of AI activation in response to emotional visual stimuli seems correlated with each participant's emotional susceptibility score (Iaria et al. 2008), suggesting a close relationship between one's subjective emotional intensities and the AI activity.

There is also evidence of AI's involvement during experience of specific categories of emotion. A robustly increased bilateral activation of the AI was observed when participants were experiencing fear due to threat of spontaneous pain (Butler et al. 2007), whereas the left insular cortex exhibited significant decrease in activity when women grieving recent romantic breakups were recalling memories of their past relationships (Najib et al. 2004). Also, bilateral FI activation was observed when participants were presented with highly aversive and violent pictures depicting injury and mutilation, and the activity in the right FI correlated with the subjective rating of the negative feelings participants were experiencing (Garrett and Maddock 2006). Fear and disgust probably are the emotions most strongly associated with this experiment. The FI also seems to play a role in emotional experiences of social nature, such as maternal love and romantic love, as the region was active in both hemispheres when mothers viewed pictures of their children and of their romantic partners (Bartels and Zeki 2004). The activity in the FI also seems correlated with the perceived funniness of humorous stimuli (Watson et al. 2006b). Considering the importance of humor in social boding, this involvement of the FI could also be construed as a social function.

Many neuroimaging studies implicate the AI in processing of empathy as well. Most of these studies have utilized pain of others as the main vehicle for instigating empathy in participants. One study used video recordings showing facial expressions of people in pain to elicit activations of the lateral FI (Botvinick et al. 2005), while another experiment utilized pictures of body parts being inflicted with pain, and observed FI activations during active rating of pain intensity in these pictures (Gu and Han 2007). An additional study found bilateral lateral FI signals when participants' loved ones were given painful stimuli (Singer et al. 2004), demonstrating that empathizing with another's pain involves FI processing. Other experiments have demonstrated that the intensity of empathy is correlated with the magnitude of the FI activity. One study used pictures depicting faces of chronic pain patients as stimuli, and observed bilateral FI activation whose strength was correlated with both the participants' estimate of the pain that the ones in the pictures were experiencing, and the participants' subjectively

perceived levels of empathy (Saarela et al. 2007). Another study showed that while people without expertise in acupuncture felt acute empathy for pain when presented with pictures of people receiving acupuncture treatments and exhibited bilateral FI activation, acupuncture specialists did not feel any concern for the pictured patients' pain, and showed significantly reduced FI activity (Cheng et al. 2007).

Some studies have studied the AI's role in empathy in the context of other types of stimuli: lateral AI activity was found in the left hemisphere (Wicker et al. 2003) and bilaterally (Jabbi et al. 2008) when participants were watching videos of others drinking liquids and making disgusted facial expressions, and hence possibility eliciting empathy, and the lateral FI in the left hemisphere was more active during viewing of faces expressing happiness or sadness, compared to during viewing non-face pictures of similar emotional contents (Britton et al. 2006).

In addition, the AI is also believed to play a role in various cognitive processes, including attention, language, speech, working memory, and memory (Kurth et al. 2010b). FI and AI appear to become active during visually presented tasks that require attention (Rubia et al. 2006), and in patients with obsessive-compulsive disorder during assignments that acquire hypervigilance (Maltby et al. 2005). Language processing was observed in the FI when the area showed increased activation during evaluation of semantic coherence in verbal stimuli (Ilg et al. 2007), listening to other people's speech (Jardri et al. 2007), and phonological assessment of words (Katzir et al. 2005). The FI also exhibited increased response when, rather than evaluating others' speech, participants produced their own speech by pronouncing syllables (Bohland and Guenther 2006; Riecker et al. 2006), and when finishing incomplete sentences (Brown et al. 2006). The role of the AI in working memory and memory was illustrated by studies in which a verbal working memory task activated the FI bilaterally (Koppelstaetter et al. 2008), the bilateral AI activity was correlated with the level of working memory load (Mayer et al. 2007), and the left lateral FI became more and more responsive as a novel object was presented repeatedly, hence helping participants memorize the object's appearance and name (van Turennout et al. 2003).

Human lesion studies of the AI support the results of the neuroimaging experiments discussed above (Ibañez et al. 2010). Patients with post-stroke damage in the right insula exhibited neglect in the visual, auditory, and tactile modalities, suggesting reduced abilities to attend to stimuli. Patients with similar lesions in the left insula did not experience such deficit (Manes et al. 1999a). Impairments in language and speech were also observed in an individual with an infarct in the left AI (Shuren 1993), a person with bilateral damage of the insula (Habib et al. 1995), and a group of patients with lesions in the anterior insula (Dronkers 1996). Moreover, patients with infarcts in the left insula exhibited reduced verbal memory, whereas those with similar damages in the right insula did not (Manes et al. 1999b). In addition, individuals diagnosed with the behavioral variant of FTD (bvFTD) tend to show impaired social cognition, such as reduced interest in social life, decreased ability to empathize, self-consciousness, and increased disinhibition and impulsiveness, while exhibiting relatively normal non-social cognitive skills. This is consistent with the rather specific atrophy of the frontal, insular, and temporal cortices in bvFTD patients (Ibañez and Manes 2012).

1.5 Known Connectivity Patterns of the Frontoinsular Cortex and Anterior Insula

1.5.1 Structural Connectivity

In the present section, I discuss in detail the connections of the human AI. As it is not possible to use the conventional method of tracer injection to study the connectivity patterns in the human brain — the tracer needs to be injected *in vivo*, which would be highly unethical — one must rely upon a set of more indirect methods for elucidating the connections of the AI. One such method is assay of the structural connectivity patterns using diffusion magnetic resonance imaging, which seeks to map the axon

fibers by measuring the movement of water molecules in the brain tissue, and will be discussed in further detail in Chapter 2. This is a non-invasive method that can be applied to live human participants in an MRI scanner.

While diffusion imaging is a method that has only recently been widely used, the small number of available studies that apply the technique to the AI yielded results that are consistent with the existing animal study results, and provided useful insights into the connectivity and function of the AI in humans. It appears that most of these studies were focused on parcellating the entire insular cortex into different regions: in one study using probabilistic fiber tractography, every single voxel in the human insular cortex ROI was used as a seed, and the resulting tracts were used to construct a connectivity correlation matrix between each pair of seeds. A Laplacian eigenmap of this matrix was computed, identifying two main categories of the seeds. Finally, these seeds were mapped back onto the insular ROI, which revealed two main portions of the insula (anteroventral and posterodorsal), with a transitional area in between. The more anterior seeds tended to connect to the amygdala, entorhinal cortex, and hippocampus, as well as the anterior frontal gyrus, whereas the posterior seeds mostly were associated with somatosensory, parietal, and posterior temporal cortical areas (Cerliani et al. 2011). In another study that also employs probabilistic fiber tractography in human diffusion images, the anteroventral portion of the insula was associated with the OFC, inferior frontal cortex, and the anterior portion of the temporal cortex (Cloutman et al. 2012).

In addition, a preliminary probabilistic fiber tractography study in the high-quality high angular resolution diffusion imaging (HARDI) data from the brain of a hyper-enriched gorilla probed the connectivity patterns in different parts of its VEN-rich FI. When the medial FI was seeded, the resulting connectivity pattern was very distinct from those of the lateral FI and the dorsal AI near the FI. The medial FI seed was observed connecting to the frontal polar cortex, amygdala, and septum. The other two seeds exhibited many overlapping connections, including the hippocampus and posterior portions of the frontal cortex (Allman et al. 2010). These results appear

consistent with those of the two human studies discussed above, and seem to support the possible cognitive, social, and emotional functions of the FI and AI.

1.5.2 Functional Connectivity

Despite the promising results from the diffusion imaging experiments described above, unfortunately there is only a small number of such studies on the AI available at present, and due to current technical limitations in the diffusion imaging, the connectivity data from the existing studies are not likely to provide a complete picture of the AI's structural connectivity patterns. However, results from functional connectivity studies, which aim to identify neural regions that are simultaneously active during the brain's resting state or during specific tasks, have supplemented our knowledge to some extent.

The existing data from resting-state functional connectivity studies seem to paint a consistent picture of the AI's association with other regions. In a study that parcellated the human insula into two portions based on functional connectivity patterns, the AI became co-activated with the middle and inferior temporal cortices, ACC, and limbic regions (Cauda et al. 2010). In studies that further categorized the AI into the dorsal and ventral parts, whereas the dorsal AI seemed associated with the middle insula, dorsal ACC (Deen et al. 2010), and dorsolateral prefrontal cortex (DLPFC), (Chang et al. 2013), the ventral AI, closer to the FI, exhibited co-varied activation with the pregenual ACC (Deen et al. 2010), superior temporal sulcus, posterolateral OFC, amygdala, and ventral tegmental area (VTA) (Chang et al. 2013). The functional network among the bilateral AI, dorsal ACC, amygdala, periaqueductal gray (PAG), VTA, substantia nigra, dorsomedial thalamus, and hypothalamus, whose strength was observed to be correlated with participants' individual anxiety scores, is called the "saliency network," based on its integration of "conflict monitoring, interoceptive-autonomic, and reward-processing" functions (Seeley et al. 2007). A meta-analysis of 1,305 functional neuroimaging experiments presenting task-based

insular activations yielded results similar to those of the above resting-state studies: the anterior portion of the insula was associated with the frontal, cingulate, and parietal cortices, as well as with the cerebellum (Cauda et al. 2012).

The endeavors described above focused mainly on distinguishing the functional connectivity patterns of the AI from that of the PI, ignoring the possibility that there might be smaller but significant variations in connectivity among different portions of the AI. One resting-state functional connectivity study, however, sought to compare two different areas – dorsal and ventral – of the AI. The authors observed a large difference between the two connectivity patterns. The dorsal AI's activity seemed correlated with an array of cortical areas, such as the posterior insula, dorsal ACC, frontal pole, inferior frontal gyrus, lateral occipital cortex, and the superior temporal pole, as well as the dorsal putamen. On the other hand, the ventral AI seed exhibited associations with the pregenual ACC, lateral OFC, superior frontal cortex, medial frontal pole, as well as subcortical regions such as the ventral putamen and substantia innominata. Both regions also co-vary with the lateral FI and the medial FI, respectively (Touroutoglou et al. 2012). While the seed placed in the dorsal AI may be a bit too dorsal to be included in the FI and hence the study does not truly address the parcellation of the FI, this experiment does seem to succeed in separating the AI functional connectivity pattern into two distinct sets.

A number of studies that assayed structural and functional connectivity in the same set of participants suggest that, in many cases, functional connections do reflect structural connections. In one such study, nine resting-state functional networks, including a functional "core network" that involves the bilateral insular cortices (that seems to contain the lateral FIs) and the ACC, which happen to be the three regions that contain VENs, were identified. And when this result was compared with the results of diffusion imaging and fiber tractography, eight of these nine functional networks, including the core network, were also found to be structural networks (van den Heuvel et al. 2009). In another study, a functional connection between the AI and the middle portion of the intra-parietal sulcus, which could be associated

with the often-proposed role of the AI in cognitive functions, was also observed as a structural association (Uddin et al. 2010). Similarly, a resting-state functional connection between the AI and the ventrolateral prefrontal cortex was confirmed to exist structurally as well. Although in this study the functional connectivity assay failed to detect a prominent connection between the AI and the OFC (Wiech et al. 2014), this may be due to the fact that the functional data were collected at rest, rather than during a specific task that engages this association.

The structural and functional connections of the AI described above seem consistent with the proposed functions of the region. In addition, a number of connectivity studies support the role of the AI in the neuropsychiatric disorders discussed earlier in this chapter. For instance, the effective connectivity between the right AI and the DLPFC was observed to be weaker in individuals with schizophrenia (Iwabuchi et al. 2014). Moreover, there is some evidence that atypical connectivity of the AI is associated with autism (Uddin and Menon 2009; Uddin et al. 2013) and alexithymia (Bernhardt et al. 2013).

Despite the promising nature of the connectivity data discussed so far, these results can be construed as rather heterogeneous due to differences in analysis methods, image qualities, number of subjects, and processing pipelines. Also, with the exception of Touroutoglou et al. 2012, these studies mostly focused on parcellating the AI from the rest of the insula, rather than attempting to investigate any subdivisions the AI. Moreover, as mentioned earlier, only one of the two seeds utilized in Touroutoglou et al. 2012 appears to be included in the FI. Therefore, although whether any subdivisions exist within the human FI remains mysterious, it may be plausible considering the patchy distribution pattern of the VENs in the FI and the variation of structural connectivity patterns within the gorilla FI (Allman et al. 2010).

1.6 Overview of Thesis

For my graduate work, I have explored in detail the connectivity patterns of the insula in a non-human primate species using the diffusion MRI technique. I have also investigated the role that the human AI plays in the olfactory hedonic experience. These studies were motivated by a number of topics in the current literature that had not yet been addressed. First, there was a lack of a high-quality, comprehensive diffusion MRI study in the field of neuroanatomy at the time of the study: while a number of studies had studied *in vivo* and *ex vivo* brains using this technique, most of these datasets were rather low in quality, and hence unable to yield very detailed results. This prompted a need for a high-quality, high-resolution diffusion data and a series of fiber tractography experiments that examine the data in a thorough manner to demonstrate the value of the technique, since this method, when used properly, could be a useful and important tool for noninvasive exploration of rare brains.

Second, as mentioned in the Section 1.4.1, there had been a lack of consensus on the relationship between the AI and hedonic value processing. It is not surprising that the past neuroimaging studies collectively do not present a very clear picture, as they tend to vary in imaging protocol and quality, behavioral task, and analysis methods. Also, most of the past studies have utilized very small number (less than five) of olfactory or gustatory stimuli that had not been well characterized or selected in any systematic manner. Considering the importance of olfactory hedonic value processing in our daily lives and perturbation of this system in many neuropsychiatric disorders (Hayes et al. 2006; Plailly et al. 2006; Atanasova et al. 2008; Atanasova et al. 2010), it would be essential to establish a better-defined model for this function through a more extensive and systematic study.

The organization of this thesis is as follows. In Chapter 2, I will describe a HARDI study of structural connectivity of the insula and the neighboring claustrum in the *Microcebus murinus*, the gray mouse lemur dataset. This study serves three different functions: investigating the evolutionary relationship between the two structures

using histology and gene expression data, and showing a clear dissociation between the their connectivity patterns, hence confirming that the connectivity and functions classically associated with the insula are indeed unique to the insula; exploring the connectivity patterns of the two regions in the species considered morphologically and behaviorally close to the common ancestor of all primates, hence furthering our knowledge about the early primate brain organization; and, through comparisons with the data from conventional tracer-injection studies, showcasing the efficacy of the HARDI and probabilistic fiber tractography techniques. Chapter 3 will be devoted to an fMRI study that explores the neural network that computes hedonic values represented in olfactory stimuli. The study especially focuses on the role of the AI in this network, and its relationship with the other regions active during passive smelling and hedonic value judgment tasks. The study also seeks to find any correlation between the data (both behavioral and neural) from the olfactory tasks and participants' moral judgment tendencies, based on the hypothesis that the primary disgust and "social/moral disgust" are functionally related. The final chapter will summarize the findings from the Chapters 2, and 3, and discuss the remaining questions and future directions in the study of the insular connectivity and function.

Chapter 2

The Structural Connectivity of Insula and Claustrum in *Microcebus murinus*

2.1   Abstract

The claustrum and the insula are closely juxtaposed in the brain of the prosimian primate, the grey mouse lemur (*Microcebus murinus*). Whether the claustrum has closer affinities with the cortex or the striatum has been debated for many decades. Our observation of histological sections from primate brains and genomic data in the mouse suggest former. Given this, the present study compares the connections of the two structures in *Microcebus* using high angular resolution diffusion imaging (HARDI, with 72 directions), with a very small voxel size (90 micra), and probabilistic fiber tractography. High angular and spatial resolution diffusion imaging is non-destructive, requires no surgical interventions, and the connection of each and every voxel can be mapped, whereas in conventional tract tracer studies only a few specific injection sites can be assayed. Our data indicate that despite the high genetic and spatial affinities between the two structures, their connectivity patterns are very different. The claustrum connects with many cortical areas and the olfactory bulb; its strongest probabilistic connections are with the entorhinal cortex, suggesting that

the claustrum may have a role in spatial memory and navigation. By contrast, the insula connects with many subcortical areas, including the brainstem and thalamic structures involved in taste and visceral feelings. Overall, the connections of the *Microcebus* claustrum and insula are similar to those of the rodents, cat, macaque, and human, validating our results. The insula in the *Microcebus* connects with the dorsolateral frontal cortex in contrast to the mouse insula, which has stronger connections with the ventromedial frontal lobe, yet this is consistent with the dorsolateral expansion of the frontal cortex in primates. In addition to revealing the connectivity patterns of the *Microcebus* brain, our study demonstrates that HARDI, at high resolutions, can be a valuable tool for mapping fiber pathways for multiple sites in fixed brains in rare and difficult-to-obtain species.

2.2   Introduction

Microcebus murinus, the grey mouse lemur, is a prosimian species native to the island of Madagascar. *Microcebus* bears many similarities to the common ancestor of primates, which motivated the early study of the microscopic anatomy of its cerebral cortex by Le Gros Clark (1931). Many sources of evidence indicate that the common primate ancestor probably lived in tropical forests and was highly arboreal, was nocturnal and small in size, weighing 500g or less, and that it fed on both fruits and small animals. *Microcebus murinus* satisfies all of these criteria (Martin, 1990), and the species' skull shape and external brain morphology closely resemble the fossil primates of the early Eocene period, 55 million years ago (Radinsky, 1975; Allman, 1977). These observations suggest a possible role of the *Microcebus* as an extant proxy for the common ancestor of primates, hence motivating us to study the species as a way of exploring the evolution of primate brains.

The claustrum is a thin, sheet-like subcortical cellular structure found in mammalian brains. In primates it is located between the putamen and the insular cortex, usually separated from each of these two structures by the external capsule and the extreme

capsule, respectively (Figures 2.1A and 2.1B). Due to the claustrum's location, size, and shape, it is very challenging to investigate the structure's connections and function using techniques that are currently available. However, the limited amount of data from other species suggest that it is extensively connected with many cortical areas including the prefrontal, temporal polar, motor, hippocampal, parahippocampal, parietal, and visual cortices (Tanné-Gariépy et al., 2002; Edelstein and Denaro, 2004). Connections with the thalamus, caudate, and amygdala have also been found (LeVay and Sherk, 1981; Arikuni and Kubota, 1985; Jiménez-Castellanos and Reinoso-Suárez, 1985; Amaral and Insausti, 1992; Edelstein and Denaro, 2004).

There has been a long debate concerning the ontogenetic origin of the claustrum, with three different views: the opinion that the structure is derived from the adjacent insular cortex (Meynert, 1868; Brodmann, 1909), the view that it is a part of the basal ganglia (Edelstein and Denaro, 2004), and the one that argues for claustrum's independence from cortical or subcortical origin (Filimonoff, 1966). Meynert (1868) and Brodmann (1909) considered the claustrum to be part of the insular layer VI, and defined the borders of the insular cortex according to the location of the claustrum. Bayer and Altman (1991a; 1991b) supported this view by demonstrating that, in rat embryos, the claustrum and the deep layer of the anterior insular cortex emerge on the same day. This view has also been supported in the context of pallidal evolution in reptiles and birds: Striedter (1997), based on comparative analysis of reptile, bird, and mammalian brains, argued that the claustrum and the endopiriform nucleus (primate ventral claustrum) are pallidal in origin. In addition, Puelles et al. (2000) have shown that the mammalian homologs of some of the genetic markers for the pallidum in the embryonic chick are expressed in the claustrum, suggesting cortical affinity. The second conception that the claustrum has its closest affinities to the striatum, rather than the insular cortex, is supported by evidence that it is possible for the claustrum to develop into a significant size in near absence of the insula, and that the human claustrum tends to extend much beyond the upper border of the insula. It has also been pointed out that the human embryonic claustrum is not

directly connected with the deep layers of the insula. Instead, it is well-separated from the cortex by the uncinate fasciculus as well as the extreme capsule, and closely connected to the amygdala in some parts (Landau, 1919). The opinion that the claustrum is neither cortical nor subcortical was supported by Ramón y Cajal (1902) and by Filimonoff (1966), who, based on an exhaustive study of human adult and embryonic brains, concluded that the claustrum is an intermediate structure between the striatum and the cortex. A recent proteomic study of the rat claustrum agreed with this view, although it also found a claustral affinity with layer VI of the insular cortex (Mathur et al., 2009).

Inspecting histological sections from primate brains available in our laboratory supports the cortical origin of the claustrum. The spatial relationship between the claustrum and insula in the *Microcebus* is illustrated in the photomicrographs of Nissl- and Gallyas-stained coronal sections (Figures 2.1A and 2.1B) and Nissl- and Heidenhain-stained horizontal sections (Figures 2.2A and 2.2B). These sections show that the two structures are only barely separated from each other. The extreme capsule is very thin and does not entirely segregate the claustrum from the insula, and the claustrum appears to be an extra layer of the insula. This is unlike most other primate brains, in which claustrum and insula are more clearly separated by the extreme capsule: Figures 2.2C-F show Nissl- and Gallyas-stained sections from the brains of a tarsier (*Tarsius bancanus*) and an orangutan (*Pongo abelii*), including the claustrum, extreme capsule, and insula. In the tarsier (Figures 2.2C and 2.2D) the extreme capsule divides only the dorsal half of the claustrum from the insula, while the ventral halves of the two structures appear fused. However, based on the width of the extreme capsule, the dorsal segregation seems quite robust. In the orangutan (Figures 2.2E and 2.2F), the claustrum is completely separated from the insula.

We have also investigated the genetic affinities of the claustrum and the insula, and compared them with those of their neighboring regions. Using Allen Institute for Brain Science's AGEA, we studied the gene expression correlation patterns based on 4,376 genes in the claustrum, insula, caudate-putamen, and the olfactory cortex in
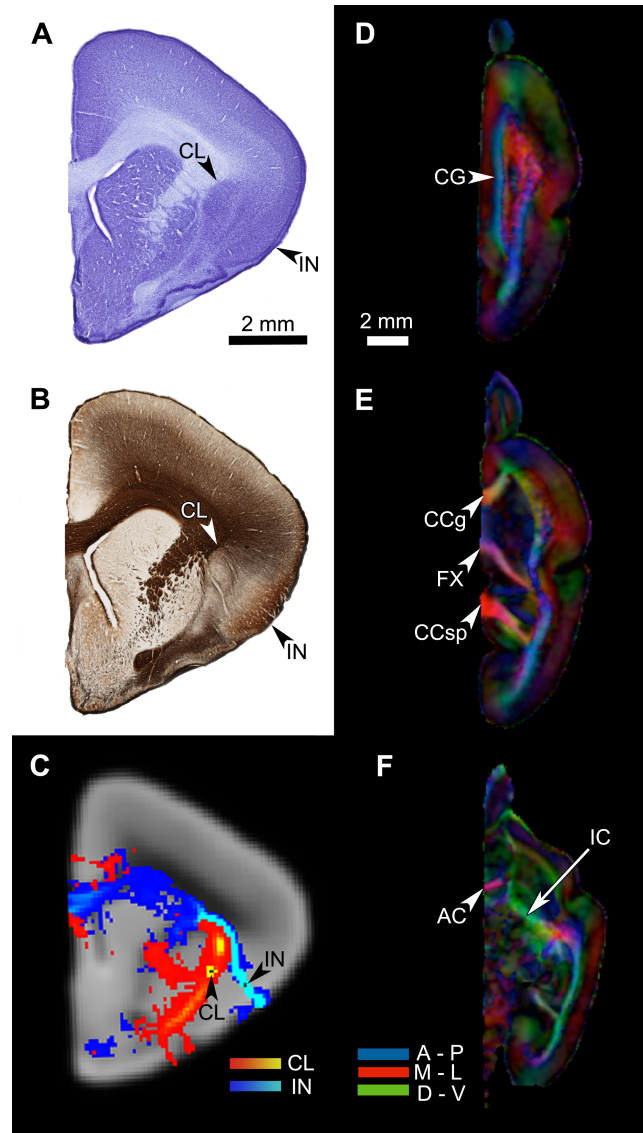
Figure 2.1: An overview of the seed placement and HARDI data quality.
(A) A coronal section of the *Microcebus murinus* brain, stained for cell body with the cresyl violet Nissl technique. The arrows point to the claustrum (CL) and the insula (IN). (B) An adjacent section, processed with the Gallyas silver staining technique, showing fiber distributions. Note the external capsule segregating the claustrum from the putamen, and the extreme capsule barely separating the claustrum from the insula. (C) A coronal cross-section of the HARDI data, at the level and cutting plane similar to those of the histological sections. The arrows indicate the locations of the claustral and mid-insular seeds. The red-yellow tract originates from the claustral seed, whereas the blue-light blue tract arises from the mid-insular seed. (D–F) The fractional anisotropy (FA) map of the HARDI data, in horizontal planes. This map reflects the distribution of fiber tracts in the brain tissue, with the colors representing fiber directions (blue = anterior-posterior; red = medial-lateral; green = dorsal-ventral). The map clearly shows a number of major fiber bundles, such as the anterior commissure (AC), cingulum bundle (CG), corpus callosum, genu (CCg), corpus callosum, splenium (CCsp), fornix (FX), and internal capsule (IC).
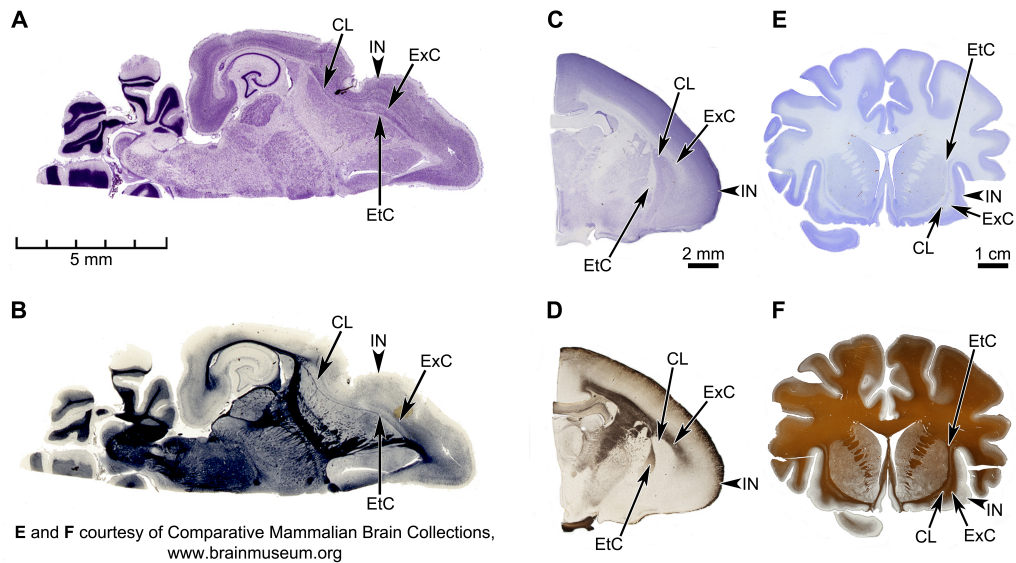
Figure 2.2: Horizontal sections of the *Microcebus* brain, and coronal sections of tarsier (*Tarsius bancanus*) and orangutan (*Pongo abelii*) brains, depicting the spatial relationship between claustrum and insula in the three species.
(A,B) Horizontal sections of the *Microcebus* brain, stained for cell bodies with the cresyl violet Nissl technique (A) and for axon fibers with the Heidenhain technique (B). (C,D) Coronal sections of the tarsier brain, stained for cell bodies with the cresyl violet Nissl technique (C) and for axon fibers with the Gallyas technique (D). (E,F) Coronal sections of the orangutan brain, stained for cell bodies with the cresyl violet Nissl technique (E) and for axon fibers with the Gallyas technique (F). In all panels, the external capsule (EtC), claustrum (CL), extreme capsule (ExC), and Insula (IN) are labeled. In the tarsier, the claustrum and the insula, while clearly segregated in the dorsal halves, appear fused together in the ventral portions. On the other hand, the extreme capsule in the orangutan is very extensive, completely separating the two structures. In the *Microcebus* the claustrum and the insula are extremely close together. Also, whereas the external capsule is relatively well defined throughout its entire length, the extreme capsule is almost absent in some parts. (A,B) Courtesy of the Comparative Mammalian Brain Collections (http://www.brainmuseum.org/), a collaborative effort among the University of Wisconsin-Madison, Michigan State University, and the National Museum of Health and Medicine, funded by the National Science Foundation and the National Institutes of Health.

the mouse. Figure 2.3 shows the expression pattern of each region: the claustrum has the strongest correlations with the deep cortical layers and a large part of the insula, whereas the caudate-putamen seems mostly self-contained in terms of genetic expressions and shows no special affinity with the claustrum. The olfactory cortex, while moderately associated with all cortical areas, is most significantly correlated with itself. Meanwhile, the anterior insula is highly correlated with the cingulate cortex as well as itself.

29
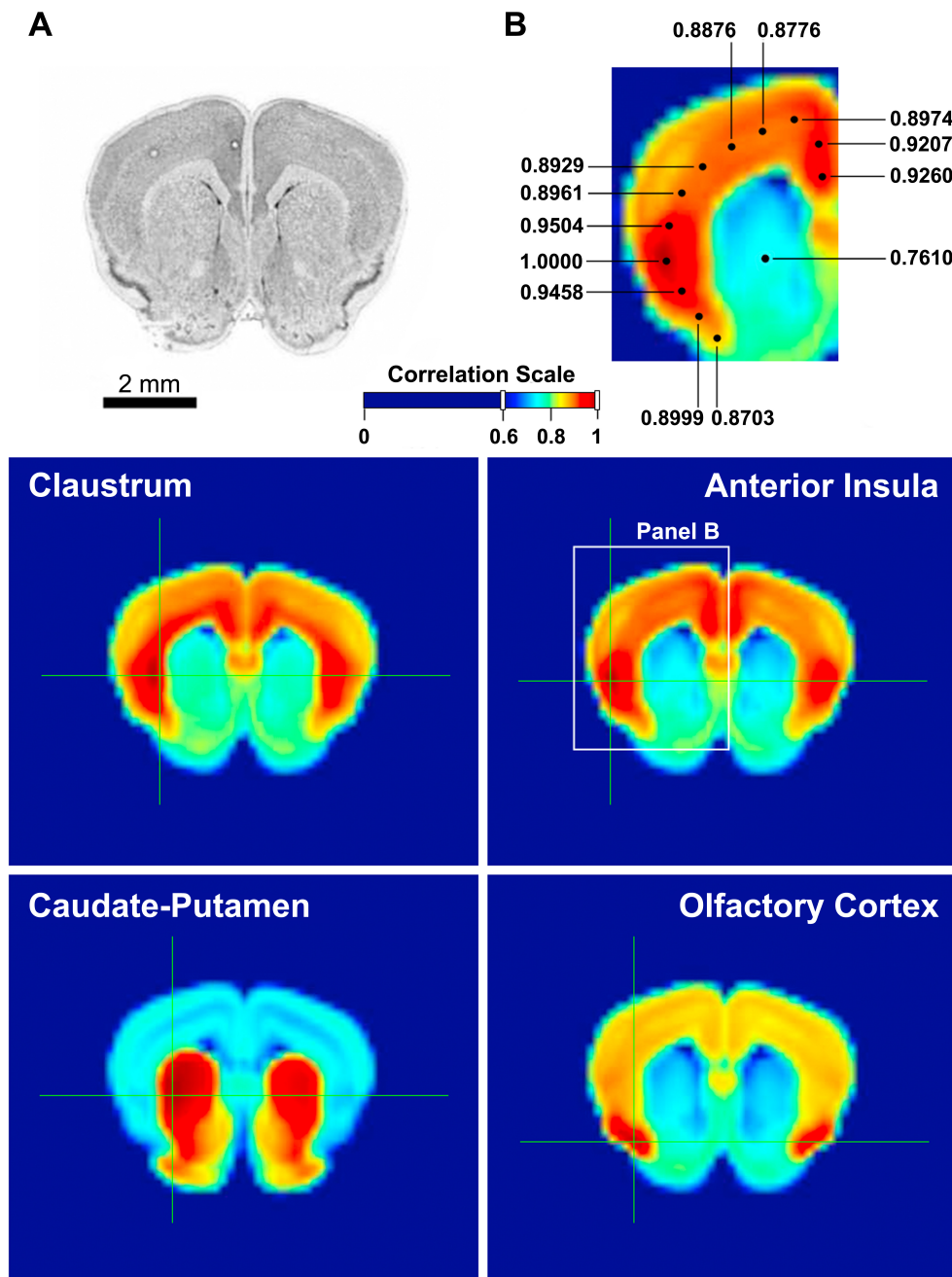
Figure 2.3: Gene expression correlation maps provided by Allen Brain Atlas AGEA.

AGEA, an on-line, open-access tool developed at the Allen Institute for Brain Science, is based on *in situ* hybridization data from the adult C57Bl/6J mouse brain, which provided the expression patterns of 4,376 genes. User can select a region of interest on the atlas and obtain a three-dimensional map of the mouse brain showing the total gene expression correlation between the region of interest and any of the other regions. AGEA also provides users with lists of genes with enhanced expression in correlated areas (Ng et al., 2009). (A) A reference section of the mouse brain, containing the claustrum, insula, caudate-putamen, and olfactory cortex. (B) A magnified view of the middle right panel, illustrating the strong correlation between the anterior insula and the cingulate cortex. Each number indicates the degree of correlation between the selected area and the location of the dot connected with the number. The dot with the correlation value of 1.0000 is where the selection crosshair was placed. Middle left: The mouse claustrum's gene expression correlation profile. According to the correlation scale [between (A,B)], the claustrum is most strongly affiliated with the deep layers of the insular cortex. Middle right: The anterior insula's gene expression is most highly correlated with the cingulate cortex, as well as itself. Bottom left: The caudate-putamen, besides a moderately high correlation with the olfactory tubercle, is mostly contained within itself. Bottom right: The olfactory cortex, other than the moderately high correlation with the cortex, is mostly correlated with itself.

From an evolutionary point of view, our histological evidence from the *Microcebus*, tarsier, and orangutan suggests a strong affinity between the claustrum and the insular cortex. Given the mouse lemur's similarities to the common primate ancestor, we believe that the two structures were closely juxtaposed in the beginning of the primate evolution, and gradually diverged due to the expansion of the extreme capsule as tarsiers, monkeys, and apes emerged. Our histological data, showing that the two structures are partially separated in the tarsier and segregated completely in the orangutan, supports this hypothesis. In addition, the gene expression profiles of the mouse claustrum and insula, provided by AGEA, indicate that the genes expressed in the claustrum are highly correlated with those present in the deep layers of the insular cortex and less correlated with gene expression in the striatum. Taken together, our anatomical and genetic evidence points to the cortical affinities of the claustrum.

Given that the claustrum appears to be a deep cellular layer closely juxtaposed with the insula in *Microcebus* and the close phylogenetic, developmental and genetic affinities of the claustrum and insula, we hypothesized that the connections of these two structures might be similar in *Microcebus*. To test this hypothesis, we have emulated standard tracer-microinjection tract tracing studies by placing single-voxel seeds within these structures in our high spatial and angular resolution diffusion imaging dataset for a fixed *Microcebus* brain. During the past decade a number of studies have explored diffusion MRI's capability of assaying fiber connectivity in post-mortem, fixed brains. Studies of various species, including the mouse (Mori et al., 2001; Guilfoyle et al., 2003; Sun et al., 2003; Zhang et al., 2003; Zhang et al., 2005; D'Arceuil and de Crespigny, 2007), cat (Takahashi et al., 2010; Takahashi et al., 2011), pig (Dyrby et al., 2007; Dyrby et al. 2011), rabbit (D'Arceuil et al., 2007), baboon (Kroenke et al., 2005), macaque (D'Arceuil et al., 2007), and human (Roebroeck et al., 2008; Miller et al., 2011; Takahashi et al., 2012), have supported this approach as an effective method of identifying and observing development of fiber bundles. It has also been shown that the anisotropy of fixed tissue does not differ significantly compared to fresh tissue (Sun et al., 2003; D'Arceuil et al., 2007),

and that fixed brain tissue retains its original diffusion property for at least 3 years (Dyrby et al., 2011). In addition, one study validated the results of probabilistic tractography in fixed pig brains by directly comparing them with the data from conventional tracer injections (Dyrby et al., 2007), showing that post-mortem diffusion imaging and probabilistic fiber tractography are viable methods. In fact, considering that these approaches are non-invasive, and could be seeded in many different regions without a limit (whereas conventional tracer injection method can assay only a few regions per brain), and that diffusion images can be sliced in many different planes for analysis, further developments of these techniques would have a significant impact on the field of neuroanatomy. However, to our knowledge there have been no studies in which an image with very high angular and spatial resolutions was produced, fiber tractography was performed with the image, and the resulting connections were validated with conventional tracer injection data. The very high resolution of our HARDI data, acquired at the magnetic field strength of 9.4 Tesla, has allowed us to study the animal's claustral connectivity at a spatial resolution (90 micra) that has not been achieved in most HARDI connectional studies.

2.3   Materials and Methods

2.3.1   Diffusion Magnetic Resonance Imaging

Two paraformaldehyde-fixed *Microcebus murinus* brains from lemurs that had died of cancer were provided by Dr. Russell Jacobs of the Beckman Institute at the California Institute of Technology. The right hemisphere of one of the brains was immersed in an inert, fluorinated fluid (Galden® HT-200 perfluoropolyether, Solvay Solexis, Inc., Thorofare, NJ) and scanned for approximately 33 hours in the Bruker 9.4-Tesla MR system (Bruker Biospin, Germany) for a high angular resolution diffusion image (Figures 2.1C – 2.1F) at the Caltech Brain Imaging Center. The HARDI data were obtained with a diffusion-weighted single spin echo sequence, using the following

parameters: number of directions = 72, TR/TE = 75 ms/22.8 ms, 256 x 160 x 112 matrix, 23.04 mm x 14.40 mm x 10.08 mm FOV, nominal b-factor = 1170 s/mm^2, ∂ = 5 ms, Δ = 10 ms. This yielded 7 non-weighted images and 72 diffusion-weighted images, with a voxel size of 90 µm isotropic. Figures 2.1D – 2.1F show the fractional anisotropy map of the HARDI data, reflecting the high quality of our image.

Only two brains were used in the present study, and only one brain was imaged, due to the scarcity of post-mortem fixed *Microcebus* brains and the very high cost of acquiring a diffusion image with high spatial and angular resolutions.

2.3.2   Histology

The imaged brain was embedded in celloidin, sectioned, and stained with thionin, but the resulting sections were low quality and could not be used for the study. Hence the second *Microcebus murinus* brain underwent sucrose and phosphate buffer saline baths for cryoprotection, was frozen on a specially designed microtome stage, and sectioned coronally at the thickness of 90 µm. The cut face of the tissue was photographed after every section. These images were used to ensure accuracy in orientation when the sections were mounted on glass slides prior to staining. All odd-numbered sections were stained with the cresyl violet Nissl technique, which visualizes neuronal cell bodies and glia (Figure 2.1A). All even-numbered sections were stained for axon fibers (Figure 2.1B) with the Gallayas method (Gallyas, 1979). Gelatinized slides were used for all Nissl sections and some of the Gallyas sections. However, agitations during the Gallyas procedure caused the tissue to peel off of gelatinized slides, and this prompted the use of SuperFrost Plus slides (Thermo Fisher Scientific, Inc., Waltham, MA), which adhere to tissue electrostatically.

2.3.3   Magnetic Resonance Image Processing and Fiber Tractography

FMRIB Software Library (FSL) algorithms (Woolrich et al., 2009; Smith et al., 2004) were used to process and analyze the HARDI data. Eddy current distortions in the diffusion-weighted images were modeled and corrected as affine transformations relative to the mean non-diffusion weighted image. Diffusion parameters were estimated using the two-fiber Bayesian inference with Markov Chain Monte Carlo sampling algorithm implemented by BEDPOSTX in FSL (Behrens et al., 2007). The non-diffusion weighted volume was re-oriented using the software Amira® (Visual Imaging, Inc., San Diego, CA), then re-sliced with Image J (National Institutes of Health, Bethesda, MD), such that its coronal cutting plane was similar to that of the histological sections. The histological sections helped us identify the claustrum and the different cytoarchitectural portions of the insula on the diffusion tensor image. We created single-voxel seeds in the two regions based on this anatomical information, and performed probabilistic fiber tractography using the PROBTRACKX algorithm implemented by FSL (Behrens et al., 2007). The same set of parameters were used for each run of probabilistic tracking: number of samples = 10,000; curvature threshold = 0.2; maximum number of steps = 4,000; and step length = 0.09 mm. The Loopcheck option was always used to exclude redundant fibers (Behrens et al., 2003a; Behrens et al., 2003b; Behrens et al., 2007). Similar tractography experiments were performed in the putamen, olfactory cortex, septum, and amygdala.

2.4   Results

To explore the connectivity patterns of the central portions of the *Microcebus* claustrum and insula, we first created a single-voxel seed mask in the center of each structure (Figure 2.1C). Fiber tractography experiments were performed using these masks and the parameters described in the Materials and methods section. The tractogra-

phy results suggest that, despite the spatial proximity between the two structures, claustrum and insula in the *Microcebus* have very distinct connectivity patterns.

Overall, the claustrum seems associated with most cortical regions and olfactory structures: as shown in Figures 2.4, 2.5, and 2.6, the claustral tract reaches the entire frontal pole, frontal cortex, premotor cortex, ventral anterior cingulate cortex, ventral temporal cortex, visual cortex, motor cortex, somatosensory cortex, olfactory cortex, and olfactory bulb, and most strongly with the entorhinal cortex. It also associates with some subcortical structures, such as the caudate (Figures 2.4C, 2.4D, 2.5B, 2.5C, and 2.6A), putamen (Figures 2.4C, 2.4D, 2.5C, and 2.6B), globus pallidus (Figures 2.4D, 2.5C, and 2.6B), lateral amygdala (Figure 2.4D), olfactory tubercle (Figures 2.5B and 2.6C), and olfactory tract (Figures 2.4A and 2.4B). The connections to the putamen and the globus pallidus appear to involve the external and internal medullary laminae of pallidum, respectively. In addition, the claustrum apparently has cross-hemispheric connections via the anterior commissure (Figures 2.4C and 2.5A) and the corpus callosum (Figures 2.4C, 2.4D, 2.5A, 2.5B, and 2.5C).
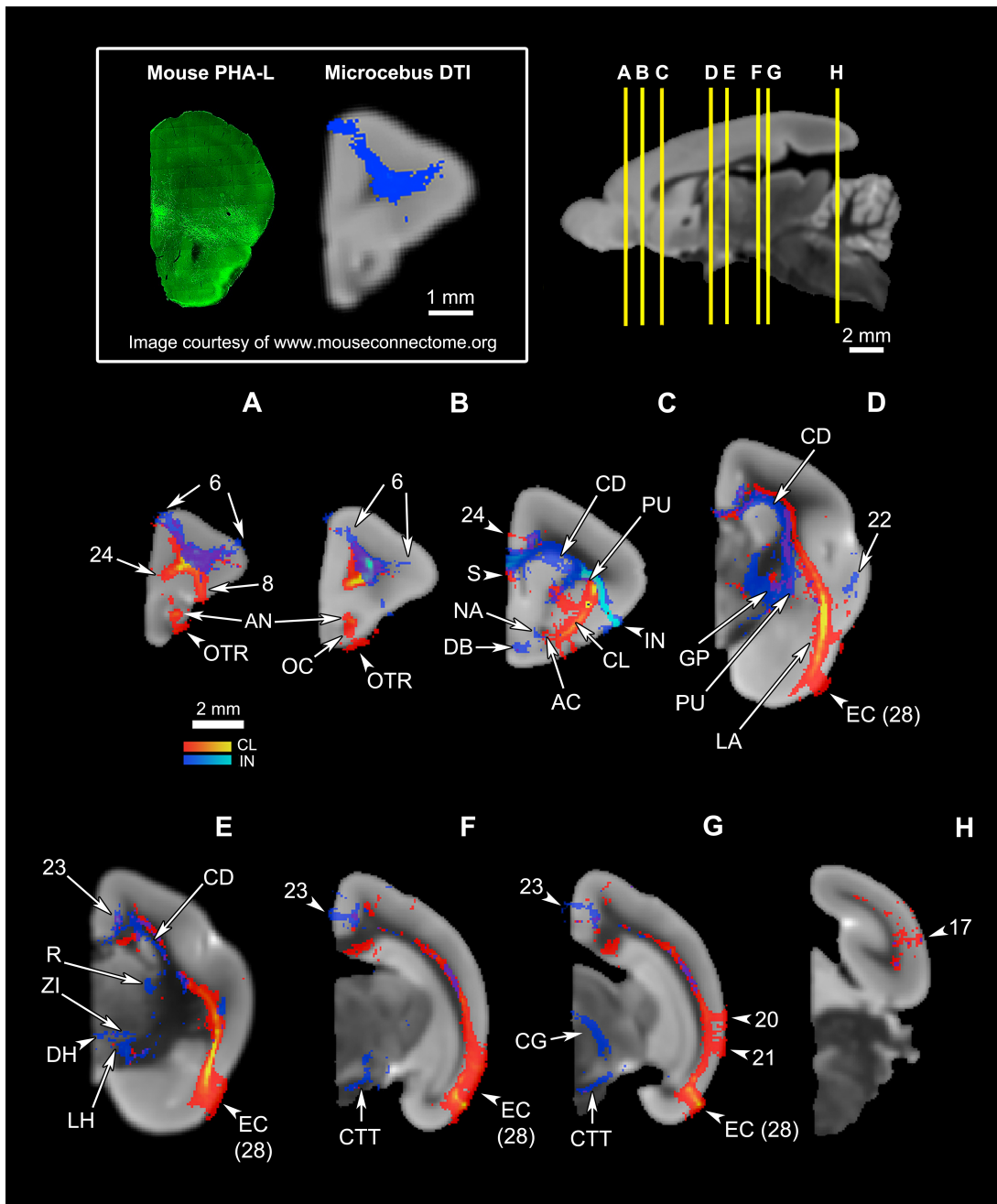
Figure 2.4: An overview of the connections of the claustral and insular tracts in coronal planes.

The claustral tracts are shown in red-yellow, with the yellow indicating connections that are more probable, while the insular tracts are shown in blue-light blue, with the light blue indicating more probable connections). The top left panel compares the insular connection to the frontal cortex between the mouse and the *Microcebus*. The image on the left shows PHA-L injected into the anterior insula of the mouse, resulting in anterograde projections to the orbitofrontal cortex, located ventrally. Image courtesy of the Mouse Connectome Project. The image on the right depicts the probabilistic fiber tractography results showing that the *Microcebus* insula connects mainly with the dorsomedial and dorsolateral frontal cortex. The top right panel describes the locations of the coronal cross-sections (A) through (H). In (A–H), since the blue tracts have been rendered transparent, the areas with overlapping claustral and insular tracts appear purple. The cortical area numbers are based on Le Gros Clark's (1931) map of *Microcebus* cortex. (A,B) The claustrum connects to the dorsal and ventral frontal cortex, cingulate cortex, olfactory cortex (OC), anterior olfactory nucleus (AN), and the olfactory tract (OTR), whereas the insula connects with the dorsomedial and dorsolateral frontal cortex. (C) The seed level. The claustral tracts travel from the claustrum (CL) to the nearby caudate (CD) and the putamen (PU), as well as the septum (S), anterior commissure (AC), and the ventral anterior cingulate cortex. The insular (IN) tracts appear in the caudate (CD), putamen (PU), septum (S), ventral cingulate cortex, nucleus accumbens (NA), and the diagonal band (DB). (D) The claustrum associates with the entorhinal cortex (EC, Area 28 in Le Gros Clark's, 1931 cortical map) at a high probability, and with the lateral amygdala (LA). The insula connects with the temporal cortex, globus pallidus (GP), caudate (CD), and putamen (PU). (E) The claustrum connects at a high probability to the entorhinal cortex (EC, Area 28 in Le Gros Clark's, 1931 cortical map). The insula connects to the caudate (CD), cingulate cortex, reticular thalamic nucleus (R), zona incerta (ZI), and dorsal lateral hypothalamus (DH, LH). (F) The claustrum continues to connect at a high probability with the entorhinal cortex (EC, Area 28 in Le Gros Clark's, 1931 cortical map), whereas the insular tracts appear in the cingulate cortex and along the central tegmental tract (CTT). (G) While the claustrum connects to the entorhinal cortex (EC, Area 28 in Le Gros Clark's, 1931 cortical map) and the more dorsal cortical areas 20 and 21, the insula continues to associate with the cingulate and central tegmental tract (CTT), and connects with the midbrain central gray (CG). (H) Both claustrum and insula connect with the visual cortex, although the insula does to a significantly lesser degree than does the claustrum.

By contrast, the mid-insular seed appears connected to more subcortical areas and does not show strong signals in the olfactory structures: the seed exhibits associations with the dorsal and lateral parts of the hypothalamus (Figure 2.4E), substantia nigra (Figure 2.5B), zona incerta (Figures 2.5B and 2.5C), thalamic areas such as the reticular nucleus (Figure 2.5C), ventral posterolateral nucleus (Figure 2.5C), and the parvocellular division of the ventral posteromedial nucleus (VPMpc) (Figure 2.5C), and with brainstem structures including the central tegmental tract (Figures 2.4E, 2.4F, 2.5A, and 2.6C), parabrachial nucleus (Figures 2.5B and 2.6B), and midbrain central grey (Figures 2.4F and 2.5A). Additional subcortical regions such as the nucleus accumbens (Figures 2.4C and 2.5B), substantia innominata (data not shown), and diagonal band (Figures 2.4C, 2.5A, and 2.5B) are also connected with the insula. We were unable to precisely identify which hypothalamic nuclei are associated with the insula, due to the limited image resolution. Overall, there appears to be a coherent system involving the central tegmental tract, parabrachial nucleus, lateral hypothalamus, zona incerta, VPMpc, midbrain central grey, and insular cortex. In contrast to the claustrum, we found no connections to the olfactory bulb or the entorhinal cortex arising from the mid-insular seed voxel, although it does have some connections with the temporal lobe outside the entorhinal cortex (Figure 2.4D). The insular seed revealed a robust trans-cortical association between the cingulate cortex and the insula (Figure 2.4C). This connection and the rest of the insular connections with the frontal cortex (Figures 2.4A and 2.4B) mainly occupy the dorsal and lateral aspects of the frontal lobe. On the other hand, the claustrum does not show such preference (Figure 2.4A). The insula's connection with the dorsolateral frontal cortex in the *Microcebus* contrasts with the mouse insula, which is mainly associated with the ventral frontal lobe (Figure 2.4, top left panel).

Some similarities between the two connectivity patterns are also observed. First, both seed regions maintain connections throughout almost the entire length of the cingulate cortex (Figures 2.4C, 2.4D, 2.4E, 2.4F, 2.5A, and 2.6A), including the part of the ventral anterior cingulate cortex that may be the primate homolog of the
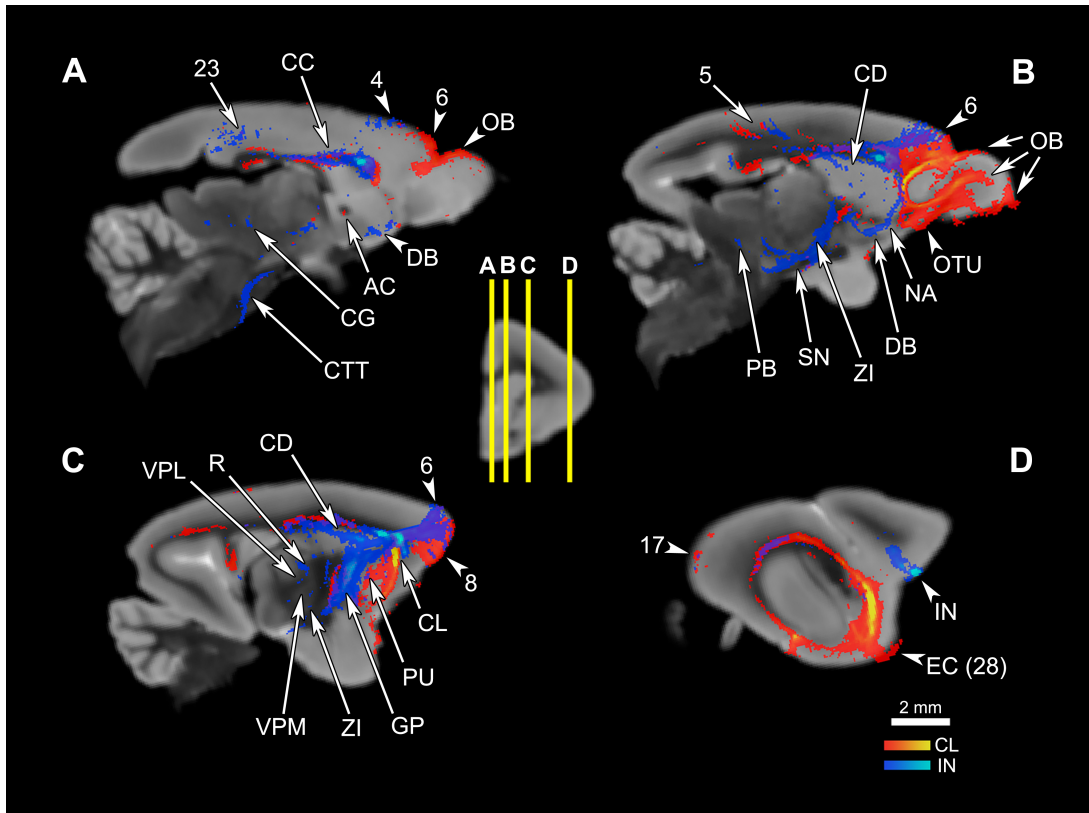
Figure 2.5: The connections of the claustrum and insula in parasagittal planes. The middle panel shows the levels of cross-section for (A–D). The cortical area numbers are based on Le Gros Clark's (1931) map of *Microcebus* cortex. (A) The claustrum connects to the olfactory bulb (OB) and the dorsal frontal cortex, and achieves cross-hemispheric connections via the anterior commissure (AC) and the corpus callosum (CC). The insula connects to the dorsal frontal cortex, posterior cingulate cortex, corpus callosum (CC), diagonal band (DB), midbrain central gray (CG), and central tegmental tract (CTT). (B) The claustrum is connected with a large portion of the prefrontal cortex, olfactory bulb (OB), olfactory tubercle (OTU), as well as the parietal cortex. The insular tracts appear in the frontal cortex, parietal cortex, caudate (CD), nucleus accumbens (NA), diagonal band (DB), zona incerta (ZI), substantia nigra (SN), and parabrachial nucleus (PB). (C) The claustrum connects to the frontal cortex and the putamen (PU), while the insula connects to the dorsal frontal cortex, globus pallidus (GP), reticular thalamic nucleus (R), ventral posterolateral thalamic nucleus (VPL), ventral posteromedial thalamic nucleus (VPM), and zona incerta (ZI). (D) The claustrum is highly probably connected to the entorhinal cortex (EC, Area 28 in Le Gros Clark's 1931 cortical map). Both claustrum and insula are connected to the cortical area 17, although the insula seems connected to a lesser degree.
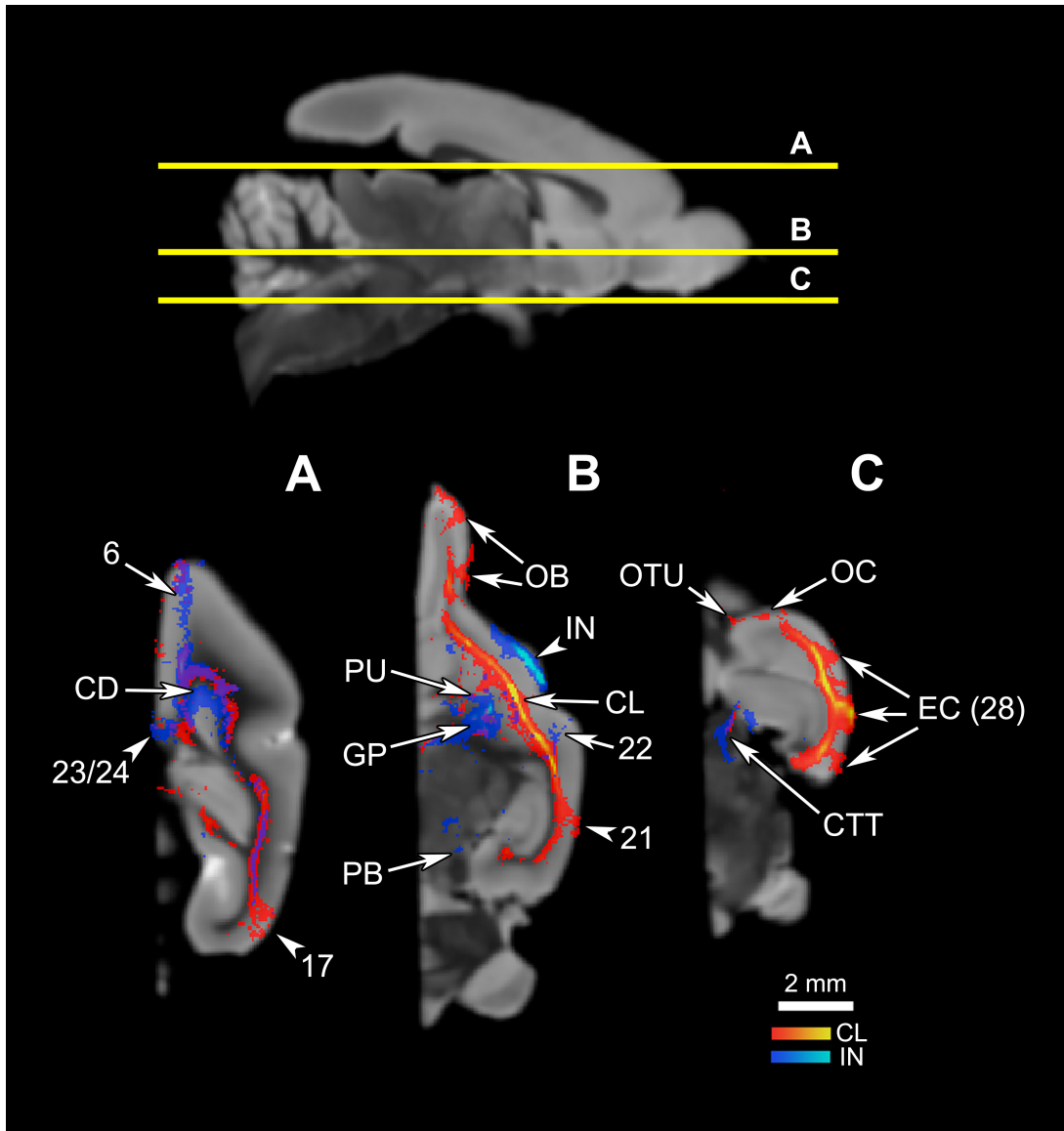
Figure 2.6: The connections of the claustrum and insula in horizontal planes. The top panel shows the levels of cross-section for (A–C). The cortical area numbers are based on Le Gros Clark's (1931) map of *Microcebus* cortex. (A) Both claustral and insular tracts appear in the frontal and cingulate cortices, caudate (CD), and the visual cortex. (B) The claustrum connects to the olfactory bulb (OB), putamen (PU), and the cortical area 21. Also note that the claustral tract is adjacent to the frontal, temporal, and occipital cortices, suggesting that the claustrum is connected to deep layers of these areas although the tract does not penetrate into upper cortical layers. The insular tract appears in the putamen (PU), globus pallidus (GP), and the parabrachial nucleus (PB). (C) The claustrum is connected to the olfactory tubercle (OTU), olfactory cortex (OC) and, at a high probability, to the entorhinal cortex (EC, Area 28 in Le Gros Clark's 1931 cortical map). Meanwhile the insula connects to the central tegmental tract.
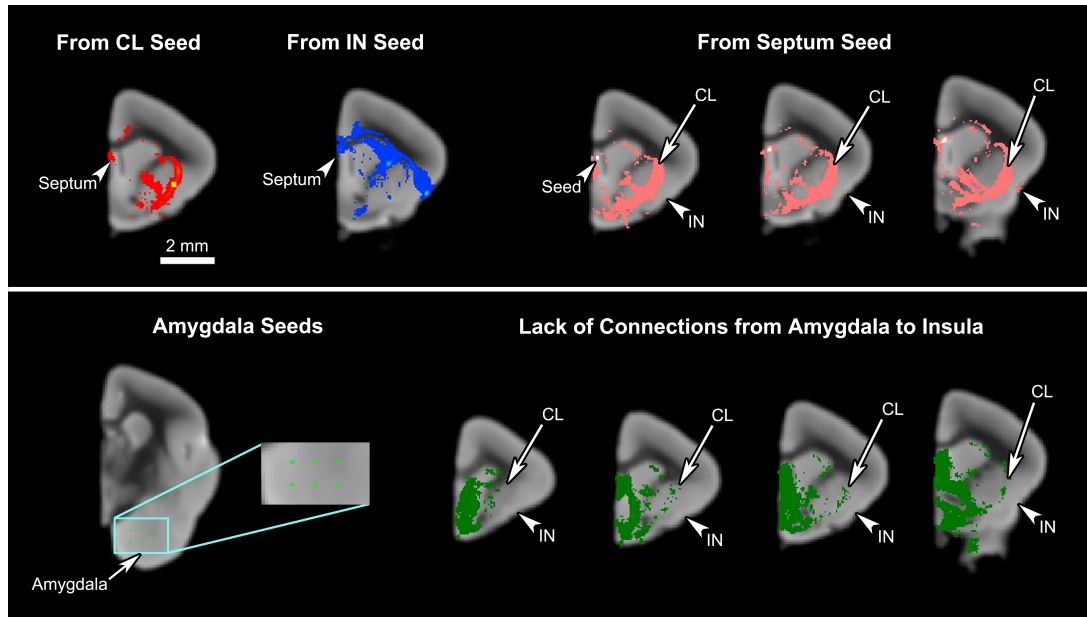
Figure 2.7: The connections of the septum and amygdala to the claustrum and insula.

Upper panel: The mid-claustral and mid-insular seeds both yield connections to the septum. A single-voxel seed placed in the septum results in tracts connecting to the claustrum (CL) and insula (IN). Lower panel: Six single-voxel seeds were placed in the basal part of the amygdala. The resulting tracts were pooled together and inspected for any connections to the insula. While some connections are observed in the claustrum, our data do not show any amygdalal tracts reaching the insula.

rodent inframlimbic and prelimbic cortices (Figure 2.4C). Second, both regions appear robustly connected to the septum: the claustral tract is seen in a large part of it while the insular tract is present in the dorsal septum (Figure 2.4C). Also, a single-voxel seed mask placed in the dorsal septum yielded a tract that reaches both the claustrum and the insula (Figure 2.7, top row). Third, both the insula and the claustrum seem associated with the parietal and occipital cortices, although the insular connections are much weaker than the claustral ones (Figures 2.4E, 2.4F, 2.4G, 2.5B, 2.5D, and 2.6A). Finally, both structures exhibit connections to the caudate and the putamen (Figures 2.4C, 2.4D, 2.5B, 2.5C, 2.6A, and 2.6B).

To investigate topographical fiber organizations in the claustrum and the insula, we placed additional single-voxel seeds along the approximate anteroposterior, mediolateral, and dorsoventral axes of each region. The mediolateral axis was not tested in

the claustrum, due to the thinness of the structure. The claustrum does not exhibit significant differences in connectivity results among the anterior, middle, and posterior seeds (Figures 2.8A – 2.8D), whereas there seems to be some spatial organization along the dorsoventral axis: the ventral claustral seed, while connecting to the same set of regions as the dorsal seed, also connects to larger areas of the olfactory bulb and the olfactory cortex compared to the dorsal seed (Figures 2.8E – 2.8H). Whereas the insula does not seem to have any significant topographic organizations along the anteroposterior or the mediolateral axes (data not shown), some differences are observed along the approximately dorsoventral axis: a seed placed in the agranular region, ventral to the mid-insular seed discussed above, exhibits connections to the olfactory bulb, olfactory cortex, and the entorhinal cortex in addition to the insular connectivity profile discussed above (Figure 2.9).

To ensure that our results from the central claustral and insular seeds mostly represent the connectivity of claustrum and insula only, and not of the surrounding regions, we placed single-voxel seeds in some of these surrounding structures and compared the resulting fiber tracts with the claustral and insular ones. A seed was placed in the putamen, the structure immediately medial to the claustrum. The most striking differences shown in the probabilistic tractography results are that a) the putamen, unlike the claustrum, does not connect with olfactory structures such as the olfactory bulb, olfactory cortex, olfactory tubercle, and entorhinal cortex, and b) the putamen connects extensively to the caudate. Some similarities are found: like the claustrum, the putamen shows connections with many cortical areas, including the frontal, entorhinal, and visual (Figure 2.10, upper panel).

We placed another seed in the olfactory cortex, the region directly ventral to both the claustrum and the insula, and compared the resulting tracts with those of the agranular insular seed. As expected, the results indicate that the olfactory cortex's connectivity profile does not significantly overlap with the connectivity patterns of the agranular insula and the claustrum, in that the olfactory cortex only connects to the olfactory bulb, olfactory tubercle, and the entorhinal cortex (Figure 2.10,
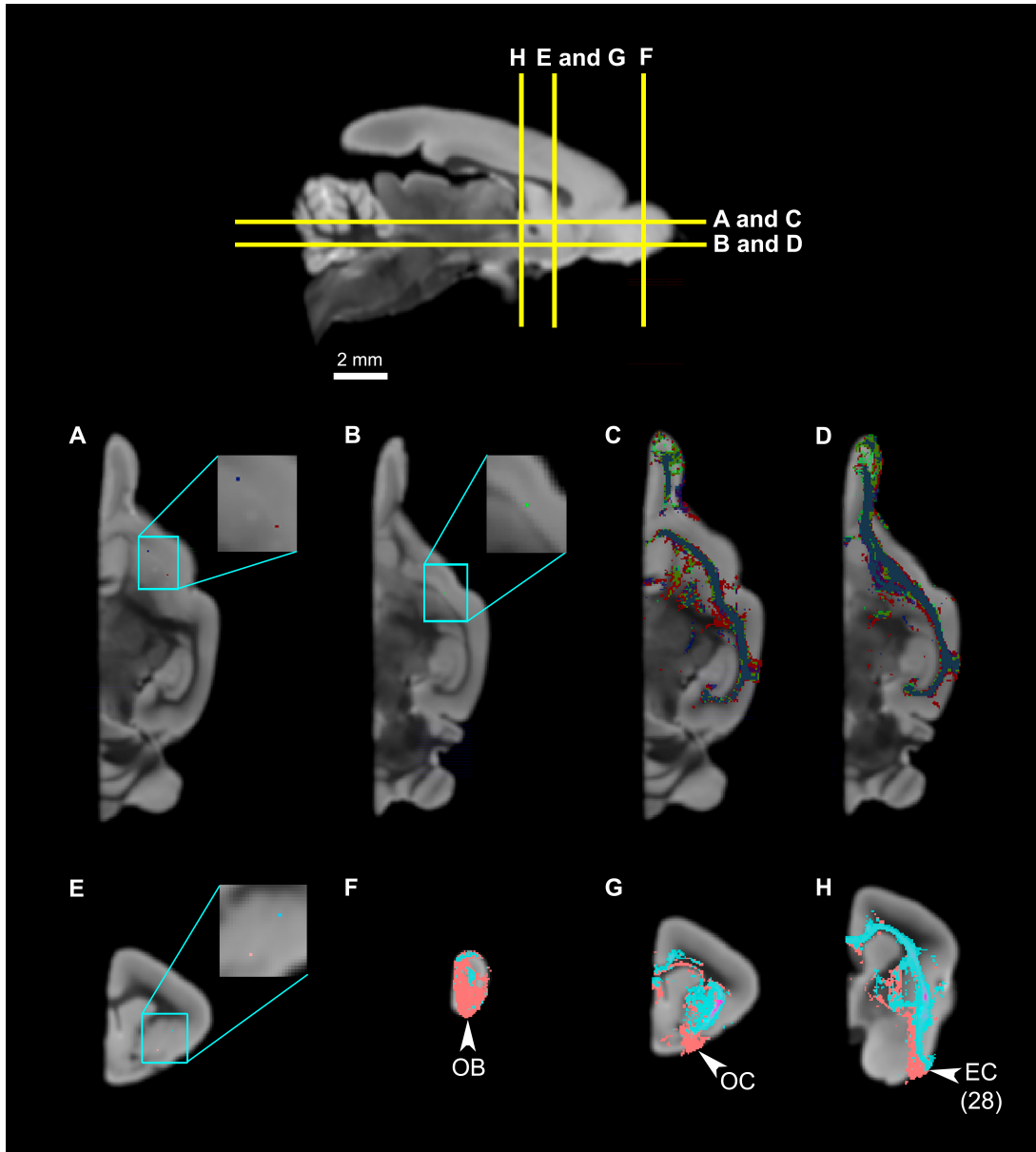
Figure 2.8: The slight spatial organization within the claustrum.

Top panel: The levels of cross-section for (A) through (H). (A) The locations of two claustrum seeds, with the blue seed in the anterior claustrum, and the red seed in the mid-claustrum. (B) The placement of the third seed, in the posterior claustrum, which is ventral compared to the anterior and middle claustrum. (C,D) illustrate the tractography results of the three seeds, demonstrating that the tracts mostly overlap with one another and there are no significant differences. (E) The locations of two claustrum seeds, with the light blue seed in the dorsal claustrum, and the pink seed in the ventral claustrum. (F,G) Claustrual connections to the olfactory bulb, olfactory cortex, and entorhinal cortex. Note that the tracts from the ventral seed (pink) occupy larger and more ventral portions of the three structures compared to those from the dorsal seed (light blue). Abbreviations: AC, anterior commissure; AN, anterior olfactory nucleus; CL, claustrum; EC, entorhinal cortex, Area 28 in Le Gros Clark's (1931) cortical map; GP, globus pallidus; OB, olfactory bulb; OC, olfactory cortex; OTR, olfactory tract; OTU, olfactory tubercle; PU, putamen.
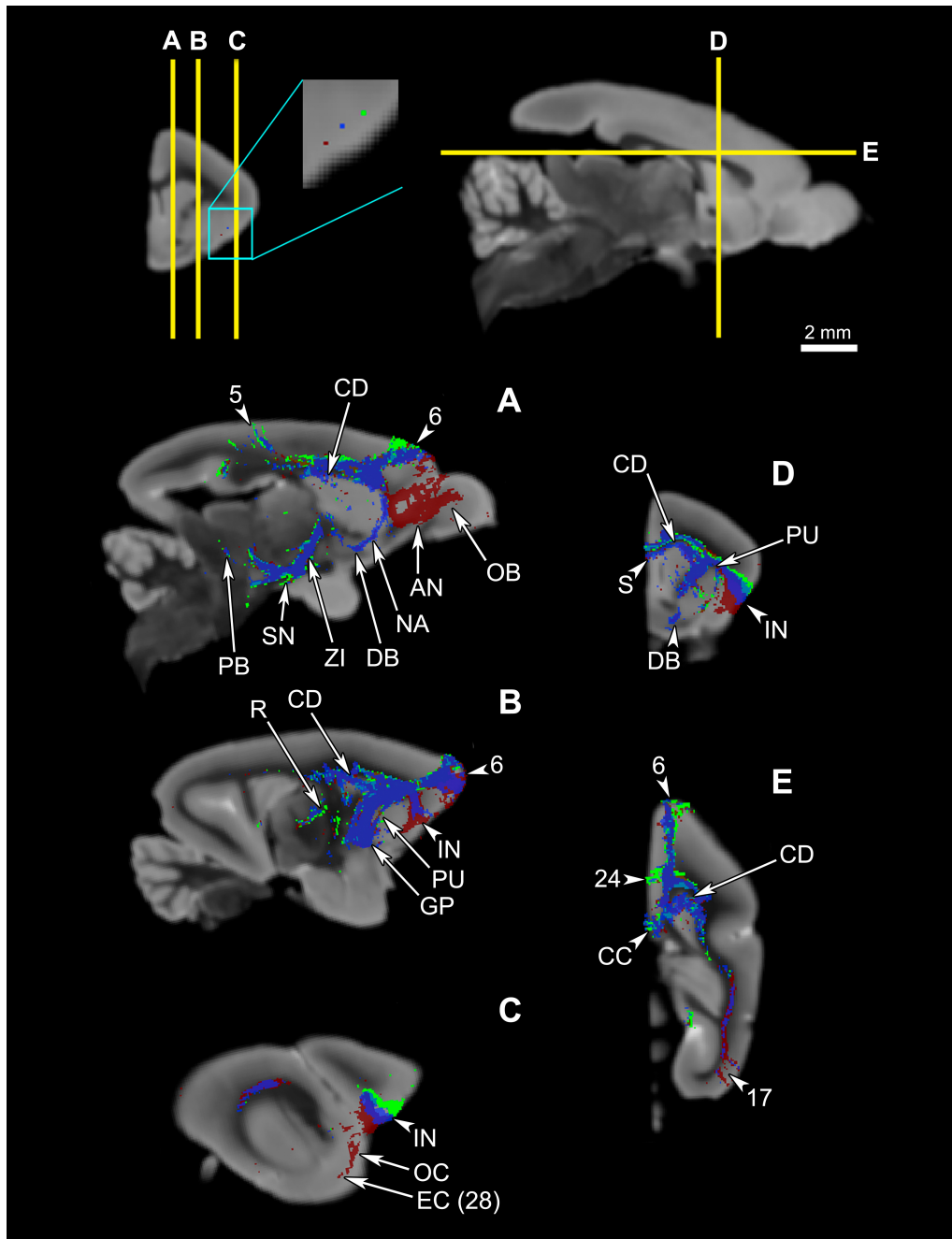
Figure 2.9: Probabilistic fiber tractography results from three seeds in the insula.

The top left panel shows the placement of the seeds: While the blue seed is in the mid-insula, the green seed is in the dorsal insula, closer to the granular insula, and the red seed is located ventrally, closer to the agranular insula. The top two panels show the levels of cross-section for (A) through (E). All panels show that the three seeds all share common tracts, and that the only significant difference is that the ventral seed connects to the olfactory bulb (A), anterior olfactory nucleus (A), olfactory cortex (C), and the entorhinal cortex (C). Note that the ventral insular seed's connection to the olfactory cortex in (C) is minimal, suggesting that the connections to other olfactory structures likely arose from the agranular insula, rather than from the adjacent olfactory cortex. (D) shows the similarities between the middle insular tracts and the ventral insular tracts. Abbreviations: AN, anterior olfactory nucleus; CC, corpus callosum; CD, caudate; DB, diagonal band; EC, entorhinal cortex, Area 28 in Le Gros Clark's (1931) cortical map; GP, globus pallidus; IN, insula; NA, nucleus accumbens; OB, olfactory bulb; OC, olfactory cortex; PB, parabrachial nucleus; PU, putamen; R, reticular thalamic nucleus; S, septum; SN, substantia nigra; ZI, zona incerta. The cortical area numbers are based on Le Gros Clark's (1931) map of *Microcebus* cortex.
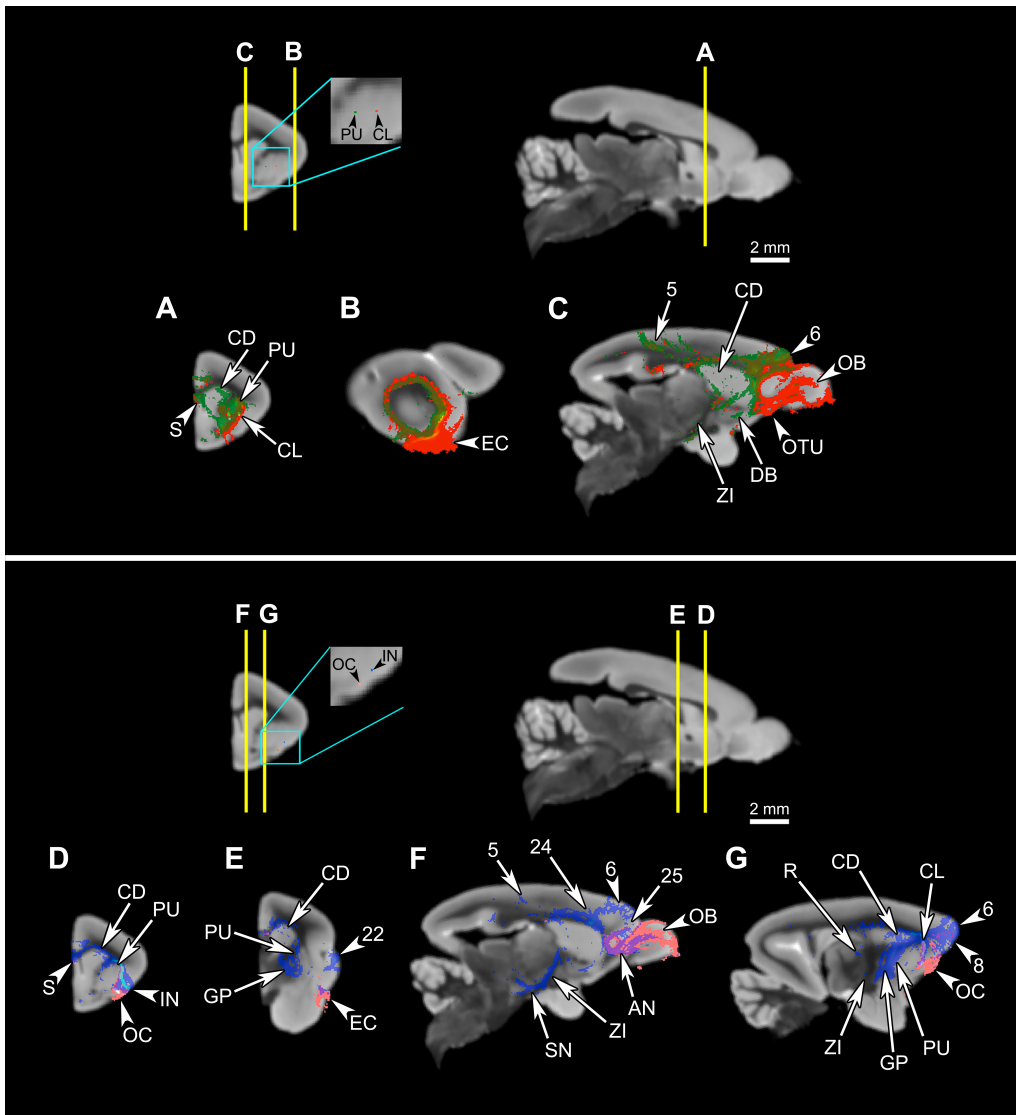
Figure 2.10: Comparison of connectivity patterns between the putamen and the claustrum, and olfactory cortex and the ventral insula.

Upper panel: Comparison of the claustral connectivity pattern with that of the putamen. The first row shows the levels of cross-section for (A–C), and the locations of the seeds in the putamen (green) and the claustrum (red). (A–C) The putamen tract shows more extensive connections to the striatum than does the claustral tract (A,C), and unlike the claustrum, the putamen does not associate with the olfactory areas, such as the olfactory bulb, olfactory tubercle, and olfactory cortex, and associates only with a small part of the entorhinal cortex (A–C). However, the two tracts share many of the cortical connections (C). Lower panel: Comparison of the insular connectivity with that of the olfactory cortex. The first row shows the levels of cross-section for (D–G), and the locations of the seeds in the olfactory cortex and the insula. (D–G) Despite the proximity of the two seeds, the tract originating from the olfactory cortex is significantly different from the insular tract, connecting to the olfactory bulb (F), anterior olfactory nucleus (F), and the entorhinal cortex (E), while avoiding most of the regions connected to the insula. Abbreviations: AN, anterior olfactory nucleus; CD, caudate; CL, claustrum; DB, diagonal band; EC, entorhinal cortex; GP, globus pallidus; IN, insula; OB, olfactory bulb; OC, olfactory cortex; OTU, olfactory tubercle; PU, putamen; R, reticular thalamic nucleus; S, septum; SN, substantia nigra; ZI, zona incerta. The cortical area numbers are based on Le Gros Clark's (1931) map of *Microcebus* cortex.

lower panel). The probabilistic connectivity results for the claustral and insular seeds mentioned above are summarized in Tables 2.1 - 2.5. The tables also include the comparison of our fiber tractography results with those of previous tracer injection studies in rodents and monkeys: since there are virtually no tracer studies done in the *Microcebus*, comparing our data to those from other species is currently the best available method of validating our data.

2.5   Discussion

Our data show that the claustrum and insula have very different connections in *Microcebus* despite their close structural, developmental, phylogenetic, and genetic affinities. Our *Microcebus* connectivity data, as shown in the Tables 2.1 – 2.5, are by and large consistent with the previously known connections of the claustrum and insula from tracer and imaging studies in other species. Our claustral connectivity pattern is comparable with the cat (Norita, 1977; Olson and Graybiel, 1980; Witter et al., 1988), macaque (Mufson and Mesulam, 1982; Pearson et al., 1982; Arikuni and Kubota, 1984; Insausti et al., 1987; Amaral and Insausti, 1992; Tanné-Gariépy et al., 2002), and squirrel monkey (Jürgens, 1983), demonstrating associations with most cortical areas. There are additional supporting data from the rat (Carey and Neal, 1985; Kowianski et al., 1998; Behan and Haberly, 1999; Lipowska et al., 2000), hedgehog (Dinopoulos et al., 1992), rabbit (Lipowska et al., 2000), mouse (Mouse Connectome Project), Galago (Carey et al., 1979), and Tupaia (Carey et al., 1979). In the cases of the rabbit and the rat, the injections were made in the endopiriform nucleus, which we consider equivalent to the ventral claustrum in primates. Although our results suggest that the *Microcebus* claustrum is connected with the putamen, globus pallidus, olfactory bulb, and olfactory tubercle, to the best of our knowledge no past tracing studies in other species have reported this. We suspect that these regions might not be directly connected with the claustrum, but rather indirectly via the cortical and subcortical areas that are associated with it.

Our results from the mid-insular seed also show a trend similar to those of the previous studies in the mouse (Mouse Connectome Project), rat (Allen et al., 1991; Shi and Cassell, 1998; McGeorge and Faull, 1988), and macaque (Mufson et al., 1981; Mufson and Mesulam, 1982; Mesulam and Mufson, 1982b; Mufson and Mesulam, 1984; Chikama et al., 1997; An et al., 1998; Öngür et al., 1998) connecting to various subcortical structures that are also associated to the insula in other species. Also, a seed placed in approximately the agranular portion of the insula connects to olfactory structures, such as the olfactory bulb, olfactory cortex, and the entorhinal cortex, which is consistent with the past literature (Mouse Connectome Project, Mesulam and Mufson, 1982b; Shi and Cassell, 1998).

Our data show some similarities to the claustral and insular connectivity patterns in the human brain as well. A human DTI study, in which selection of the seed regions were guided by microsurgical dissection of the claustrum and its surrounding fibers, suggests that the human claustrum is associated with a wide variety of cortical regions, including the prefrontal cortex, orbitofrontal cortex, temporal pole, parietal cortex, and occipital cortex (Fernández-Miranda et al., 2008). The human insula's structural connections with the entorhinal cortex, prefrontal cortex, premotor cortex, and parietal cortex, and the functional associations with the frontal cortex, cingulate cortex, supplementary motor area, parietal cortex, and visual cortex, are consistent with our findings (Taylor et al., 2009; Deen et al., 2010; Menon and Uddin, 2010; Uddin et al., 2010; Cerliani et al., 2011). However, these studies report the structure's connections with multiple regions not included in our results. This disagreement might be mostly due to the increased complexity of the human brain that may have enlarged the claustral and insular connections.

The results from the insular seed appear to contain a coherent system including the central tegmental tract, parabrachial nucleus, midbrain central grey, and the VPMpc of the thalamus. A tracer injection study in the macaque nucleus of the solitary tract (NST) revealed that the rostral NST projects to the VPMpc via the central tegmental tract, the caudal NTS connects to the parabrachial nucleus, midbrain central grey, and

ultimately the VPMpc, and the intermediate portion of the nucleus is associated with the VPMpc and the parabrachial nucleus (Beckstead et al., 1980). The connection to the NST seems to have been lost in our results, but the insular connections are present for all of the other structures in the system, and its association with the central tegmental tract is especially strong. In macaque monkeys, tracer injections have demonstrated that the agranular insula is reciprocally connected with the same part of the midbrain central grey that is associated with the insula in our study (An et al, 1998).

The tracer data from the mouse show that the insula is connected to the frontal cortex ventrally, while our tractography results suggest that insula and the prefrontal cortex are associated more dorsally in the *Microcebus*. This divergence may be due to the expansion of the dorsal and lateral frontal cortex in the primate brain, relative to non-primate mammalian brains (Khokhryakova, 1978; Fuster, 2008). Since the dorsal and lateral frontal cortices are relatively larger in the *Microcebus* than in rodents, it seems plausible that the insula might be more strongly connected to the dorsolateral frontal cortex in the *Microcebus* than in the mouse. A tracer injection study in the macaque, showing that connections exist between the insula and the dorsolateral frontal cortex in addition to the orbitofrontal cortex (Mesulam and Mufson, 1982b), supports this conclusion.

In addition, our data reflect differences in connectivity pattern between the granular and agranular insula, with the latter, unlike the former, connecting to olfactory structures. This is consistent with past tracer studies in the primate insula in which the agranular portion of the structure has been implicated in olfactory processing (Mesulam and Mufson, 1982b). While this could conceivably result from the seed's proximity to the olfactory cortex, the ventral insular seed does not connect to the portion of the anterior olfactory cortex directly adjacent to the insula (Figure 2.10, lower panel), thus supporting the interpretation that these tracts indeed represent the connectivity pattern of the agranular insula, rather than that of the olfactory cortex.

In our results, the region that was most probabilistically connected to the claustral

seeds was the entorhinal cortex. This cortical region has been of interest to those studying the neural mechanism of navigation and spatial memory, because it contains special classes of neurons that appear to process one's perceived location and direction of movement. For example, "border cells" encode the animal's location relative to local boundaries (Solstad et al., 2008), while "grid cells" represent one's position and, in some cases, direction within a field map composed of equilateral triangular grids anchored to external landmarks (Doeller et al., 2010; Hafting et al., 2005). In addition, "path cells" in the human entorhinal cortex encode whether one is headed clockwise or counterclockwise (Jacobs et al., 2010), whereas similar "path equivalent cells" found in rodents react to locations in different but similar – "equivalent" – trajectories (Frank et al., 2000). The frequent loss of visuo-spatial orientation in the early stages of Alzheimer's disease (AD) has been attributed to the degeneration of entorhinal cortex and hippocampus (Iachini et al., 2009). The portion of the human claustrum that is connected with the entorhinal cortex has been reported to show more severe AD pathology than the rest of the structure (Morys et al., 1996). This suggests that the claustrum contributes to the spatial function of the entorhinal cortex, and that the loss of spatial memory in AD may be due not only to degeneration of the entorhinal cortex and the hippocampus, but also to destruction of the integrating function of the claustrum. This is plausible, considering the claustrum's extensive connections with cortical areas and its implications in perception and consciousness.

Our data suggest that, despite the close juxtaposition between the claustrum and insula, the two structures have completely different connections. This is confirmed by the conventional tract tracer results in other species. In addition, tractography experiments in the adjacent putamen and olfactory cortex show that our insular and claustral results are more or less region-specific. The seeds in the putamen and the claustrum do seem to share some of their tracts, and although it is possible that this is due to the proximity of the two structures and the limited resolution of our image, we believe that the more likely cause may be the claustrum's robust connection to the putamen, making the tract originating from the putamen seed a natural part of

the claustral tract.

It is not yet clear if the claustrum and the insula are directly connected with each other. Associations between the two structures have been observed in the rat (Allen et al., 1991; Shi and Cassell, 1998; Behan and Haberly, 1999), mouse (Mouse Connectome Project), and the cat (Witter et al., 1988), via tracer injections into the insula. However, considering the close proximity between these regions, it is uncertain whether the labeling in the claustrum reflects a true connection between the two regions or merely the spread of the injections. A similar labeling was observed in the macaque, but was attributed to the spread of the tracer injected into the insula (Mufson and Mesulam, 1982). Meanwhile, direct injection into the claustrum has been avoided due to the sheet-like morphology of the structure, hence limiting the amount of available data. Although in our data the claustrum and the insula do appear connected to each other, the connection is quite weak and hence unable to offer a conclusive view.

Some aspects of our results are not consistent with the tracer studies. First, we find no connection between the insula and the amygdala, whereas previous studies indicate otherwise (Mouse Connectome Project; Allen et al., 1991; Shi and Cassell, 1998, Mufson et al., 1981). The lack of connection between the insula and amygdala in our results was confirmed by additional fiber tractography with six single-voxel seeds placed in the various nuclei at the basal portion of the amygdala (Figure 2.7, lower panel). The resulting tracts suggest that while these seeds do connect to the claustrum, they are not at all associated with the insula. In fact, the tracts entering the claustrum seem very selective, cleanly avoiding the insula. This difference might be anatomically valid, demonstrating the mouse lemur's inherent biological difference from the rodents and higher-level primates. It is also possible that this lack of connection is unique to the particular individual that was studied. Although it might also reveal a technical limitation of HARDI in this instance, it is worth noting that we did previously find a robust connection between the FI and amygdala in the gorilla using HARDI and probabilistic fiber tractography (Allman et al., 2010).

Second, our results, while showing connections to many of the regions known to be associated with the claustrum and the insula in other species, including small structures such as the parabrachial nucleus and zona incerta, in some parts fail to provide as much detail as the tracer studies can. For instance, whereas injecting tracers in the macaque insula demonstrated minuscule connections to many small thalamic nuclei (Mufson and Mesulam, 1984), our results are able to clearly show tracts to only three thalamic nuclei.

Third, as discussed in the Results section, while our data suggest the differences between the connectivity patterns of the granular and agranular insula, the results do not show much topographical fiber organizations within the claustrum. Many tracer studies have found the claustrum to be topographically organized (Dinopoulos et al., 1992; Fernández-Miranda et al., 2008; Kowianski et al., 1998; Norita, 1977; Olson and Graybiel, 1980; Pearson et al., 1982; Tanné-Gariépy et al., 2002), hence indicating that our results do not reflect the differential fiber organization that is likely to exist. While the limited resolution of our image might have caused this, strong connections within the claustrum – like the long-range connection found within the rat claustrum (Behan and Haberly, 1999; Smith and Alloway, 2010) – might also have influenced our results. Considering the integrative nature of the claustral function, intra-claustral associations are indeed plausible, and it seems possible that such connections, by unifying the claustrum into one unit, prevented our results from properly reflecting the topographical organization of the claustrum. However, our data do suggest that the ventral claustrum may be affiliated to a greater extent than does the dorsal claustrum with the olfactory bulb, olfactory cortex, and the entorhinal cortex. This is consistent with Striedter's argument that the ventral claustrum originates from the olfactory cortex (Striedter 1997).

Despite these inconsistencies, our experimental approach has demonstrated that, at a very high resolution, HARDI and probabilistic fiber tractography can achieve results that are comparable with those from tracer injection studies. Besides the high spatial and angular resolutions of our image, the most significant aspect of the present study

is that, thanks to the high quality of the image, we were able to obtain detailed results using single-voxel seeds, placed in the grey matter. This emulates the conventional tract tracing method, and is in stark contrast to most previous studies using diffusion imaging and fiber tractography, in which all voxels in a region have to be used as seeds, or seeds had to be placed in the white matter in order to acquire viable results. Our method may raise concerns, though, as only one or two voxels were used to represent the entire claustrum and insula. We have dealt with these concerns by repeating tractography in other parts of the structures and verifying that, in our specific dataset, the seeds that we have used yield the tracts that sufficiently represent the regions. The fact that our results are largely consistent with the results of tracer injection studies also suggests that our single-voxel seeding method is viable.

HARDI and probabilistic fiber tractography has the advantages that they are non-destructive; require no surgical interventions; and the connection of each and every voxel can be mapped with full knowledge of the anatomical context, whereas in conventional tractography only a few specific tracer injection sites can be assayed. Also, the brain can be sectioned computationally into any desired plane for analysis. Although the diffusion fiber tractography results are bidirectional and cannot determine whether a connection is afferent or efferent, and currently available diffusion images obviously do not have the fine resolution of conventional tract tracing, this method will still be helpful in extending the study of axonal fiber connectivity to the animals that are rare, cannot be investigated through injections of track tracers, and can only be accessed post-mortem. The method also has potential applications to high-resolution studies of connectivity in fixed human brain tissue.

2.6   Acknowledgments

This study was conducted in collaboration with Dr. Mike Tyszka and Professor John Allman. We wish to thank Dr. Russell Jacobs of the Beckman Institute at California Institute of Technology for providing the *Microcebus* brains, and Dr. Jason Kaufman

for helping process the imaging data. This study was supported by the James S. McDonnell Foundation.

Table 2.1: Comparison of claustral connectivity in the cat and the *Microcebus*. The leftmost column and the bottom row of the table both present the comprehensive list of all regions connected with the claustrum in at least one of the two species. While the column highlights in blue the regions associated with the *Microcebus* claustrum, the row highlights in yellow the structures shown to connect with the claustrum in cat tracer studies. The red squares mark the structures that are connected to the claustrum in both species. Studies cited: [1]Norita (1977); [2]Olson and Graybiel (1980); [3]Witter et al. (1988). Abbreviations: SMA, supplementary motor area.

Microcebus DTI \ Monkeys	Amygdala, lateral[6]	Anterior olfactory nucleus	Caudate[4]	Cingulate cortex[1,3]	Entorhinal cortex[1,5]	Globus pallidus	Insular cortex	Motor cortex[2,7]	Olfactory bulb	Olfactory cortex[1]	Olfactory tubercle	Orbitofrontal cortex[1,2]	Parietal cortex[1,2]	Perirhinal cortex	Prefrontal cortex (area 8)[1]	Premotor cortex/SMA (area 6)[2,7]	Putamen	Septum pellucidum	Somatosensory cortex[2]	Temporal cortex[1,2]	Visual cortex[2]	Zona incerta
Amygdala, lateral	■																					
Anterior olfactory nucleus																						
Caudate			■																			
Cingulate cortex				■																		
Entorhinal cortex					■																	
Globus pallidus																						
Insular cortex																						
Motor cortex								■														
Olfactory bulb																						
Olfactory cortex										■												
Olfactory tubercle																						
Orbitofrontal cortex												■										
Parietal cortex													■									
Perirhinal cortex																						
Prefrontal cortex (area 8)															■							
Premotor cortex/SMA (area 6)																■						
Putamen																						
Septum pellucidum																						
Somatosensory cortex																			■			
Temporal cortex																				■		
Visual cortex																					■	
Zona incerta																						

Table 2.2: Comparison of claustral connectivity in the rhesus macaque (*Macaca mulatta*), the common squirrel monkey (*Saimiri sciureus*), and the *Microcebus*.
The configuration is the same as that of Table 2.1. Studies cited: [1]Mufson and Mesulam (1982), macaque; [2]Pearson et al. (1982), macaque; [3]Jürgens (1983), squirrel monkey; [4]Arikuni and Kubota (1985), macaque; [5]Insausti et al. (1987), macaque; [6]Amaral and Insausti (1992), macaque; [7]Tanné-Gariépy et al. (2002), macaque. Abbreviations: SMA, supplementary motor area.

Rat \ Microcebus DTI	Amygdala[1,2]	Caudate[3]	CM of thalamus[2]	Cingulate cortex[2]	Claustrum[1,2]	Diagonal band	DLPFC	DMPFC	Entorhinal cortex[2]	Globus pallidus	Infralimbic area[2]	Lateral hypothalamus[1,2]	MD of thalamus[1,2]	Midbrain central grey	Motor cortex	Nucleus accumbens[3]	Olfactory bulb	Olfactory cortex[2]	Olfactory tubercle[2]	Orbital cortex[2]	Parabrachial nucleus[1]	Parietal cortex	Perirhinal cortex[2]	Prelimbic cortex[2]	Putamen[2]	PVN of thalamus[2]	R of thalamus[1]	Septum pellucidum	Somatosensory cortex[2]	Substantia innominata	Substantia nigra	Temporal cortex	Ventral PF of thalamus[2]	Visual cortex	VPL/VPLpc of thalamus[1,2]	VPM/VPMpc of thalamus[1,2]	Zona incerta
Amygdala																																					
Caudate		■																																			
CM of thalamus																																					
Cingulate cortex				■																																	
Claustrum					■																																
Diagonal band																																					
DLPFC																																					
DMPFC																																					
Entorhinal cortex									■																												
Globus pallidus																																					
Infralimbic area											■																										
Lateral hypothalamus												■																									
MD of thalamus																																					
Midbrain central grey																																					
Motor cortex																																					
Nucleus accumbens																■																					
Olfactory bulb																																					
Olfactory cortex																		■																			
Olfactory tubercle																			■																		
Orbital cortex																				■																	
Parabrachial nucleus																					■																
Parietal cortex																																					
Perirhinal cortex																							■														
Prelimbic cortex																								■													
Putamen																									■												
PVN of thalamus																																					
R of thalamus																											■										
Septum pellucidum																																					
Somatosensory cortex																													■								
Substantia innominata																																					
Substantia nigra																																					
Temporal cortex																																					
Ventral PF of thalamus																																					
Visual cortex																																					
VPL/VPLpc of thalamus																																			■		
VPM/VPMpc of thalamus																																				■	
Zona incerta																																					

Table 2.3: Comparison of insular connectivity in the rat and the *Microcebus*. The configuration is the same as that of Tables 2.1 and 2.2. Note that since the *Microcebus* anteroventral cingulate cortex appears to be the homolog of the rat infralimbic and prelimbic cortices, the rat infralimbic and prelimbic connections were treated as cingulate connections as well. Studies cited: [1]Allen et al. (1991); [2]Shi and Cassell (1998); [3]McGeorge and Faull (1989). Abbreviations: CM, centralmedialnucleus; DLPFC, dorsolateralprefrontalcortex; DMPFC, dorsomedialprefrontalcortex; MD, medialdorsalnucleus; PF, parafascicular nucleus; PVN, paraventricular nucleus; R, reticular nucleus; VPL, ventral posterolateral nucleus; VPLpc, ventral posterolateral nucleus, parvocellular part; VPM, ventral posteromedial nucleus; VPMpc, ventral posteromedial nucleus, parvocellular part.

Comparison matrix — rows (Mouse) and columns (Microcebus DTI): Amygdala, Bed nucleus, Caudate, Cingulate cortex, Claustrum, Diagonal band, DLPFC, DMPFC, Dorsal peduncular area, Entorhinal cortex, Globus pallidus, Infralimbic area, Lateral hypothalamus, Midbrain central grey, Midline thalamus, Motor cortex, Nucleus accumbens, Olfactory bulb, Olfactory cortex, Olfactory tubercle, Orbital cortex, Parabrachial nucleus, Parietal cortex, Perirhinal cortex, Prelimbic cortex, Putamen, PVT of hypothalamus, R of thalamus, Septum pellucidum, Somatosensory cortex, Substantia innominata, Substantia nigra, Temporal cortex, Visual cortex, VPL/VPLpc of thalamus, VPM/VPMpc of thalamus, Zona incerta.

Filled (red) cells:
- Cingulate cortex × Cingulate cortex
- Diagonal band × Diagonal band
- Entorhinal cortex × Entorhinal cortex
- Infralimbic area × Infralimbic area
- Lateral hypothalamus × Lateral hypothalamus
- Midbrain central grey × Midbrain central grey
- Nucleus accumbens × Nucleus accumbens
- Olfactory bulb × Olfactory bulb
- Olfactory cortex × Olfactory cortex
- Orbital cortex × Orbital cortex
- Parabrachial nucleus × Parabrachial nucleus
- Putamen × Putamen
- Septum pellucidum × Septum pellucidum
- Substantia innominata × Substantia innominata
- VPM/VPMpc of thalamus × VPM/VPMpc of thalamus
- Zona incerta × Zona incerta

Table 2.4: Comparison of insular connectivity in the mouse and the *Microcebus*. The configuration is the same as that of Tables 2.1, 2.2, and 2.3. Note that since the *Microcebus* anteroventral cingulate cortex appears to be the homolog of the mouse infralimbic cortex, the mouse infralimbic connection was treated as both infralimbic and cingulate. All mouse data from the Mouse Connectome Project, www.mouseconnectome.org. Abbreviations: DLPFC, dorsolateral prefrontal cortex; DMPFC, dorsomedial prefrontal cortex; R, reticular nucleus; VPL, ventral posterolateral nucleus; VPLpc, ventral posterolateral nucleus, parvocellular part; VPMpc, ventral posteromedial nucleus, parvocellular part. Also, the "midline thalamus" consists of reuniens, medial part of mediodorsal nucleus, paraventricular nucleus, and intermediodorsal nucleus.

Table comparing insular connectivity — matrix of brain regions (Macaque rows vs. Microcebus DTI columns). Filled (red) cells lie along the diagonal, matching each row region to its corresponding column region:

Row regions (top to bottom): Amygdala, Caudate, Cingulate cortex, Claustrum, Diagonal band, DLPFC, DMPFC, Entorhinal cortex, Globus pallidus, Lateral hypothalamus, Limitans, MD of thalamus, MG/MGpc of thalamus, Midbrain central grey, Motor cortex, MVL of thalamus, Nucleus accumbens, Olfactory bulb, Olfactory cortex, Olfactory tubercle, Orbitofrontal cortex, OVL of thalamus, Parabrachial nucleus, Parietal cortex, Perirhinal cortex, PF of thalamus, Premotor cortex, Pulvinar, Putamen, R of thalamus, Reuniens, Septum pellucidum, Somatosensory cortex, Substantia innominata, Substantia nigra, Suprageniculate nucleus, Temporal cortex, Visual cortex, VPL/VPLpc of thalamus, VPM/VPMpc of thalamus, Zona incerta.

Column headers (Microcebus DTI / Macaque): Amygdala[1], Caudate[5], Cingulate cortex[23], Claustrum, Diagonal band, DLPFC[23], DMPFC, Entorhinal cortex[2], Globus pallidus, Lateral hypothalamus, Limitans[4], MD of thalamus[4], MG/MGpc of thalamus[4], Midbrain central grey[6], Motor cortex[4], MVL of thalamus[4], Nucleus accumbens[5], Olfactory bulb, Olfactory cortex[23], Olfactory tubercle, Orbitofrontal cortex[23], OVL of thalamus[4], Parabrachial nucleus, Parietal cortex[23], Perirhinal cortex[23], PF of thalamus[4], Premotor cortex[23], Pulvinar[4], Putamen[5], R of thalamus[4], Reuniens[4], Septum pellucidum, Somatosensory cortex[23], Substantia innominata, Substantia nigra, Suprageniculate nucleus[4], Temporal cortex[23], Visual cortex, VPM/VPMpc of thalamus[4], VPL of thalamus[4], Zona incerta[4].

Filled cells (diagonal matches): Caudate, Cingulate cortex, DLPFC, Entorhinal cortex, Midbrain central grey, Motor cortex, Nucleus accumbens, Olfactory cortex, Orbitofrontal cortex, Parietal cortex, Perirhinal cortex, Putamen, R of thalamus, Somatosensory cortex, Temporal cortex, VPL/VPLpc of thalamus, VPM/VPMpc of thalamus, Zona incerta.

Table 2.5: Comparison of insular connectivity in the rhesus macaque (*Macaca mulatta*) and the *Microcebus*.

The configuration is the same as that of Tables 2.1, 2.2, 2.3, and 2.4. Studies cited: [1]Mufson et al. (1981); [2]Mufson and Mesulam (1982); [3]Mesulam and Mufson (1982b); [4]Mufson and Mesulam (1984); [5]Chikama et al. (1997); [6]An et al. (1998); [7]Öngür et al. (1998). Abbreviations: DLPFC, dorsolateral prefrontal cortex; DMPFC, dorsomedial prefrontal cortex; MD, medial dorsal nucleus; MG, medial geniculate nucleus; MGpc, medial geniculate nucleus, parvocelluar part; MVL, medial division of ventral lateral nucleus; OVL, oral divison of ventral lateral nucleus; PF, parafascicular nucleus; R, reticular nucleus; VPL, ventral posterolateral nucleus; VPLpc, ventral posterolateral nucleus, parvocellular part; VPM, ventral posteromedial nucleus; VPMpc, ventral posteromedial nucleus, parvocellular part.

Chapter 3

Neural Processing of Olfactory Hedonic Values

3.1 Abstract

The ability to evaluate odors, especially to judge their hedonic values — pleasantness and unpleasantness — are crucial to one's quality of life and even survival. Smell, when combined with odor, helps create flavor, which is central to one's eating experience, and inability to accurately judge olfactory hedonic values can result in dangerous actions, such as ingestion or inhalation of harmful materials. Despite such importance of olfactory hedonic evaluation, and despite the fact that this function is often disrupted in a number of psychiatric disorders and cause further deterioration of patients, the neural process in which this function occurs is not very well established.

This study attempts to improve our understanding of the olfactory hedonic evaluation process by creating a rich set of neural and behavioral data generated by 33 human participants making smell judgments in the MRI scanner. Based on a hypothesis that the FI would play a central role in hedonic value evaluation, a large number of odorants, systematically selected, were utilized as stimuli, and a variety of models were employed to explore the neural signals generated in response to odors of different hedonic values. The results suggest a pattern of laterality of the FI, in which the right

FI is more sensitive to unpleasantness of odors while the left FI responds better to pleasant ones. Another dichotomous arrangement, in which the medial FI tracks the magnitude of olfactory hedonic values while the lateral FI tracks the valence, is also suggested. The OFC also appears to be involved in tracking hedonic value magnitude, but not valence. This study has generated a very large set of data, some of which remains to be evaluated, and we hope that further work into these data will help validate this observation.

3.2   Introduction

The purpose of the study discussed in this chapter is to investigate the mechanism in which the human brain computes the hedonic values – the degree of pleasantness, ranging from sheer disgust to absolute pleasure – of odors. We seek to systematically approach this goal, using multiple odorants represented throughout a potential human olfactory perception space, a calibrated olfactometer, and measurement of human brain activity through the use of fMRI.

In addition to investigating the potentially crucial role of the AI in olfactory processing that was discussed in Chapter 1, the great importance of olfactory hedonic evaluation in clinical neuroscience motivated our study. Many clinical studies have implicated disturbance of olfactory functions in neurological and psychological disorders, with olfactory impairments predicting the emergence of degenerative symptoms in Alzheimer's and Parkinson's diseases, and the increased risk of death from all causes (Hummel et al. 2010; Wilson et al. 2009; 2011a; 2011b). The evaluation of hedonic values in odors appears especially affected: patients with schizophrenia or depression exhibit olfactory anhedonia (Plailly et al. 2006; Atanasova et al. 2008; Atanasova et al. 2010), and individuals with obsessive-compulsive disorder tend to be more sensitive to unpleasant odors than those without (Husted et al. 2003), while those with Parkinson's disease or Huntington's disease appear impaired in feeling olfactory disgust (Hayes et al. 2006; Hummel et al. 2010), and frontotemporal lobar

degeneration patients exhibit changes in food preference that suggest reduction in olfactory disgust (Whitwell et al. 2007; Woolley et al. 2007). These findings indicate the importance of olfactory hedonic evaluation in these disorders, and motivate us to investigate the underlying mechanism.

Olfactory hedonic evaluation also plays an important role in one's quality of life, and even survival. As pointed out originally by Jean Anthelme Brillat-Savarin in his 1825 book *The Physiology of Taste*, and later reiterated in Gordon Shepherd's *Neurogastronomy*, retronasal smell – the odor of chewed food that travels from the back of the mouth into the nasal cavity via exhaling – is a major component of flavor perception. Hence impairment in olfactory hedonic evaluation may significantly lower one's interest in food and diet, and reduce the quality of life. This poses especially high risks for the elderly, in whom impaired olfaction is very common. Moreover, the perceived hedonic values of odors greatly influence one's everyday decision-making and sense of well-being, as evidenced by the prevalent use of pleasant odors in product marketing and the existence of the huge fragrance industry devoted to this purpose. In addition, unpleasant odors are typically produced by hazardous substances such as toxic chemicals and sources of bacterial infection (contaminated food, for instance) that may threaten the life of the individual. Therefore the ability to perceive and assess the hedonic qualities of odors is crucial in survival.

A small number of functional imaging studies have in fact explored the neural activities that occur during judgment of olfactory hedonic values. While some of these studies suggest that the OFC is strongly involved in representing pleasantness of odors and the insula is involved in representing unpleasantness (Royet et al. 2003; Grabenhorst et al. 2007; Grabenhorst and Rolls 2009), others present different results (Fulbright et al. 1998; Katata et al. 2009), and to the best of our knowledge there is not a strong general consensus on which regions compute olfactory hedonic values. This is not surprising, considering that these studies used only five or fewer different odor stimuli that were chosen rather arbitrarily (Fulbright et al. 1998; Grabenhorst et al. 2007; Grabenhorst and Rolls 2009; Katata et al. 2009), or relied simply on

the direction of the perceived hedonic valence (pleasant or unpleasant) instead of taking into account the magnitude of the experienced hedonic values (how pleasant or how unpleasant, on a scale of -5 or +5, for example) (Royet et al. 2003). Hence it seemed that conducting a study that involves a relatively large number of odorants that are systematically selected, as well as a parametric analysis of neural data using quantitative measures of odor hedonic values, would help provide more concrete and complete results. The present study aimed to employ both of these strategies.

To address the issue of disorganized selection of a small number of odorants, we selected a relatively large number — 24 — of odorants in a systematic manner to represent the range of a possible human olfactory perception space proposed by a recent computational study (Koulakov et al. 2011). A graphical representation of this putative space is shown in Figure 4.1. It has been derived from a standardized database containing 146-dimensional descriptions of 144 odorants by 140 highly trained odor evaluators (Dravnieks 1985). Using a principal component analysis — a statistical method which identifies the variables that describe the variance of the data most effectively (principal components), hence reducing the dimensionality of the dataset — Koulakov et al. collapsed the 146-dimensional data into an approximately two-dimensional map that illustrates the nature of human odor perception. The two dimensions represented in this map are a) the odor's hedonic quality, which is negatively correlated with the molecular weight of the odorant, and b) the affinity of the odor molecule to water, which makes it smell more "chemical" and "medicinal" or, at the other extreme, "burnt" and "moldy." Along the main (hedonic) dimension of this map, the odors near the north pole signal substances that are potentially harmful to eat due to contamination with pathogenic micro-organisms, while those near the south pole signal substances that are safe and nutritious to eat, like ripe fruit. This is consistent with the crucial role of olfaction and hedonic judgment in health and survival. This map represents olfactory hedonicity as a gradient in which a range of hedonic values is possible, rather than an all-or-nothing system where an odor is judged as only either pleasant or unpleasant. This gradient representation accurately

SICKENING
PUTRID, FOUL, DECAYED
RANCID
SWEATY
SHARP, PUNGENT, ACID
HEAVY
MUSTY, EARTHY, MOLDY
BURNT, SMOKY
OILY, FATTY
SOUR, VINEGAR

Elevation

ETHERISH, ANAESTHETIC
CHEMICAL
MEDICINAL
DISINFECTANT, CARBOLIC
SHARP, PUNGENT, ACID
GASOLINE, SOLVENT
COOL, COOLING
CLEANING FLUID
PAINT
CAMPHOR

BURNT, SMOKY
NUTTY (WALNUT ETC)
WOODY, RESINOUS
MUSTY, EARTHY, MOLDY
ALMOND
POPCORN
PEANUT BUTTER
OILY, FATTY
WARM
DRY, POWDERY

Azimuth

FRAGRANT
SWEET
PERFUMERY
FLORAL
LIGHT
FRUITY, OTHER THAN CITRUS
AROMATIC
COOL, COOLING
FRUITY, CITRUS
ROSE

Figure 3.1: Illustration of the approximately 2-dimensional putative human olfactory perception space.
The elevation (ranging from putrid to fragrant) and azimuth (ranging from medicinal/chemical to smoky/earthy) are the two axes of this space. The odor qualities that contribute to large elevation/azimuth coefficients are listed. Adapted from Koulakov et al. 2011.

reflects the reality in which multiple odors can vary in terms of the degree of pleasantness, and a single odor can even be assigned different hedonic values depending on the context in which it is perceived. The use of Dravnieks' extensive and comprehensive database and the olfactory space derived by Koulakov et al. provided a method of systematically selecting the odors to be used as stimuli in the experiment, as they were based on standard profiles of a large number of odors, logically organized by a computational method. I expected that this would help the results of the present study establish a more complete picture than the previous studies have on olfactory hedonic value computation.

Topographic organization of the brain's olfactory perception mechanism according to odor hedonicity, to the best of our knowledge, has not been shown in the mammalian

olfactory system. Odor molecules are detected initially by olfactory sensory neurons (OSNs) in the nasal mucosa, which relay the information to the olfactory bulb. While the OSNs are randomly scattered in the nasal mucosa, the olfactory bulb exhibits a neat spatial organization in which two glomeruli receive inputs from all the OSNs that have the same odorant receptors, and the location of each glomerulus is roughly the same across different individuals. However, this spatial organization disappears as the odorant information is relayed to the olfactory cortex, the main site of higher-level odor processing (Buck 2005; Sosulski et al. 2011).

Despite the lack of spatial organization in the olfactory cortex, however, it seems likely that some form of organization is present in other higher-level neural structures involved in odor processing, as there are strong evolutionary pressures arising from the need for efficient neuronal wiring that favor the formation of functional maps in the brain (Allman 2000; Chklovskii and Koulakov 2004). Therefore it appears that one or more topographically organized, hedonicity-based maps that correspond to Koulakov et al.'s olfactory perceptual space might exist in higher-level olfactory areas, and that given the importance of olfactory hedonicity in survival-related decisions, such organization, if present, might represent one of the main decision mechanisms in the human brain. It is probable that these maps do not exist in the lower olfactory centers, as they are not directly coupled to behavioral decisions.

Based on the evidence presented earlier in Chapter 1, we hypothesized that the AI would be one of the main regions containing the olfactory hedonic map. In addition, we expected to see the OFC to participate in processing the hedonic values of olfactory stimuli. A small number of studies implicate the OFC as one of the centers of hedonic evaluation of odors, given its activity during detection of pleasant odors (Royet et al. 2003; Grabenhorst et al. 2007; Grabenhorst and Rolls 2009). In addition, this structure is heavily involved in hedonic evaluation in other reward modalities such as food (Small et al. 2001; Gottfried et al. 2003), visual beauty (O'Doherty et al. 2003), and monetary gain or loss (O'Doherty et al. 2001), thus suggesting that it computes the hedonic values of the individual's general environment, regardless of the

modality. Given this information, it seems possible that AI and the OFC work closely together to mediate olfactory hedonic judgments, either complementing each other as suggested by past studies (with the AI computing the degree of unpleasantness and the OFC computing the degree of pleasantness), or one structure relaying information to the other for further processing and representation (for example, the AI computing hedonic values specific to the olfactory domain, and relaying it to the OFC where the information becomes combined with other hedonic values in the environment to form the general hedonic state of the individual).

To test the above hypothesis, we provided human participants with olfactory stimuli and measured the brain-oxygenation-level dependent (BOLD) signals using the fMRI technique while the stimuli were being implicitly or explicitly judged. Utilization of a larger number of odorants, systematic, educated selection of odorants, and parametric analysis of the imaging data were used to ameliorate the methodological shortcomings of past imaging studies on olfactory hedonicity.

3.3 Materials and Methods

3.3.1 Participants

34 (16 female, 18 male) healthy volunteers participated in this study. These participants were recruited from the subject pool of a long-term behavioral and neuroimaging project at Caltech, for which they had been screened for any significant neurological, psychological, and other health issues. For the purpose of the present study, the participants were also screened for anosmia using the Brief Smell Identification Test (Doty, 1996). Out of these 34 participants, 1 male participant, previously flagged for a history of depression, exhibited anhedonic behavior towards the odor stimuli, as well as scored as "mildly depressed" on the Beck Depression Inventory-II (Beck et al. 1996) and showed flat affect in general in his interactions with the researchers. This

	Age	IQ	Approx. Education Length	Mean Odor Intensity Rating	Gender
Group Mean	30.15	108.70	15.18	4.81	16 Women
Standard Dev.	5.39	10.79	1.51	0.78	
Median	29	107	16	4.90	17 Men
Range	21 - 40	90 - 132	12 - 21	1 - 7	

Table 3.1: A general profile of the participant pool.

To compute the numbers in the "Mean Odor Intensity Rating" column, all intensity ratings of each subject for non-blank odors presented during the scan session were averaged. These values, which act as a proxy for individual subjects' olfactory sensitivity, were pooled together across subjects, and the group mean, standard deviation, median, and range of these values were calculated.

led to the exclusion of this participant, hence reducing the actual number of subjects for this study to 33. The general profile of these 33 participants is shown in Table 3.1.

The experimental protocol described below has been reviewed and approved by Caltech's Institutional Review Board.

3.3.2 Olfactory Stimuli

The odorants used in this study were selected from the Atlas of Odor Character Profiles (Dravnieks, 1985) based on the following criteria:

1. The odorant must be strongly associated with only one or two descriptors - that is, given the odorant, one must be able to grasp the characteristic of the odor almost immediately and without ambiguity, and there must be a consensus among multiple people on said characteristic

2. The descriptor(s) of the odorant must be lie at one of the four extremes of the quasi-two-dimensional olfactory perception map discussed above

3. The odorant must not be harmful for human use

This selection process yielded the following 24 odorants. The odorants were purchased from laboratory supply providers or essential oil manufacturers, and diluted in mineral oil or propylene glycol (both are odorless solvents not harmful to humans at low levels of exposure) depending on their solubility profiles. The concentrations to which the odorants were diluted were determined empirically: all odorants were initially diluted to 5% solutions by volume (with exception of 6-methyl-1,2,3,4-tetrahydroquinoline, which is a solid at room temperature and hence whose diluted concentrations were calculated by mass), tested on the author for intensity, and increased or decreased in concentration such that the author could easily perceive all of the odors, without finding them overpowering. Here, note that the author was chosen as a random, healthy subject to test all odor concentrations on behalf of the participants, as it is very difficult to standardize odor intensity across all participants, unless all participants are carefully screened to all have similar olfactory sensitivity levels.

The odorants chosen for this study, their suppliers, solvents used, and final concentrations are listed in Table 3.2.

3.3.3   Odor Delivery System

The odor stimuli were delivered to participants using an OLFACT-fMRI^{TM}unit (Osmic Enterprises, Inc., Cincinnati, OH). This unit consists on two major parts: a main controller that houses the electronic circuits, valves, an air pump, and pressure gauges; and a metal-free odorant box, consisting entirely of plastic and glass, that carries eight vials containing odorant solutions. The two parts are connected to each other via a bundle of Tygon® tubing, which each strand of tubing connecting a valve in the controller with its corresponding vial in the odorant box. While the former stays outside of the scanning room, the latter is MR-safe and sits on participant's chest during the experiment. The odorant box is smaller than the average adult torso (approximately 26 cm x 35 cm x 11 cm), is light (approximately 1.15 kg), and its surface that touches subject's body is padded with sponge for participant's comfort.

Odorant	Descriptor(s)	Supplier	Solvent used	Concentration
2-Ehtyl pyrazine	Peanut butter	Sigma	Mineral oil	5%
2,5-Dimethylpyrazine	Etherish, anaesthetic	Sigma	Mineral oil	10%
6-isopropylquinoline	Musty, earthy, moldy	MP Biochemicals	Mineral oil	10%
6-methyl-1,2,3,4-tetrahydroquinoline	Mothballs	TCI Chemicals	Dipropylene glycol	10% by mass
Anethole	Anise (licorice)	Sigma	Mineral oil	10%
Benzaldehyde	Almond	Sigma	Mineral oil	5%
Cedarwood oil	Woody, cedarwood	Eden's Garden	Mineral oil	20%
Cinnamon bark oil (Ceylon)	Cinnamon	Eden's Garden	Mineral oil	5%
Clove oil	Clove-like	Eden's Garden	Mineral oil	5%
Ethyl 3-methyl-3-phenyl glycidate	Sweet, fruity, fragrant	Sigma	Mineral oil	10%
Ethyl octanoate	Soapy	Sigma	Mineral oil	10%
Eucalyptus oil	Eucalyptus	Eden's Garden	Mineral oil	5%
Gamma-nonalactone	Coconut	Sigma	Mineral oil	10%
Garlic oil	Garlic	Eden's Garden	Mineral oil	0.1%
Guiacol	Burnt, smoky	Sigma	Mineral oil	5%
Hexanoic acid	Sour, acid, sweaty, rancid	Sigma	Mineral oil	5%
Isoamyl acetate	Banana	Sigma	Mineral oil	5%
Litsea oil	Fruity (citrus), lemon	Eden's Garden	Mineral oil	5%
Methyl thiobutyrate	Sickening, putrid	Sigma	Mineral oil	1%
Perfume "Charlie" by Revlon	Perfumery, fragrant	Revlon	Mineral oil	5%
Phenylethyl alcohol	Floral, rose, fragrant	Sigma	Dipropylene glycol	20%
Spearmint oil	Minty, spearmint, peppermint	Eden's Garden	Mineral oil	5%
Tetrahydro thiophene	Sickening, sharp, pungent	Sigma	Mineral oil	0.1%
Vanilla oil	Vanilla, sweet, chocolate	Eden's Garden	Mineral oil	5%

Table 3.2: List of odorants used, their descriptors, suppliers, solvents used, and concentrations.

Figure 3.2: The Olfactometer Setup.
Shown in the upper panel is the general setup of the olfactometer, modeled on a subject situated in a mock scanner. The main controller unit (shown on the right in a blue and gray casing) is connected to the odorant box on the subject's chest. The lower panel shows the odorant box placed on the subject's chest. A plastic tubing emerging from the box is fixed onto the head coil and aimed at the subject's nostrils from about an inch away.

In fact, all of the participants reported that they felt comfortable with the placement of the odorant box. The unit, modeled on a subject, is shown in Figure 3.2.

For the present experiment, a script written in MATLAB® and executed on a Macintosh laptop (OS X 10.9) was used to operate and control the olfactometer. Once the script executed a command to either open or close one of the valves in the olfactometer, the signal was transmitted from the laptop to a data acquisition (DAQ) module (model USB-1208FS, Measurement Computing Corporation, Norton, MA), which in turn sent the digital signal to the olfactometer main controller's circuit, causing the valve of interest to open or close.

During the entirety of each scan the air pump connected to the olfactometer's controller was active and pumping air into the unit. When a valve was opened, the air was passed through the open valve and through the tubing connecting the valve with

the corresponding vial in the odorant box on participant's chest. The air then was pumped into the vial and mixed with the odor-carrying air in the vial's headspace. This created a puff of odor-infused air that was subsequently pumped out of the vial and into a one-foot-long Tygon® tubing whose end was aimed at participant's nostrils from about one inch away. When the script executed a command to close the valve, it simultaneously opened and passed all air through a makeup valve not associated with any of the odorant vials. The air going through the makeup valve bypassed all vials and delivered non-odor-carrying, clean air to participant's nose. Therefore, throughout the entire scan, participants experienced a constant, gentle flow of air, which occasionally carried odors according to the experiment protocol. Unlike other commercially available olfactometers, our model did not humidify the air. This provided advantage of preventing any mold from growing in the tubing, but also posed a small risk of drying out participant's nasal passage and causing discomfort. To overcome this issue, saline nasal sprays were made available to all participants, and those who used the sprays reported finding it helpful in maintaining nasal comfort.

As mentioned earlier each odorant box carries eight vials of odorant, and because we wished to use 24 different odors for this study, three odorant boxes were used. Prior to each scan, the 24 odorants were divided into two groups (roughly pleasant and roughly unpleasant) using the author's subjective criteria (which may or may not match the participants' personal criteria, since olfactory preferences differ rather widely among people), and a MATLAB® script was used to randomly select four odorants out of each group to be included in one of the three odorant boxes, hence assigning to each box a group of four pleasant and four unpleasant odorants. The odorant-solution-containing vials were then manually loaded into the odorant boxes according to the output of the script.

3.3.4 Experiment Protocol

The experimental procedure was divided into three main portions:

Session	Image Type	Approx. Length
Session 1	Localizer	10 seconds
	B0 Fieldmap	2 minutes
	Functional - Passive Run	5 minutes
	Functional - Active Run	10 minutes
	Anatomical - T1	5 minutes
Break/Odorant Set Switch		
Session 2	Localizer	10 seconds
	B0 Fieldmap	2 minutes
	Functional - Passive Run	5 minutes
	Functional - Active Run	10 minutes
	Anatomical - T1	5 minutes
Break/Odorant Set Switch		
Session 3	Localizer	10 seconds
	B0 Fieldmap	2 minutes
	Functional - Passive Run	5 minutes
	Functional - Active Run	10 minutes
	Anatomical - T2	1 minute

Table 3.3: Structure of the scanning portion of the experimental procedure.

1. a 90-minute MR scan with olfactory tasks consisting of three sessions, with two breaks in between sessions

2. a 30-to-40-minute post-scan break, during which participants were asked to fill out various questionnaires

3. a 45-minute out-of-scanner olfactory task

The first portion was structured as shown in Table 3.3. The scan was divided into three sessions to accommodate the three separate odorant boxes: each box was used in each session, and the boxes were switched during the break instituted in between sessions. Since the boxes were placed upon participant's chest, she/he was required to be pulled out of the scanner during each break/odorant box switch. Because many participants requested to re-adjust their positions during these breaks, localizer and B0 fieldmap scans were performed for each session to ensure accurate positioning and unwarping of the subsequently acquired images.

Participants were asked to complete olfactory tasks during both the passive and active runs of the functional scan. For the passive run, the task involved passively smelling an odor dispensed by the olfactometer for nine seconds, without explicitly thinking about any specific qualities of the odor. On the other hand, the corresponding active run asked participants to rate the hedonic value and intensity value of the same set of odor, upon being presented with the same set of odors for the same amount of time.

Each functional run of the scan was accompanied by a visual presentation constructed and executed with Psychtoolbox Version 3.0.12 (Figure 3.3). For both passive and active runs, each trial began with a five-second visual countdown signaling the imminent odor release. Participants were asked to prepare themselves during this countdown by adjusting their breathing pattern, such that they were beginning to inhale at the end of the countdown window. This was to help ensure that participants inhaled, and hopefully perceived, at least some of the odor that was subsequently being released, rather than missing the odor due to exhalation. After the countdown, an odor was continuously released by the olfactometer for nine seconds, during which participants were presented with a visual cue, "Odor is being released." Participants had been instructed to relax and breathe as naturally as possible, and refrain from sniffing, during this time.

During a passive run, the trial ended after the odor release, and a new trial began following an inter-trial interval whose length was selected randomly between zero - three seconds. On the other hand, during an active run, the odor release window was followed, one second later, by a rating screen for the hedonic value of the odor, with the question, "How pleasant was the odor?" Participants were given five seconds to enter the rating, and the rating screen was replaced with a fixation screen if the rating was entered before the five-second deadline, while a negative feedback screen that said, "You missed the rating!" was presented if no rating was entered within five seconds, to discourage participants from missing any more ratings. After a one-second gap, participants were presented with a screen for rating the intensity value of the odor, with the question, "How strong was the odor?" The timeline of this rating was
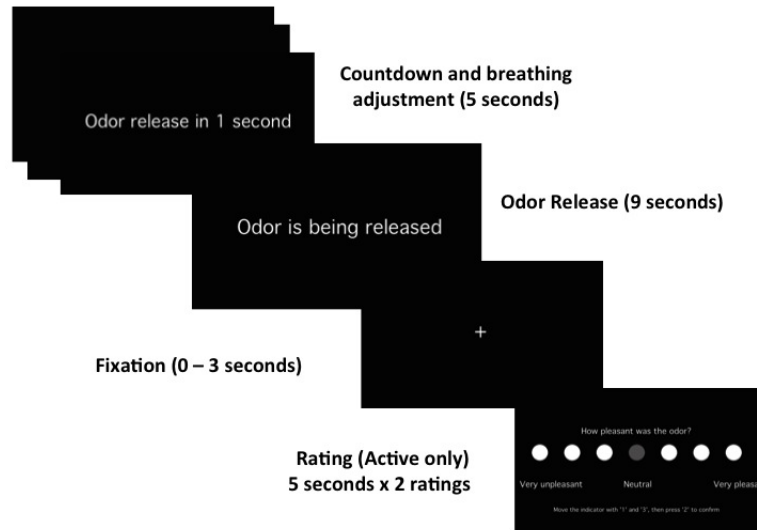
Figure 3.3: Visual Cues for Each Trial.

identical to that of the hedonic value rating.

Each rating was collected on a seven-point Likert scale. For the hedonic value rating, the leftmost end of the scale represented "very unpleasant," while the middle represented "neutral" and the rightmost end signified "very pleasant." Similarly for the intensity value rating, the leftmost end meant "couldn't smell it," the middle represented "neutral," and the rightmost end represented "very strong." Participants moved the cursor, a gray circle initially placed in the middle of the scale, using a set of three buttons placed in their right hands (with the exception of one left-handed participant).

In both types of run each of the eight odors in the session-specific set was presented twice. In addition to these 16 trials, four "blank" trials — during which participants were presented with the same visual odor-release and rating cues as during any other trials, but were not given any actual odor stimuli — were included in each run. These 20 trials were presented in a random order, hence each participant was given odor stimuli in an order unique from those of the other participants.

A number of physiological recordings were made during each functional scan. A bellows connected to a Siemens wireless respiration module was utilized to monitor and measure breathing, and a similar pulse oximeter module was clipped to participants' left thumbs (with the exception of one left-handed participant, who preferred to have the unit clipped to his right thumb) to measure pulse. In addition, an infrared camera (Thorlabs, Inc., Newton, NJ) and accompanying recording software (UC480) were used to record participants' right eyes. Such videos were collected for all participants and all functional runs, except for two functional runs from two of the male participants, as hardware malfunction caused recording failure. The videos, as will be discussed later, were used to measure participants' pupil sizes.

During the second portion of the experiment, participants were asked to complete the following questionnaires, using Qualtrics online data collection system (Qualtrics, Provo, UT):

1. A scan debriefing questionnaire, on which participants were asked about their general experience during the in-scanner olfactory tasks

2. Disgust Scale - Revised (Haidt, McCauley & Rozin 1994, modified by Olatunjet al. 2007), which measures one's sensitivity to possibly disgusting situations

3. Engagement with Beauty Scale by (Diessner et al. 2008), which measures one's sensitivity to beauty in the natural, artificial (artistic), and moral domains

4. An edited version of the Duke adult picky eating survey (Wildes et al. 2012), which explores one's sensitivity to, and preference for, food items

5. A moral judgment questionnaire devised by the author, based on the autographical memories collected from 100 participants (Escobedo and Adolphs 2010) that have been shortened and standardized (Knutson et al. 2010). On this questionnaire, 18 short moral scenarios were presented, and each was followed by questions concerning legal permissibility of the character's action, the action's violation of social and cultural rules, moral rightness and wrongness, harshness

of the punishment that the character deserves, and degree of guilt the character might be feeling

6. For a small number of participants who had been flagged for history or possibility of depression, Beck Depression Inventory-II (Beck et al. 1996)

During the final portion of the experiment, participants were asked to smell the same set of odors from the in-scanner tasks, but make a larger number of ratings for further evaluation. During this task, participants sat upright at a desk with the odorant box placed upon it, held the odor-dispensing tubing with their left hands, and aimed it at their noses, while controlling the stimulus laptop with their right hands to enter ratings. Throughout the task, participants' faces were recorded using a digital camcorder to monitor automatic facial expressions triggered by the odors.

As in the scanner, this portion was divided into three sessions interleaved by quick breaks for switching the odorant sets, but this time each session consisted of only eight trials, as no blank or repeat trials were included in the out-of-scanner task. During each trial, participants were shown a five-second countdown as described earlier, followed by nine seconds of continuous odor release. This was succeeded by four questions asking to rate (using the seven-point Likert scale setup described above):

1. whether the odor smelled more "burnt," or closer to "chemical/medicinal," to explore the second dimension of human olfactory perception suggested by Koulakov et al.

2. how familiar the odor was to participant

3. how pungent the odor was to participant, focusing mainly on the tactile sensation in the nose associated with the odor

4. whether the odor caused participant to feel any strong emotions

After participants entered the above ratings, the same odor was administered again for nine seconds, in order to remind participants of what the odor smelled like. They were then asked to make the following three ratings:

1. how willing participant would be to eat something that smells like the odor

2. whether participant would move away from or toward something that smells like the odor

3. whether participant found the odor interesting enough to smell it again

Finally, participants were asked to verbally describe the odor, as well as discuss any memories that might have been elicited by the odor. Participants were given 30 seconds to speak their response into the built-in microphone on the stimulus laptop, while a MATLAB® script generated the audio recording of the response.

3.3.5 Image Acquisition

Scans were acquired at the Caltech Brain Imaging Center, using a 3.0-Tesla Siemens Tim Trio scanner and a 32-channel head coil. For each of three passive runs, 300 volumes of T2*-weighted echo-planar image (EPI) were acquired (for one of the 33 subjects, due to an error, only 295 volumes per passive run were obtained) and for each of three active runs, 540 volumes were acquired. The EPI parameters used were: TR = 1050 ms, TE = 30 ms, number of slices = 64, flip angle = 60°, FOV = $192mm^2$, voxel size = 2mm isotropic. As participants were taken out of the scanner bore after each run, a B_0 fieldmap was acquired for each of the six runs for accurate unwarping of each EPI. In addition, two high-resolution anatomical T1-weighted images, with TR = 2300 ms, TE = 2.96 ms, and voxel size = 1 mm isotropic, inversion time = 900 ms , were obtained for each subject.

3.3.6 Analysis

3.3.6.1 Respiration Data Analysis

Over the course of the study, it was discovered that the respiration data from the first passive runs were, due to system malfunction, never recorded for eight of the 32 subjects. It was important for the missing data to be recovered, as the imaging data analysis required us to establish the times at which participants were inhaling. Hence for these eight passive runs, the periodic y-direction head motion (which mainly describes the natural nodding of participant's head during respiration), extracted from the head motion correction data generated by FSL FEAT, was used as the proxy for respiration data. The head motion data tended to be noisy, a robust Loess smoothing method was used to correct the baseline and filter the data. The value of the span parameter used in this process was determined empirically by, under the assumption that participants' respiratory and head motion behaviors tended to be pretty consistent among the three passive runs, applying the smoothing process to the other passive runs of the same subject (for which both head motion and respiration data were available), finding the span values that resulted in the best match between the two types of signals, and using the average of the span values from the two passive runs (for all eight subjects the two values were very close to each other, which suggested that they would also work well for the first passive run's head motion data). And, as it was observed that the respiration data tended to lag very slightly (by less than half a second) behind the head motion data (as the initial expansion of the chest in the beginning of inhalation produces the head motion, closely followed by conspicuous change in the lower torso volume), a delay was introduced to the head motion data to correct this. Again, the amount of the delay was determined by finding the optimal delay amount for the second and third passive runs through direct comparison with the respiration data, and averaging out the two values.

While it is impossible, for obvious reasons, to assay how effectively the head motion data replaced the missing respiration data for these eight passive runs, we attempted

Participant ID	CC0003	CC0024	CC0059	CC0063	CC0069	CC0071	CC0091	CC0104
% match - Passive 2	89.77	89.3	74.87	66.7	77.18	85.3	87.03	86.6
% match - Passive 3	92.7	91	72.23	74.27	63.73	86.73	88.4	88.78

Table 3.4: Comparison of inhalation data generated from head motion and respiration signals.

to demonstrate the method's efficacy by comparing the respiration and corrected head motion signals for the second and third passive runs (those with actual respiration data available) of these eight subjects. Since in the present study we're only interested in the inhalation times of subjects (since inhalation times represent the direct olfactory stimulation times), the first derivatives of the two sets of signal were computed, and boxcar functions representing the inhalation times for these signals were generated. The percentage of the timepoints on which these two boxcar functions match in value was then computed.

In addition, note that as the respiration and head motion signals tended to be rather noisy, they were drastically smoothed out by automatic identification of major peaks (representing the inhalation maxima and exhalation minima) and interpolation between these peaks, before the boxcar functions were generated. This smoothing process should not have any deleterious effect on the analysis, but in fact improve it, as the smoothed data would produce boxcar functions that more accurately represent the inhalation windows (without smoothing, the resulting boxcar functions will be extremely choppy). The smoothing procedure was followed by resampling of the data so that the new sampling frequency is 10 Hz. The results of the comparisons are presented in Table 3.3.

The respiration data for all other runs and participants were processed using the same method as described above. They were smoothed via automatic peak selection and interpolation, and resampled such that a data point was present every 0.1 second. Then their first derivatives were computed and boxcar functions illustrating the inhalations were generated.

3.3.6.2 Pupillometry

The size of the pupils in the eye videos described above were computed using in-house, Python-based software (MrGaze, Mike Tyszka, Caltech). A number of screenshots were extracted from the videos recorded during 8 functional runs (selected for the videos' reasonably high qualities), and manually categorized into "positives" (eyes open, both wide and half-open) and "negatives" (eyes closed). The pupil positions in the "positives" screenshots were notated, and the pupil-detection algorithm was trained using these data. Pupillometry was then performed on all available eye videos using this trained algorithm. The results were then cleaned up to exclude any unrealistically large values caused by blinks, and the average pupil size over each of the nine-second odor release windows was computed. These values were later used as parametric modulators during the statistical analysis of the functional imaging data.

3.3.6.3 Imaging Data Analysis

All imaging data analysis was performed mainly using FMRIB Software Library (FSL; Oxford, UK; Jenkinson et al. 2012). The T1 structural images were averaged using FSL FLIRT (Jenkinson and Smith 2001; Jenkinson et al. 2002), and the resulting image underwent brain extraction using optiBET (Lutkenhoff et al. 2014). The functional images, using FSL FEAT, were first preprocessed for motion correction, B0 unwarping, spatial smoothing at 5mm, highpass temporal filtering with cutoff at 100s, and registration with the brain-extracted average T1 data. The resulting preprocessed functional image was then fed to FSL MELODIC independent component analysis (ICA) algorithm, which identified an automatically estimated number of independent components contained in the BOLD data. These components, representing either actual neural signals or noise generated by motion, respiration, pulse, or scanner drift, were then categorized using FSL FIX (Salimi-Khorshidi et al. 2014; Griffanti et al. 2014). The FIX algorithm had been trained with 10 of the functional runs from the present study (five active and five passive runs), whose independent components

had been manually identified as "signal" or "noise" using the criteria identified in Kelly, Jr. et al. 2010, as well as careful inspection of high-frequency oscillations at respiration- or pulse-like frequencies. The trained algorithm was then tested and its parameter was fine-tuned based on the results. Once the algorithm's performance became satisfactory, the algorithm was run with the ICA data of all functional runs from the 33 participants, and the components identified as noise were filtered out from the functional images, hence yielding "clean", preprocessed images ready for statistical analysis.

The "clean" images were then analyzed using univariate general linear models for whole-brain analysis, via FSL FEAT. The specific models used will be described in the Results section. During this process, outstanding motion confounds were eliminated from the timeseries. Each stimulation was convolved with the double-gamma hemodynamic response function (HRF), and temporal derivatives were added to make up for any inaccurate temporal fit. The higher-level analysis (across sessions and subjects) were carried out by FSL FLAME, which enabled fixed-effect modeling when pooling data across sessions within each individual, and mixed-effect modeling when pooling across subjects. After confirming that there were no significant differences between the passive and active run group-level results, the data were pooled across session types to minimize effect size. The resulting clusters were thresholded at $Z > 2.3$ and $p < 0.05$. ROI analysis was carried out using FSL Featquery and binary (non-weighted) ROI masks created based on anatomical or functional evidence.
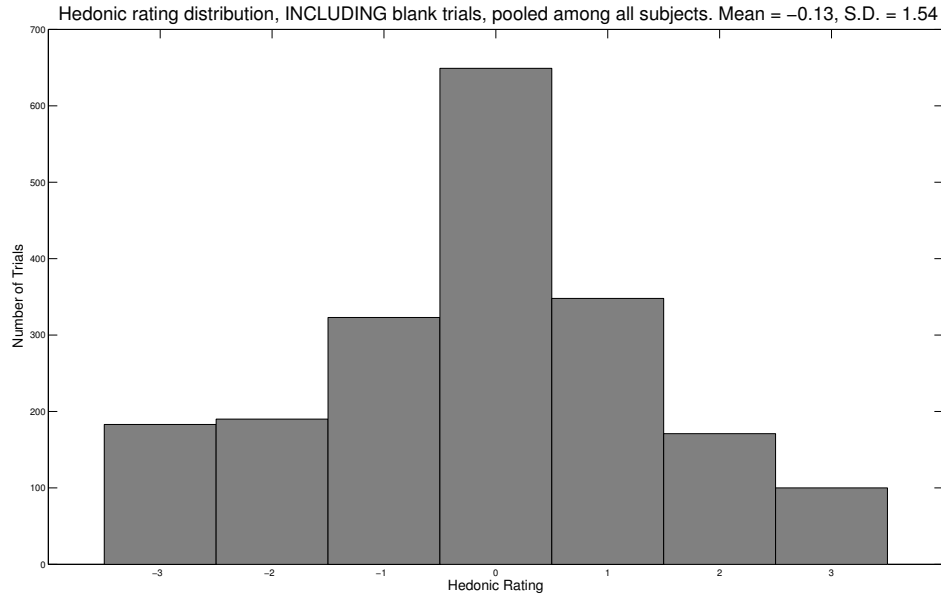
Figure 3.4: Distribution of hedonic value ratings, including blank stimuli.

3.4 Results

3.4.1 Behavioral Data

3.4.1.1 Hedonic and Intensity Values

When pooled across all subjects, sessions, and stimuli including blank trials, the hedonic value ratings from the active runs seemed to be distributed in a normal fashion, with the overall mean of -0.13 and standard deviation of 1.54, on a -3 to 3 scale (Figure 3.4). And when the blank trials are excluded due to the fact that their ratings do not necessarily reflect subjects' behavior toward the odor stimuli, the distribution still behaves similarly (mean = -0.15; S.D. = 1.70), with the only main difference of the middle, "neutral" peak being halved by the exclusion (Figure 3.5). This indicates that participants, overall, found a large portion of the stimuli to be rather neutral, while perceiving a smaller number of the odors as extremely pleasant or extremely noxious.
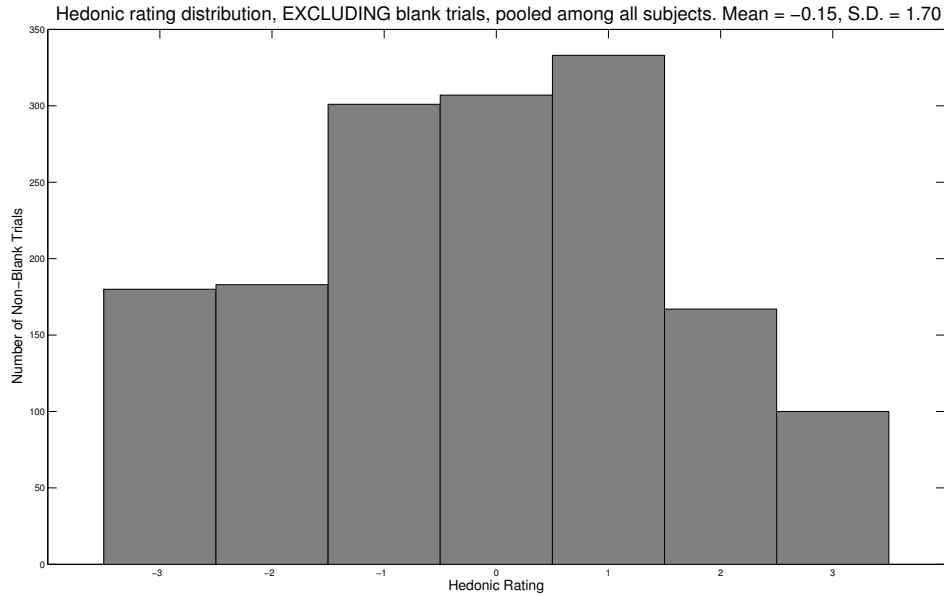
Figure 3.5: Distribution of hedonic value ratings, excluding blank stimuli.

The overall distribution of the intensity ratings reflected a dichotomy in participants' perception patterns. As shown in both Figure 3.6 and Figure 3.7, regardless of inclusion of blank trials, a larger peak at ratings higher than or equal to five and a smaller peak at ratings lower than or equal to three were observed, accompanied by a rather small number of ratings at the intensity value of four. The skew of the distribution toward the higher intensity ratings indicates that the majority of odorants utilized in this study were presented at concentrations that enabled most participants to perceive them, although it appears possible that some of them might have been too intense for many individuals. The strong absence of ratings at the middle intensity suggests that many participants might have been using an interesting heuristic, in which one rates the odor at a number higher than four (in many cases, five) if the odor smells vaguely strong, and rates it at a number lower than four (in many cases, three) if it smells vaguely weak. If this conjecture is true, then it may reflect a psychological tendency to dichotomize judgment of odor intensity as either "weak" or "strong," rather than making a more gradated assessment as we've observed in participants' hedonic value rating data.
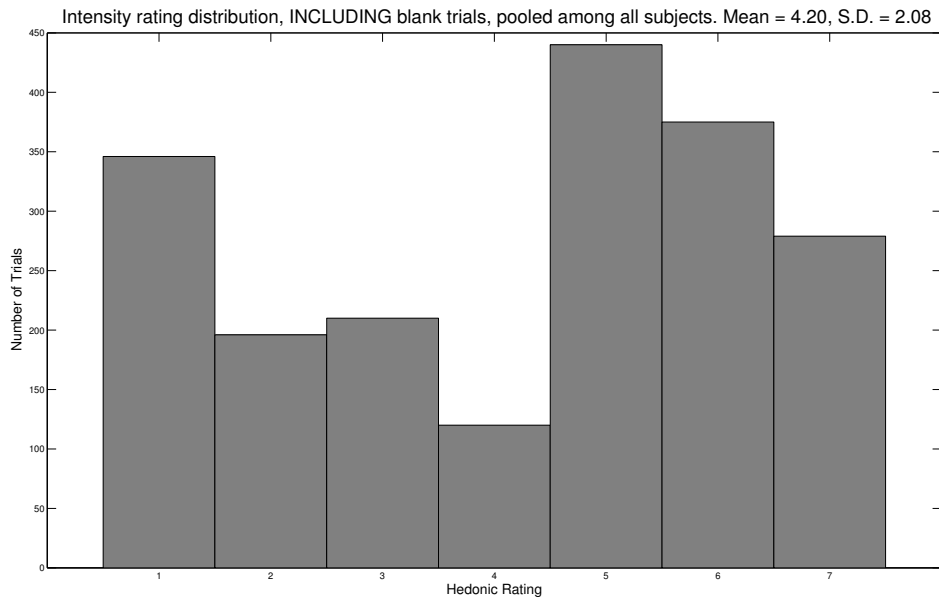
Figure 3.6: Distribution of intensity value ratings, including blank stimuli.
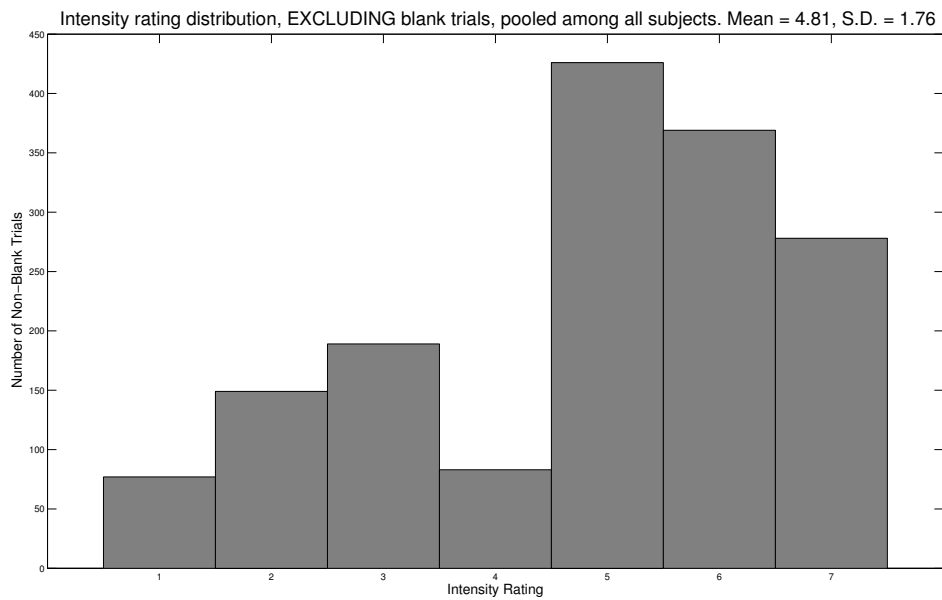
Figure 3.7: Distribution of intensity value ratings, excluding blank stimuli.

At both group and individual levels, we did not find any notable overall relationship between the odor stimuli's hedonic value and intensity ratings. According to the first group-level analysis, in which each subject's overall hedonic and intensity ratings for all odors were averaged and compared across subjects in Figure 3.8, even though a small number of extremely unpleasantness-sensitive and extremely pleasantness-sensitive participants tended to be give higher intensity ratings, the general trend, with a Pearson correlation coefficient of -0.24, was weak. In the second group-level analysis, in which each odor's overall hedonic and intensity ratings from all subjects were averaged and the mean values were plotted (Figure 3.9), a similar trend was found (Pearson correlation coefficient = -0.24), where some very unpleasant stimuli and very pleasant stimuli were rated at high intensity levels, but most of the odors did not appear to follow any specific overall pattern. The individual-level rating patterns generally mirror this, with the average correlation coefficient over all 33 subjects of -0.14 (standard deviation = 0.22; range -0.61 to 0.43). A representative plot from one participant (participant # 21) is shown as Figure 3.10.

As each participant had rated each stimulus' hedonic and intensity values twice, the within-subject variability of the ratings was also assessed. We predicted a small degree of variability due to contextual effects (e.g. an odor that is not particularly pleasant or unpleasant might be perceived as quite pleasant, when preceded by a very noxious odor; an odor might be perceived as very strong when followed by a blank stimulus), but otherwise constant ratings, for most odors. As predicted, most within-subject rating differences in same-odor pairs were 0, 1, or -1 with small portions of pairs showing larger differences (Figure 3.11).

To find any patterns present in these re-rating differences, all non-blank odor pairs were grouped in various ways and the distributions of their rating differences were examined. First, the odor pairs were categorized according to the across-subject mean of their perceived hedonic values, such that group one comprised the odors that were generally pleasant (the group means of their hedonic values fell between +1 and +3, inclusively), group two consisted of those that were generally neutral
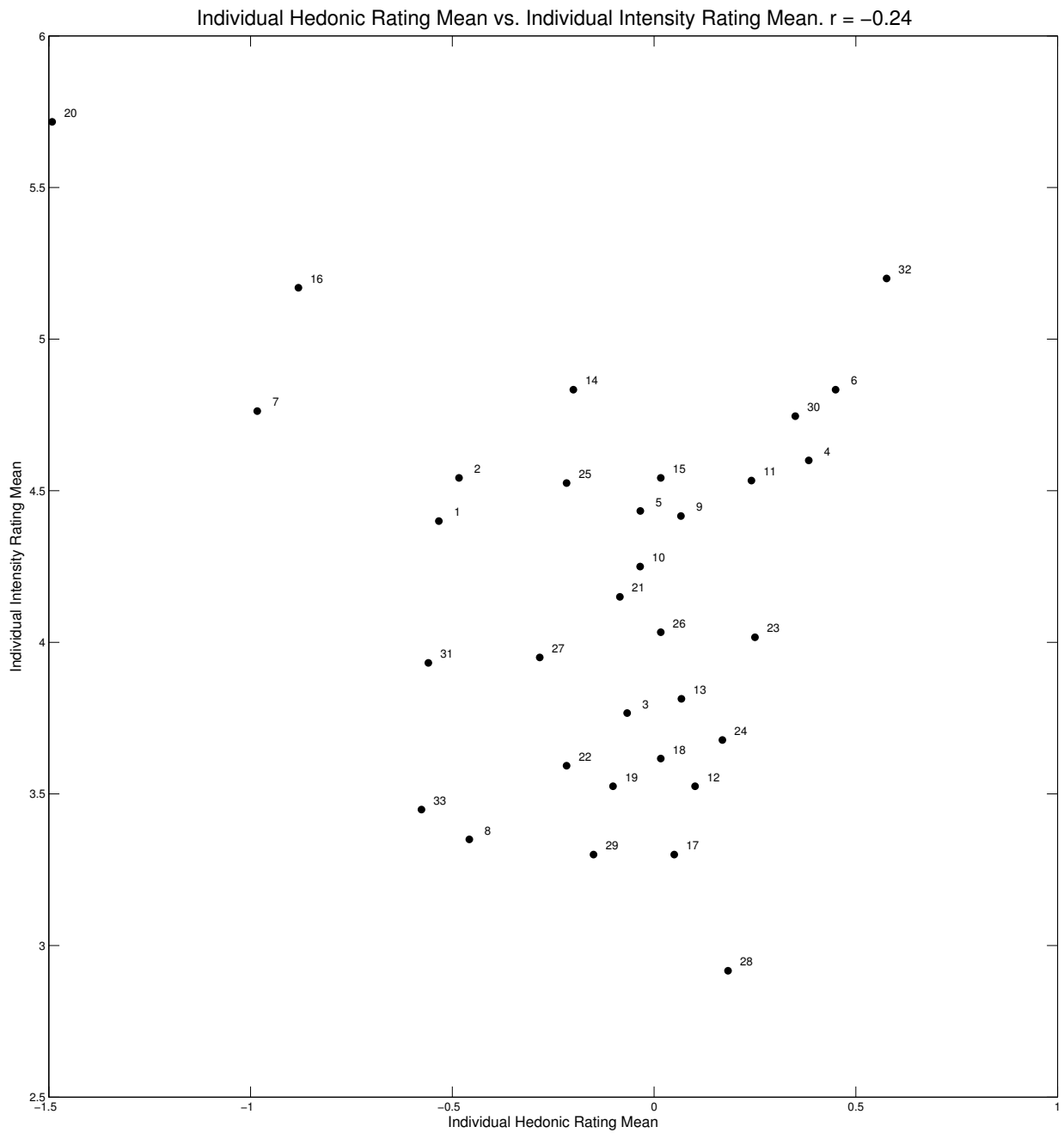
Figure 3.8: Relationship between individual subject mean hedonic ratings and individual subject mean intensity ratings.
Each dot represents one participant, and is labeled with the participant number.
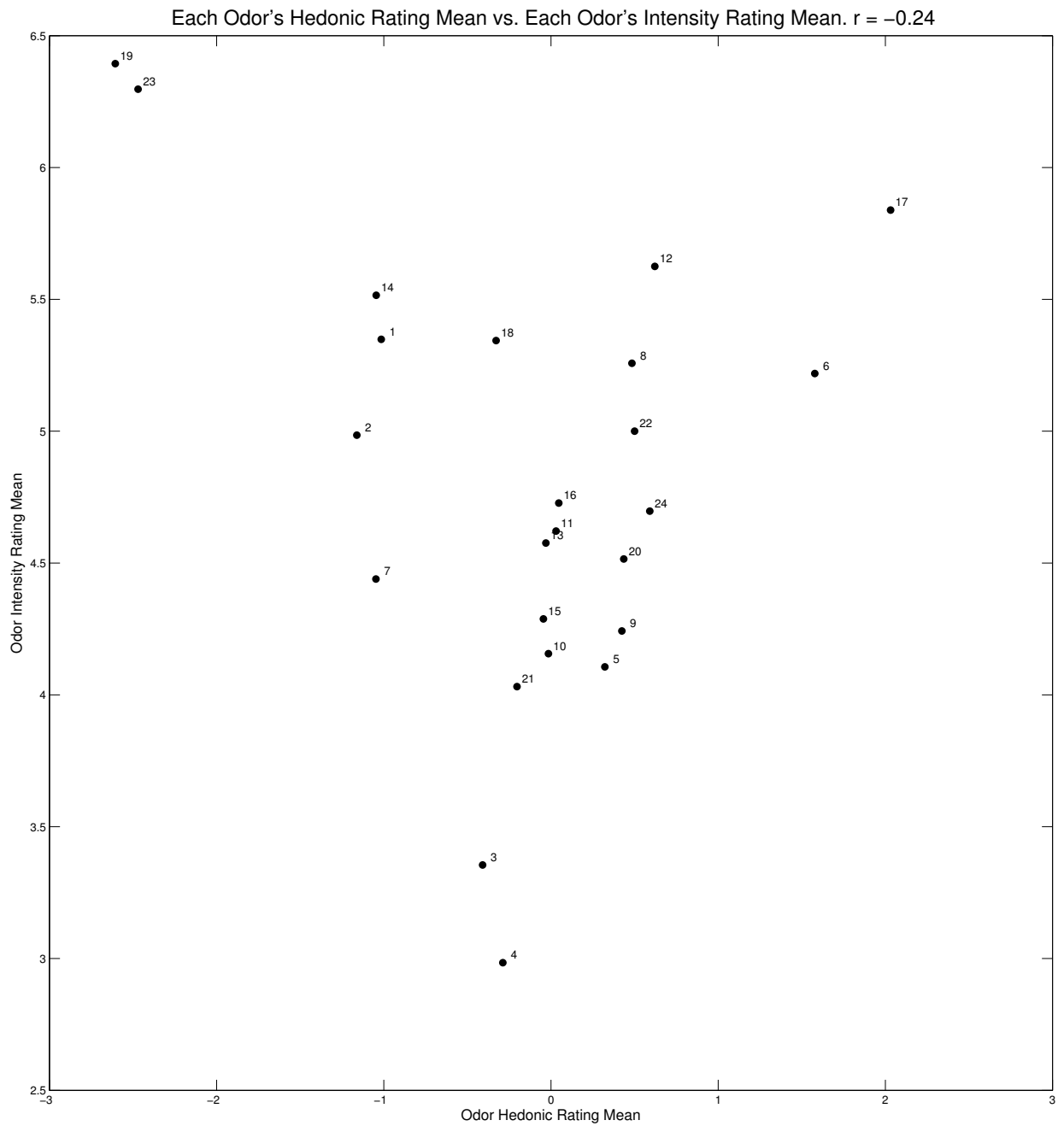
Figure 3.9: Relationship between individual odor mean hedonic ratings and individual odor mean intensity ratings.
Each dot represents one odor, and is labeled with the odor number.
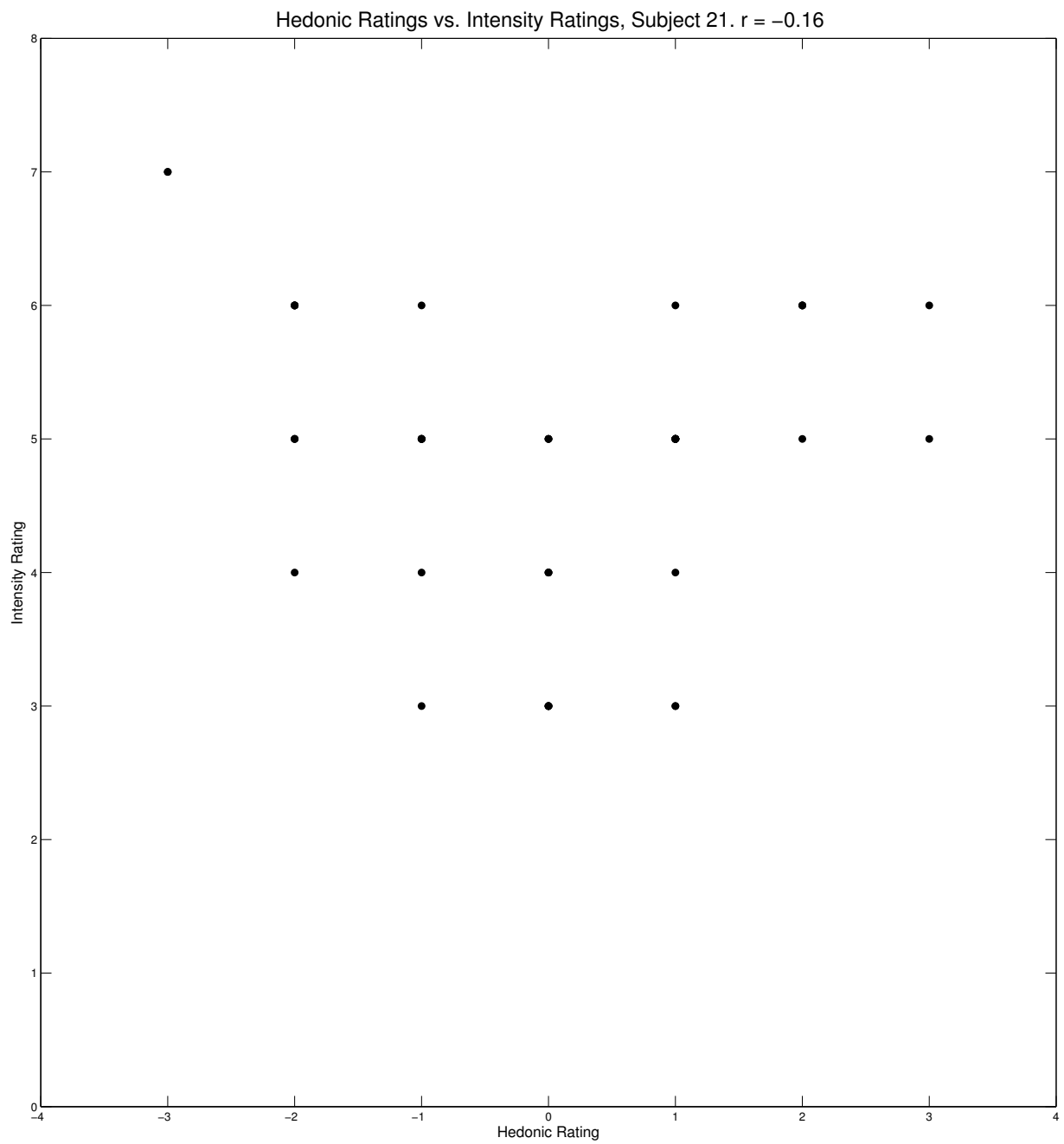
Figure 3.10: Relationship between hedonic ratings and intensity ratings, subject #21.
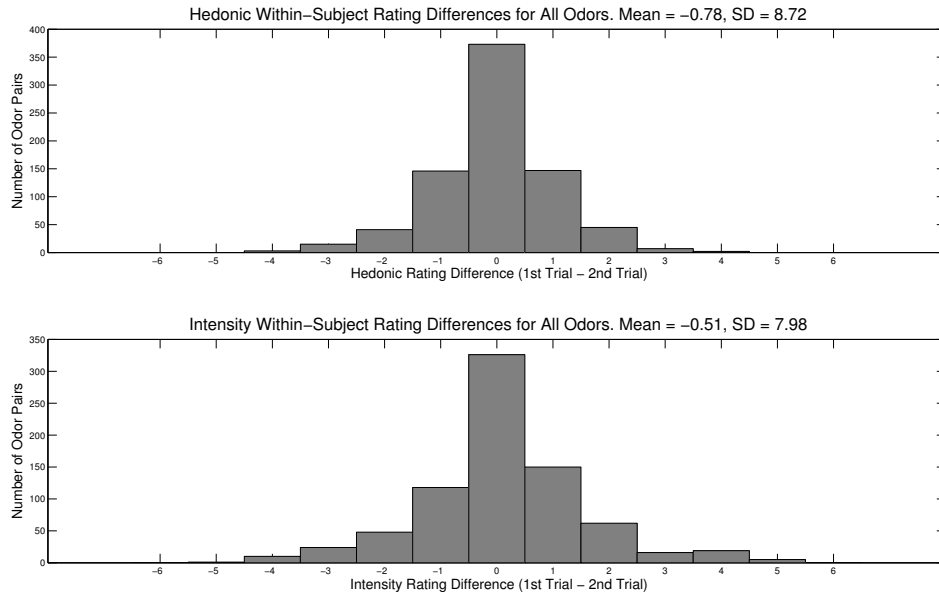
Figure 3.11: Distributions of within-subject rating differences for hedonic (top) and intensity (bottom) values.

(mean hedonic values between -1 and 1, inclusively), and group three was formed by those that were generally perceived as unpleasant (mean hedonic values between -3 and -1, inclusively). The within-subject hedonic rating difference distributions of these three groups are shown in Figure 3.12, while their within subject intensity rating difference distributions are shown in Figure 3.13. The results indicate that these three groups only exhibit very small statistical differences, although the generally unpleasant odors' hedonic value re-rating differences tended to exhibit slightly larger consensus — smaller standard deviation — compared to the other two groups, and the intensity value re-rating differences tended to be somewhat more spread out compared to the other two groups. These observations suggest that hedonic judgment of unpleasant odors might be slightly less resistant to the effect of presentation context than more pleasant ones might be, while hedonically neutral odors tend to be somewhat more vulnerable to contextual effects when it comes to intensity judgments, possibly due to their relatively lower saliency.

A similar assay was performed by dividing the odor pairs into two intensity-based
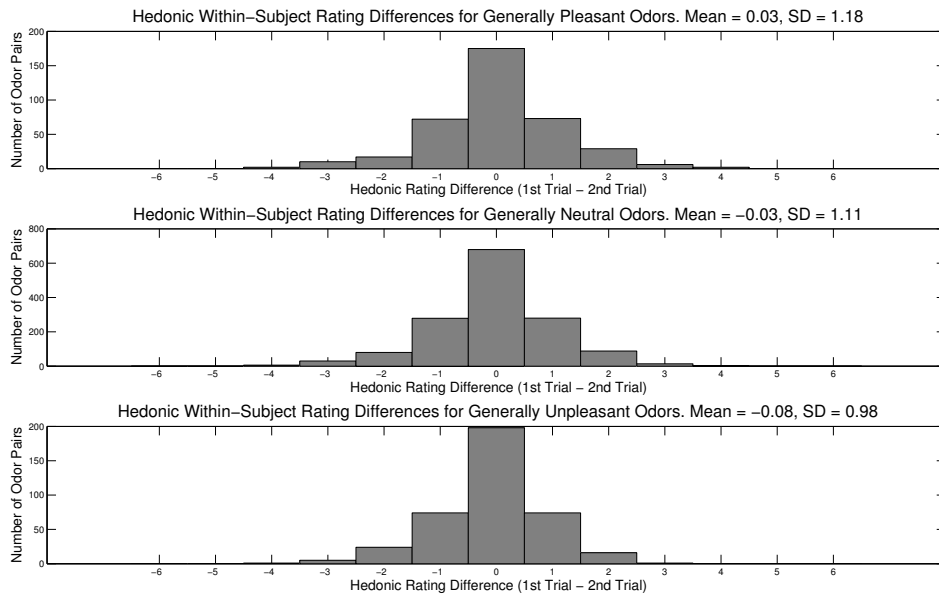
Figure 3.12: Distributions of within-subject re-rating differences of hedonic values for different hedonic categories.
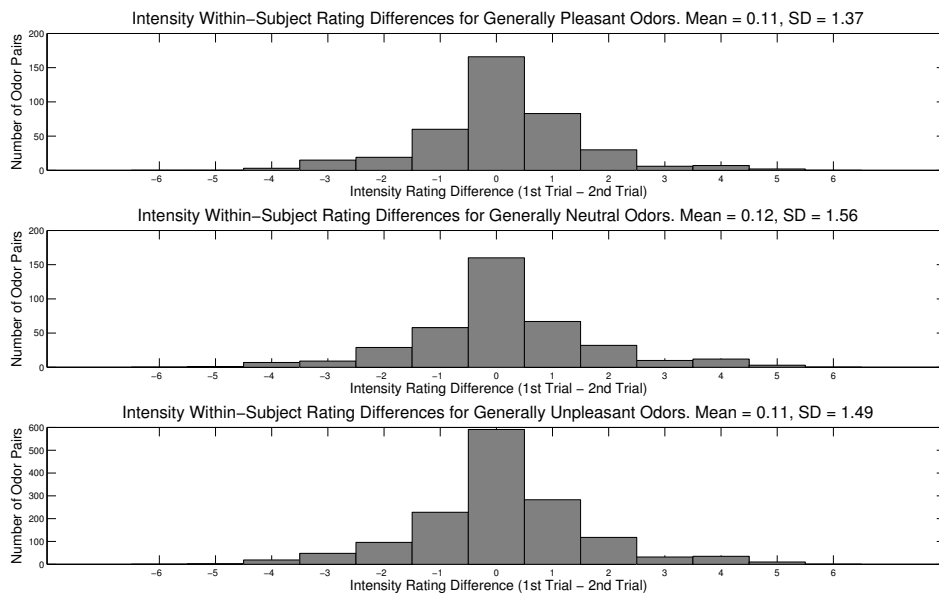
Figure 3.13: Distributions of within-subject re-rating differences of intensity values for different hedonic categories.
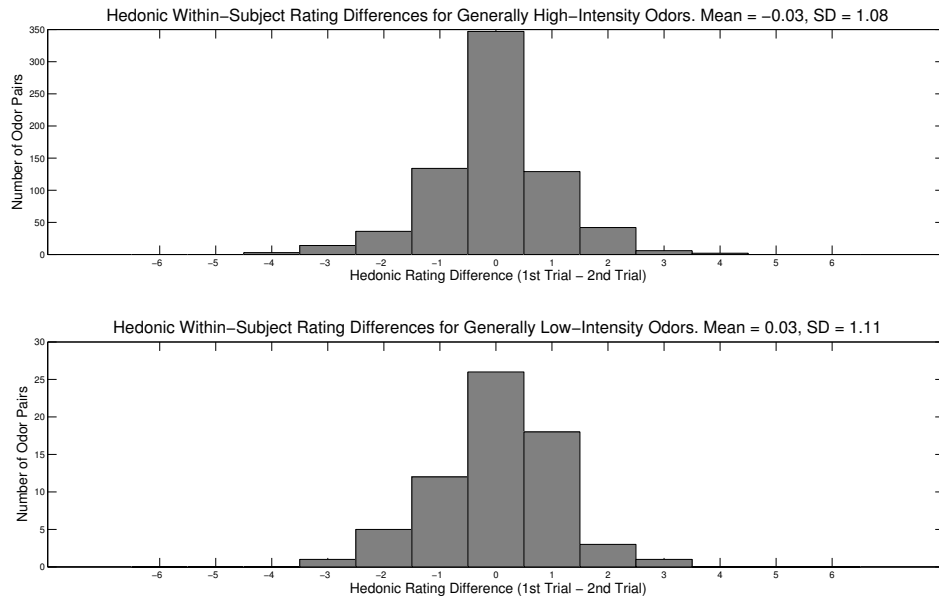
Figure 3.14: Distributions of within-subject re-rating differences of hedonic values for different intensity categories.

groups: one group consisting of the odors that were generally stronger in intensity (with the group means of intensity ratings higher than four), and another group of the odors that were generally perceived as weaker (those with group-mean intensity values lower than four). The results are illustrated in Figure 3.14 and Figure 3.15. The results suggest a very slight bias towards an increase in hedonic value rating upon repeated exposure to higher-intensity odors, and the opposite effect during exposure to low-intensity odors, yet the effect is extremely small and there are far fewer low-intensity odor pairs than high-intensity ones, so no clear assertion could be made at this point. The results also indicate a slight bias towards a general reduction in intensity ratings upon repeated exposure to stronger odors, while a relatively large increase is observed for weaker odors. Although the effects here are also rather weak, it appears possible that subjects were becoming sensitized to low-intensity odors after their initial presentations. Also, the slightly larger standard deviation in the intensity ratings for weaker odors indicates that, as one would imagine, less intense odors tend to be more vulnerable to any contextual effects that might cause re-rating variability.
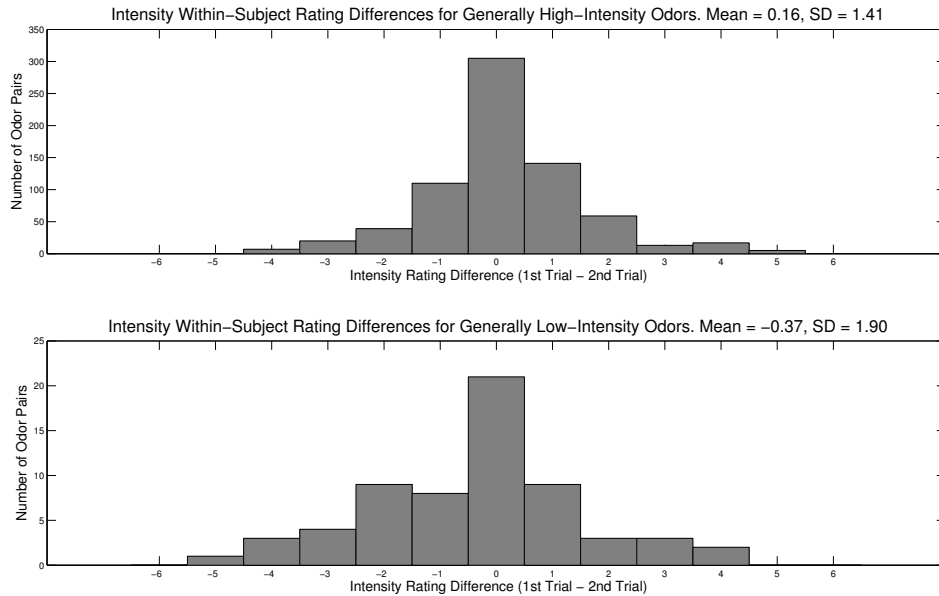
Figure 3.15: Distributions of within-subject re-rating differences of intensity values for different intensity categories.

To find if any specific odors or subjects were driving the effect of within-subject rating variability, the odor pairs whose absolute values of re-rating differences exceeded two were identified across all subjects, and visualized in Figure 3.16 and Figure 3.17. The results suggest that while the effect in hedonic ratings is indeed driven by a small number of odors (such as odors 2, 5, and 20) and participants (such as participants 4, 5, 9, and 22), it is spread out over larger numbers of stimuli and subjects in the case of intensity ratings. This seems to indicate that odor intensity judgment is significantly more vulnerable to contextual and other cognitive effects than is hedonic value judgment.

The relationship between the odor pair presentation distance — i. e. the number of trials between the first presentation of an odor and its second presentation — and the within-subject re-test variability was also examined. As shown in Figure 3.18, we did not observe any notable correlation between the two factors, which together exhibit very low Pearson correlation coefficients of 0.031 (hedonic value re-rating) and -0.193 (intensity value re-rating). In addition, when the re-rating variability
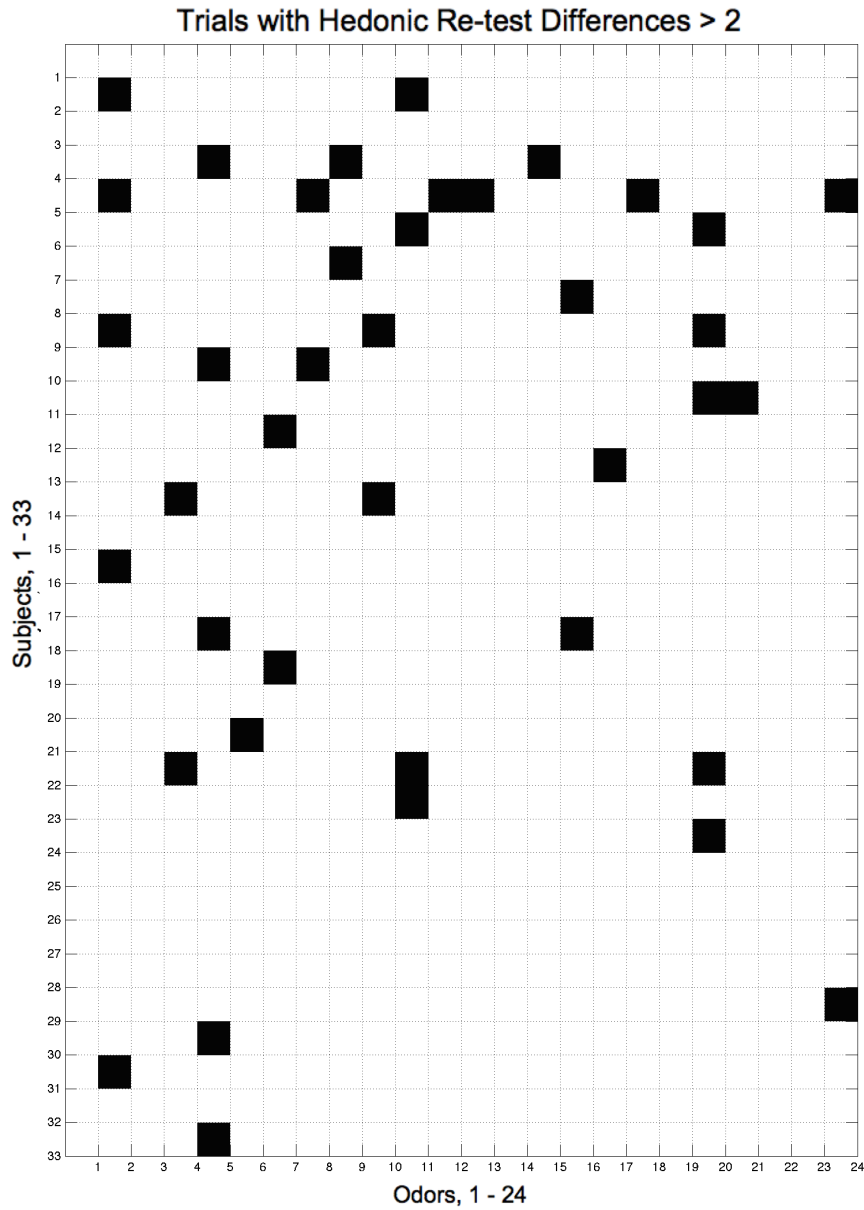
Figure 3.16: Subjects and odors with within-subject hedonic value re-rating difference magnitudes larger than two.
The x-axis represents the 24 odors, while the y-axis represents the 33 participants. The subject-odor pairs with hedonic value re-rating difference absolute values larger than two are marked with black squares.
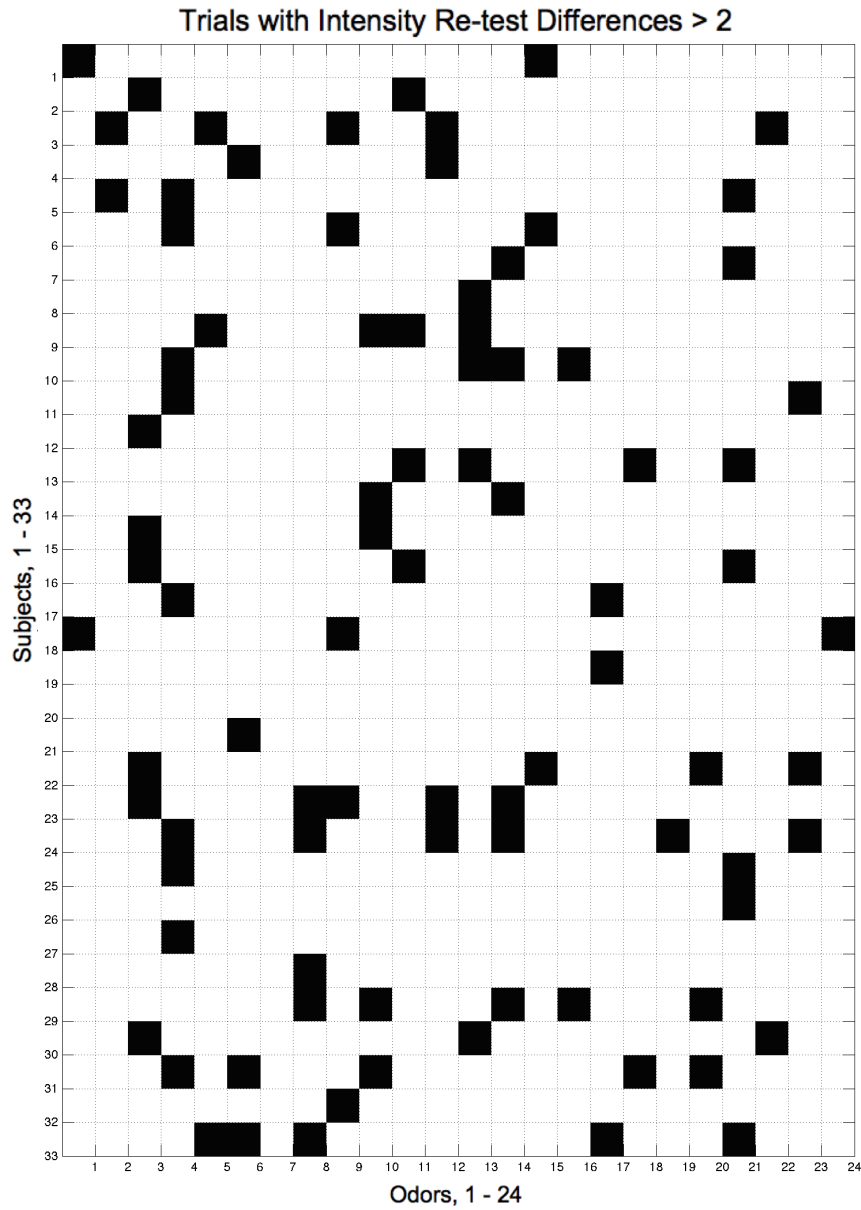
Figure 3.17: Subjects and odors with within-subject intensity value re-rating difference magnitudes larger than two.
The x-axis represents the 24 odors, while the y-axis represents the 33 participants.
The subject-odor pairs with intensity value re-rating difference absolute values larger than two are marked with black squares.
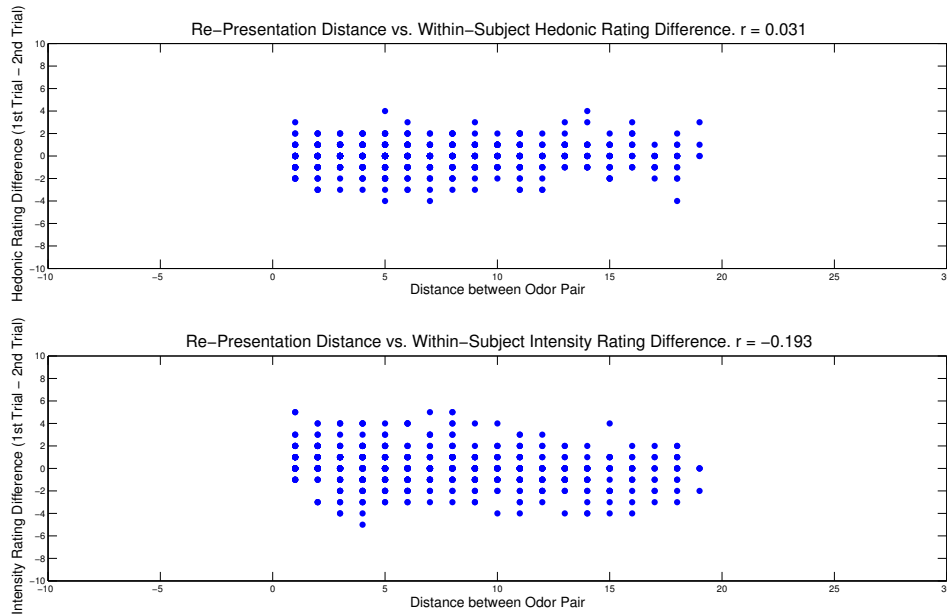
Figure 3.18: Relationship between re-rating variability and the number of trials between same-odor pairs, for hedonic ratings (top) and intensity ratings (bottom).

was compared with each subject's full scale IQ (Figure 3.19) and auditory working memory score (Figure 3.20), which had been collected earlier as part of a large-scale study at Caltech Conte Center, no significant correlation was found between within-subject rating variability and one's intelligence or working memory. Taken together, these results strongly indicate that changes in re-rating variability was not an effect of subjects' remembering their previous rating for the odor and simply repeating it. Rather, this variability appears to have been based on subjects' actual experiences of the repeated odor presentations.

3.4.1.2 Comparisons with Other Behavioral Measures

As briefly mentioned earlier, the participants of this study form a part of a larger-scale, long-term study at Caltech Conte Center, and their behaviors and personalities have been thoroughly characterized through a large number of tests. We have utilized some of these data to examine whether any of the participants' behavioral measures
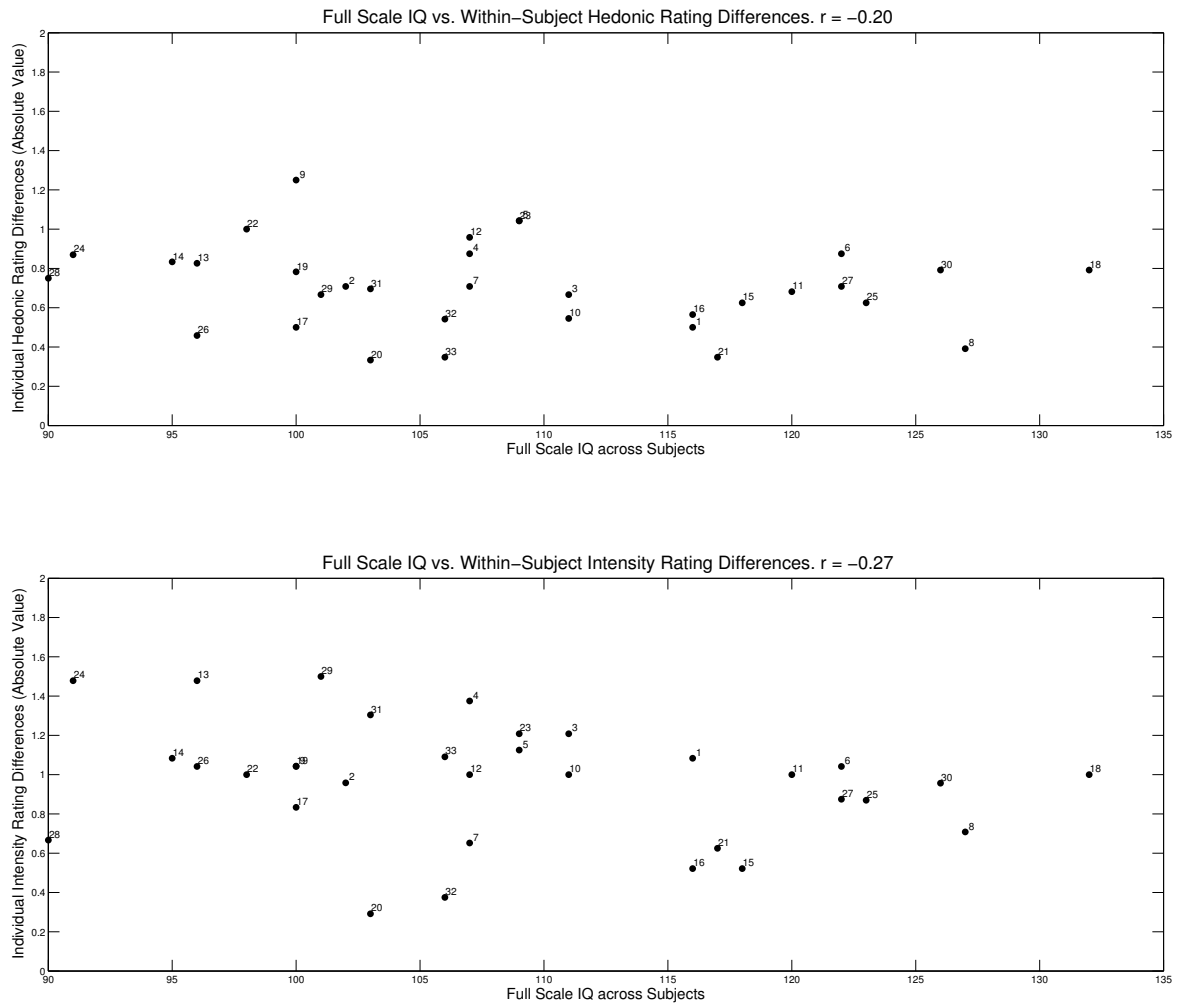
Figure 3.19: Relationship between re-rating variability of each subject and their full-scale IQ, for hedonic ratings (top) and intensity ratings (bottom).
Each dot represents a participant, and is labeled with the participant number.
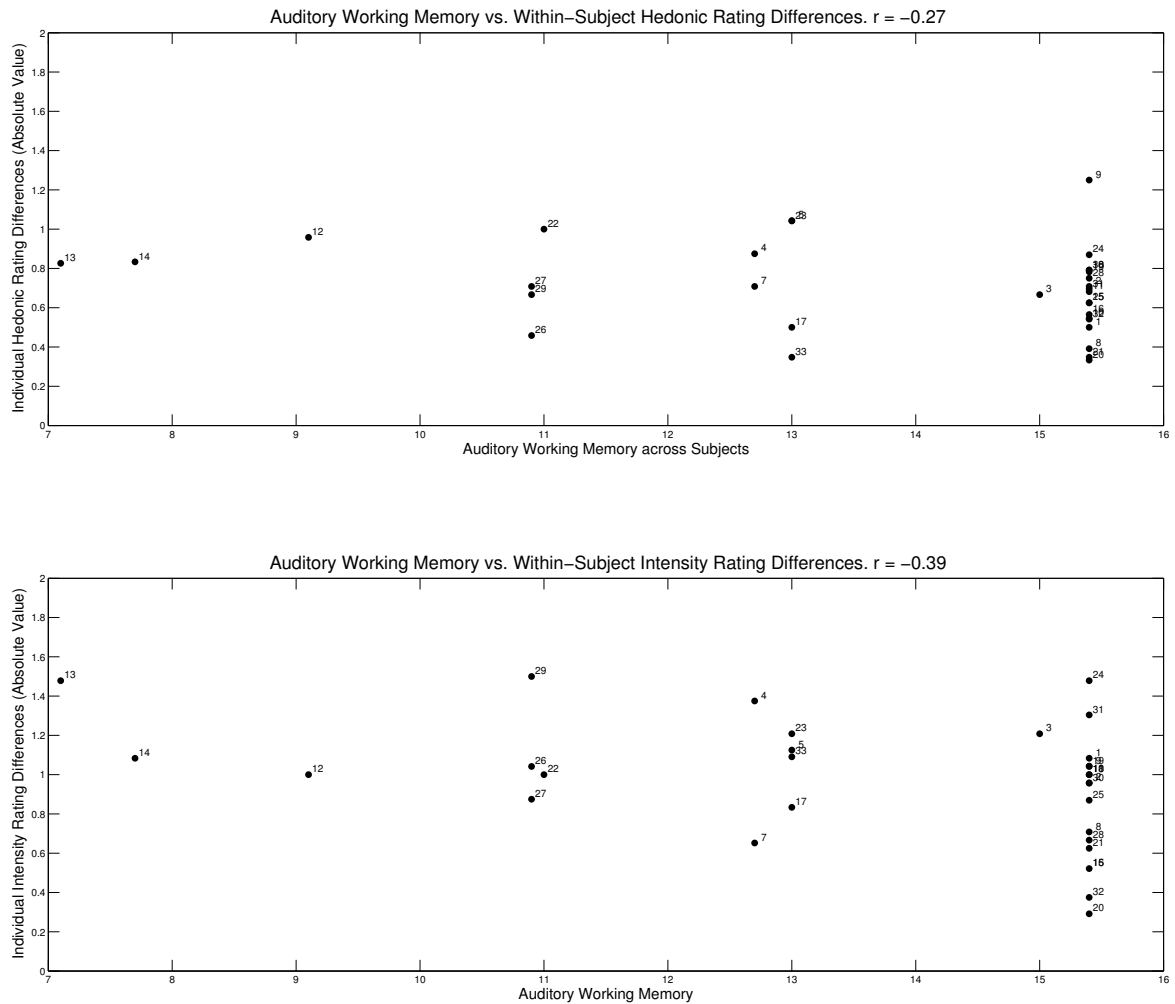
Figure 3.20: Relationship between re-rating variability of each subject and their auditory working memory score, for hedonic ratings (top) and intensity ratings (bottom). Each dot represents a participant, and is labeled with the participant number.

were related to their hedonic value or intensity rating patterns. The data that we used had been collected through the following tests:

1. Mayer-Salovey-Caruso Emotional Intelligence Test (MSCEIT) (Mayer et al. 2002)

2. Social Network Index (SNI) (Cohen et al. 1997)

3. Positive and Negative Affect Schedule (PANAS) (Watson et al. 1988)

4. State-Trait Anxiety Inventory (STAI) (Spielberger et al. 1983)

For MSCEIT, the overall emotional intelligence score and the "perceiving" score — a measure of test taker's emotional perception in stimuli such as faces, objects, and music — were plotted against the standard scores of each participant's mean hedonic rating, mean intensity rating, hedonic rating variance, and intensity rating variance. For SNI, the number of people in subjects' social networks was compared with the four sets of Z-scores. The positive affect Z-score and negative effect Z-score were used as the PANAS results of interest, and both state and trait anxiety scores from STAI were compared with the olfactory rating standard scores. The results are presented in Figure 3.21, Figure 3.22, Figure 3.23, Figure 3.24, Figure 3.25, Figure 3.26, and Figure 3.27. As shown in these figures, no notable correlations were observed from these comparisons, which indicates that odor ratings themselves are not strongly associated with one's emotional, social, affect, and anxiety-related traits. However, it may still be possible to find these individual differences reflected in the neural imaging data, and the assay to explore this will be discussed later in this chapter.

3.4.1.3 Out-of-Scanner Ratings

As a fairly large number of questions were asked during the out-of-scanner tasks, in order to concentrate our analytical efforts to a smaller set of more interesting
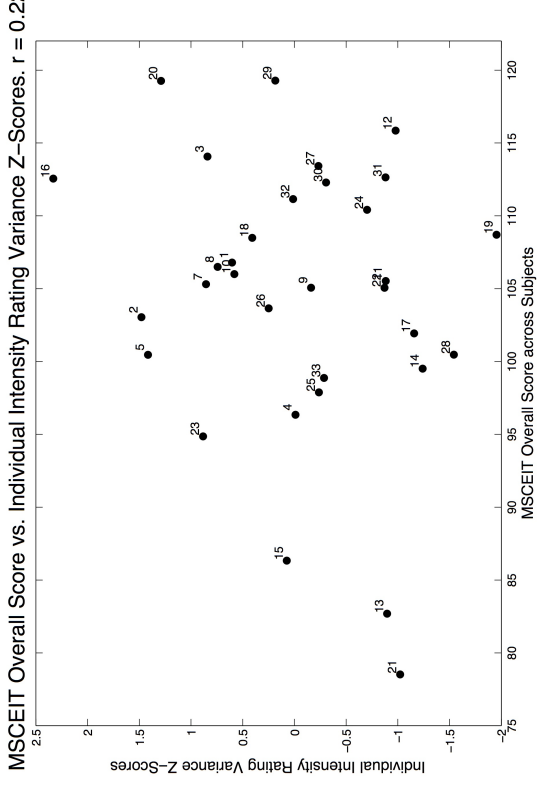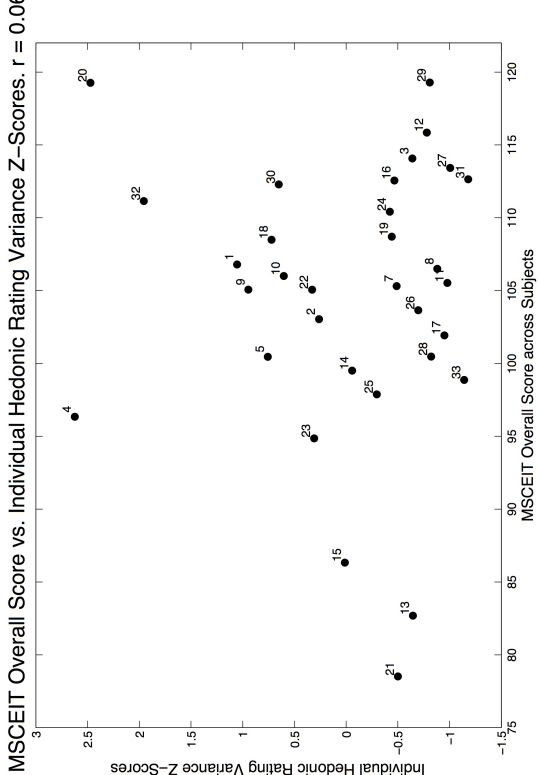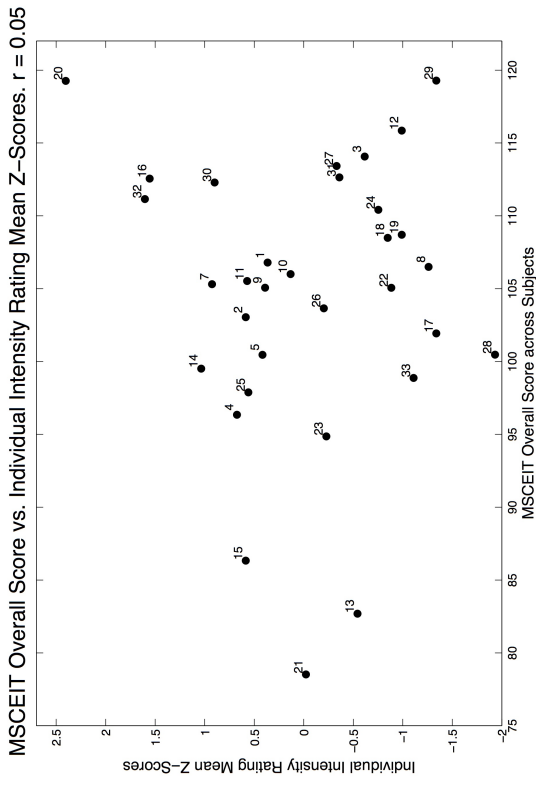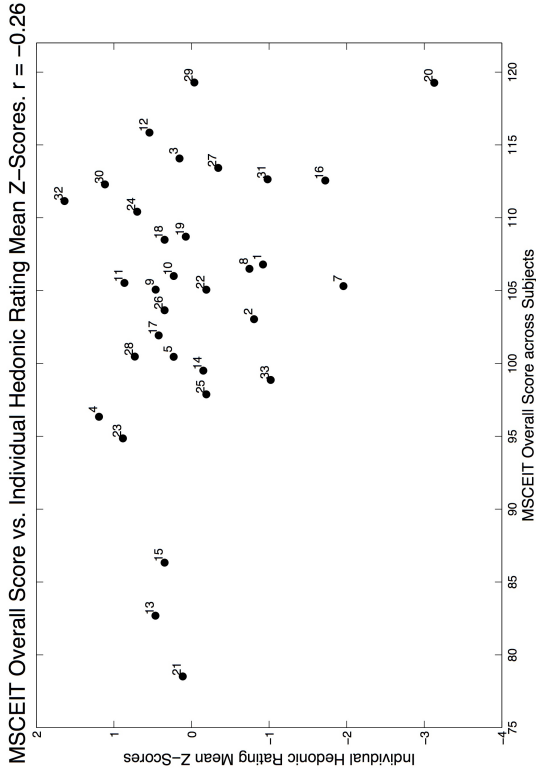
Figure 3.21: Relationship between the overall emotional intelligence scores measured by MSCEIT and the standard scores of individual participants' rating patterns.
MSCEIT overall scores are compared with hedonic rating means (top left), intensity rating means (top right), hedonic rating variance (bottom left), and intensity rating variance (bottom right). Each dot represents a participant, and is labeled with the participant number.
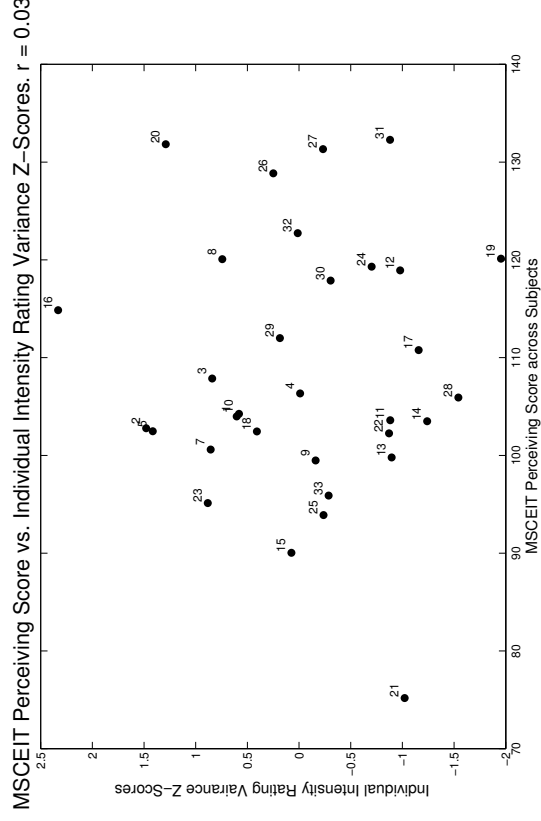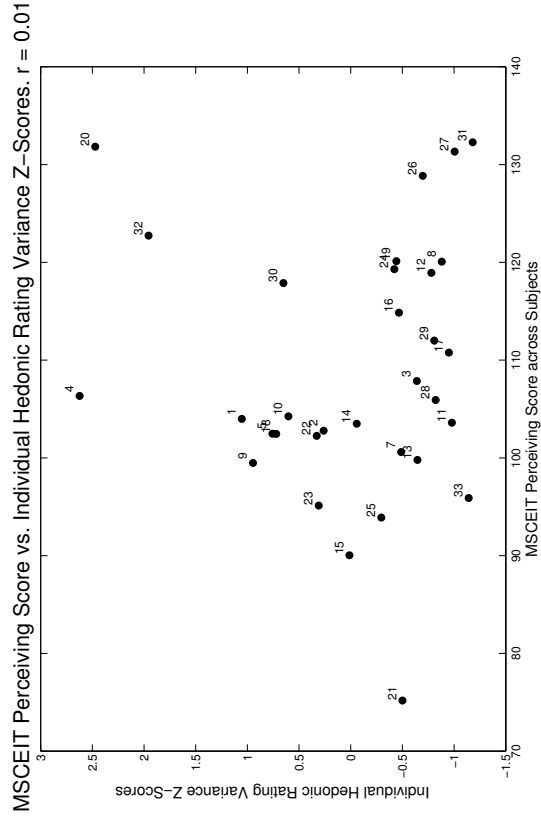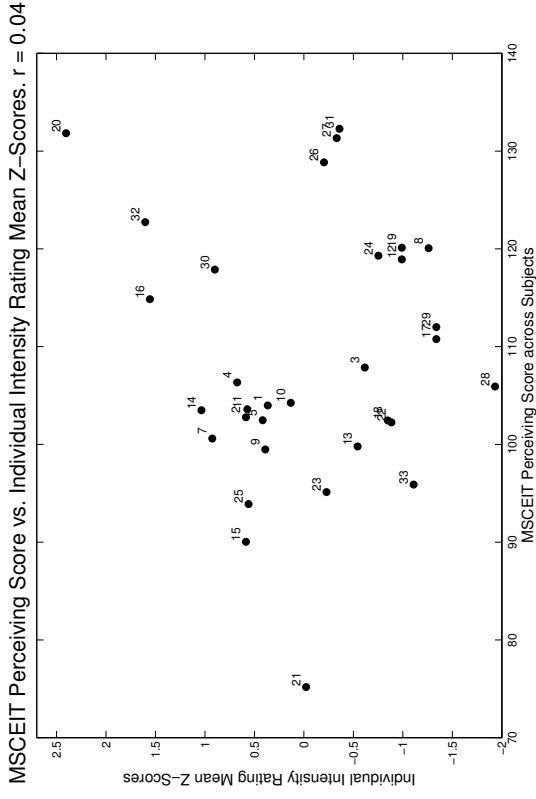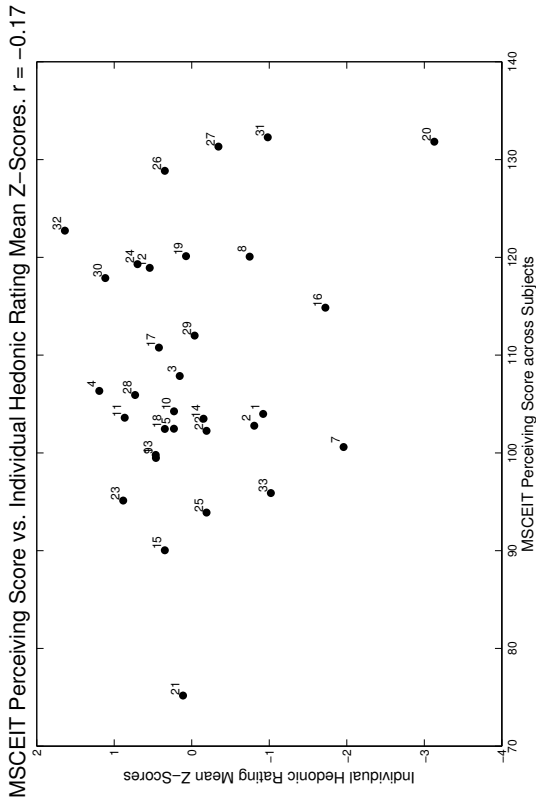
Figure 3.22: Relationship between the emotional perceiving scores measured by MSCEIT and the standard scores of individual participants' rating patterns.
MSCEIT perceiving scores are compared with hedonic rating means (top left), intensity rating means (top right), hedonic rating variance (bottom left), and intensity rating variance (bottom right). Each dot represents a participant, and is labeled with the participant number.

Figure 3.23: Relationship between the number of people in social networks measured by SNI and the standard scores of individual participants' rating patterns.

SNI scores are compared with hedonic rating means (top left), intensity rating means (top right), hedonic rating variance (bottom left), and intensity rating variance (bottom right). Each dot represents a participant, and is labeled with the participant number.
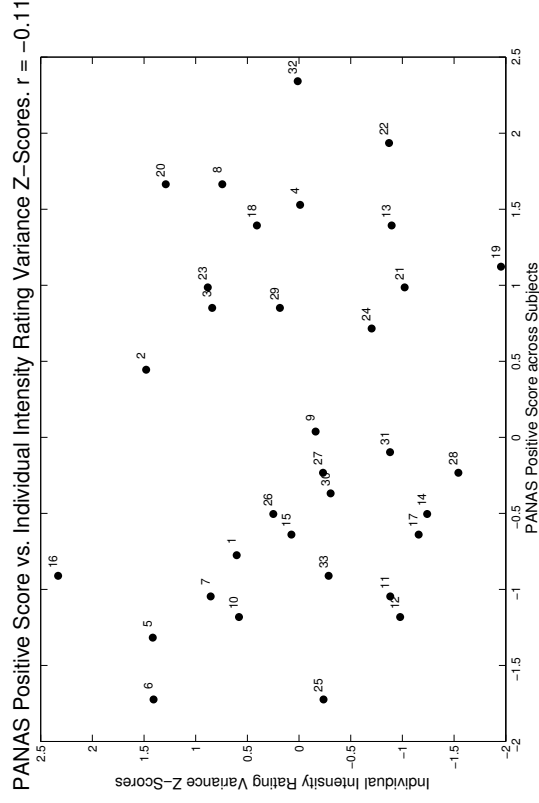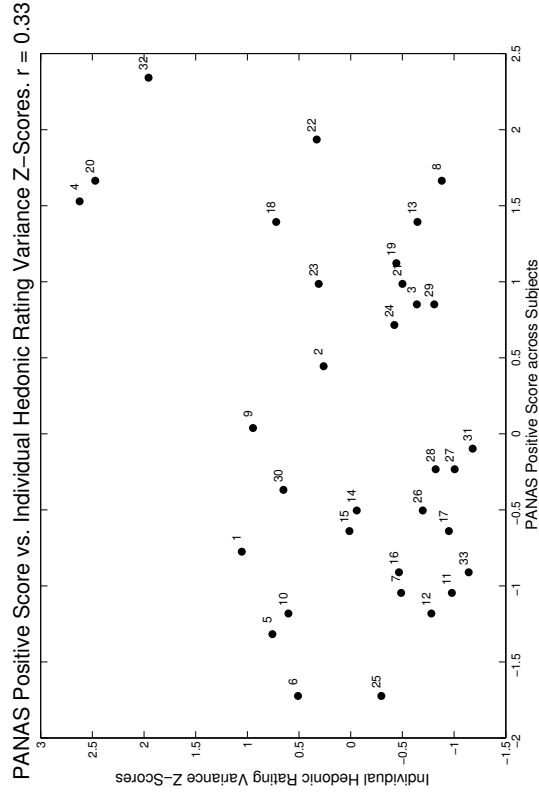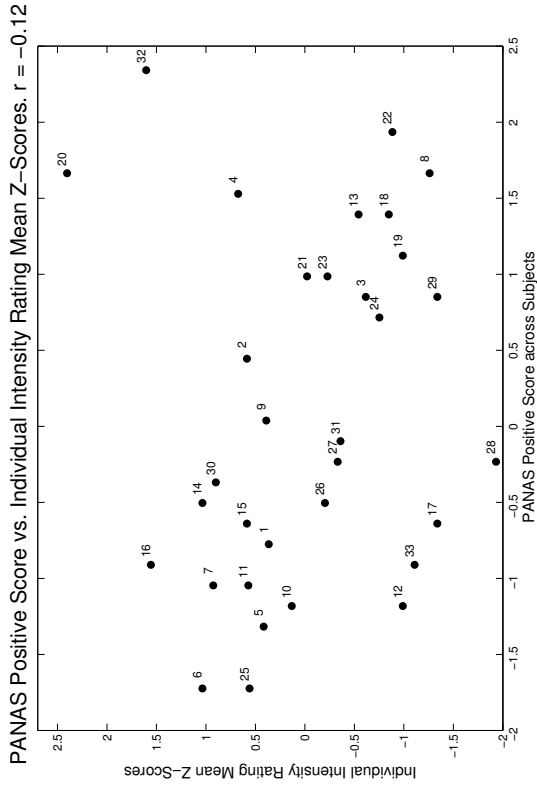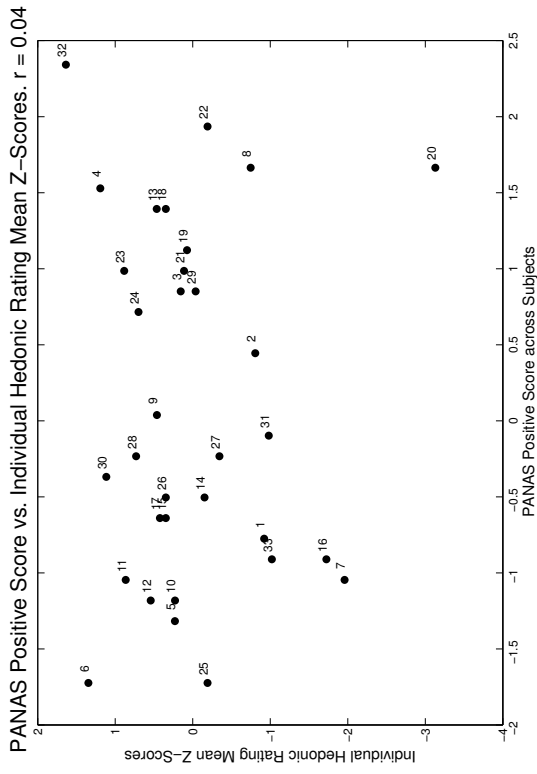
Figure 3.24: Relationship between the positive affect scores measured by PANAS and the standard scores of individual participants' rating patterns.
Positive affect scores are compared with hedonic rating means (top left), intensity rating means (top right), hedonic rating variance (bottom left), and intensity rating variance (bottom right). Each dot represents a participant, and is labeled with the participant number.
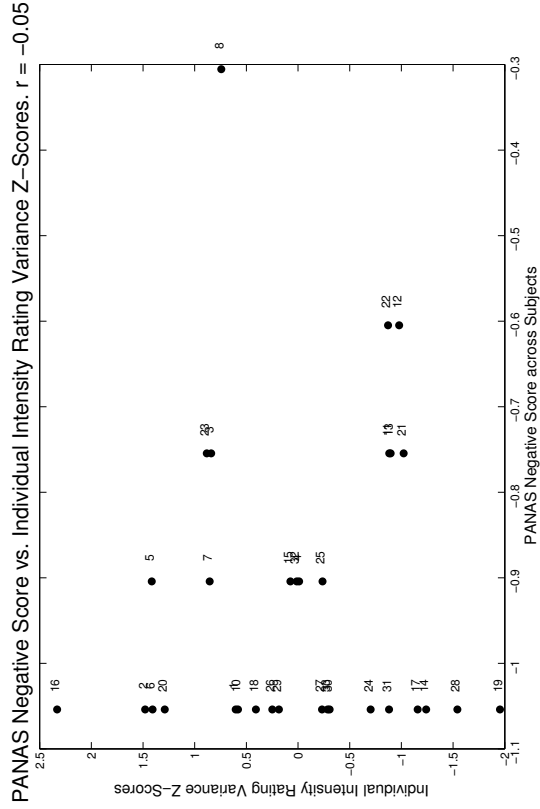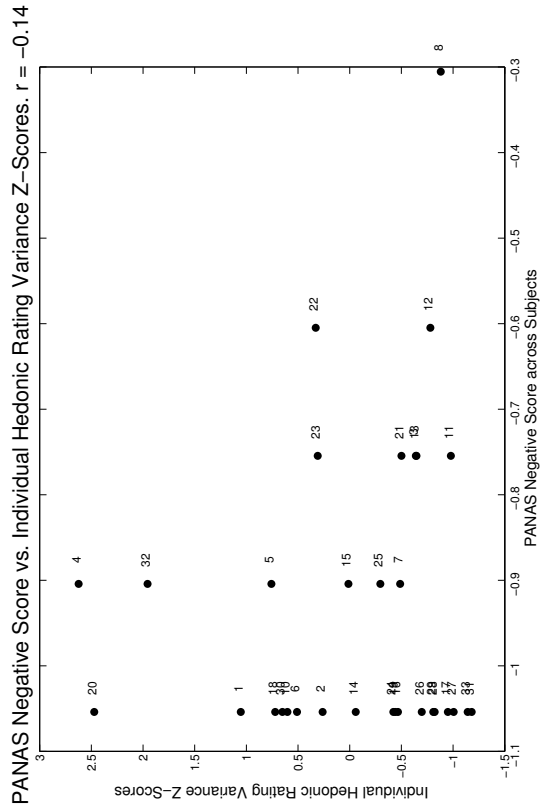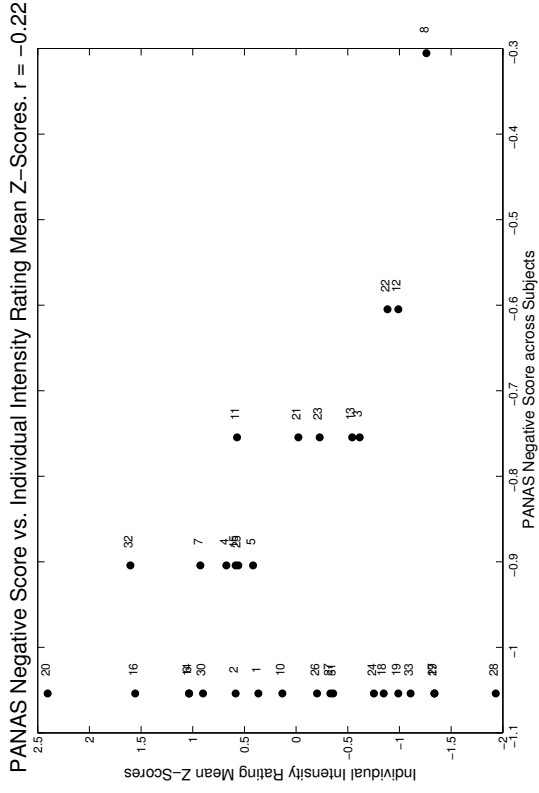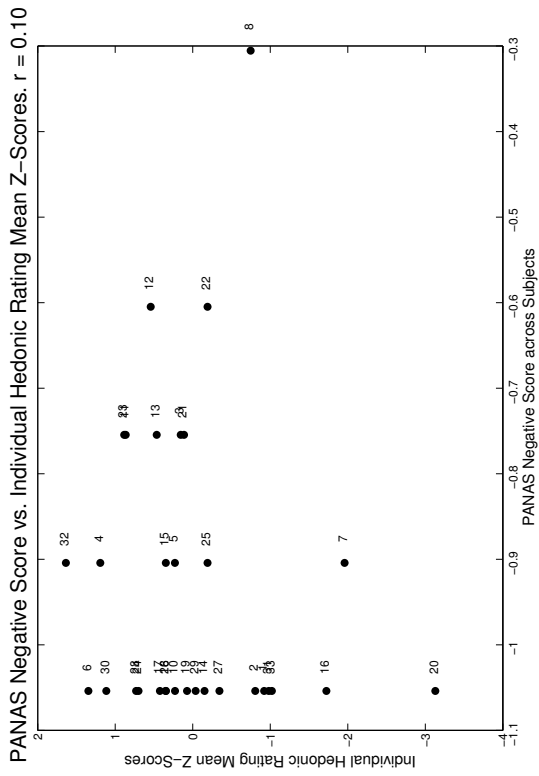
Figure 3.25: Relationship between the negative affect scores measured by PANAS and the standard scores of individual participants' rating patterns.
Negative affect scores are compared with hedonic rating means (top left), intensity rating means (top right), hedonic rating variance (bottom left), and intensity rating variance (bottom right). Each dot represents a participant, and is labeled with the participant number.

103
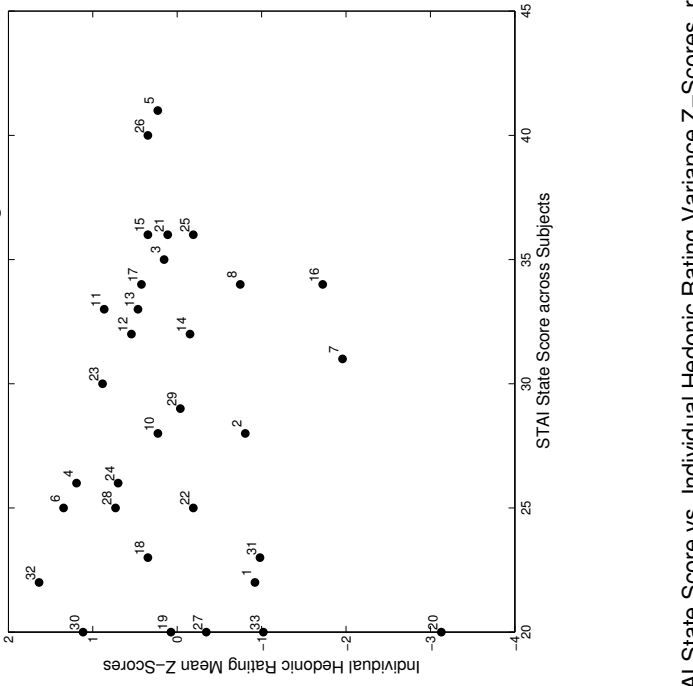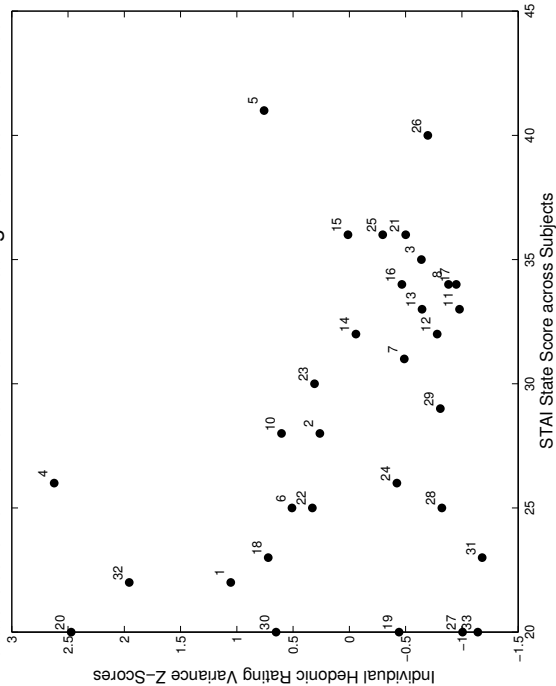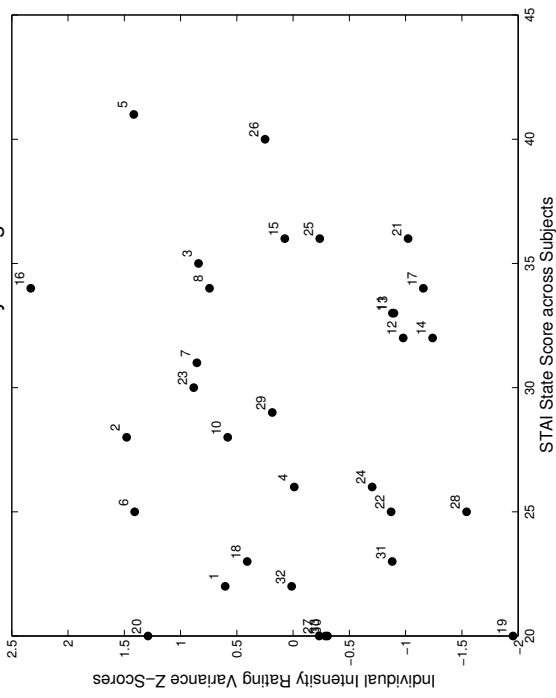
Figure 3.26: Relationship between the state anxiety scores measured by STAI and the standard scores of individual participants' rating patterns.
State anxiety scores are compared with hedonic rating means (top left), intensity rating means (top right), hedonic rating variance (bottom left), and intensity rating variance (bottom right). Each dot represents a participant, and is labeled with the participant number.
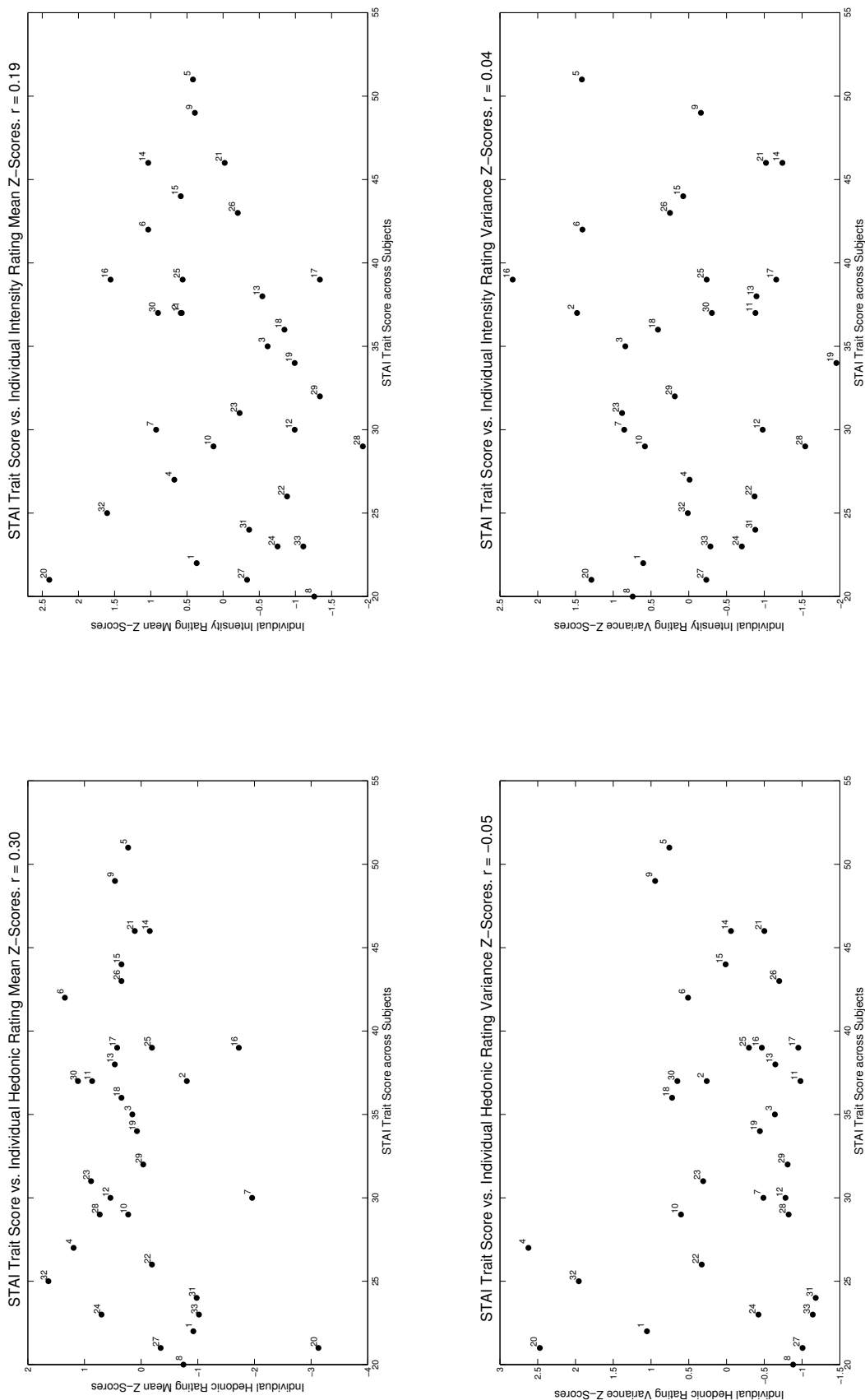
Figure 3.27: Relationship between the trait anxiety scores measured by STAI and the standard scores of individual participants' rating patterns.

Trait anxiety scores are compared with hedonic rating means (top left), intensity rating means (top right), hedonic rating variance (bottom left), and intensity rating variance (bottom right). Each dot represents a participant, and is labeled with the participant number.
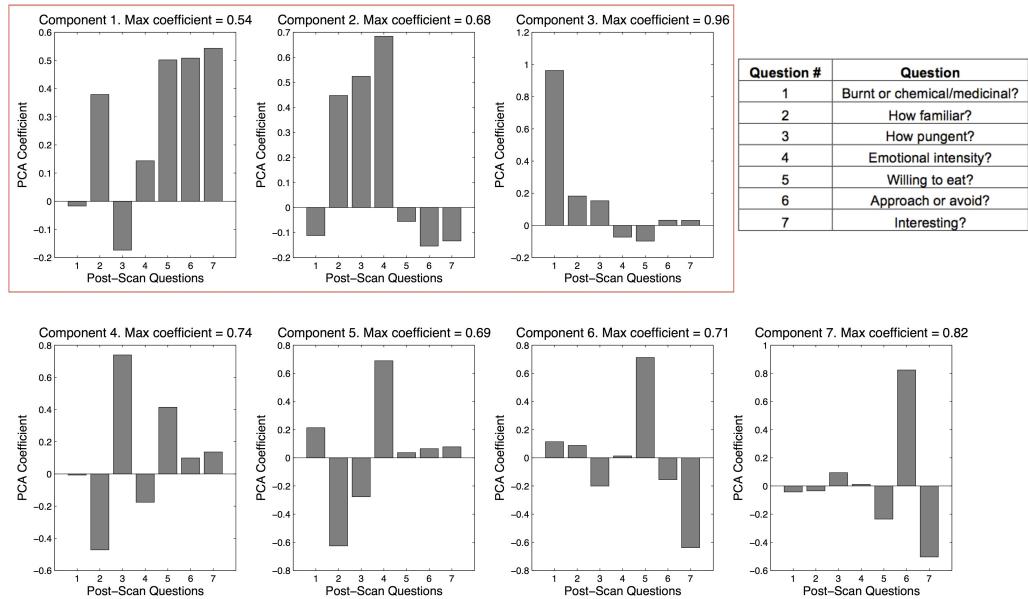
Figure 3.28: Results from PCA of out-of-scanner rating data.
The 3 main components are indicated by the red box. The table at the top right corner describes the out-of-scanner rating questions that correspond to the numbers shown on the x-axes of the bar graphs.

questions, a principal component analysis (PCA) was performed on all of the out-of-scanner ratings across all subjects. This process identified seven components (Figure 3.28), and the three strongest components were selected to be analyzed. Component 1 was most strongly represented by the questions, "how willing would you be to eat something that smells like this?," "would you move away from or toward something that smells like this?," and "is this odor interesting enough for you to want to smell it again?" Out of these questions, the one pertaining to the interesting-ness of the odor exhibited a slightly larger PCA coefficient, and because the three questions appeared to be rather similar to one another (all pointing to the hedonic value of the odor), the interesting-ness question was selected as the first question of interest. The second component was represented best by the question, "does this odor make you feel any intense emotions?," while the third component was formed almost solely by the question, "does this smell more burnt, or more chemical/medicinal?"

The rating distributions for the three questions of interest are shown in Figure 3.29,
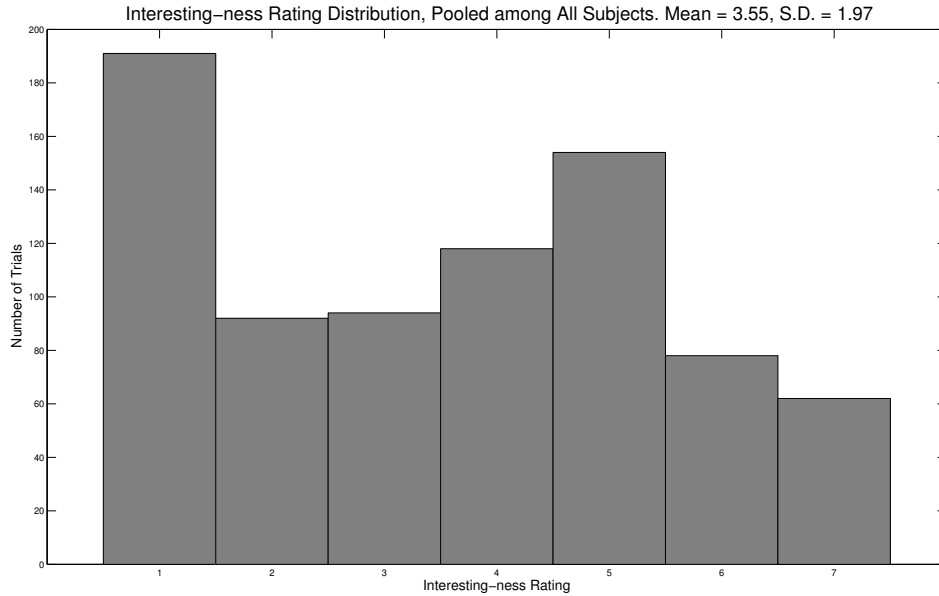
Figure 3.29: Distribution of interesting-ness ratings.

Figure 3.30, and Figure 3.31. The emotional intensity ratings (mean = 3.42, S.D. = 1.92) were somewhat evenly distributed along the entire scale of one to seven, except for a large peak at rating one ("did not feel any intense emotions"). A similar-looking distribution was observed for the question concerning the odors' interesting-ness (mean = 3.55, S.D. = 1.97), although this particular distribution exhibited a moderate peak at five, suggesting that while subjects found a large number of stimuli not interesting enough (possibly due to fatigue towards the end of the experiment) or found them too aversive to smell them again, there were still a good amount of stimuli that subjects did find rather interesting.

The "burnt vs. chemical" ratings were skewed toward the more chemical (toward seven) side of the scale (mean = 4.44, S.D. = 1.59), and the highest peak in the distribution was at the middle of the scale. This might possibly be that the majority of the odors that were used in this study, in fact, smelled more chemical than burnt. Although efforts were made in the beginning of the study to allocate roughly equal numbers of odorants to the four extremes of the putative principal axes of human olfactory map, there were still a number of odorants that might have been ambiguous
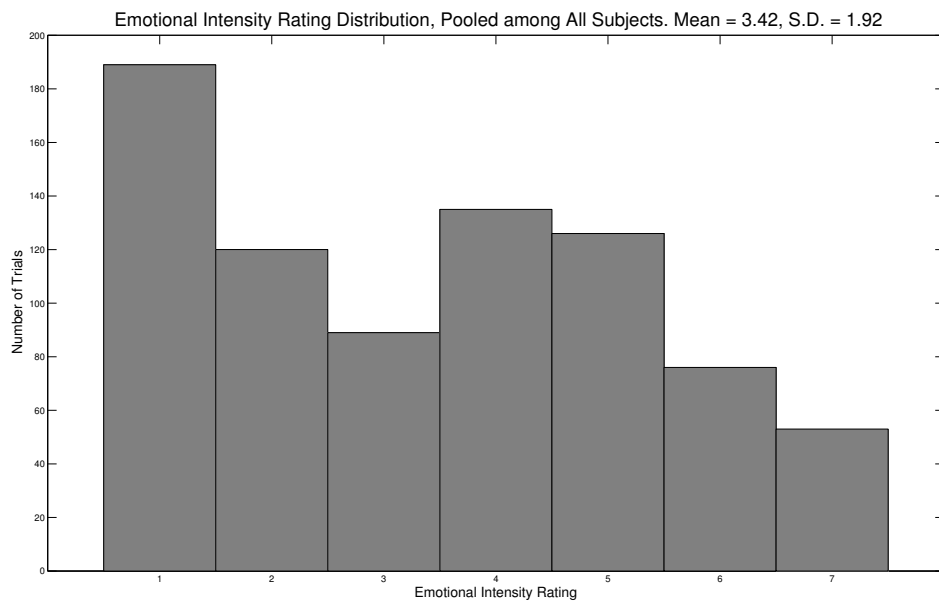
Figure 3.30: Distribution of emotional intensity ratings.
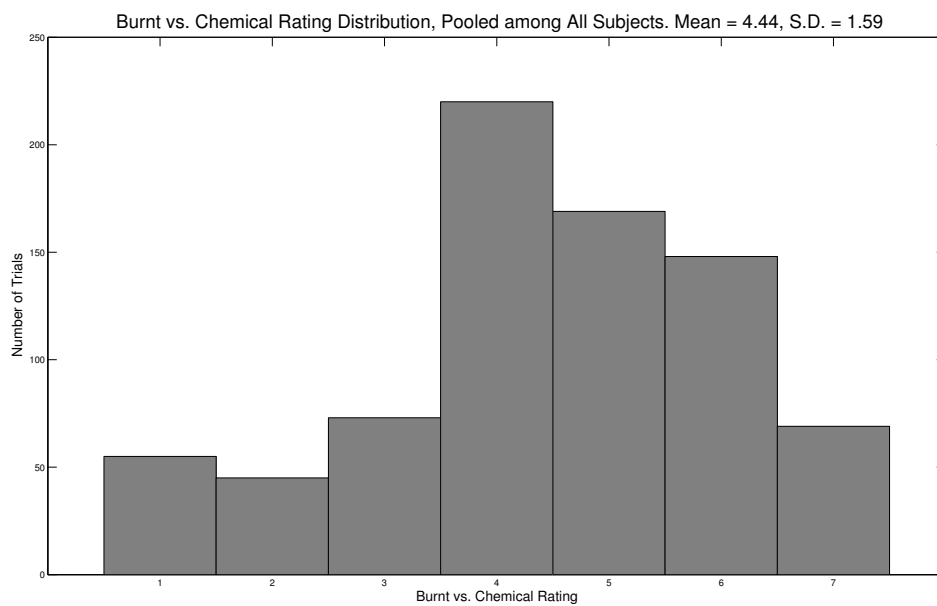
Figure 3.31: Distribution of "burnt vs. chemical" ratings.
On the rating scale of 1 - 7, 1 represents "definitely smells burned" and 7 represents "definitely smells chemical."

in terms of burnt- or chemical-ness (a number of participants commented after the experiment that this was a particularly difficult question for some of the odors), and many of the participants might have decided that they were mostly chemical, either because they are indeed slightly more chemical-like than burnt-smelling, or because subjects were somehow biased toward identifying odors as chemical-like.

To find any patterns in the three out-of-scanner ratings, for each question, each odor's group rating mean and its across-subject rating variance were plotted against each other. The resulting graphs (Figure 3.32) show a notable inverse correlation between the two for the "burnt vs. chemical" ratings (Pearson's correlation coefficient = -0.42), and a positive correlation for the emotional intensity ratings (correlation coefficient = 0.67). The former seems to suggest that while there is less consensus among participants on the odors that some has rated as closer to burnt-smelling (lower mean rating), the consensus is stronger for identifying odors as chemical-smelling. The latter suggests that higher emotional intensity is generally associated with larger individual differences, which is to be expected considering that a large component of emotional intensity would be based on one's memories and personal experiences.

3.4.2   Neuroimaging Data

3.4.2.1   Whole Brain Analysis

a. Effect of Odor Perception

To gain neurological evidence that subjects were indeed receiving and perceiving the odor stimuli, three simple models assayed for the effect of odor perception:

1. a model in which the "odor release" times of the trials that subject has rated as perceptible (intensity score higher than one) were contrasted against those of the trials rated as non-perceptible (intensity score of one)
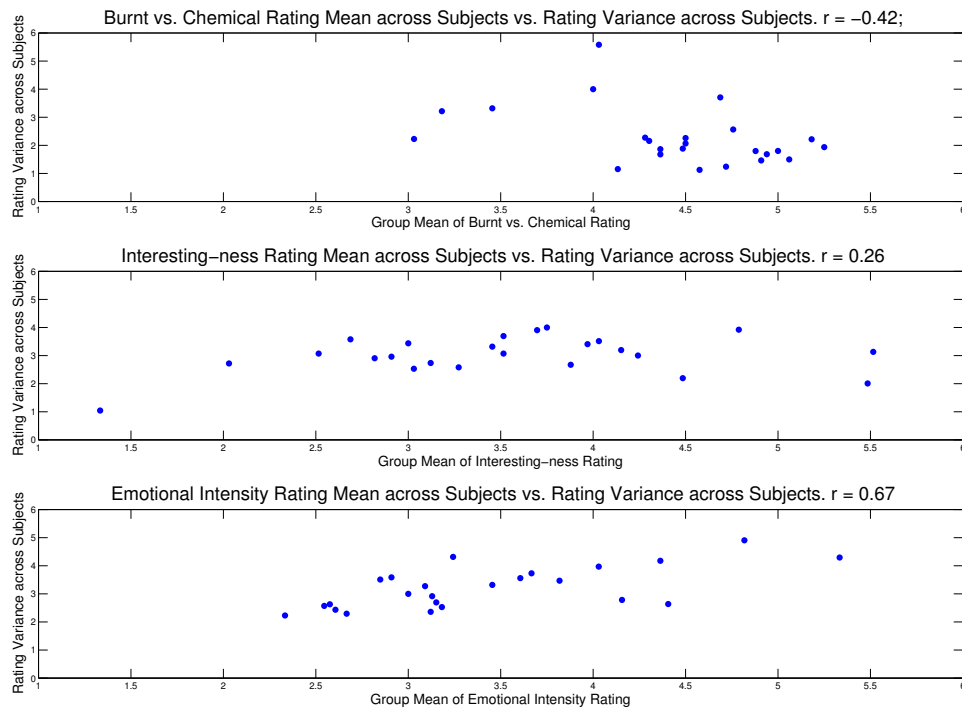
Figure 3.32: Relationship between individual odors' rating means and variances across all subjects for the three main out-of-scanner questions. Each dot represents an odor.

2. a model in which the "odor release" times for any non-blank stimuli, regardless of subject rating, were contrasted against those of the blank trials

3. a model in which the "odor release" times for the stimuli rated as relatively strong (intensity score higher than four) were contrasted against those of the stimuli rated as weaker (intensity score lower than four).

For each model, two effects were computed:

1. the effect of odor perception (for model one), non-blank odor stimulation (for model two), or stronger odor stimulation (for model three)

2. a contrast in which the non-perceptible/blank/weaker odors' effects were subtracted from those of perceptible/non-blank/stronger odors.

The above models and contrasts were computed for passive as well as active runs,

by directly applying the intensity ratings from the active runs to the corresponding trials in the passive runs.

The resulting group-level clusters from the three models were remarkably similar, indicating that our analysis methods were not able to clearly distinguish the subtle differences among them. Hence in this thesis, only the results from the first model will be discussed.

Table 3.5 and Figure 3.33 illustrate the locations and sizes of the clusters discovered in the two effects described above, from the group-level passive, active, and [passive + active] conjunction analyses. The effect of simple perception of odors (Figure 3.33(a)), as expected, is quite global, with strong bilateral signals in the OFC, the entire insula including the FI, and the piriform cortex, all of which have been, as discussed earlier in the Introduction, implicated in perceiving odors. The very large activation in the visual areas are most definitely from the visual cue, "Odor is being released," which was shown to participants during the nine-second olfactory stimulation windows. It is also possible that the brightness of the rating screen, which immediately followed the odor release window during the active runs, might also have contributed to this effect. The signals in the posterior cingulate cortex (PCC) and the angular gyrus may reflect the attentional state of participants during the smelling task. When the effect of not being able to detect the stimulus is subtracted from these signals (Figure 3.33(b)), only the signals in the left posterior OFC, bilateral dorsal amygdala, and bilateral posterior FI remain.

b. Valence-Specific Hedonic Effect

In order to investigate the effect of the odors' hedonic values, a simple model comparing three valence groups — non-blank odors that were rated as positive (hedonic value rating higher than zero), neutral (hedonic value rating of zero), and negative (hedonic value rating lower than zero) — were contrast against one another. Table 3.6 and Figure 3.34 describe the significant clusters discovered from these contrasts: although the [negative - neutral], [positive - negative], and [negative - positive] con-
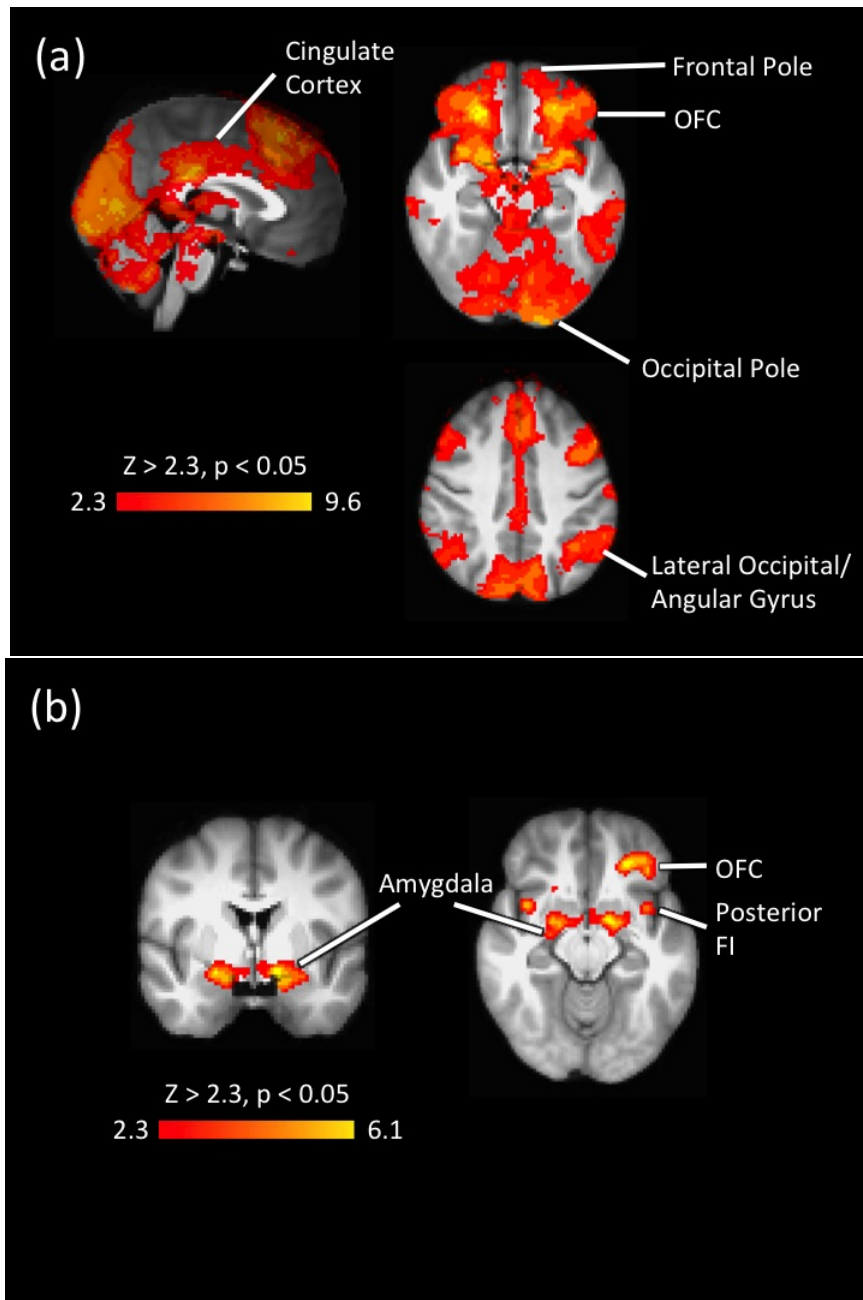
Figure 3.33: Clusters of Significance from the Effect of Odor Perception (a) and the [Odor Perception - Odor non-perception] Contrast (b).

Region	Hemisphere	Number of Voxels	p-Value	Peak MNI Coordinates		
				x	y	z
Effect of Odor Perception Alone						
Lateral occipital cortex; angular gyrus	Right	1097	3.77e-05	50	-60	40
Lateral occipital cortex; angular gyrus	Left	2568	5.01e-10	-44	-54	52
A large cluster including the frontal pole; OFC; whole insula including FI; piriform cortex; cingular cortex	Both	72006	0	22	34	-16
[Odor Perceived - Odor Not Perceived] Contrast						
Posterior OFC	Left	437	0.00488	-26	36	-12
Amygdala; piriform cortex	Right	554	0.00085	22	0	-14
Amygdala; piriform cortex	Left	608	0.000395	-14	0	-12

Table 3.5: List of Clusters from the Whole-Brain Odor Perception Effect Analysis.

trasts yielded over-the-statistic-treshold results, the [positive - neutral] contrast did not survive the analysis. This appears to be due to the relatively small numbers of the positively and neutrally rated trials.

The results of the [negative - neutral] contrast (Figure 3.34(a)) suggest activations in the FI, left OFC, and the amygdala, all of which were also observed to be active in the [odor perception - non-perception] contrast. However, while the previous contrast has shown signals in bilateral posterior FI, a smaller portion of the left OFC, and bilateral amygdala, the present effect implicates a slightly different pattern: the right FI, left OFC, and left amygdala might contribute more strongly to the processing of unpleasant odors compared to their contralateral counterparts, and the OFC signal is spread to larger, more bilateral areas. The FI signal is also larger in the present effect, spanning most of the region.

The signals yielded from the [positive - negative] contrast (Figure 3.34(b)) seems to indicate increased readiness to the rating task in pleasant-odor tasks compared to negative-odor ones, as they arise from the areas related to action planning and memory.

The [negative - positive] contrast (Figure 3.34(c)) seems to provide results that are consistent with those of the [negative - neutral] contrast: the FI signal is much

Region	Hemisphere	Number of Voxels	p-Value	Peak MNI Coordinates		
				x	y	z
[Negative - Neutral] Contrast						
Lingual gyrus	Left	468	0.00542	0	-72	2
FI; OFC	Both	1709	5.87e-09	38	12	-12
Superior frontal gyrus; ACC	Both	3262	1.63e-14	8	14	62
Amygdala	Left	3517	2.48e-15	-20	-4	-12
[Positive - Negative] Contrast						
Primary somatosensory; motor cortex	Left	300	0.0415	-36	-26	66
Frontal pole	Right	458	0.00303	2	70	12
Precuneous; posterior cingulate cortex	Right	467	0.00263	4	-60	30
Parahippocampal gyrus	Right	569	0.000572	34	-28	-28
Medial primary somatosensory; motor cortex	Both	830	1.65e-05	2	-28	62
[Negative - Positive] Contrast						
Posterior frontal pole	Left	293	0.0469	-22	54	32
Intracalcarine cortex/primary visual cortex	Left	795	2.59e-05	-14	-74	10
Inferior frontal gyrus, pars opercularis; lateral FI	Left	1043	1.19e-06	-58	10	6
Supramarginal gyrus	Right	1325	5.96e-08	66	-28	34
Supramarginal gyrus	Left	1668	1.3e-09	-64	-52	36
Superior frontal gyrus	Right	2951	1.03e-14	18	2	76
Inferior frontal gyrus, pars opercularis; lateral FI	Right	3259	8.13e-16	42	32	4

Table 3.6: List of Clusters from the Whole-Brain Hedonic Valence Analysis.

stronger in the right hemisphere than in the left, and the ACC and superior frontal gyrus activations are still present. The main notable difference between the two effects is that the medial and anterior FI and bilateral OFC signals are not present in the [negative - positive] contrast. This could possibly be construed as an indication that the medial/anterior FI and the OFC are engaged in processing of both pleasant and unpleasant types of stimuli, and not as strongly involved in computing neutral hedonic sensations.

c. Parametric Effect of Subjective Hedonic Value

A parametric model was built to explore the parametric effect of subjects' hedonic ratings on the neural signals. To achieve this, an explanatory variable (EV) listing the onset and duration of all non-blank odor stimuli's release times were added to the model. The EV also described, as the amplitude of each trial, the normalized
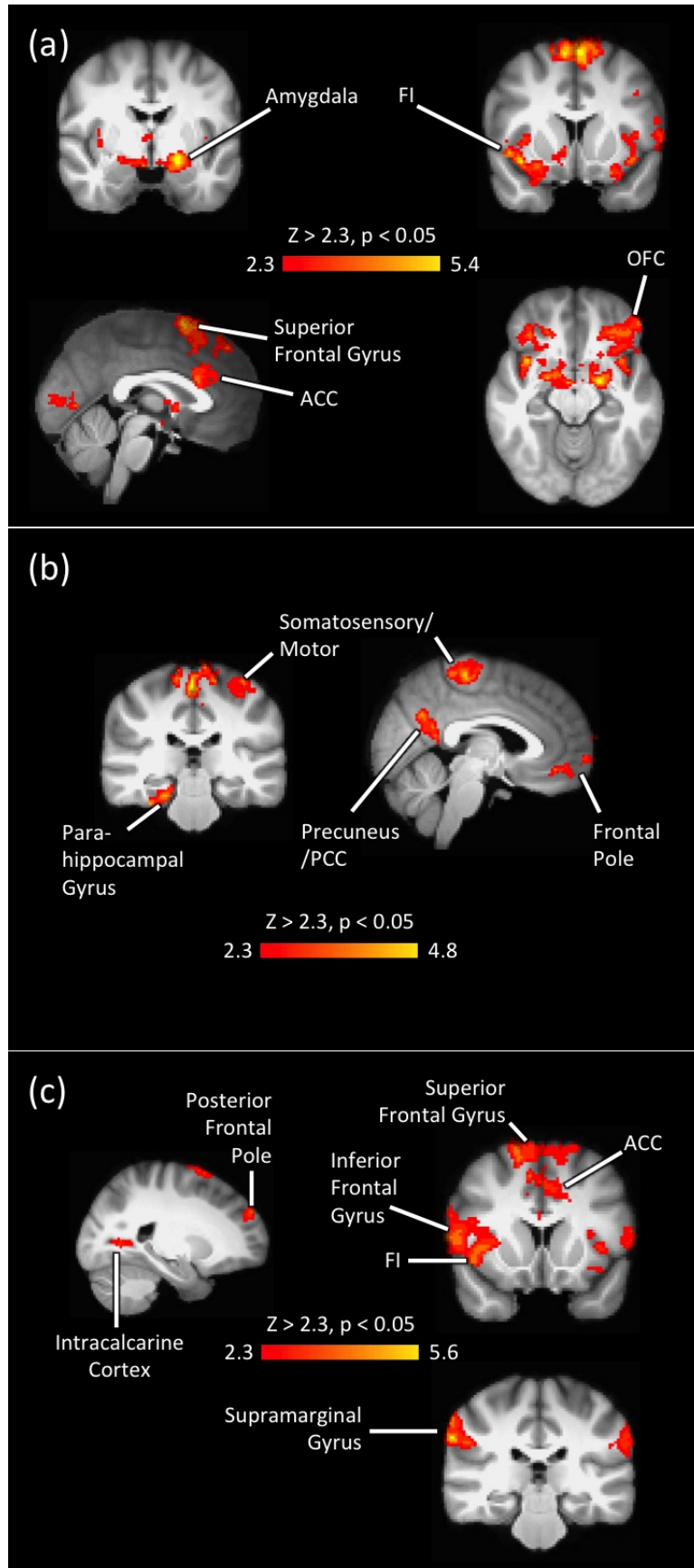
Figure 3.34: Clusters of Significance from the Effect of [Negative - Neutral] (a), the [Positive - Negative] (b), and [Negative - Positive] (c).

value of its hedonic rating. This third parameter modeled the effect of increasing and decreasing subjective hedonic ratings. Table 3.7 and Figure 3.35 present the clusters discovered from the analysis.

The FI signal found here is especially interesting, given the context of the previously discussed contrasts. Unlike the negative-valence contrasts, in which the right FI activation is observed, the present contrast yielded a left FI activation, which suggests that negative-valence odors are mainly processed in the right FI, while the left FI's contribution increases as the odor becomes more pleasant. Also, the left FI signal is observed in the area's lateral and posterior portion, which is consistent with the possibility, postulated earlier, that the medial/anterior FI might be involved in processing the magnitude, but not the direction, of odors: since our parametric model heavily takes into account the sign of the hedonic rating, it makes sense that any regions processing only the magnitude would not survive the analysis. This is also consistent with the lack of OFC signals in the parametric model results.

The parametric effect is also consistent with that of the [positive - negative] results, with signals from the ACC and the frontal pole present in both sets of results. It is surprising that the rest of the parametric effects also did not appear in the [positive - negative] effect, but this may be due to the decreased sensitivity of the latter model to smaller variations among different hedonic value signals.

d. Parametric Effect of Subjective Intensity Value

In the same parametric model discussed above, another EV, fashioned similarly to the hedonic value EV and delineating instead the normalized intensity value of each non-blank trial, was included to model the increasing and decreasing effects of perceived intensity. The resulting clusters are listed in Table 3.8. As one can observe in Figure 3.36, the increasing effect of odor strength seems mostly encoded by the posterior OFC (more or less consistent with the [odor perception - non-perception], which showed a signal in the left posterior OFC) and bilateral anterior insula including the FI, with perhaps a slight bias toward the left hemisphere. This effect also includes activations

Region	Hemisphere	Number of Voxels	p-Value	Peak MNI Coordinates		
				x	y	z
Effect of Increasing Hedonic Value						
Anterior cingulate cortex; paracingulate	Both	464	0.00123	14	36	20
Lateral frontal pole	Both	1841	2.53e-11	-48	42	12
A very large bilateral cluster including occipital pole; occipital fusiform gyrus; lateral occipital cortex; supramarginal gyrus; superior temporal gyrus; posterior cingulate cortex; inferior frontal gyrus; dorsal anterior insula; lateral/posterior FI; putamen; claustrum; periaqueductal gray; parts of cerebellum	Both	58673	0	-8	-102	-8
No effects of decreasing hedonic value survived.						

Table 3.7: List of Clusters from the Whole-Brain Hedonic Parametric Analysis.
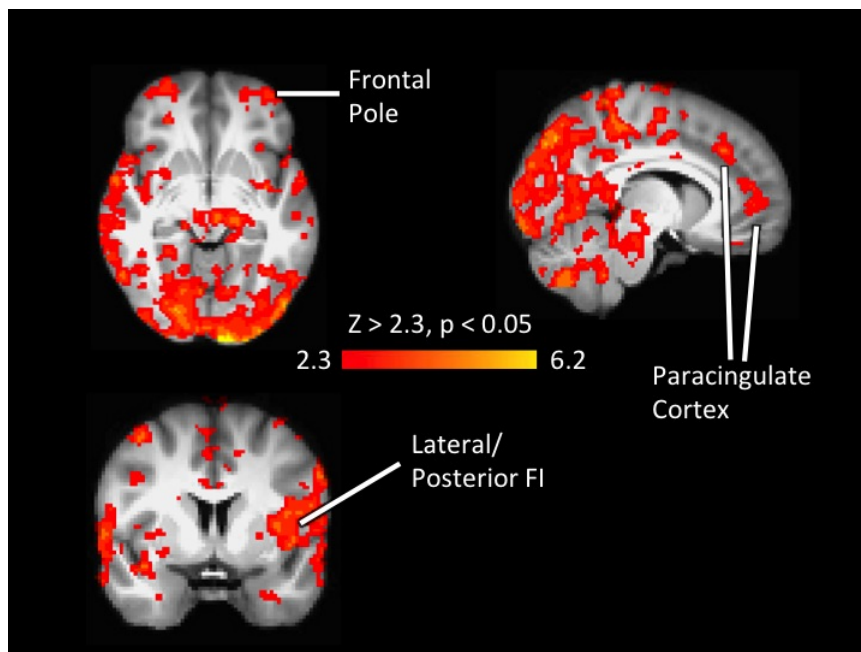
Figure 3.35: Clusters of Significance from the Effect of Increasing Hedonic Value.

Region	Hemisphere	Number of Voxels	p-Value	Peak MNI Coordinates		
				x	y	z
Effect of Increasing Intensity						
Primary somatosensory cortex	Both	627	0.000187	-66	-20	34
Dorsal AI; FI	Both	2131	7.2e-12	-30	28	4
Paracingulate gyrus; ACC; supplementary motor cortex	Both	2293	1.56e-12	-2	14	44
Inferior frontal gyrus; posterior OFC; frontal operculum	Both	3257	3.24e-16	44	28	4
Occipital pole	Both	4614	7.93e-21	-8	-100	-12
Effect of Decreasing Intensity						
Frontal pole	Left	553	0.000556	-38	56	-8
Middle frontal gyrus	Right	810	1.5e-05	40	30	48
Angular gyrus; lateral occipital cortex	Right	834	1.1e-05	48	-52	18

Table 3.8: List of Clusters from the Whole-Brain Intensity Parametric Analysis.

in the paracingulate gyrus, ACC, and the supplementary motor cortex, which might reflect increased readiness for judgment in stronger odors with less ambiguity involved. On the other hand, the effect of decreasing odor intensity seems to suggest increased mental effort in thinking about weaker odors.

e. Other Models Examined

In addition to the four main models described above, three more parametric models were utilized to investigate the effects of increasing and decreasing interesting-ness, emotional intensity, and the burnt-or-chemical-like quality of the odors, as rated during the out-of-scanner tasks. Unfortunately all but the "decreasing emotional intensity" model failed to provide notable activation clusters that appear convincing, and the clusters that did survive the significance threshold are documented here (Table 3.9, Figure 3.37). Both of the clusters resulting from this analysis are located in the frontal pole, which may indicate a sort of increased cognitive processing related to reduced emotional immersion in the stimulus.

f. Parametric Model with Sensory Classification Regressors

Given the rather noisy data provided by the hedonic value parametric model described above, a new attempt was made during revision of this thesis to improve the data
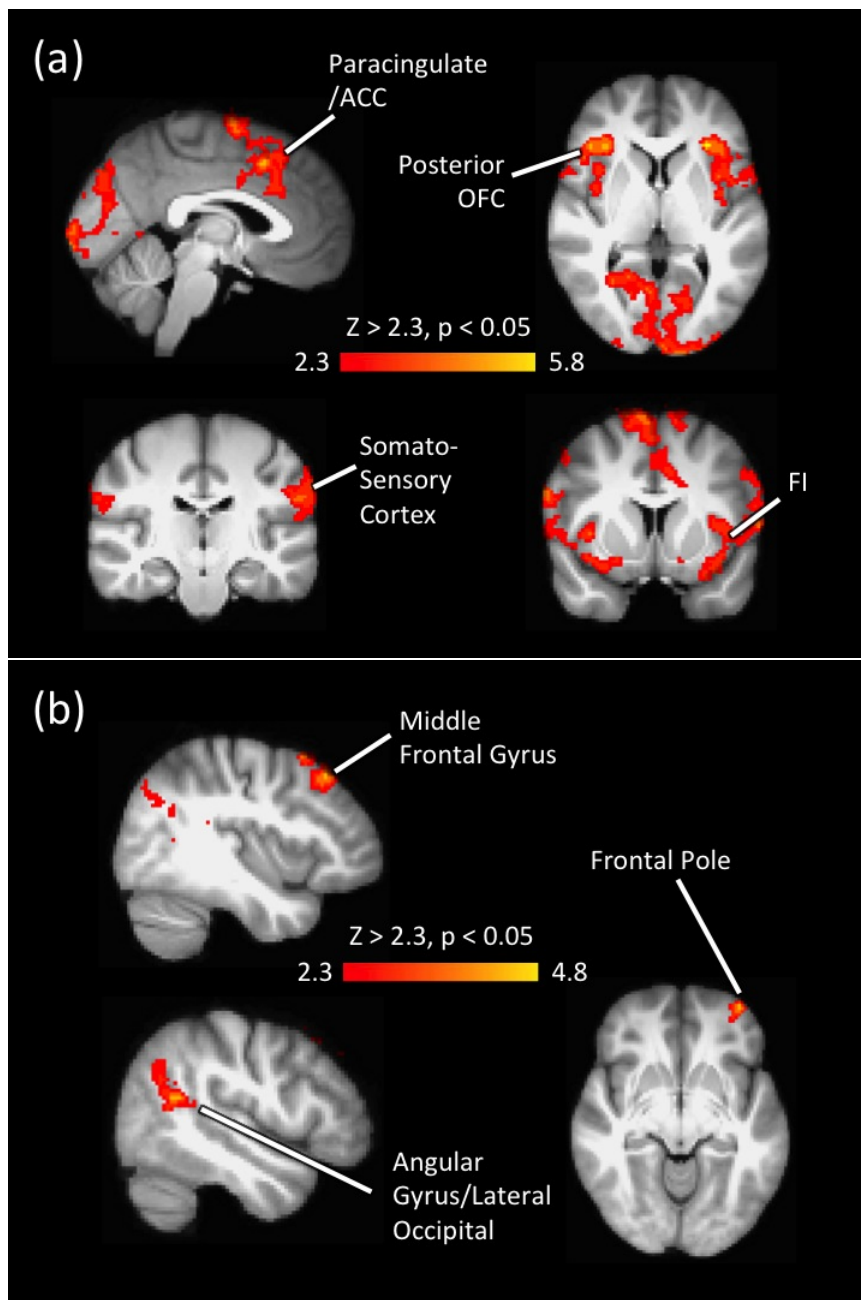
Figure 3.36: Clusters of Significance from the Effect of Increasing (a) and Decreasing (b) Odor Intensity.

Region	Hemisphere	Number of Voxels	p-Value	Peak MNI Coordinates		
				x	y	z
Effect of Decreasing Emotional Intensity						
Frontal pole	Right	344	0.0165	34	50	-10
Superior/posterior frontal pole	Right	451	0.00277	36	44	34

Table 3.9: List of Clusters from the Whole-Brain Emotional Intensity Parametric Analysis.
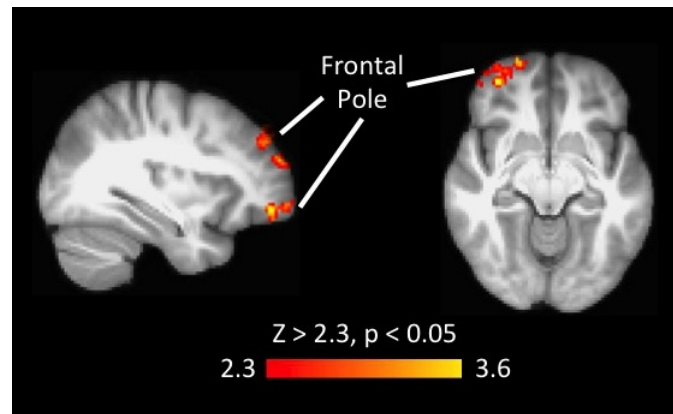
Figure 3.37: Clusters of Significance from the Effect of Decreasing Emotional Intensity.

quality. This was done by taking each odor stimulus in all imaging runs into one of the following 4 sensory categories, defined by the putative human olfactory perception space described earlier in this chapter:

1. Odors that were rated as pleasant and chemical

2. Odors that were rated as pleasant and burnt

3. Odors that were rated as unpleasant and chemical

4. Odors that were rated as unpleasant and burnt

The categorized odors then were included in the parametric model as regressors, with each category serving as one regressor. The expectation was that these regressors would help clean up the results of the hedonic value parametric model by controlling for the different sensory features in the data.

The results, however, suggested that the 4 regressors absorbed the majority of the neural signals being modeled, as most of the models did not yield any statistically viable results. While the models for the increasing hedonic value, decreasing intensity value, and decreasing interesting-ness yielded activation patterns that were somewhat similar to those from the old parametric models, no signals survived for all of the other parametric models.

g. Differences between Passive and Active Runs in Whole-Brain Analysis Results

For each of the whole-brain analysis models described above, group-level contrasts investigating the activation pattern difference between the passive and active runs were computed. We initially hypothesized that the active runs would in general exhibit stronger effects related to hedonic value and intensity judgements, as subjects had been instructed to explicitly think about these factors during active runs. On the other hand, we expected the passive runs to provide a richer dataset pertaining to the other qualities of the odors, as subjects had been asked to experience each stimulus as a whole, rather than focusing on its hedonic quality and strength.

The results of the contrasts, for most of the models, were either null in both directions, or null in the [passive - active] contrasts and consisting entirely of visual area and cerebellar signals in the [active - passive] contrasts. This indicates that the ratings screens in the active runs, which are much brighter than the cue screens shown in the passive runs, greatly increased the activity in participants' visual areas, and that some of this effect, along with some motion-induced cerebellar signals, was introduced to our analysis in the BOLD modeling process. The result also suggests participants' experiences were not significantly different between the passive and active runs. Consistent with this observation, the majority of participants reported, in a quick scan de-briefing questionnaire, automatically thinking about the hedonic quality and intensity of odor stimuli even during the passive runs, for which they had been instructed not to think specifically about these two factors.

The only contrasts that yielded real differences between the two session types were:

1. The simple effect of odor perception, in which [passive - active] resulted in a large cluster in the medial frontal pole and the anterior cingulate, and [active - passive] provided small clusters in the inferior frontal gyrus as well as the visual and cerebellar ones

2. The [odor perception - non-perception] contrast, in which the active run did not have any surviving clusters

3. The decreasing effect of odor intensity, in which [passive - active], interestingly, yielded visual and motor areas and [active - passive] did not provide any clusters (the model design was double-checked to make sure that this was not due to a simple mistake).

3.4.2.2   ROI Analysis

a. Insular Regions

In order to further investigate the neural signals by taking into account those that did not make the cluster threshold, we performed region of interest (ROI) analysis utilizing a set of 23 brain area masks (20 of which were used in the original draft of this thesis, and 13 of which were used in the revision). First, a set of nine insular ROIs were defined and their degrees of signal change were observed. Table 3.10 lists each insular ROI's name, number of voxels, sources from which it was derived, and the motivation for including or excluding the ROI in or from the analysis. Figure 3.38 illustrates the ROIs' locations by overlaying them onto an anatomical brain image. While the whole insula ROI was derived directly from the atlas built in FSL and trimmed to better fit the region, the whole FI ROI was defined by hand by an expert of FI anatomy (John Allman). The medial and lateral FIs were then defined by dividing the FI mask into half. The non-FI insular ROI was created by simply

subtracting the whole FI ROI from the whole insula mask. The four functionally derived areas — implicated in processing of empathy, olfaction, emotion, and pain — have been derived in a meta-analysis of 1768 insular functional imaging studies by Kurth et al. (Kurth et al. 2010), which identified various functional clusters in the insula. Out of the many different categories of insular functions treated in this meta-study we only selected the four, as they appeared to be related to hedonic value evaluation. The functions of interest were generated by taking the peak MNI coordinates of the clusters shown in the paper, entering them to the standard MNI image, and creating small spheres around the peak voxels, such that they sufficiently covered the areas of interest, and did not significantly encroach upon neighboring areas. Note that the "conventional analysis" clusters — those including voxels that might not be specific to one type of function — rather than the "specific analysis" clusters — those consisting of voxels that only belong to one functional category — were employed in the present study as ROIs, as most of the specific analysis regions appeared to be too small for effective analysis.

In the initial ROI analysis performed for the original draft of this thesis ("Original Analysis"), each region was first defined in both hemispheres and analyzed for % signal changes in both active and passive runs. Then each ROI was divided according to hemisphere, and separately analyzed. The resulting hemisphere-specific results were then analyzed for any significant effect of the hemispheric or active/passive difference. During the revision of this thesis, the ROI analysis was re-perfomed ("Revised Analysis") using a similar approach, but using raw signal change values rather than % signal signal changes, and treating the passive and active runs separately throughout the assay. Also, a slightly different set of ROIs was used for the revised analysis.

b. Insular Regions - Original Analysis Results

The results of the non-hemisphere-specific analyses suggest that while the activation patterns of the whole insula, FI, and non-FI insula are overall similar, there is a small

Region	Hemisphere	Number of Voxels	Source	Reason for Inclusion
Whole Insula	Both	2501	Harvard-Oxford Atlas	To assay olfactory value processing in the insula, regardless of categories within the region
Medial FI	Both	591	Drawn by Expert	To test for any differences between medial and lateral FIs
Lateral FI	Both	582	Drawn by Expert	To test for any differences between medial and lateral FIs
Whole FI	Both	1173	Drawn by Expert	To study FI's role in olfactory hedonic value processing
Non-FI Insula	Both	1913	Whole Insula - FI	To distinguish between olfactory value processing in FI and the part of the insula that excludes the FI
"Empathy Areas"	Both	172	Kurth et al. 2010	To test whether the putative "empathy-processing areas" also participate in olfactory value processing, as positive and negative valences tend to be strongly implicated in feelings of empathy
"Olfaction Areas"	Both	66	Kurth et al. 2010	To test whether the putative "olfaction-processing areas" also participate in olfactory value processing, among other olfactory functions
"Emotion Areas"	Both	165	Kurth et al. 2010	To test whether the putative "emotion-processing areas" also participate in mediation of olfactory evaluation, among other emotional experiences
"Pain Areas"	Both	99	Kurth et al. 2010	To test whether the putative "pain-processing areas" also participate in olfactory value processing, as pain can be categorized as a type of negative hedonic experience

Table 3.10: List of Insular ROIs.
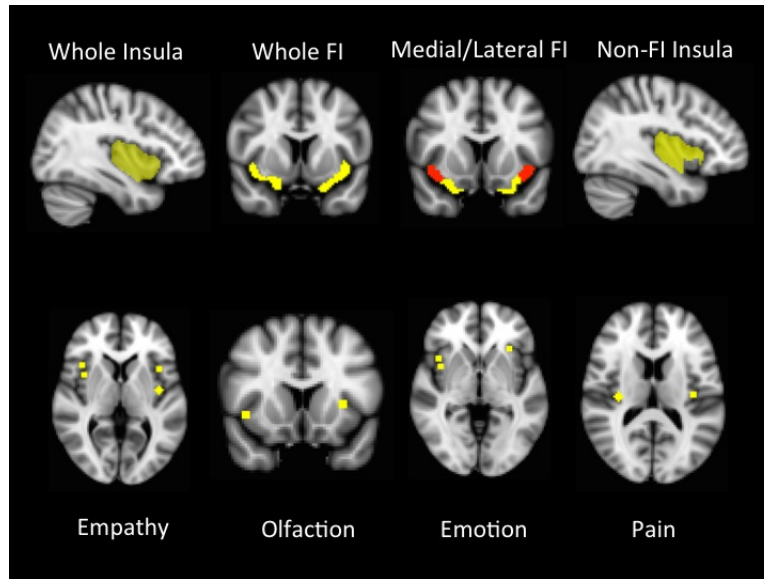
Figure 3.38: Insular ROIs Used.

trend in which the FI distinguishes itself from the other two regions by exhibiting slightly higher levels of signal induced by the [negative - neutral] contrast (Figure 3.39). The FI also marginally differed from the two other regions' signal patterns by being more attenuated in the hedonic value parametric model, and slightly more active in the model of increasing emotional intensity. This serves as a small piece of evidence that while the insula as a whole is somewhat sensitive to the hedonic and intensity values of odor stimuli, the FI by itself presents a unique processing pattern that seems more highly tuned to their noxious and emotional qualities.

The other insular regions' ROI analysis results were very comparable to the data shown in Figure 3.39, and hence will not be discussed here. The pain-related insular ROI, though, exhibited a very different pattern, with a rather high level of positive signal change with increasing hedonic values of odors, a moderate level of negative signal change in reaction to decreasing interesting-ness, and no notable signal changes for the other effects (Figure 3.40). This is surprising, since one would expect an area normally active while receiving pain or viewing other people's painful experiences to be more sensitive to decreasing hedonic values, rather than increasing.

The hemisphere-specific assay did not demonstrate any statistically significant differ-
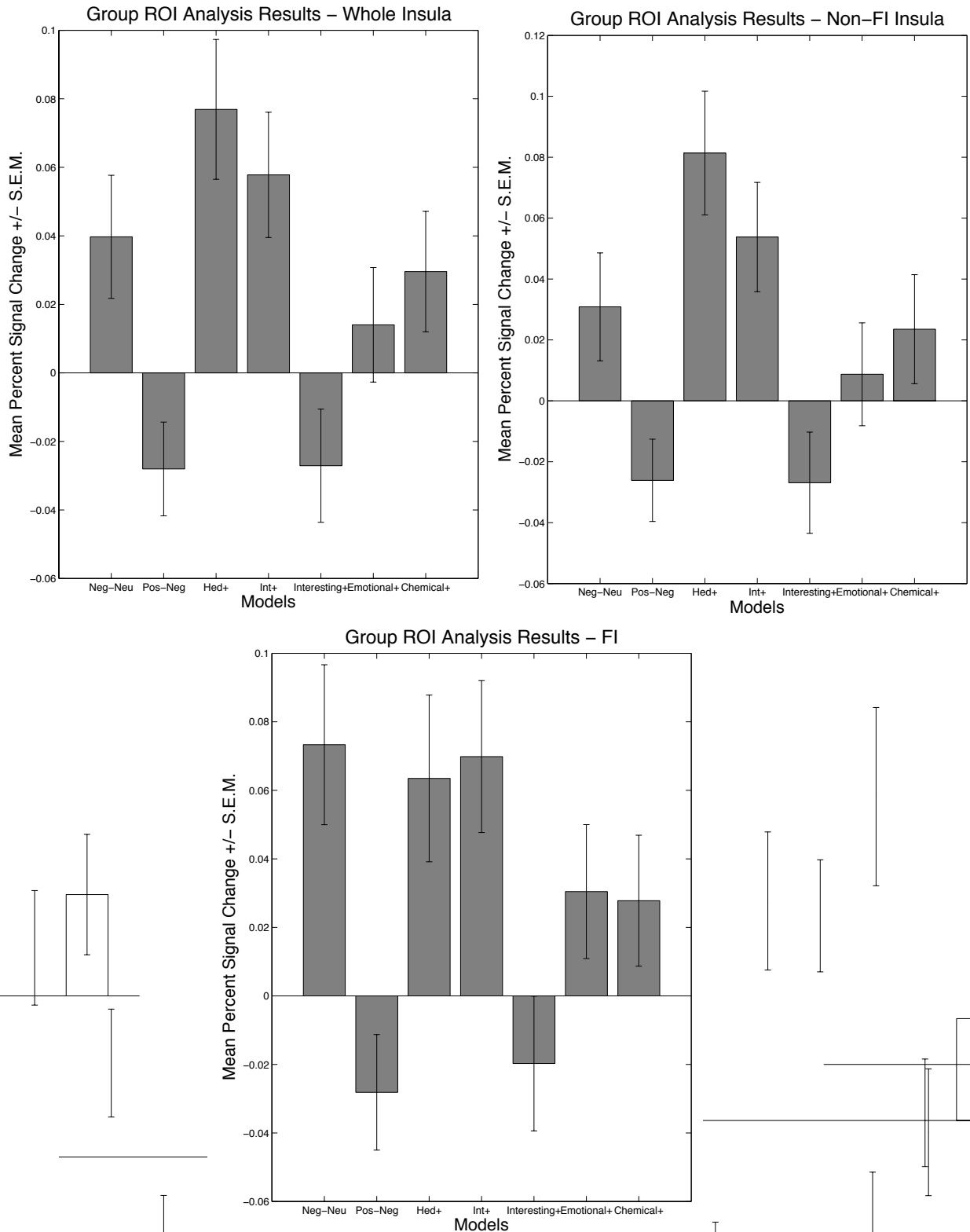
Figure 3.39: Partial Results of Insular ROI Analyses, Non-Hemisphere-Specific. Models: Neg-Neu = [Negative - Positive]; Pos-Neg = [Positive - Negative]; Hed+ = Effect of Increasing Hedonic Value; Int+ = Effect of Increasing Intensity Value; Interesting+ = Effect of Increasing Interesting-ness; Emotional+ = Effect of Increasing Emotional Intensity; Chemical+ = Effect of Increasing Chemical-like Quality.
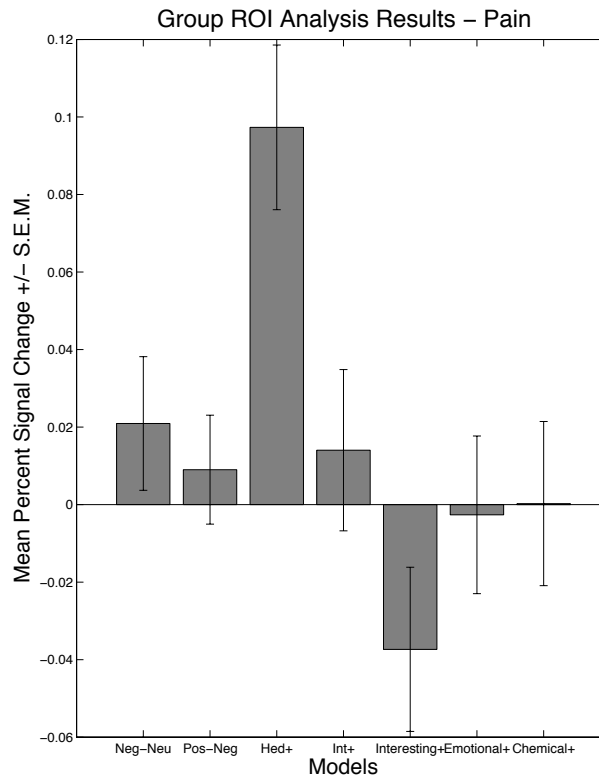
Figure 3.40: Results of Pain-Related Insular ROI Analyses, Non-Hemisphere-Specific. Models: Neg-Neu = [Negative - Positive]; Pos-Neg = [Positive - Negative]; Hed+ = Effect of Increasing Hedonic Value; Int+ = Effect of Increasing Intensity Value; Interesting+ = Effect of Increasing Interesting-ness; Emotional+ = Effect of Increasing Emotional Intensity; Chemical+ = Effect of Increasing Chemical-like Quality.

ences between the left and right hemispheres (some of the results are shown in Figure 3.41), which is surprising given the differential patterns observed in the insula during the whole-brain analysis. The two-way analysis of variance (ANOVA) exploring the effect of the hemisphere and passivity/activity of the session, however, did show a statistically significant difference between the passive and active sessions for the lateral FI ($F(1,1) = 4.65$, $p = 0.033$) in the [positive - negative] condition (Figure 3.41, upper row, third column). In addition, a paired t-test on the signal change patterns between the medial and lateral FI failed to detect any significant differences.

c. Insular Regions - Revised Analysis Results

As mentioned above, the revised ROI analysis treated the signal changes observed during passive and active tasks separately, rather than lumping them together, and hence allowed a more granular view of the ROI signal changes in each model.

The overall signal change profiles in the 5 main insular ROIs - whole insula, FI, non-FI insula, medial FI, and lateral FI - were very similar, but when the data from passive and active tasks were compared, different effects by the two task types were suggested (Figures 3.42 and 3.43). The signal change trends in the insular regions for the [negative - neutral] contrast were similar between the passive and active runs. On the other hand, the [positive - negative] contrast signal change appeared slightly more pronounced in the passive runs than was in the active runs, with the former showing observable decrease, while the latter was close to zero. And whereas the data suggested that the signal change for the hedonic parametric model was greater than that of the intensity parametric model in the passive runs, the opposite effect was observed in the active runs. The effects for the chemical parametric model were barely observed in the passive runs, but some decrease in signal was observed in the active runs. The interesting-ness parametric model elicited a small amount of positive signal change in both passive and active runs. Finally the effects for the emotional parametric model tended to be near zero in the passive runs, while some increase in signal was observed in the active runs.
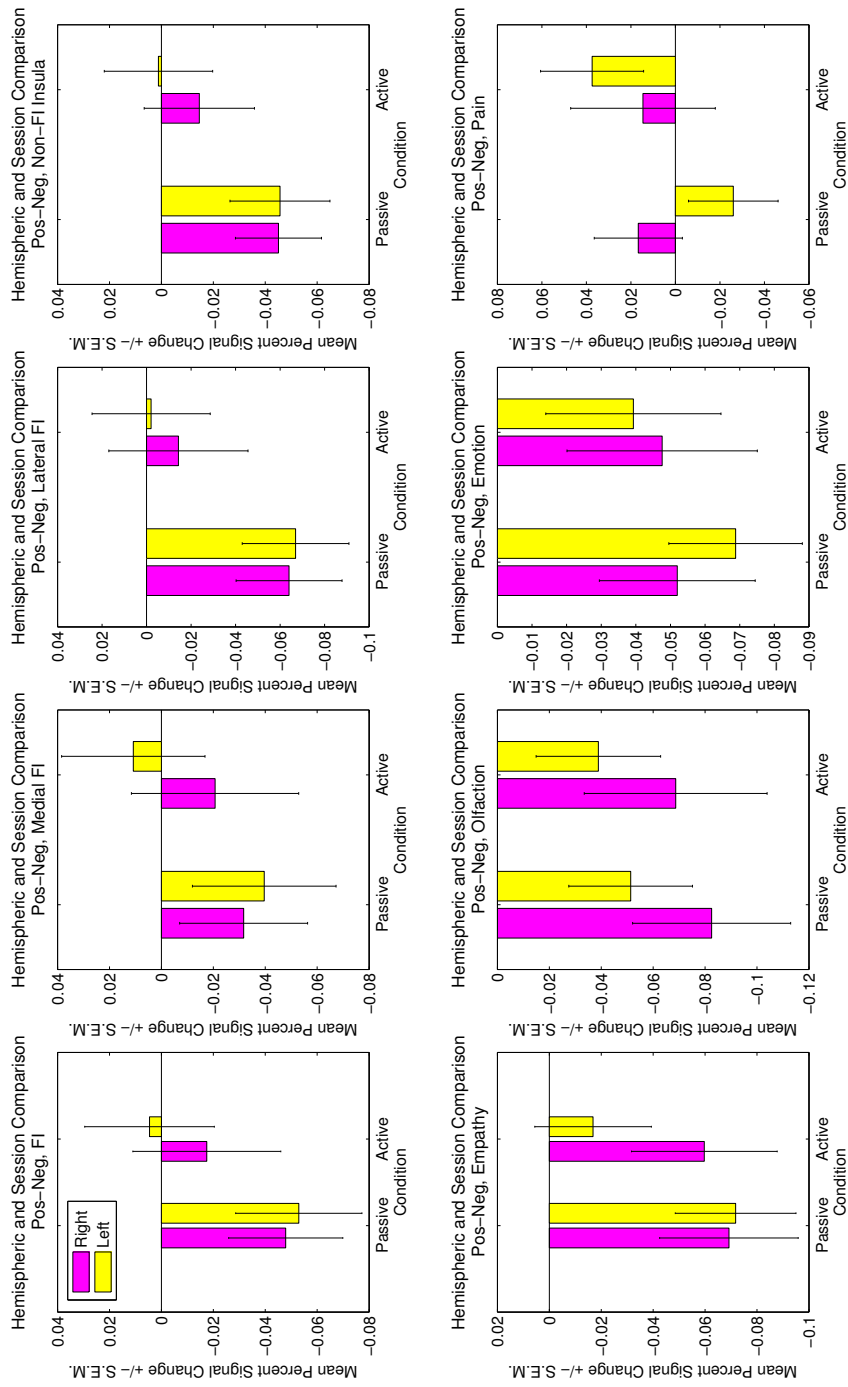
Figure 3.41: Results Insular ROI Analyses for the [Positive - Negative] Model, Hemisphere-Specific.
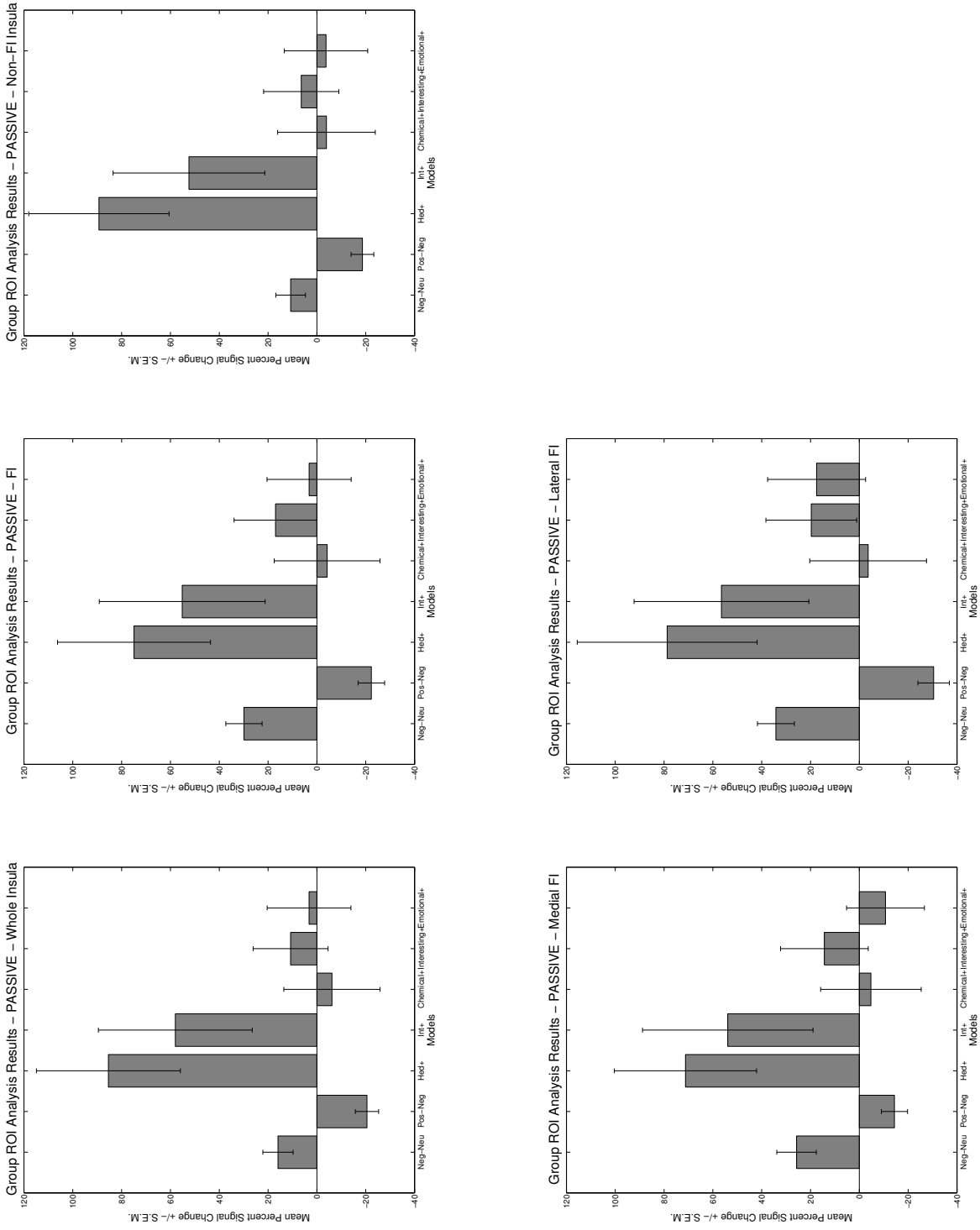
Figure 3.42: Revised ROI Analysis Results for the 5 Main Insular Regions, for Passive Runs in Both Hemispheres Models: Neg-Neu = [Negative - Positive]; Pos-Neg = [Positive - Negative]; Hed+ = Effect of Increasing Hedonic Value; Int+ = Effect of Increasing Intensity Value; Interesting+ = Effect of Increasing Interesting-ness; Emotional+ = Effect of Increasing Emotional Intensity; Chemical+ = Effect of Increasing Chemical-like Quality.
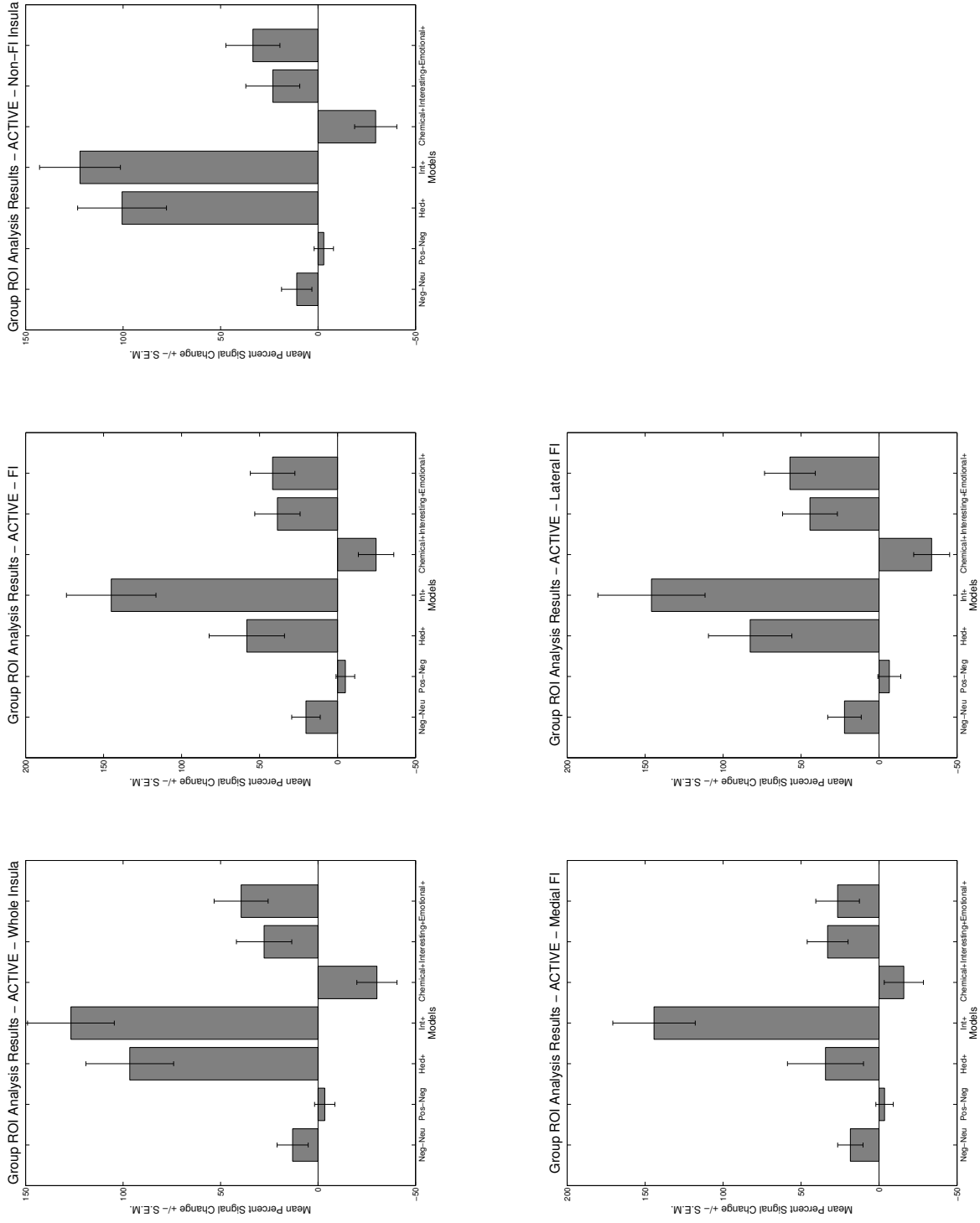
Figure 3.43: Revised ROI Analysis Results for the 5 Main Insular Regions, for Active Runs in Both Hemispheres Models: Neg-Neu = [Negative - Positive]; Pos-Neg = [Positive - Negative]; Hed+ = Effect of Increasing Hedonic Value; Int+ = Effect of Increasing Intensity Value; Interesting+ = Effect of Increasing Interesting-ness; Emotional+ = Effect of Increasing Emotional Intensity; Chemical+ = Effect of Increasing Chemical-like Quality.

The effects described above were similarly suggested by the passive and active task data for the left-hemisphere-only and right-hemisphere-only ROIs of the 5 main insular regions. However, the right-hemisphere-only analysis revealed that the signal change levels for the hedonic and intensity parametric models were very similar in the passive runs, rather than the hedonic signal change being greater than the intensity signal change (Figure 3.44). Also, the right-hemisphere passive signal changes for the interesting-ness parametric model were near zero, while some positive signal changes were observed in all other (right-hemisphere active, left-hemisphere active and passive) analyses.

In order to test the hypothesis, formed based on the whole-brain analysis results, that there exists a dichotomy between the hedonic value processing in the medial and lateral FI, two-tailed, paired t-tests were performed to compare the signal changes in the two regions for both hemispheres, the left hemisphere only, and the right hemisphere only. The analysis yielded only 3 instances of "significant" — with p-values lower than 0.05 — results:

1. $p = 0.016$, between the left medial FI and left lateral FI for passive [positive - negative] contrast, with the lateral FI showing more signal decrease than the medial FI;

2. $p = 0.020$, between the medial FI and lateral FI in both hemispheres, for passive [positive - negative] contrast, with the lateral FI showing more signal decrease than the medial FI (likely to be driven by the first effect);

3. $p = 0.039$, between the medial FI and lateral FI in both hemispheres, for active emotional parametric model, with the lateral FI showing larger signal increase.

The entirety of the medial FI vs. lateral FI t-test data can be found in the Appendix.

The overall signal change profiles of the empathy, olfaction, emotion, and pain functional areas were, for both passive and active runs, similar to those of the 5 main
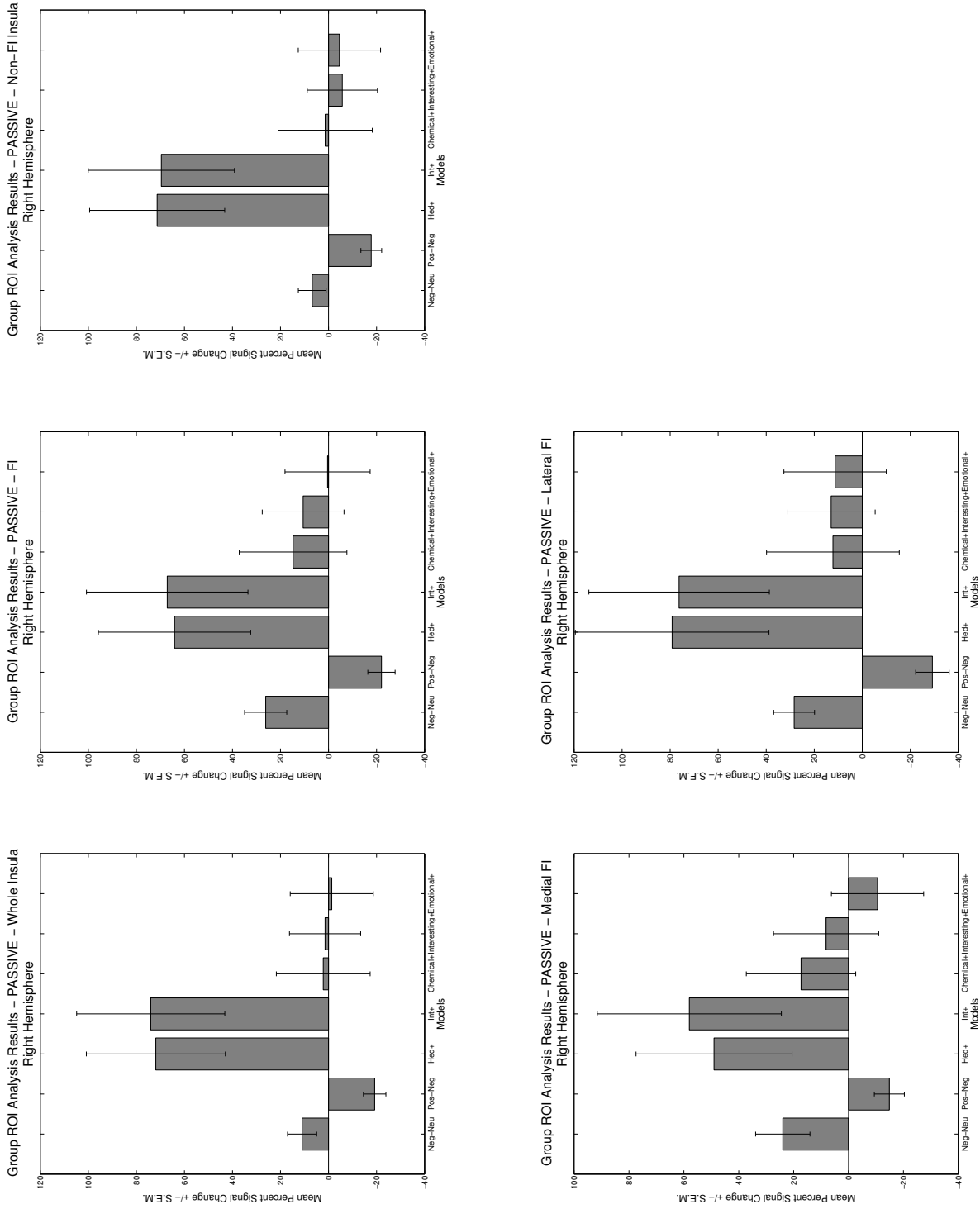
Figure 3.44: Revised ROI Analysis Results for the 5 Main Insular Regions, for Right-Hemisphere-Only Passive Runs Models: Neg-Neu = [Negative - Positive]; Pos-Neg = [Positive - Negative]; Hed+ = Effect of Increasing Hedonic Value; Int+ = Effect of Increasing Intensity Value; Interesting+ = Effect of Increasing Interesting-ness; Emotional+ = Effect of Increasing Emotional Intensity; Chemical+ = Effect of Increasing Chemical-like Quality.

insular regions discussed above (Figures 3.45 and 3.46). However, the pain functional areas yielded interesting results, in which most signal changes for the passive run were concentrated on the hedonic parametric model. The active run results for these areas, while showing most of the signal change patterns observed in the other insular regions for the active run, yielded a larger signal change for the hedonic parametric model compared to the intensity parametric model, hence showing that the hedonic value processing tends to dominate the pain-processing insular regions. Also, when only the right-hemisphere pain areas were examined, a hedonic-model-dominated pattern shown in the passive runs was found (Figure 3.47).

d. Non-Insular Regions of Interest

In addition to the insular regions discussed above, 14 non-insular ROIs were selected and their signal changes levels were assayed. Table 3.11 lists the ROIs, and Figure 3.48 illustrates their locations. While 11 non-insular ROIs were used in the original draft of this thesis, in the revision process of this thesis, 3 more OFC ROIs — Lateral OFC (Revision), Middle OFC (Revision), and Medial OFC (Revision) — were included, in order to more accurately represent the different portions of the OFC than we had done using the two "Older" OFC ROIs. Also, a number of ROIs used in the original assay — Lateral OFC (Older), Medial OFC (Older), Frontal Medial Cortex, Frontal Orbital Cortex, Frontal Pole, Anterior STS, DMPFC, VMPFC, PCC, and TPJ — were omitted in the revised analysis, due to poor region definition and/or lack of proper justification for including in the analysis.

The amygdala was defined based on an amygdala atlas, which was created using standardized MR images of a large number of human subjects (Tyszka and Pauli, in preparation), while the frontal medial cortex, frontal orbital cortex, frontal pole, lateral OFC (older version), and medial OFC (older version) ROIs were created based on the Harvard-Oxford Atlas available on FSL: the frontal pole ROI was edited so that it covers only the relatively ventral portion of the frontal pole, while the lateral OFC (older version) and medial OFC (older version) ROIs are hand-edited versions of the Harvard-Oxford Atlas' frontal medial and orbital cortex masks. The 3 "Revision" OFC
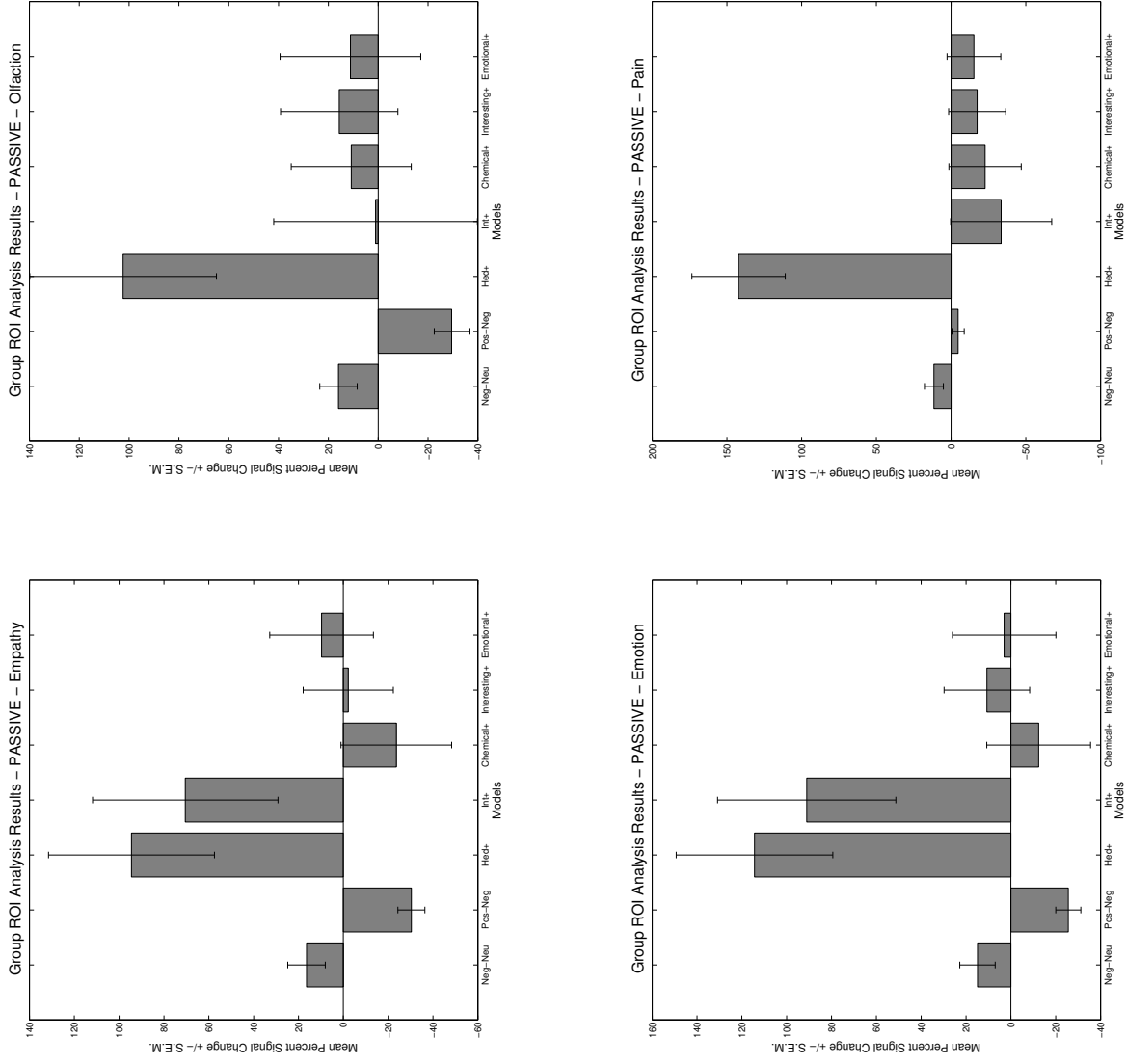
Figure 3.45: Revised ROI Analysis Results for the Functional Insular Regions, for Passive Runs in Both Hemispheres Models: Neg-Neu = [Negative - Neutral]; Pos-Neg = [Positive - Negative]; Hed+ = Effect of Increasing Hedonic Value; Int+ = Effect of Increasing Intensity Value; Interesting+ = Effect of Increasing Interesting-ness; Emotional+ = Effect of Increasing Emotional Intensity; Chemical+ = Effect of Increasing Chemical-like Quality.
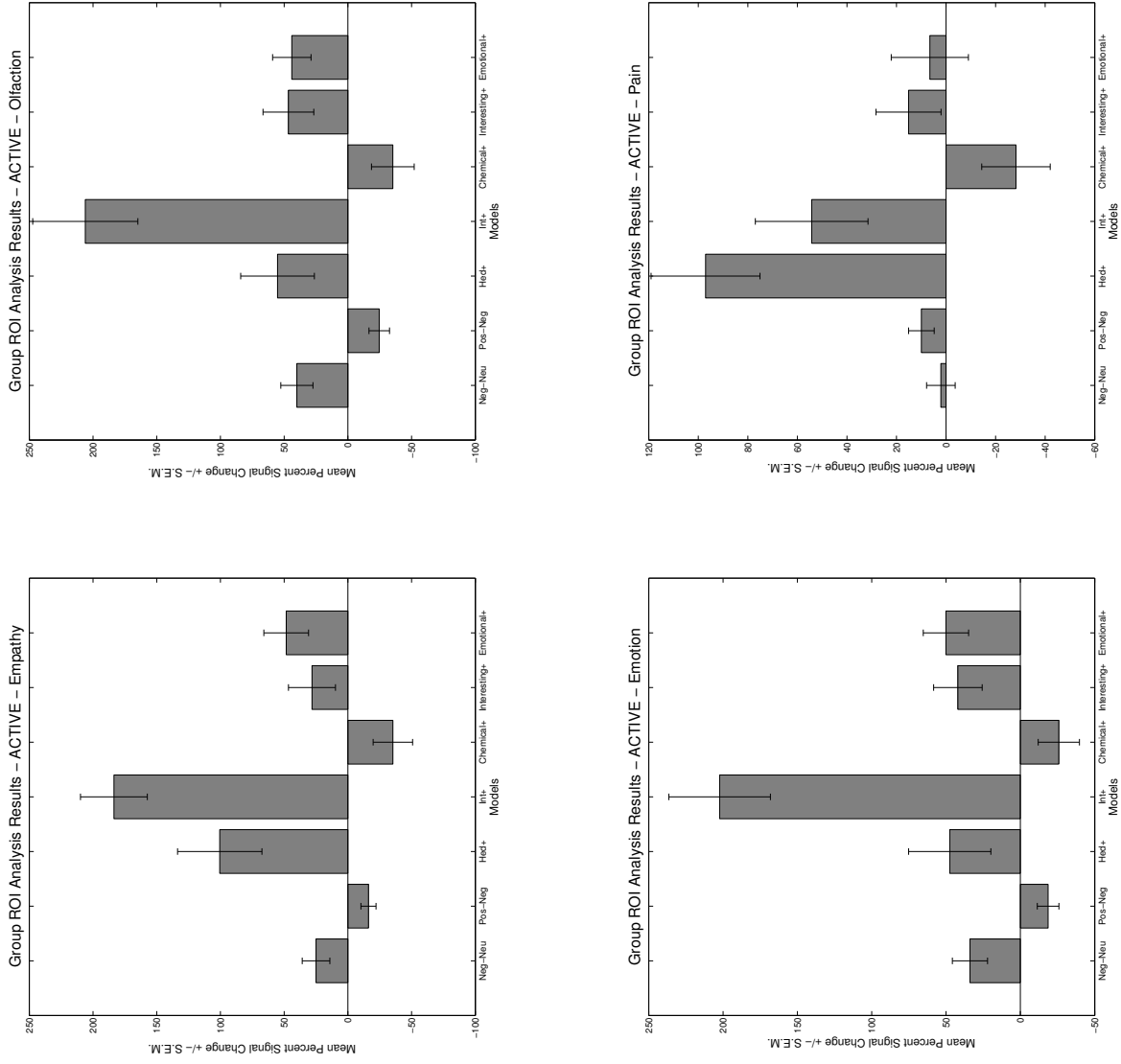
Figure 3.46: Revised ROI Analysis Results for the Functional Insular Regions, for Active Runs in Both Hemispheres Models: Neg-Neu = [Negative - Positive]; Pos-Neg = [Positive - Negative]; Hed+ = Effect of Increasing Hedonic Value; Int+ = Effect of Increasing Intensity Value; Interesting+ = Effect of Increasing Interesting-ness; Emotional+ = Effect of Increasing Emotional Intensity; Chemical+ = Effect of Increasing Chemical-like Quality.
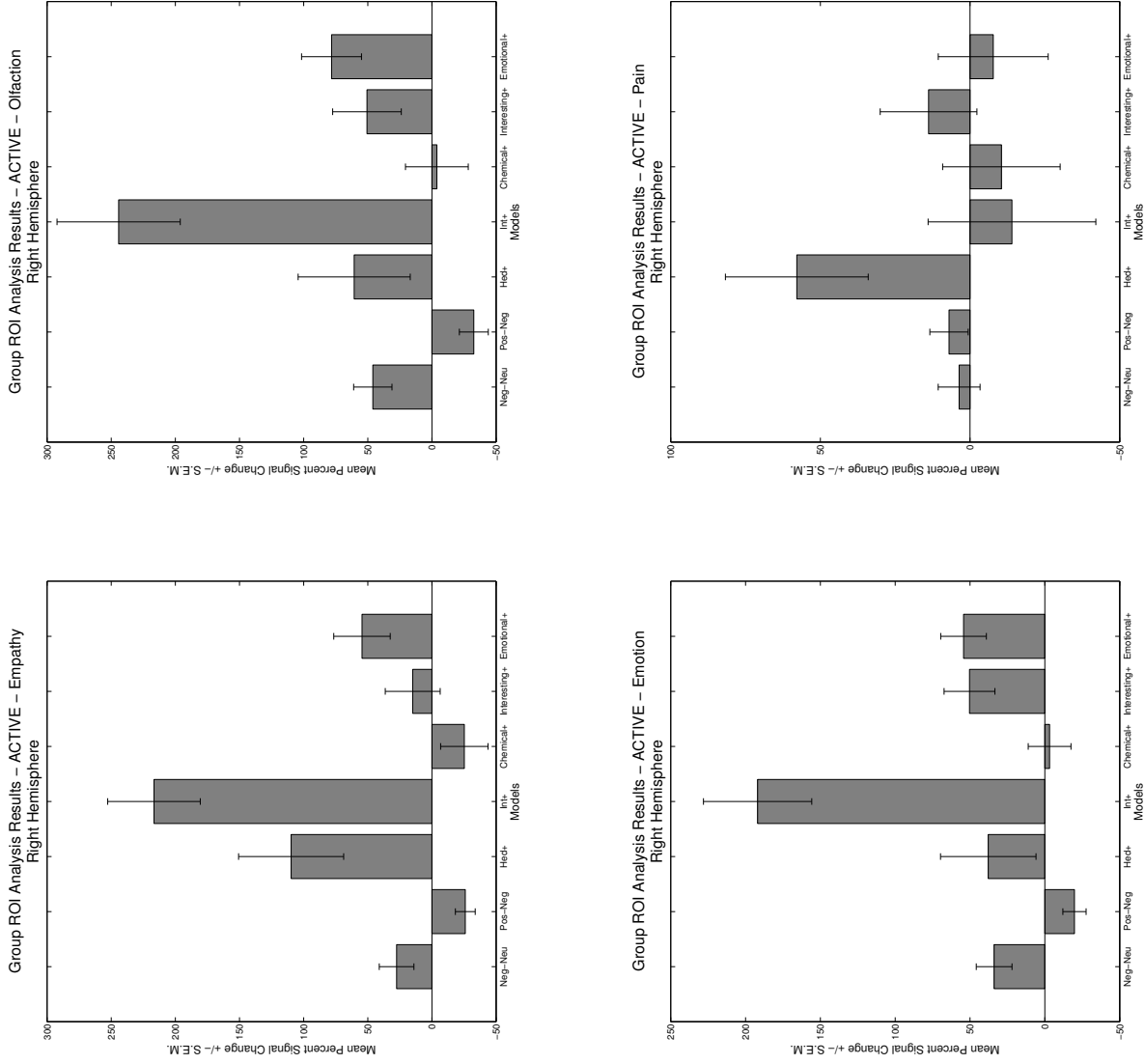
Figure 3.47: Revised ROI Analysis Results for the Functional Insular Regions, for Active Runs in the Right Hemisphere Only Models: Neg-Neu = [Negative - Positive]; Pos-Neg = [Positive - Negative]; Hed+ = Effect of Increasing Hedonic Value; Int+ = Effect of Increasing Intensity Value; Interesting+ = Effect of Increasing Interesting-ness; Emotional+ = Effect of Increasing Emotional Intensity; Chemical+ = Effect of Increasing Chemical-like Quality.
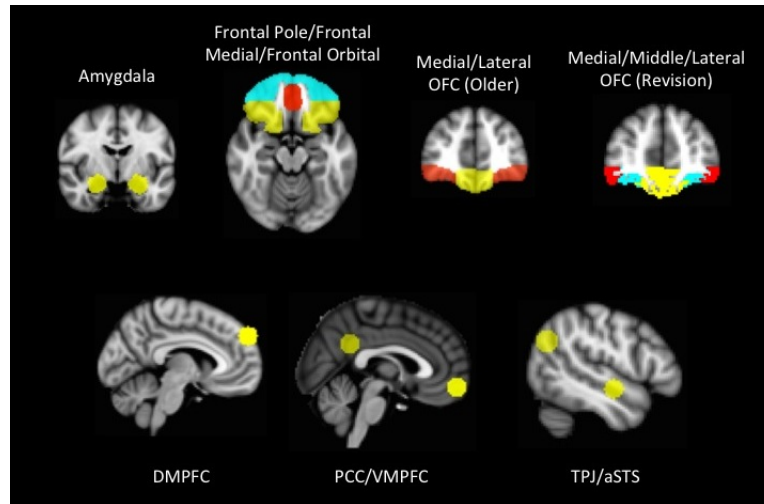
Figure 3.48: Non-Insular ROIs Used.

masks were first hand-drawn by the author based on the standard gyral structure, then reviewed by an expert in OFC structure and function (John O'Doherty) to ensure accuracy.

The anterior superior temporal sulcus (STS), dorsomedial frontal cortex (DMPFC), posterior cingulate cortex (PCC), ventromedial prefrontal cortex (VMPFC), and temproro-parietal junction (TPJ) ROIs were all derived from a functional mentalizing network defined in Spunt and Adolphs (2015). The anterior STS and DMPFC ROIs were created only in the left hemisphere, since the original study had shown the network to be left-lateralized. The PCC and VMPFC ROIs straddled both hemispheres due to their medial location, and while TPJ mask had originally been defined only in the left hemisphere, a mirror-image, right-hemisphere mask was also created, due to the fact that other studies in ToM had found the TPJ activity to be right-lateralized (Saxe and Wexler 2005).

e. Non-Insular Regions - Original Analysis Results

While the entirety of the data is available in the Appendix, we would like to focus the discussion of the group ROI on the OFC. As shown in Figure 3.49, the frontal orbital cortex ROI shows signal change patterns that reflect the findings of the whole-brain analysis: robust activation in the effects of the [negative - positive] contrast and

Region	Hemisphere	Number of Voxels	Source	Reason for Inclusion
Amygdala	Both	948	Atlas in preparation	To further investigate the role of amygdala in olfactory value processing, based on the amygdalal signals in the whole-brain analysis and the role of the structure in emotion processing
Frontal Medial Cortex	Both	1380	Harvard-Oxford Atlas	Excluded in the revision due to better coverage by the new OFC masks
Frontal Orbital Cortex	Both	4207	Harvard-Oxford Atlas	Excluded in the revision due to better coverage by the new OFC masks
Frontal Pole	Both	4138	Adopted from Harvard-Oxford Atlas	Excluded in the revision due to better coverage by the new OFC masks
Lateral OFC (Older)	Both	4056	Adopted from Harvard-Oxford Atlas	Excluded in the revision due to better coverage by the new OFC masks
Medial OFC (Older)	Both	3550	Adopted from Harvard-Oxford Atlas	Excluded in the revision due to better coverage by the new OFC masks
Lateral OFC (Revision)	Both	2277	Hand-drawn Based on Gyral Structure, and Reviewed by Expert	To further investigate the area's role in olfactory value processing and any differences among various portions of the OFC, based on the whole-brain analysis results
Middle OFC (Revision)	Both	1449	Hand-drawn Based on Gyral Structure, and Reviewed by Expert	To further investigate the area's role in olfactory value processing and any differences among various portions of the OFC, based on the whole-brain analysis results
Medial OFC (Revision)	Both	3696	Hand-drawn Based on Gyral Structure, and Reviewed by Expert	To further investigate the area's role in olfactory value processing and any differences among various portions of the OFC, based on the whole-brain analysis results
Anterior STS	Left	515	Spunt and Adolphs 2015	Excluded in the revision due to not enough justification to include in the analysis
DMPFC	Left	515	Spunt and Adolphs 2015	Excluded in the revision due to not enough justification to include in the analysis
PCC	Both	515	Spunt and Adolphs 2015	Excluded in the revision due to not enough justification to include in the analysis
VMPFC	Both	515	Spunt and Adolphs 2015	Excluded in the revision due to not enough justification to include in the analysis
TPJ	Both	1030	Spunt and Adolphs 2015	Excluded in the revision due to not enough justification to include in the analysis

Table 3.11: List of Non-Insular ROIs.

increasing hedonic values, as well as increasing intensity values, while showing mean reduction in signals in the [positive - negative] contrast. This is somewhat echoed in the results from the lateral OFC ROI, with a trend of higher signal change in the [negative - neutral] and the hedonic parametric effects, although some positive signal change in the [positive - negative] contrast can be found here. The medial OFC ROI yielded results that are different from the other two, with attenuated mean signal in the [negative - neutral] contrast and higher degrees of signal increase for the [positive - negative] and increasing hedonic value effects. However, the overall magnitude of signal change in this ROI is smaller than those of the other two OFC regions, which suggests that this result should be taken with caution.

f. Non-Insular Regions - Revised Analysis Results

The signal changes that occurred in the three "Revision" OFC regions (lateral, middle, and medial) and the amygdala during the passive runs were quite different from those that occurred during the active runs (Figures 3.50 and 3.51). This is rather surprising, given the seemingly similar activation patterns between the two types of runs suggested by the whole-brain analysis data.

In the passive runs, the lateral, middle, and medial OFC's signal change seemed rather dominated by the hedonic value parametric model; some signal changes were observed for the other contrasts, but they tended to be smaller in magnitude. The hedonic signal change level for the medial OFC was much lower than those of the middle and lateral OFC.

On the other hand, the medial OFC for the active runs suggested a more distributed signal change pattern (with only small signal changes for all contrasts). The middle OFC for the active runs, while exhibiting a large signal change in response to the hedonic parametric contrast, also implied some additional, albeit smaller, signal changes for the [positive - negative] and intensity contrasts. The lateral OFC for the active runs, rather than showing the large hedonic signal changes observed in the passive runs, suggested sizable changes in the intensity and interesting-ness parametric
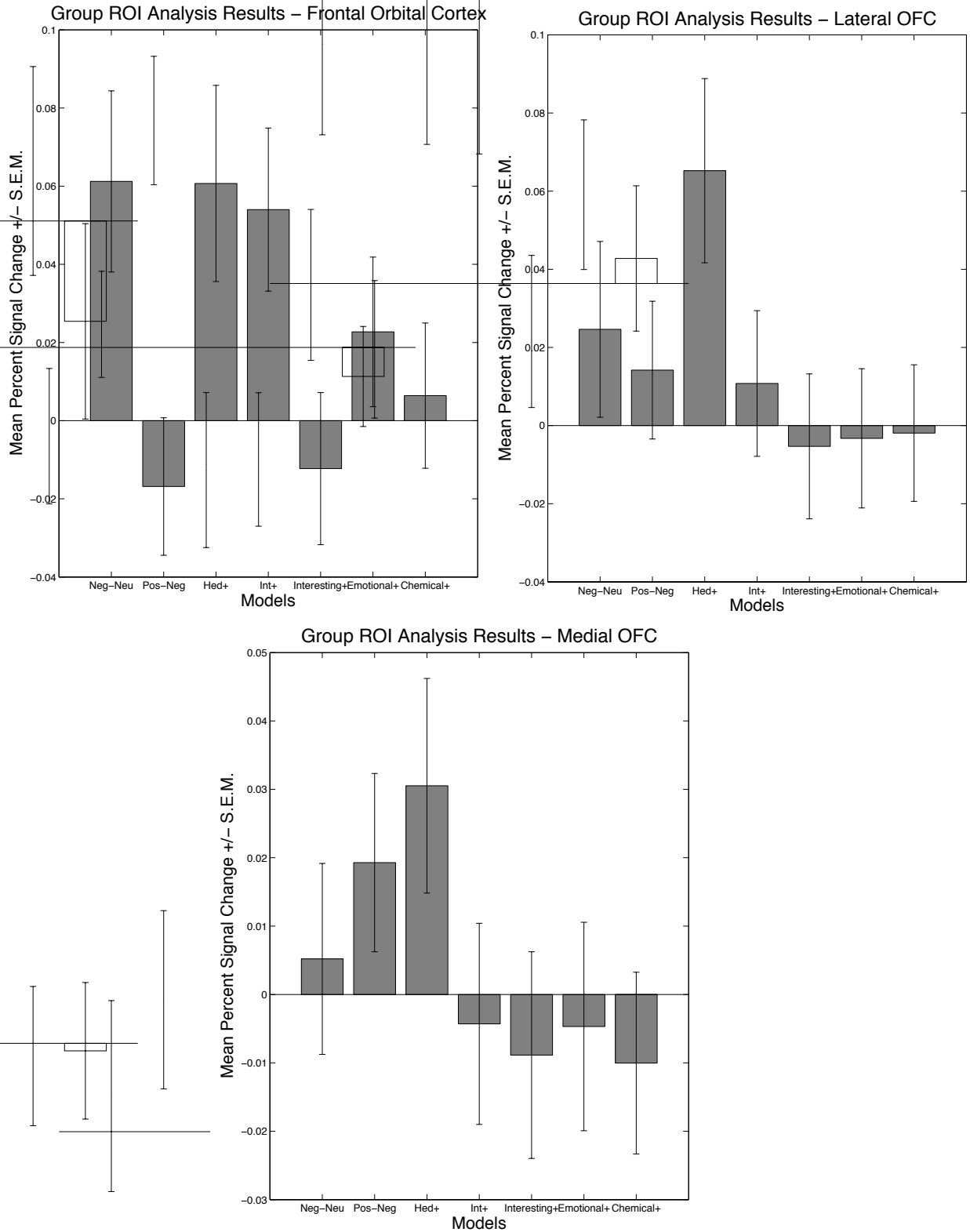
Figure 3.49: Partial Results of OFC ROI Analyses, Non-Hemisphere-Specific. Models: Neg-Neu = [Negative - Positive]; Pos-Neg = [Positive - Negative]; Hed+ = Effect of Increasing Hedonic Value; Int+ = Effect of Increasing Intensity Value; Interesting+ = Effect of Increasing Interesting-ness; Emotional+ = Effect of Increasing Emotional Intensity; Chemical+ = Effect of Increasing Chemical-like Quality.
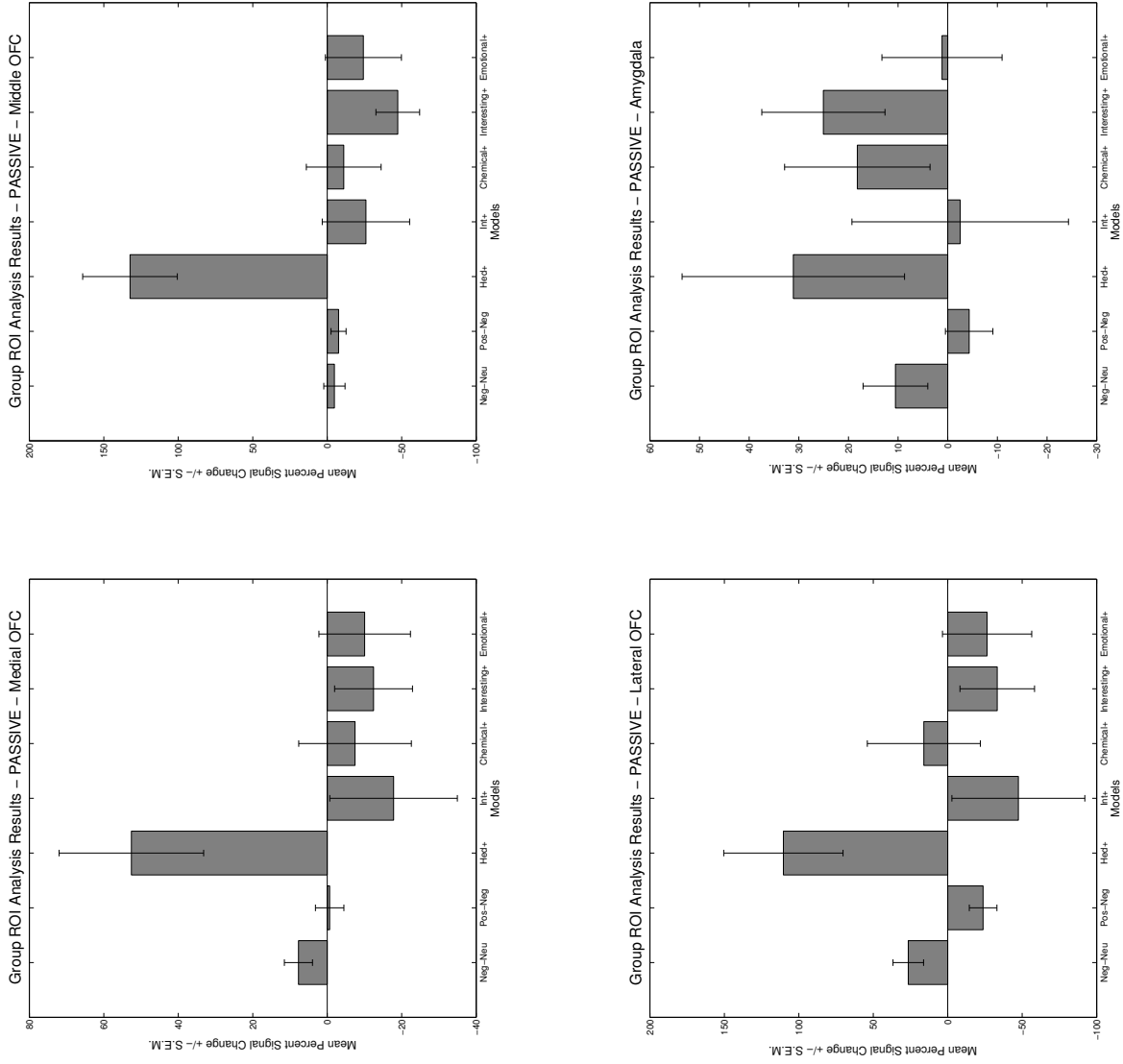
Figure 3.50: Revised ROI Analysis Results for the OFC and Amygdala, for Passive Runs in Both Hemispheres Models: Neg-Neu = [Negative - Positive]; Pos-Neg = [Positive - Negative]; Hed+ = Effect of Increasing Hedonic Value; Int+ = Effect of Increasing Intensity Value; Interesting+ = Effect of Increasing Interesting-ness; Emotional+ = Effect of Increasing Emotional Intensity; Chemical+ = Effect of Increasing Chemical-like Quality.
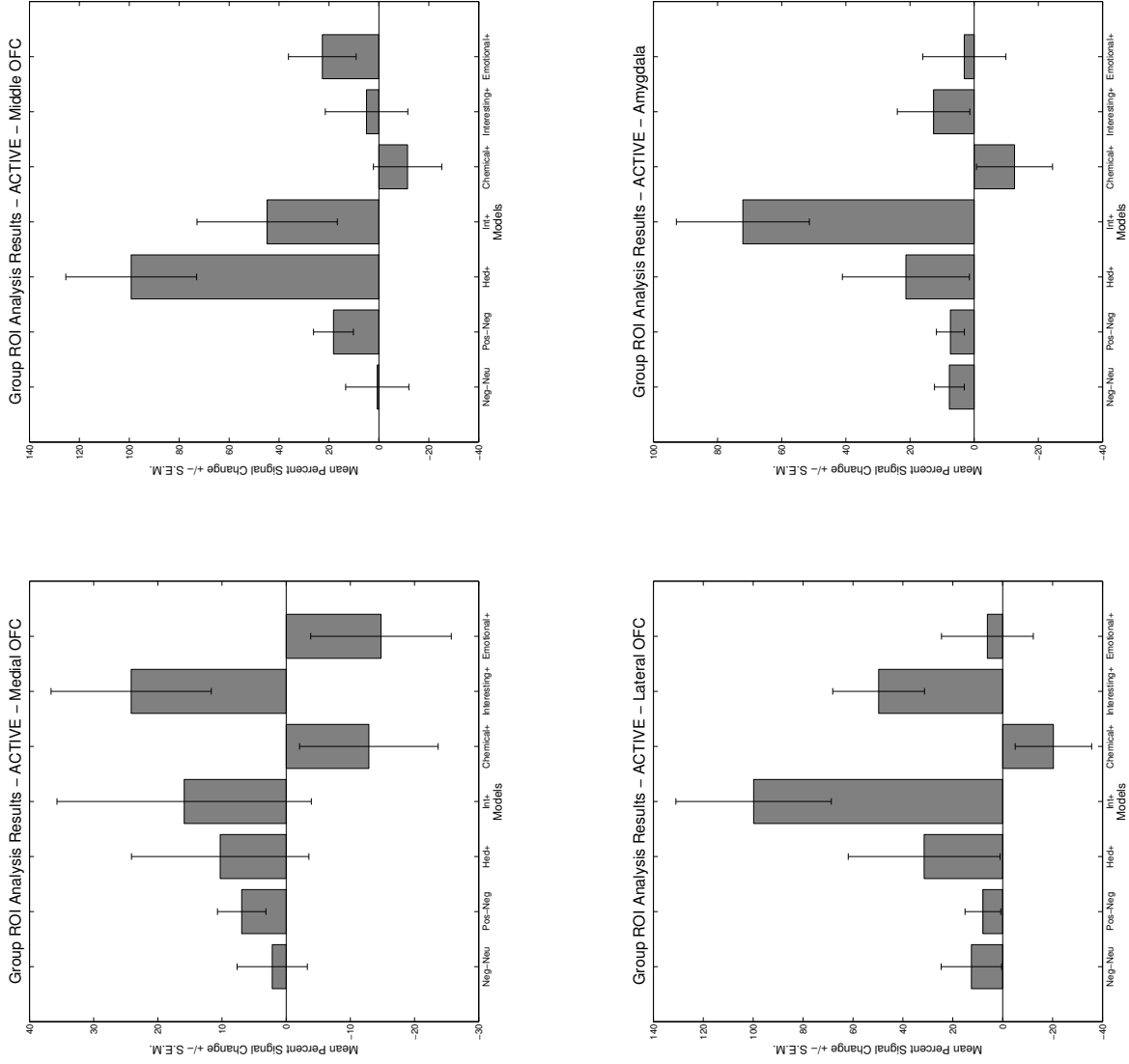
Figure 3.51: Revised ROI Analysis Results for the OFC and Amygdala, for Active Runs in Both Hemispheres Models: Neg-Neu = [Negative - Positive]; Pos-Neg = [Positive - Negative]; Hed+ = Effect of Increasing Hedonic Value; Int+ = Effect of Increasing Intensity Value; Interesting+ = Effect of Increasing Interesting-ness; Emotional+ = Effect of Increasing Emotional Intensity; Chemical+ = Effect of Increasing Chemical-like Quality.

models.

In the passive runs, the amygdala seemed to show some smaller signal changes for the [negative - neutral], hedonic parametric, chemical parametric, and interesting-ness parametric contrasts. On the other hand, during the active runs, the region suggested signal changes mainly for the hedonic (to a relatively small degree) and intensity (to a larger degree) parametric models, and near-zero changes for the other models.

The right-hemisphere- and left-hemisphere-specific results were similar to the both-hemisphere results that were discussed above.

Any ROI analysis figures not discussed earlier can be found in the Appendix.

g. ANOVA: Passive vs. Active and Left Hemisphere vs. Right Hemisphere - Revised Analysis Results

During the revision of this thesis, a two-way ANOVA was performed for each ROI and each model, in order to examine the differential effects of passive and active tasks, and of the ROIs' hemispheric laterality. For these analyses no interactions between the two variables were considered, as it seemed unlikely that such interactions should exist. Table 3.12 summarizes notable ($p < 0.05$) results. All of the p-values and F-ratios from the ANOVA can be found in the Appendix.

h. Individual Behavioral Effects - Original Analysis Results

In addition to performing the assays described above, we have compared the mean % signal changes in insular ROIs from each individual subject with the various behavioral measures discussed earlier in section 3.4.1.2. We hypothesized that the olfactory hedonic processing network may overlap with those computing social and emotional values, and that some of our neural data, especially those estimating the effect of hedonic value evaluation, would be relatively well-correlated with many of these behavioral measures. The overall and perceiving scores of MSCEIT, positive and negative scores of PANAS, and the social network size measure from SNI were considered as the best

ROI	Model	Variable	p	F (1,1)
Non-FI Insula	Hedonic	Left/Right	0.03068	429.90828
Empathy	Chemical	Left/Right	0.04101	240.31724
Empathy	Emotional	Passive/Active	0.0131	2,359.89
Olfaction	[Negative - Neutral]	Passive/Active	0.0005	1,634,563.08
Olfaction	[Negative - Neutral]	Left/Right	0.00099	413,290.96
Emotion	Chemical	Left/Right	0.0191	1,110.49
Emotion	Emotional	Passive/Active	0.00967	4,336.29
Emotion	Emotional	Left/Right	0.0404	247.64722
Amygdala	Emotional	Left/Right	0.04444	204.58347
Medial OFC	Hedonic	Passive/Active	0.03367	356.89006
Lateral OFC	[Negative - Neutral]	Passive/Active	0.00612	10,833.68
Lateral OFC	[Negative - Neutral]	Left/Right	0.00465	18,770.53

Table 3.12: Summary of Notable Findings from Passive vs. Active and Left vs. Right Two-Way ANOVA

candidates for these correlations, as they seem to directly illustrate one's emotional and hedonic tendencies. In this section, only the relationships that appear relatively coherent (with fairly high correlation coefficients, and upon visual inspection, not clearly driven by outliers) will be discussed.

Table 3.13 summarizes the notable findings. Out of the findings listed, the comparison between the negative PANAS scores and the emotional intensity parametric model for the passive runs, as an example of a relatively clear relationship, is presented in Figure 3.52.

Consistent with our initial hypothesis, the perceiving and overall scores of MSCEIT, positive and negative scores of PANAS, and to a small degree the SNI score correlated with some of the ROI analysis data. The trait anxiety score from STAI also exhibited some correlation. Some of these relationships appear relatively easy to interpret: the inverse correlation between the PANAS negative affect score and the FI activity in the hedonic and emotional intensity parametric models shown in Figure 3.44 suggests that the region's hedonicity- and emotion-tracking role may be central to formation of affect. In specific, one could hypothesize based on these results that the ability to richly experience the hedonic and emotional aspects of an odor may somehow be
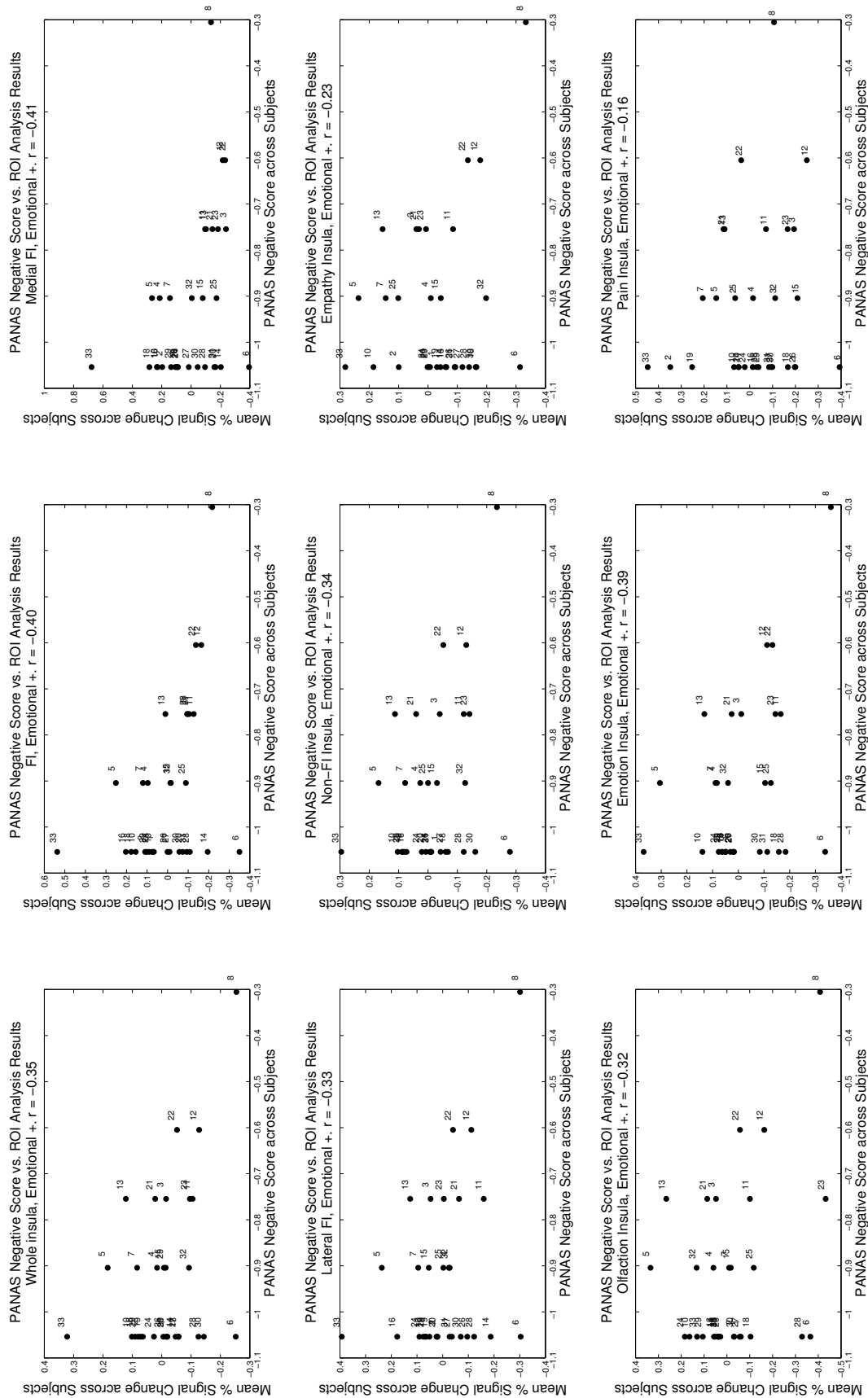
Figure 3.52: Comparison of Negative PANAS Scores with Insular Signal Changes in Emotional Intensity Parametric Model ROI during Passive Runs.

Session Type	Measure	Model	Notable ROIs (r)
Passive	MSCEIT - Overall	[Pos - Neg]	"Pain" Insula (0.34)
	MSCEIT - Overall	Int +	FI (-0.26)
	MSCEIT - Perceiving	[Pos - Neg]	"Pain" Insula (0.36);
	MSCEIT - Perceiving	Emotional +	"Empathy" Insula, (-0.32)
	PANAS - Negative	Hedonic +	Whole FI (-0.28), with Med/Lat FI
	PANAS - Negative	Emotional +	FI (-0.40); All ROIs Notable
Active	PANAS - Positive	Interesting +	Whole Insula and FI, appear quadratic
	PANAS - Negative	[Pos - Neg]	Medial FI (0.40)
	SNI	Chemical +	"Pain" Insula (0.40)
	STAI - Trait	Chemical +	Whole Insula (0.41)

Table 3.13: Summary of Notable Findings from Behavioral Measure vs. ROI Signal Change Comparison

protective against experiencing negative feelings. However, these results should be interpreted carefully and the hypothesis should undergo rigorous testing, as a) the ROI analysis results seem rather noisy, b) it is difficult to make a clear conclusion based on 33 data points, and c) the PANAS score only reflects a recent trend in a subject's affect, rather than being a long-term, trait-based measure.

i. Individual Behavioral Effects - Revised Analysis Results

During the revision of this thesis, the newly computed raw signal changes in all of the ROIs were compared with the overall and perceiving scores of MSCEIT, positive and negative Z-scores of PANAS, and the social network size from SNI, measured from each participant. STAI was excluded from this revisional effort, as further consideration suggested that there was not enough *a priori* justification for believing that comparing one's state and trait anxiety scores and the BOLD signal changes in the ROIs in response to our models would yield very meaningful results. For each comparison, a Pearson correlation coefficient and a Spearman correlation coefficient were calculated, in order to measure both linear and (not necessarily linear) monotonic degrees of correlation.

The entirety of the correlation coefficient data for each ROI and each region can be found in the Appendix; in this section, only the correlations with coefficients that

exceed an arbitrary cut-off point of |0.5| (i.e. greater than 0.5 or less than -0.5) are discussed.

Several ROIs and models exhibited high Pearson correlation coefficients with the SNI social network size measure when their signal changes in the chemical parametric model were considered, but upon graphical inspection of the data, it was noted that these effects were mainly driven by one outlier that has an exceptionally high social network size, as well as large signal changes in the tested ROIs. When this subject was excluded, the correlations were no longer notable.

A number of ROIs (lateral OFC, medial OFC, and left empathy functional areas) demonstrated high Pearson and Spearman correlation coefficients with the negative PANAS Z-scores, when compared in the context of the interesting-ness parametric model signal changes. These relationships appear very similar to those discussed in the above section ("Individual Behavioral Effects - Original Analysis Results") and shown in Figure 3.52, with some of the correlation measures likely to have been influenced by the multiple occurrence of the same, lower PANAS Z-scores over a large span of mean signal change values.

The signal changes in a few regions highly correlated with the perceiving scores of MSCEIT when the interesting-ness parametric model (bilateral amygdala, left pain functional areas) or the [negative - neutral] model (left olfaction functional areas) was considered. In addition, the signal changes in the left amygdala in response to the emotion parametric model correlated highly with the positive PANAS Z-scores. These results are shown in Figure 3.53.
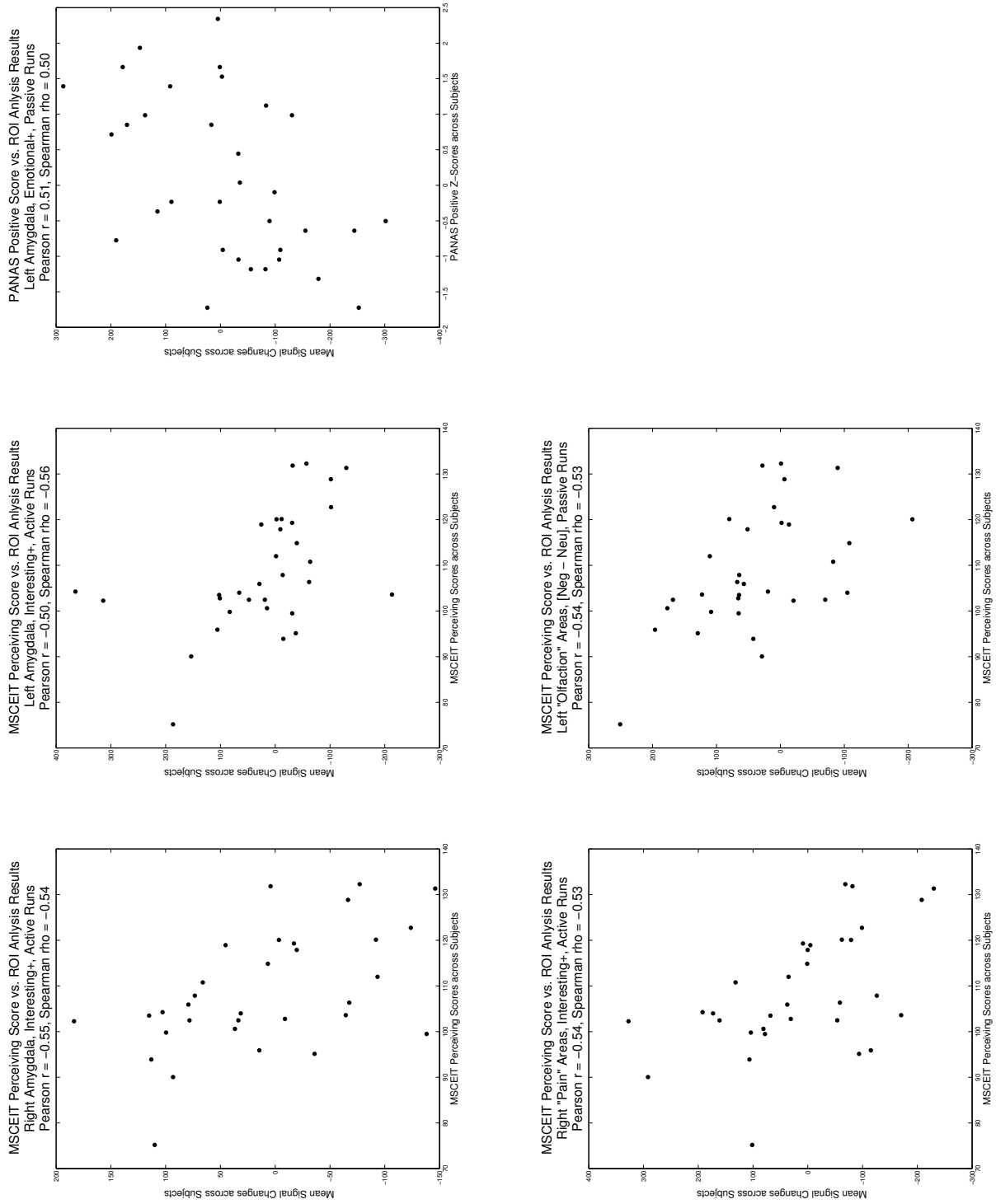
Figure 3.53: Revised Comparison of Perceiving MSCEIT and Positive PANAS Scores with ROI Signal Changes.

3.5 Discussion

3.5.1 Summary and Discussion of Findings

The analysis of subjects' rating behavior indicates that, although some individual differences do exist in personal preference of and sensitivity to odors, the overall odor hedonic value and intensity judgment behavioral pattern in each person is not notably influenced by basic individual traits such as IQ and memory, and that its correlations with personality traits are also fairly weak. Some individual variations have been observed in the degree of within-subject difference between repeated ratings, but based on our analysis, this should be attributed to the ambiguity presented in the odors themselves, and the effect of presentation context, which had been randomly varied for each subject, rather than on specific traits in personality or intelligence. This serves as evidence that the human tendency in odor judgment forms a behavioral pattern that is fairly stable across neurotypical individuals, and hence that the neural data based on these behavioral patterns can be interpreted as standard across individuals, rather than only applicable to a small subset of the population.

The main findings of the whole-brain analysis are as follows:

1. As initially hypothesized, the FI and OFC appear to be involved in computing the odor stimuli's hedonic and intensity values. The amygdala, also highly implicated in value processing (Baxter and Murray 2002, Morrison and Salzman 2010), also exhibited increased BOLD signals in response to odor hedonic values and intensity.

2. There might be a division of roles in hedonic value encoding between the lateral and medial FI, with the lateral and posterior FI being more sensitive to the valence of hedonic values (positive or negative), and the medial and more anterior parts of the FI responding more strongly to the magnitude, but not the valence, of the hedonic value.

3. There might be another division, between the left and right FI, with the right FI being more heavily involved in the processing of negative hedonic values, while the left FI is more biased toward positive hedonic values.

4. The entire FI, as well as the dorsal AI, is involved in tracking the intensity of odor stimuli.

5. The OFC and amygdala seem to follow a similar pattern of activity as does the FI, with increased sensitivity to the magnitude of odor hedonic value and intensity rather than to the valence. However, no hemispheric dichotomy was found in these regions.

6. No significant activation was found using the parametric model of the "burnt vs. chemical" axis from the putative human olfactory map. This may reflect the non-linearity of the axis' neural processing, rather than its non-existence, hence prompting further analysis.

Our whole-brain analysis results differ from those of many previous studies on olfactory hedonic value processing. The past olfactory value studies' main findings were in the OFC, with different portions of the structure found to be active in response to odor stimuli of different valences (Kringelbach 2005, Grabenhorst et al. 2007, Katata et al. 2009) and without significant focus on the insular signals. However in the present study, while both the FI and the OFC were found to be actively involved in hedonic value processing, no significantly fine-grained observations were made for different portions of the OFC, while some spatial organization in hedonic valence processing was suggested in the FI. This is not entirely against the existing olfactory and hedonicity literature, however, as the presence of FI activations in our results appear consistent with a number of previous studies discussed earlier in Section 1.4.1. But these studies did not make any strong assertions about spatial differences within the FI for processing different qualities of odors. This seems to be the first olfactory study to be doing so, as well as the first study in which a larger number of systematically

selected odors were used to probe not only the processing of hedonic judgement, but other qualities of odors (such as burnt-ness, and emotional intensity) as well.

Our finding of FI laterality seems consistent with a combination of two autism studies: in one, children with autism were observed maintaining similar sniffing amplitudes when smelling pleasant and unpleasant odors, while neurotypical children exhibited much shallower sniffs when smelling unpleasant odors (Rozenkrantz et al. 2015); in the second study, individuals with autism have been shown to have less active right FI compared to neurotypicals when performing social tasks. (Di Martino et al. 2009). Given our results, it seems plausible that the attenuated right FI function in autism might be affecting negative-valence-specific olfactory processing, and that this may lead autistic children to differently experience the odors that are generally considered unpleasant by neurotypical children. However, more rigorous statistical testing, such as voxel-wise statistical contrast, must be performed in order to validate our findings.

The results of our original ROI analysis, performed in order to find and examine any signals that did not necessarily survive the statistical thresholds imposed during the whole-brain analysis, did not provide very robust evidence supporting our interpretation of the whole-brain analysis results concerning the spatial organization of the FI. It seemed possible that the inconclusiveness of the original ROI analysis had stemmed from inappropriate selection of the ROIs, very small mean % signal changes, and large standard errors, rather than from the lack of effect. Also, the process of converting the effect of ROI signal changes into their percentage of the whole range of neural signals in the individual might have introduced a great deal of noise to the data. In addition, lumping together the data from the passive and active tasks in the original analysis might have erased some interesting effects created by inherent differences between the two types of tasks. Therefore, in the revised ROI analysis a different approach was taken: the raw amplitudes of the ROI signal changes — rather than % changes — were analyzed, a number of improved ROIs were added, the poorer ROIs were excluded, and the passive and active tasks were treated separately.

The signal change patterns tended be similar among the insular ROIs, when the re-

gions were compared to one another under the same hemispheric (bilateral, left, or right) and passive/active conditions: most of the signal changes occurred in response to increasing hedonic and/or intensity values, with some smaller signal changes in response to other odor qualities. This finding is consistent with the strong neural signals yielded from the hedonic and intensity parametric models in the whole-brain analysis. This result also suggests that either all portions of the insula are similarly engaged during various judgments of odor qualities, or that the neuroimaging assay and computational data processing performed in the present study were not quite sensitive enough to make fine-grained distinction among different parts of the structure during odor judgment. While the latter may be of a higher possibility due to the limited resolution and quality of functional neuroimaging and various issues in the currently available imaging data processing tools, it may not be entirely wise to dismiss the former; considering that the posterior portion of the insula mediates the processing of somatic sensations, which are not completely separate from the complex olfactory experience, there is a small chance that the more posterior, non-olfactory parts of the insula were indeed engaged during the odor judgment tasks.

The new medial, middle, and lateral OFC ROIs and the amygdala ROI also seemed most sensitive to the increasing hedonic and intensity values of the odors, although some larger signal changes in response to the increasing chemical quality and emotional intensity were also observed in some instances. Although not conclusive, the data indicate some distinction among the medial, middle, and lateral OFC: during both passive and active runs the medial OFC showed diminished sensitivity to the increasing hedonic value of the odors compared to the other OFC ROIs. Also, during the active runs, while the middle OFC trended towards being more sensitive to the hedonic value tracking than to the intensity value tracking, the lateral OFC showed the opposite trend.

Although the whole-brain analysis did not show a great deal of difference between the neural signals elicited during the passive and active imaging runs, some noticeable differences were found as a result of the ROI analysis. For example, during passive

runs, the ROIs overall appeared to be more sensitive to the increasing hedonic values of the odors than to any other odor qualities modeled, whereas during active runs higher sensitivity to the increasing intensity values, as well as the chemical and emotional qualities of the odors, were observed. A similar trend was also observed in the OFC and amygdala ROIs, with the increasing hedonic value being tracked more sensitively than the other odor qualities during the passive runs, and slightly higher sensitivity to non-hedonic odor qualities during the active runs. This, to a small degree, suggests that different types of neural processing occurred during the two types of runs. For instance, during the passive runs, without the need to report the intensity of the presented odors, the subjects might have automatically focused on the odor quality that was the most salient to them — the hedonic value. On the other hand, the rating requirements during the active runs may have forced the subjects to attend more heavily to the intensity of the odors, hence engaging the insular regions to track the intensity values more closely.

The pain-processing functional areas were the only insular ROIs that did not exhibit the signal change patterns similar to those shown by the other insular regions. As discussed above, all insular ROIs except for the pain areas tended to be more sensitive to the increasing hedonic value during the passive runs and to the increasing intensity value during the active runs. Unlike these regions, the pain functional areas suggested higher sensitivity to the increasing hedonic values than to the other odor qualities, regardless of whether the imaging runs were active or passive. While this outcome is not tremendously unexpected, given the heavy involvement of pleasantness and unpleasantness processing in pain perception, it is very puzzling to observe that the areas that are sensitive to noxious stimuli, such as painful experiences, are also sensitive to tracking increasing pleasantness, rather than unpleasantness (reflected in the [negative - neutral] model, to which the region is not quite sensitive), in odors. This seems to suggest a complex relationship between pain perception and hedonic value processing: for instance, it seems plausible that pain processing in the insula is a complex procedure that not only takes into account the noxious stimulus, but also

sensitizes the organism to any pleasant and/or pain-relieving sensations, so that the organism can be protected from further negative physical effects of feeling pain. The relationship between pain processing and pleasantness processing in the insula may be an interesting topic that warrants further investigation.

The results of the two-way ANOVA, examining the effect of laterality and passive/active-ness of the imaging run, suggest that these two factors may or may not play a significant role in neural activity in response to various qualities of odors depending on the region and the odor quality being modeled. From the data presented, it is difficult to perceive a clear pattern in which regions and models are more susceptible to the effects of laterality and passive-/active-ness of the imaging run. However, it appears that the insular regions in the two hemispheres, as suggested by a number of studies discussed earlier in this thesis and the results of our whole-brain analysis, are differentially sensitive to the effect of the odors. Also, as we have observed earlier in this chapter, some significant differences exist between the neural processing during the passive tasks and the active tasks.

Out of the ANOVA results that were statistically notable, two laterality effects — one in the non-FI insula for the hedonic parametric model, and the other in the olfaction functional areas for the [negative - neutral] model — tie together hemispheric laterality and hedonic processing in the insula. In order to gauge the direction in which the laterality factor impacts the signal changes in these insular regions (i.e. whether, in accordance with the interpretation of the whole-brain analysis, the left insular regions tend to be more sensitive to the positive values of odors, while the right insular regions show the opposite effect), simple bar charts comparing the mean signal changes for these regions and models were created (Figure 3.54).

Figure 3.54 suggests that, during passive tasks, the non-FI insula in left hemisphere may be sensitive to the increasing hedonic values of the odors. On the other hand, the right olfactory functional areas, which are included in the right FI (see Figure 3.38), seem to show more signal changes when modeled for the negative valence of the odors. Such effects do not seem to occur during active runs. These results
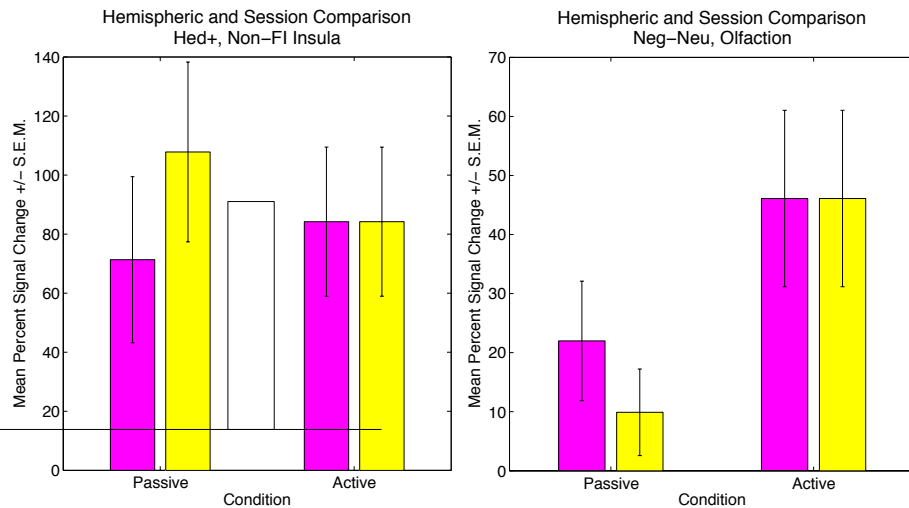
Figure 3.54: Comparison of the Mean Signal Changes in Insular Areas and Models with Significant Laterality Effects.
Colors: Pink = Right Hemisphere; Yellow = Left Hemisphere.
Models: Hed+ = Effect of Increasing Hedonic Value; Neg-Neu = [Negative - Positive]

do not contradict the interpretation of the whole-brain analysis results, with the right hemisphere appearing to be more sensitive to negative odor hedonic values, and the left seemingly responding more strongly to the positive values. However, it is somewhat puzzling that the non-FI insular region shows this laterality effect, when the whole-brain analysis suggested this effect in the FI. Perhaps, as discussed earlier, given the great similarity exhibited among most of the insular areas tested in the revised ROI analysis, the effect is in fact present in the entire insula, rather than only the FI, but simply was not picked up by the whole-brain analysis, or the technological limitations have failed to distinguish the neural signals in the FI from those in the rest of the insula. Also, it is very interesting that this effect only appears to exist in the context of passive odor judgment tasks, and that it seems to disappear during the active tasks. Given the generally higher sensitivity to odor hedonic values during the passive runs and higher sensitivity to other, non-hedonic odor qualities during the active runs, suggested by the revised ROI data, it appears possible that significantly different neural processes occurred during the two types of runs due to different attentional demands, and that this altered the hemisphere-specific olfactory

hedonic value processing. In addition, as the two area-model pairs shown here are the only ones that statistically support the hypothesis that there are hemispheric differences in the FI olfactory hedonic value processing, the evidence presented so far is inconclusive and must be interpreted very cautiously.

The comparison between the medial and lateral FI provides some support for the interpretation of the whole-brain analysis results, that the lateral FI is more sensitive to the valence than is the medial FI, as the absolute values of signal changes in the lateral FI were found to be larger than those in the medial FI for the [positive - negative] contrast. In this case the contrast is associated with negative signal changes, which is consistent with the signal increase observed in the region after the [negative - positive] contrast during the whole-brain analysis. Given this evidence, it seems plausible that the lateral FI is indeed sensitive to tracking the valence of odor hedonic values. However, the data do not support the hypothesis that the medial FI is necessarily more sensitive to tracking the magnitude of the olfactory hedonic values.

The comparison of the revised ROI analysis data with the individual behavioral measures yielded 3 notable categories of correlation patterns. First, there was a negative correlation between the perceiving scores of MSCEIT and the signal changes in the bilateral amygdala in response to the increasing interesting-ness of the odors. The MSCEIT perceiving score measures one's ability to perceive emotions in others and oneself, taking into account not only the general sensitivity to emotion perception, but also the accuracy with which one identifies the perceived emotions (Mayer et al. 2002). This suggests a relationship between lower ability in reading emotions and increased sensitivity of the amygdala to stimuli that are considered interesting. This appears consistent with a past finding that individuals with severe social anxiety and phobia, who tend to exhibit hyperactivity in the amygdala in response to faces conveying various emotions when compared to neurotypicals (Stein et al. 2002, Straube et al. 2005, Phan et al. 2006), also score lower than neurotypicals in the experiential portion of MSCEIT, which includes the perceiving score component (Jacobs et al. 2008). Based on these data, it seems plausible that the over-active amygdala

could distort one's ability to correctly identify emotions. This argument could also be applied the fact that the interesting-ness signals in the pain-associated insular ROIs exhibited a very similar relationship with the MSCEIT perceiving score. However, the present evidence should be treated with caution and its interpretation must be validated through future studies.

Second, our analysis found a negative correlation between the MSCEIT perceiving score and the signal changes in the olfaction-associated insular ROI, in response to the [negative - neutral] contrast. This seems to imply that the inability to accurately read emotions is somehow related to the increased insular response to the negative, or simply high-magnitude (regardless of valence), hedonic values of odors. Perhaps this result could be interpreted along the same line as the amygdala ROI data discussed in the previous paragraph, which is to say that the more sensitive one is to the negative or other salient stimuli, the more this sensitivity distorts one's perception of the stimuli's emotional content, hence leading to inaccurate emotional perception.

Third, we found a positive correlation between the signal changes in the left amygdala in response to increasing emotional intensity of the odors and the individual participants' positive affect scores measured via PANAS. This relationship between positive emotional state and amygdalal sensitivity is somewhat puzzling, as past functional imaging studies point out that the amygdala's sensitivity to emotions is increased in individuals with depression (Sheline et al. 2001, Siegle et al. 2007). However, there is also some evidence that this increased amygdala sensitivity in depression is mood-congruent, with the increase in depressed individuals being mostly in response to negative emotional content, and with these individuals' amygdala showing decreased neural signals in reaction to positive emotional contents (Suslow et al. 2010). This possibly implies that the amygdala in the individuals with positive affect may respond more strongly to positive emotions. Based on this, perhaps it is plausible that most of the participants in the present study, when asked to rate the emotional intensity of an odor, associated the quality with positive emotions, rather than with negative emotions. In fact, most of the subjects, during the instruction session before

beginning their out-of-scanner rating tasks, were given an example scenario in which a person smells roses, is reminded of her grandmother's perfume, and feels intense positive emotions remembering the grandmother. This example might have biased the participants toward rating positive emotions, rather than negative emotions, as emotionally more intense. And this might have led to a positive correlational effect between positive affect and left amygdalal activity during emotional experience.

The outcome of the present study may contribute some insight into the mechanism in which the brain computes the value of external reward or punishment. According to the results of our whole-brain analysis, the magnitude and valence of the olfactory hedonic values may be processed separately, as there is some evidence that some areas' BOLD signals correlated selectively with the hedonic value magnitude, while the others' signals correlated selectively with the valence. This is supported by the evidence from electroencephalogram (EEG) suggesting dissociation between representation of the valence and magnitude of reward (Yeung and Sanfey 2004), as well as by a number of studies that found selective encoding of reward magnitude in the amygdala (Anderson et al. 2003, Small et al. 2003), although it seems likely that some neurons in the amygdala do represent reward valence (Morrison and Salzman 2010), as would be expected given the wide array of neuronal responses found in various parts of the amygdala (Baxter and Murray 2002).

According to our analysis, the FI, OFC, and amygdala are some of the main regions observed to be active in response to various hedonic qualities of odors: the FI was associated with both the valence and magnitude of hedonic values, and while the OFC and amygdala only seemed to track hedonic magnitude in the whole-brain analysis, the ROI analysis data revealed some weaker signal changes related to hedonic valence, which might have been reduced by relatively smaller number of the odors that were perceived as very pleasant. The past literature on value processing offers a wealth of evidence that suggests heavy involvement of the OFC and amygdala in encoding of the intensity and valence of reward and punishment, and hence these two regions are, along with the striatum, considered the primary areas in which value

representation occurs (O'Doherty et al. 2001, Baxter and Murray 2002, Elliott et al. 2003, O'Doherty 2004, Morrison and Salzman 2010). On the other hand, as one might have observed from the discussion of the known insular functions earlier in this thesis, the insula is not considered a region in which fundamental value computation is mediated — instead, the insula, particularly the anterior insula, is believed to be a high-level integrator of various sensory and cognitive representations (Kurth et al. 2010). However, the anterior insula is connected very robustly with the amygdala and the OFC (Singer et al. 2009), and thus it is very possible that these three structures form a part of a network in which a subjective experience of reward or punishment, at least in the olfactory domain, becomes synthesized. In such a network, the amygdala and OFC might compute and project to the anterior insula the information on the olfactory stimulus as a reward or a punishment, and the anterior insula might in turn represent and integrate input with the various sensory information received from other regions to form a conscious experience of pleasant or disgusting smell. Such a process may only be limited to processing the value of odors, or other biological rewards such as food, but it is also possible that utility of other, higher-level stimuli, such as money or social interactions, could be processes in the same network.

The details of exactly which components of the value signal might be computed by which neurons in the amygdala and OFC, and which pathways might relay such information to the anterior insula, is out of the scope of this thesis. However, we believe that the data presented in this study provide support for this theoretical model that could be tested in the future using various experimental methods.

In addition, the present experiment revealed some differences — not significantly picked up by the whole-brain analysis, but revealed by the ROI analysis — in underlying neural processes between passive and active tasks. This provides insight into the subtle differences in the human olfactory judgment behavior, and informs one that, in the future experiments probing the neural processing of value, one may need to be cautious about whether judgments should be passive and implicit, or active and explicit, as this decision might possibly lead to different neural data outcomes.

3.5.2   Caveats and Future Directions

The present study, while providing interesting results, has a number of caveats and the data should in general be interpreted cautiously. First, during the experimental procedure, many subjects experienced issues with background odors caused by residue of odorants adhering to the various plastic tubings carrying odorous air. While efforts were made to keep the tubing clean and replace them frequently, there were many parts that could not be cleaned or replaced without taking the olfactometer apart, and hence the background odor could not be completely removed. Many participants have reported not having been affected too much by these background odors, or reported having learned to ignore them, yet a small number complained that the background odors had prevented them from making accurate judgements of the actual odor stimuli. In addition to the residue odorants remaining in plastic parts, participants sometimes experienced odors from previous trials lingering in the scanner bore for 10 - 20 seconds. While the fan inside the scanner was always used to minimize this effect, due to the closed nature of the bore and the strength of some of the odors, it was not entirely avoidable. Also, due to the relatively long duration of the experiment (the scan took about 90 minutes, and the entire experiment including the out-of-scanner tasks was about four hours long), many subjects experienced nasal fatigue and dryness toward the end of the experiment. Nasal saline solution was provided to each subject for optional use in order to minimize this, but it is possible that this fatigue has influenced subjects' ratings during the out-of-scanner tasks.

Second, many of the models utilized in this study have failed to yield any significant results. There may be multiple reasons for this. For instance, it is possible that the effects being modeled for in fact exist in the neural signal, but that the models themselves are poor because the participants were unable to accurately report some of the odor qualities that they had been asked to judge. In fact, as mentioned earlier, many participants felt that they simply could not decide whether an odor smelled more chemical or burnt, and ended up picking a random number or guessing, and it is very plausible that this has led to inaccurate reporting of many parameters used

for modeling. It is also possible that some of the models did not work due to simple lack of statistical power, and/or that we did use of appropriate models for the effects for which we were assaying (for example, a fully linear parametric model could have failed to yield any results because the process itself is not linear). Therefore, before submitting the present study for peer-reviewed publication, we will construct and try various non-linear models, as well as explore the pre-existing models at lower statistical thresholds.

Third, the exact relationship between the passive and active runs is not entirely clear. Although the whole-brain analysis did not detect any significant and meaningful differences in activation patterns, and even though many of the subjects reported having been thinking about hedonic and intensity values during the passive runs as well as the active runs, the revised ROI analysis discovered some underlying differences between the two types of tasks. While one can easily posit that this is due to the more focused and explicit nature of the active judgment task, the mechanism in which active judgment and reporting altered the BOLD signals is not apparent. In addition, a larger sample size may be needed to ascertain that the differences that we observed are indeed real in the first place.

Fourth, the comparison between the individual personality trait measures and the individual ROI analysis results provide some interesting results that may imply an overlap between the odor hedonic value processing and social and emotional networks. However, as mentioned repeatedly earlier, these results should be treated very cautiously, as some of the ROI signal changes have very small group means and very large standard deviations across individuals. Hence rather than being considered as evidence for a real effect, these results should be treated as starting points for new hypotheses, upon which meaningful future studies can be built.

Finally, the present experiment has generated a very large amount of rich data, some of which have not yet been addressed due to time constraints and technical issues. These data include the various questionnaires on moral decision-making, eating habits, and hedonic sensitivities, as well as pupillometry data from all scan sessions. In addition,

as our participants form a part of a large-scale study at the Conte Center and a subset have undergone (and are undergoing) other neuroimaging studies involving mentalizing, moral decisions, and food choice, there is a large trove of data that could be compared with the present study's results. Thus our hope is to thoroughly address these data before publishing this study, so that our results can be interpreted in a full, data-rich context.

3.6   Acknowledgments

Chapter 4

Summary, Conclusion, and Future Directions

In the context of the structure and function of the insula, the two studies in this thesis address three important questions. First, the study of the insular and claustral structural connectivity in the *Microcebus murinus* explores the question, "are the connections — and hence functions — generally attributed to the insula actually unique to the insula, or do some of them belong to the claustrum?" Meanwhile, the study of human olfactory processing tries to answer the questions, "how are the various odor dimensions represented in the insula," and "how do these representations relate to the social, emotional, and cognitive processing taking place in the same structure?"

The results of these thesis suggest the following: the insular connections are very distinct from from those of the claustrum, despite the high genetic similarity between the two structures. The odor-evaluation functions in the insula, in the hedonic dimension, seem concentrated in the FI portion, with possible divisions of roles between the right and left FI, and between the medial and lateral FI in each hemisphere. Moreover, it is possible that the olfactory hedonic values are encoded and processed in a network in which the amygdala and OFC compute the fundamental components of the odor value, and the information is sent to the FI, which integrates it with other sensory data to produce the perceived experience of olfactory pleasantness/unpleasantness. In addition, based on comparison of the neural data with behavioral measures, it is

plausible that there is some degree of interaction between olfactory value computation and higher-level emotional processing.

Based on the results of these two studies, one could posit that the insula, especially the anterior insula, acts a high-level sensory value integrator that combines the valence and magnitude of stimulus value with various olfactory, gustatory, emotional, and/or somatosensory inputs to create the hedonic and emotional experience that we feel every day. This function may only apply to biological rewards such as odors, but it is also possible that it can be generalized to all types of value stimuli, including abstract ones. And perhaps the claustrum, as a global integrator that rolls up all of the cortical processes occurring in the brain at a time, facilitates the conscious experience of self.

There are several main ways in which the ideas presented in the above paragraph could, and should, be further explored. First, more rigorous testing, such as voxel-wise statistical contrast, should be employed to validate the main findings of the whole-brain analysis of the functional imaging study, and the comparison of neural data with individual behavioral measures. Second, in order to further investigate the relationship between olfactory and social/emotional processes in the insula, new imaging studies in which both modalities are separately and simultaneously engaged in a controlled fashion should be carried out. Third, there must be careful studies in the structural and functional connectivity among the amygdala, OFC, and anterior insula in the context of value processing, in order to test the theoretical model suggested above. Such experiments must be performed using primary, biological rewards and punishments (e.g. odors, food rewards), as well as with more abstract rewards and punishments (e.g. money, social acceptance), so that one can test whether the model applies to the former, the latter, both, or neither. Finally, additional studies must be performed to find any fine-grained functional differences, similarities, and interactions between the insula and the claustrum in humans. The results from such experiments may help test the roles of the two structures as integrators, as well as ascertain the functional differences between them and reveal any important interactions

that may occur.

Chapter 5

Appendix

The ROI analysis data not discussed in the previous chapter are shown in this Appendix.
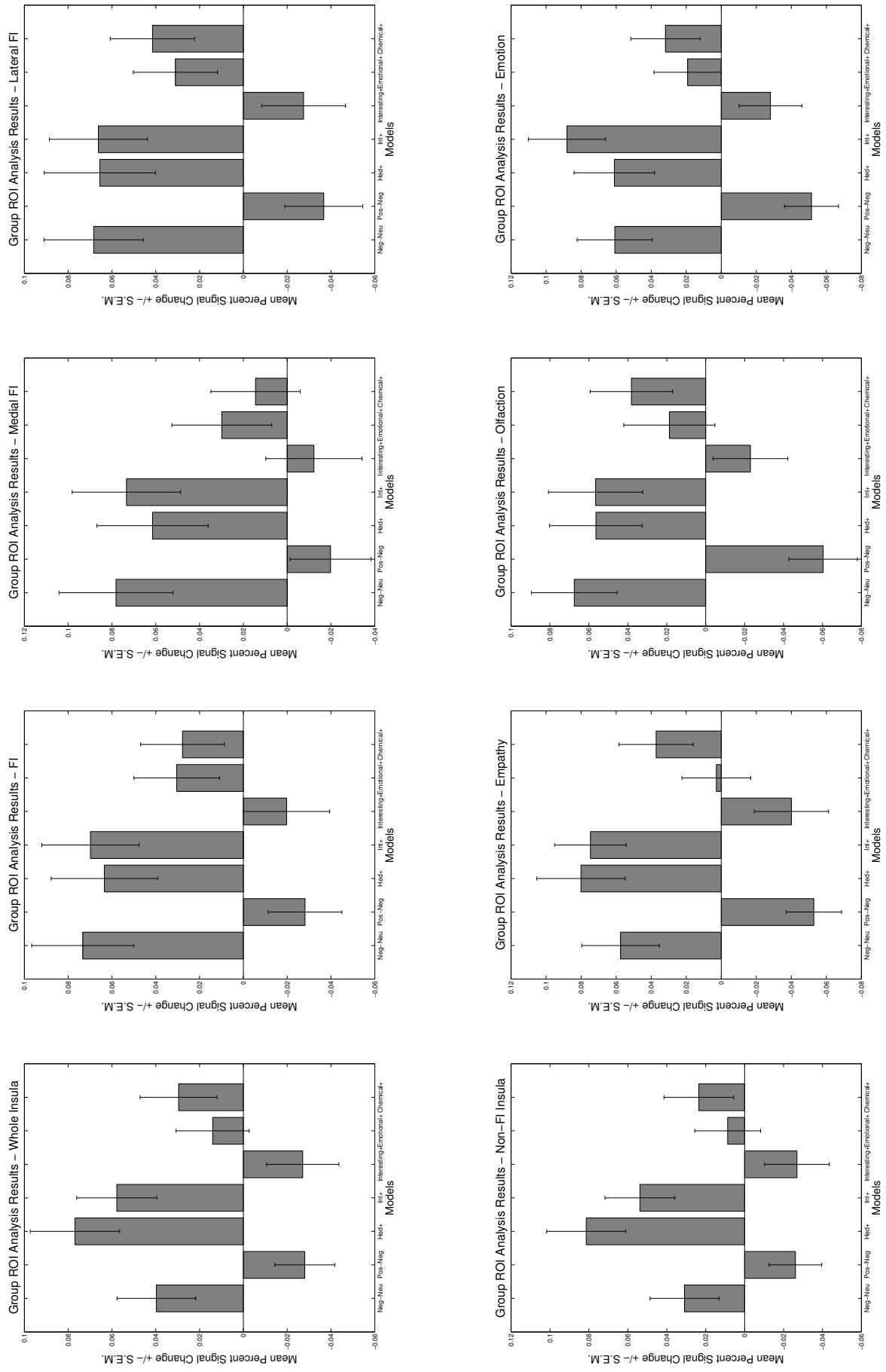
Figure 5.1: First Set of Results from the Original Group ROI Analyses, Non-Hemisphere-Specific.

Models: Neg-Neu = [Negative - Positive]; Pos-Neg = [Positive - Negative]; Hed+ = Effect of Increasing Hedonic Value; Int+ = Effect of Increasing Interesting-ness; Emotional+ = Effect of Increasing Emotional Intensity; Chemical+ = Effect of Increasing Chemical-like Quality.
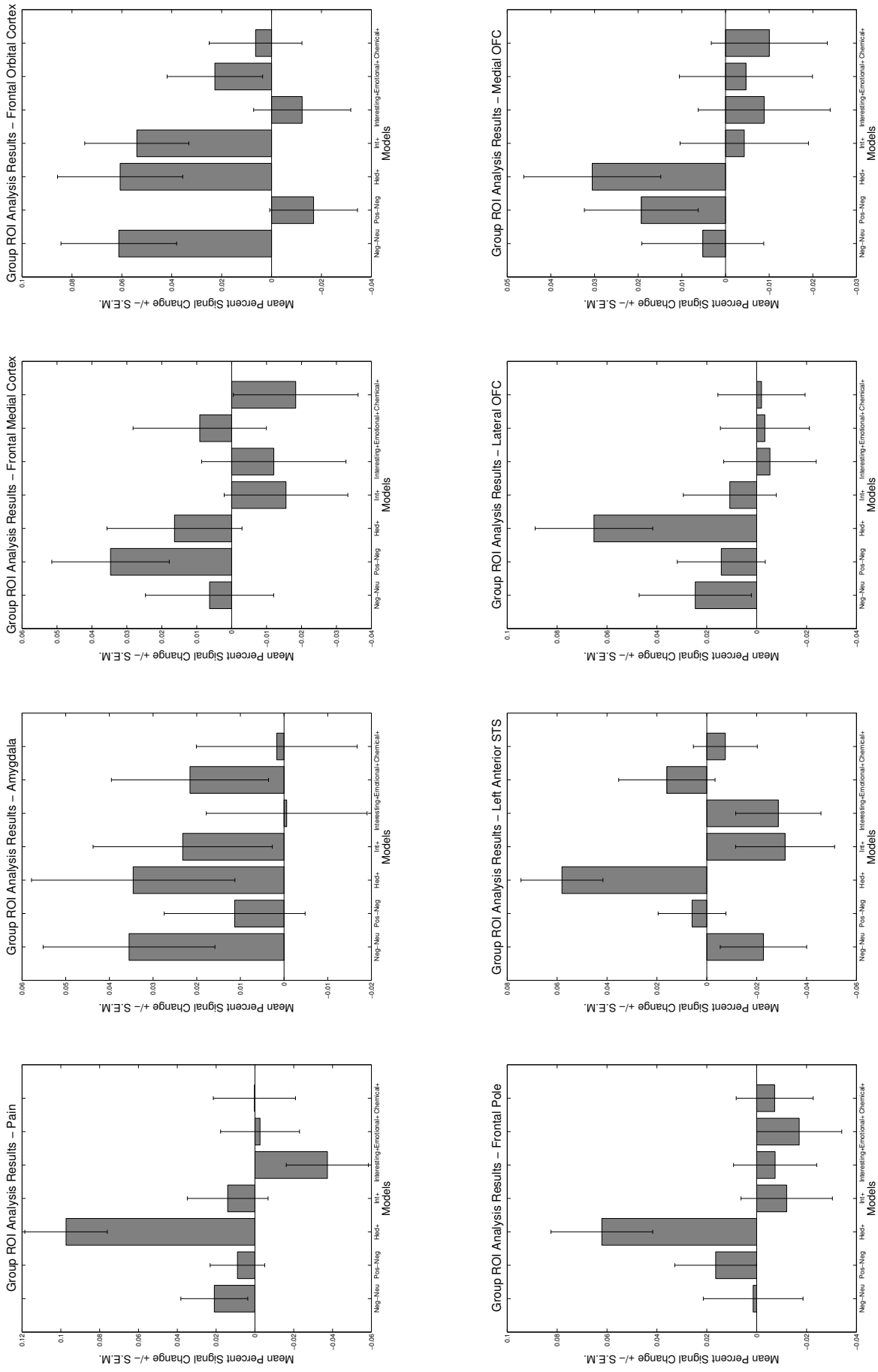
Figure 5.2: Second Set of Results from the Original Group ROI Analyses, Non-Hemisphere-Specific.
Models: Neg-Neu = [Negative - Positive]; Pos-Neg = [Positive - Negative]; Hed+ = Effect of Increasing Hedonic Value; Int+ = Effect of Increasing Interesting-ness; Emotional+ = Effect of Increasing Emotional Intensity; Chemical+ = Effect of Increasing Chemical-like Quality.
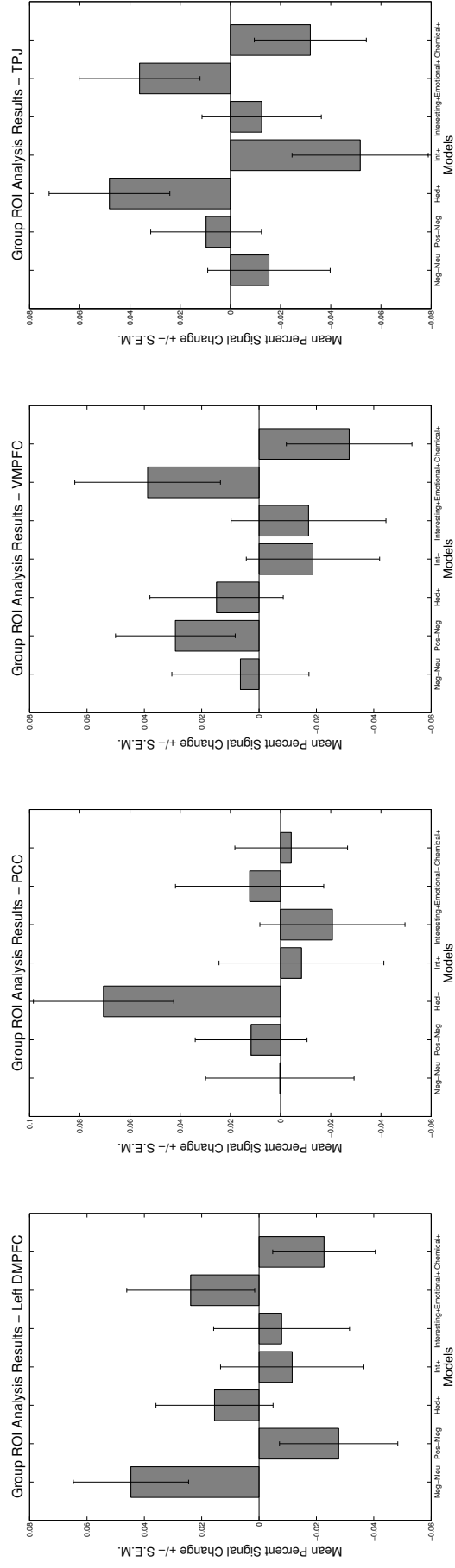
Figure 5.3: Third Set of Results from the Original Group ROI Analyses, Non-Hemisphere-Specific.
Models: Neg-Neu = [Negative - Positive]; Pos-Neg = [Positive - Negative]; Hed+ = Effect of Increasing Hedonic Value; Int+ = Effect of Increasing Intensity Value; Interesting+ = Effect of Increasing Interesting-ness; Emotional+ = Effect of Increasing Emotional Intensity; Chemical+ = Effect of Increasing Chemical-like Quality.
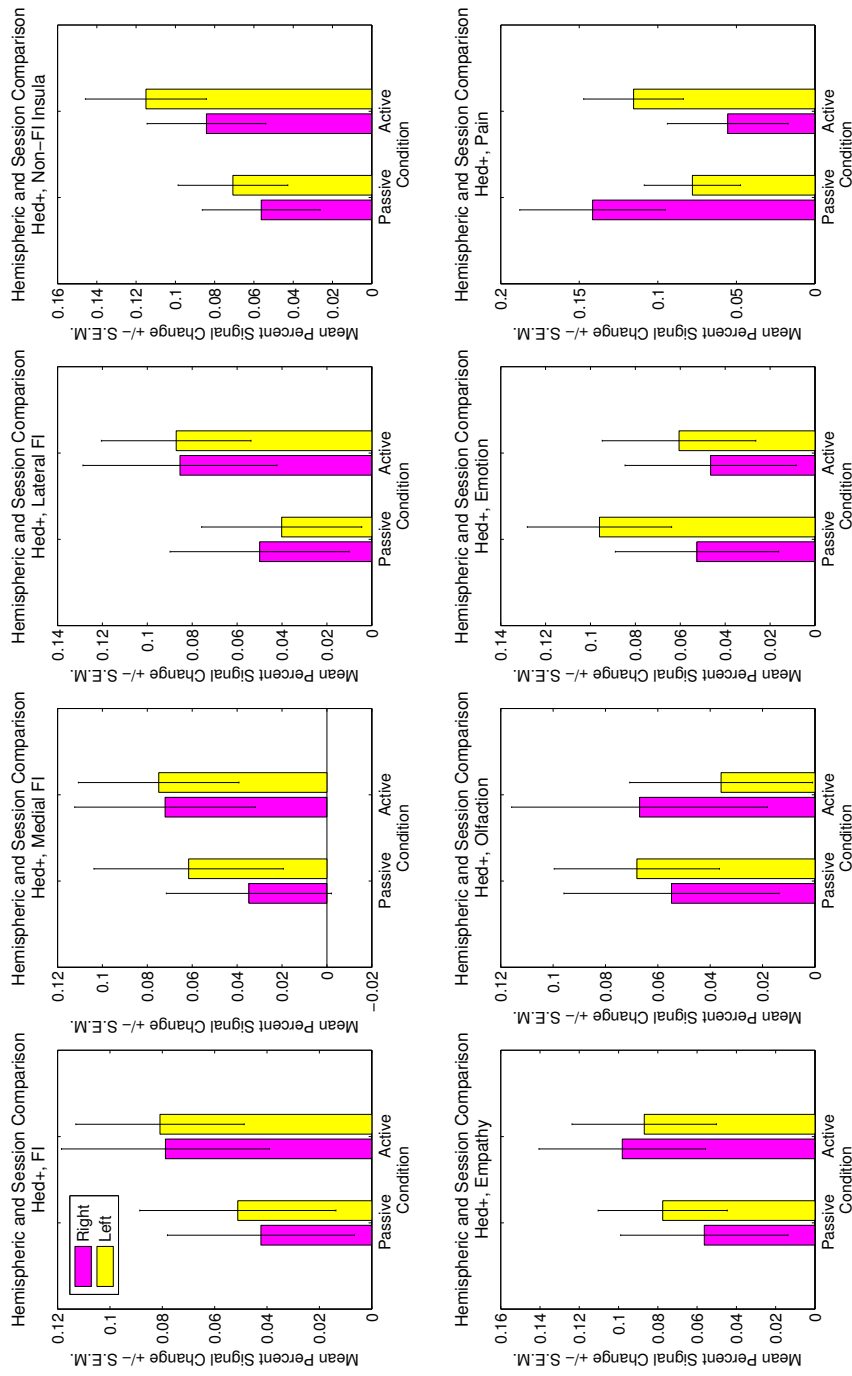
Figure 5.4: Results of the Original Insular ROI Analyses for the Hedonic Value Parametric Model, Hemisphere-Specific.
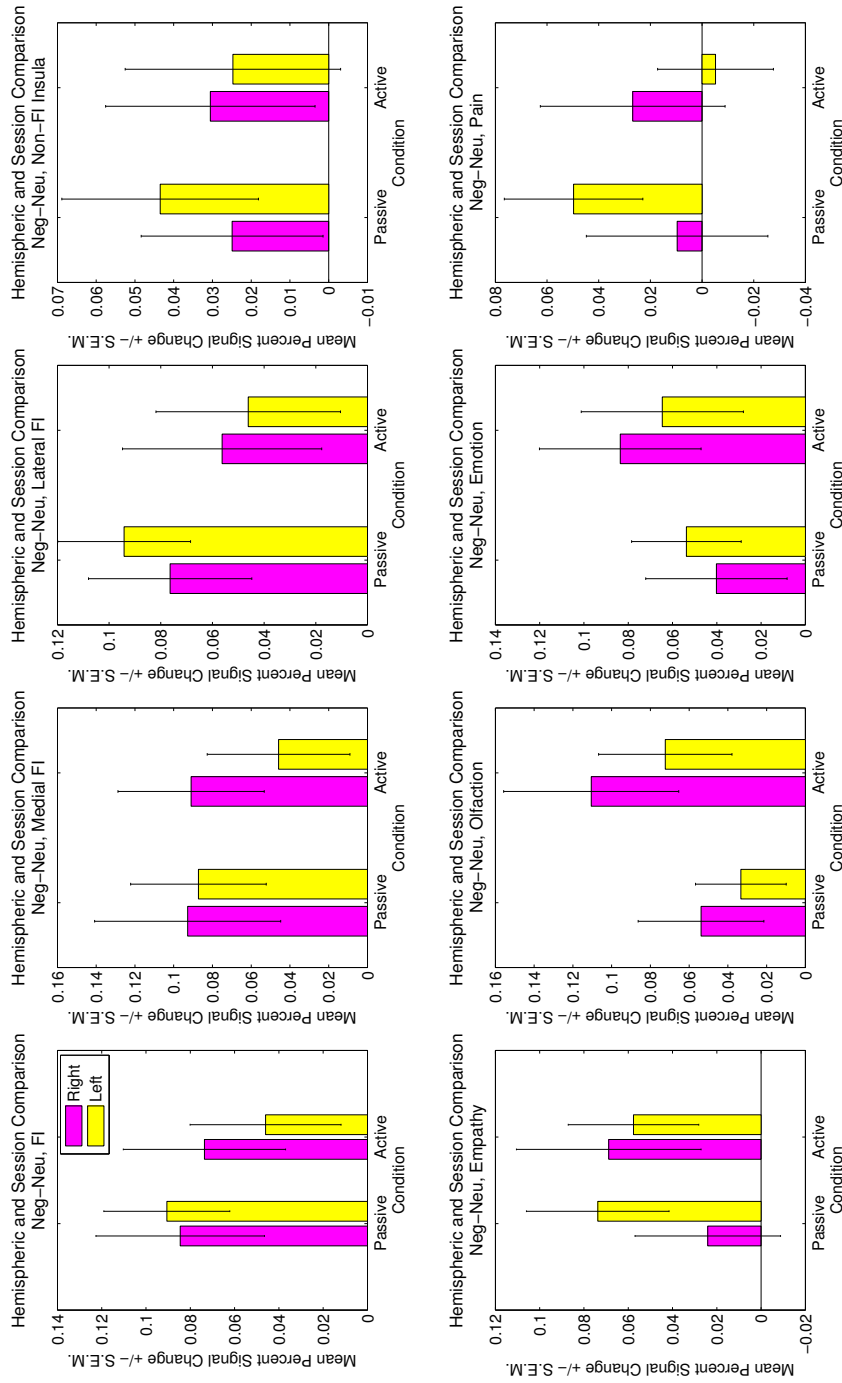
Figure 5.5: Results of the Original Insular ROI Analyses for the [Negative - Neutral] Model, Hemisphere-Specific.
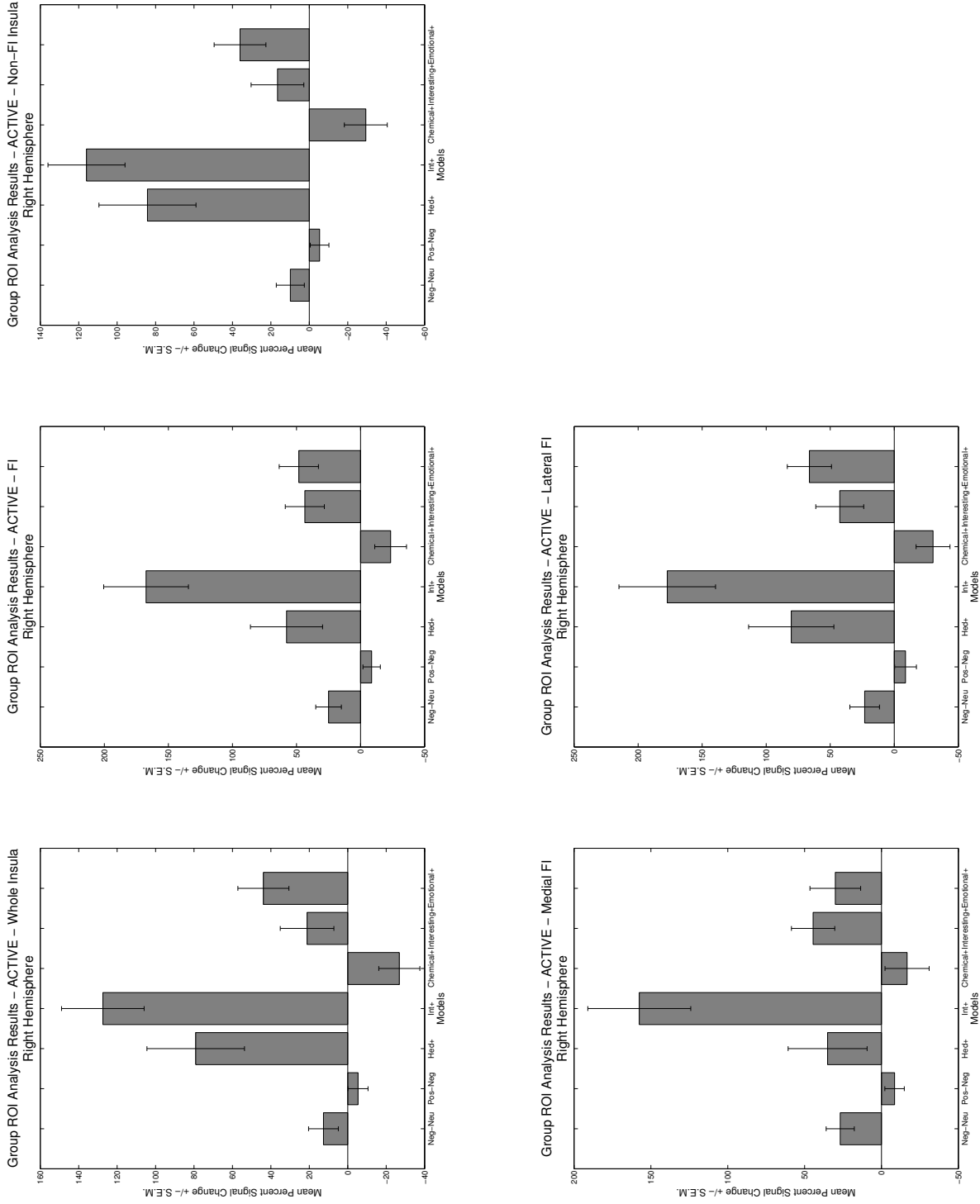
Figure 5.6: Revised ROI Analysis Results for the 5 Main Insular Regions, for Right-Hemisphere-Only Active Runs
Models: Neg-Neu = [Negative - Positive]; Pos-Neg = [Positive - Negative]; Hed+ = Effect of Increasing Hedonic Value; Int+
= Effect of Increasing Intensity Value; Interesting+ = Effect of Increasing Interesting-ness; Emotional+ = Effect of Increasing
Emotional Intensity; Chemical+ = Effect of Increasing Chemical-like Quality.
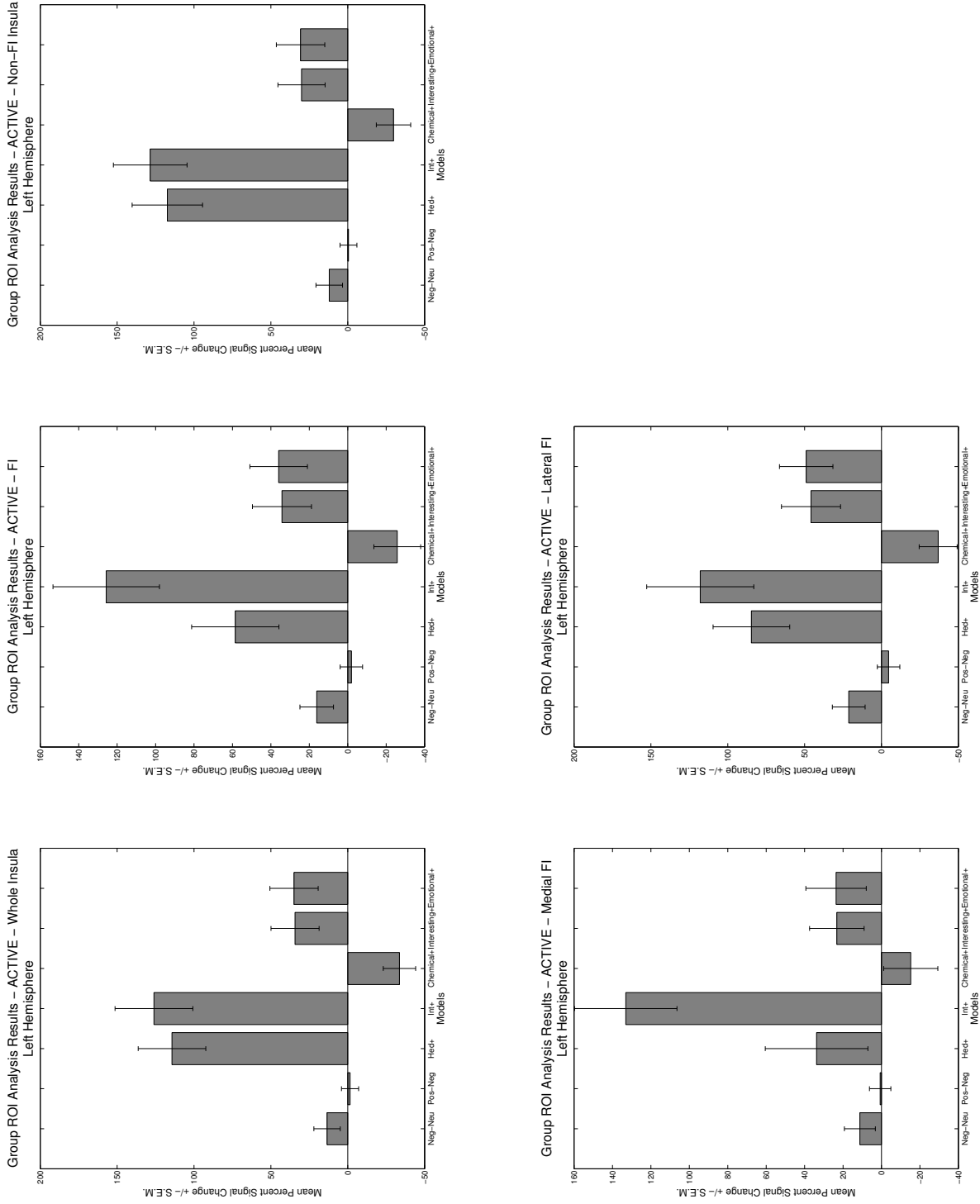
Figure 5.7: Revised ROI Analysis Results for the 5 Main Insular Regions, for Left-Hemisphere-Only Active Runs Models: Neg-Neu = [Negative - Positive]; Pos-Neg = [Positive - Negative]; Hed+ = Effect of Increasing Hedonic Value; Int+ = Effect of Increasing Intensity Value; Interesting+ = Effect of Increasing Interesting-ness; Emotional+ = Effect of Increasing Emotional Intensity; Chemical+ = Effect of Increasing Chemical-like Quality.

174
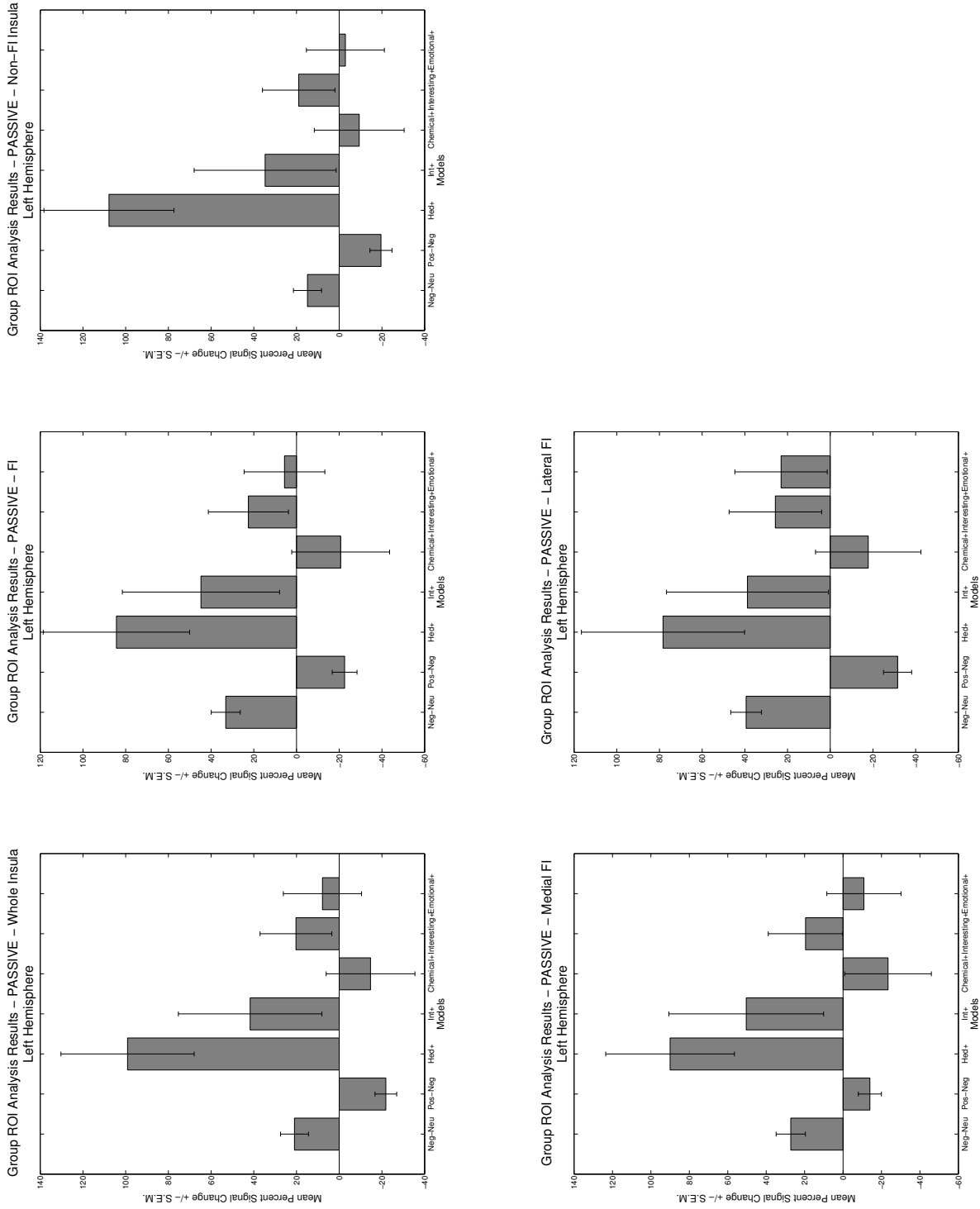
Figure 5.8: Revised ROI Analysis Results for the 5 Main Insular Regions, for Left-Hemisphere-Only Passive Runs Models: Neg-Neu = [Negative - Neutral]; Pos-Neg = [Positive - Negative]; Pos-Neg = [Positive - Negative]; Hed+ = Effect of Increasing Hedonic Value; Int+ = Effect of Increasing Intensity Value; Interesting+ = Effect of Increasing Interesting-ness; Emotional+ = Effect of Increasing Emotional Intensity; Chemical+ = Effect of Increasing Chemical-like Quality.
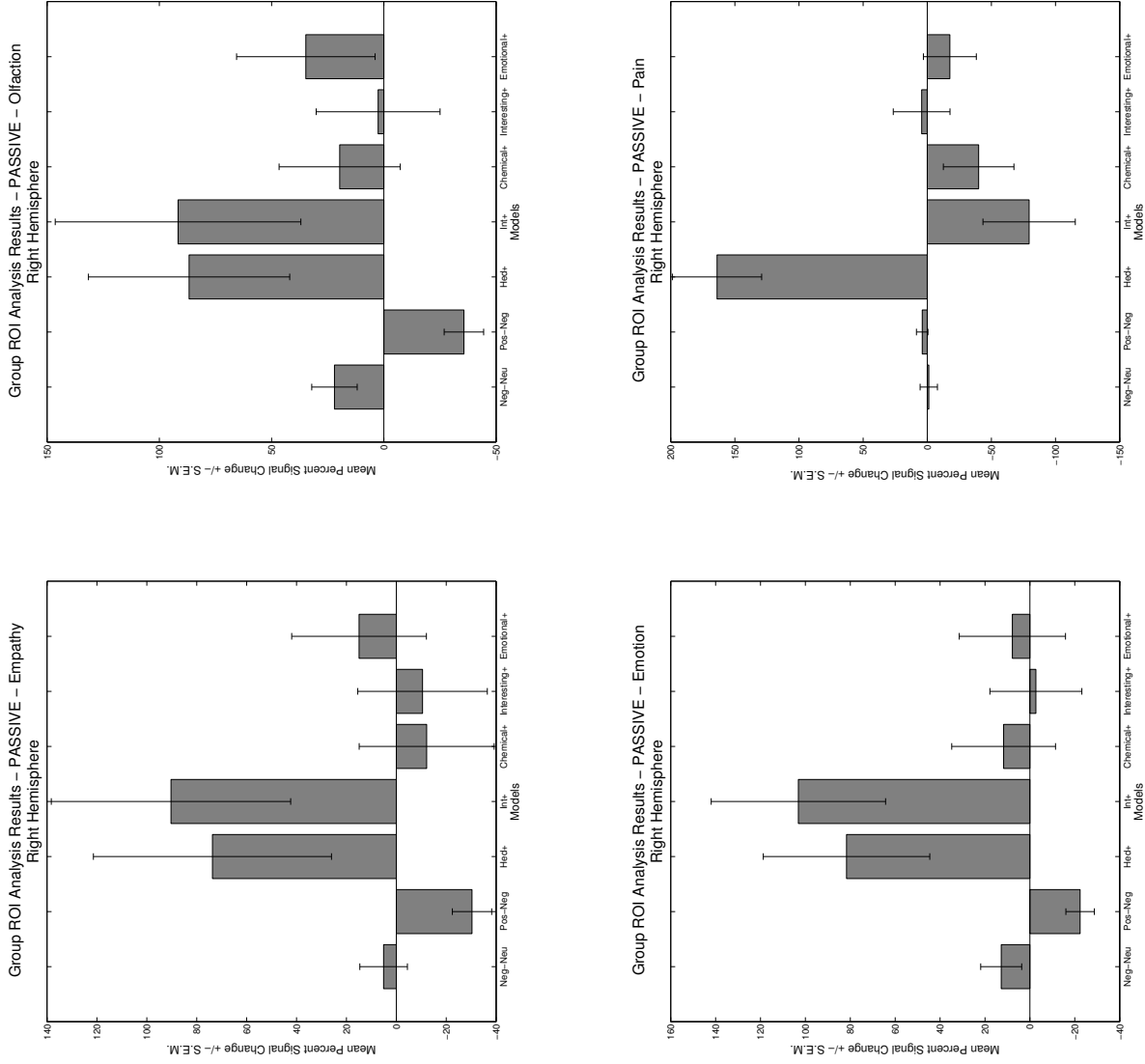
Figure 5.9: Revised ROI Analysis Results for the Functional Insular Regions, for Right-Hemisphere-Only Passive Runs Models: Neg-Neu = [Negative - Positive]; Pos-Neg = [Positive - Negative]; Hed+ = Effect of Increasing Hedonic Value; Int+ = Effect of Increasing Intensity Value; Interesting+ = Effect of Increasing Interesting-ness; Emotional+ = Effect of Increasing Emotional Intensity; Chemical+ = Effect of Increasing Chemical-like Quality.
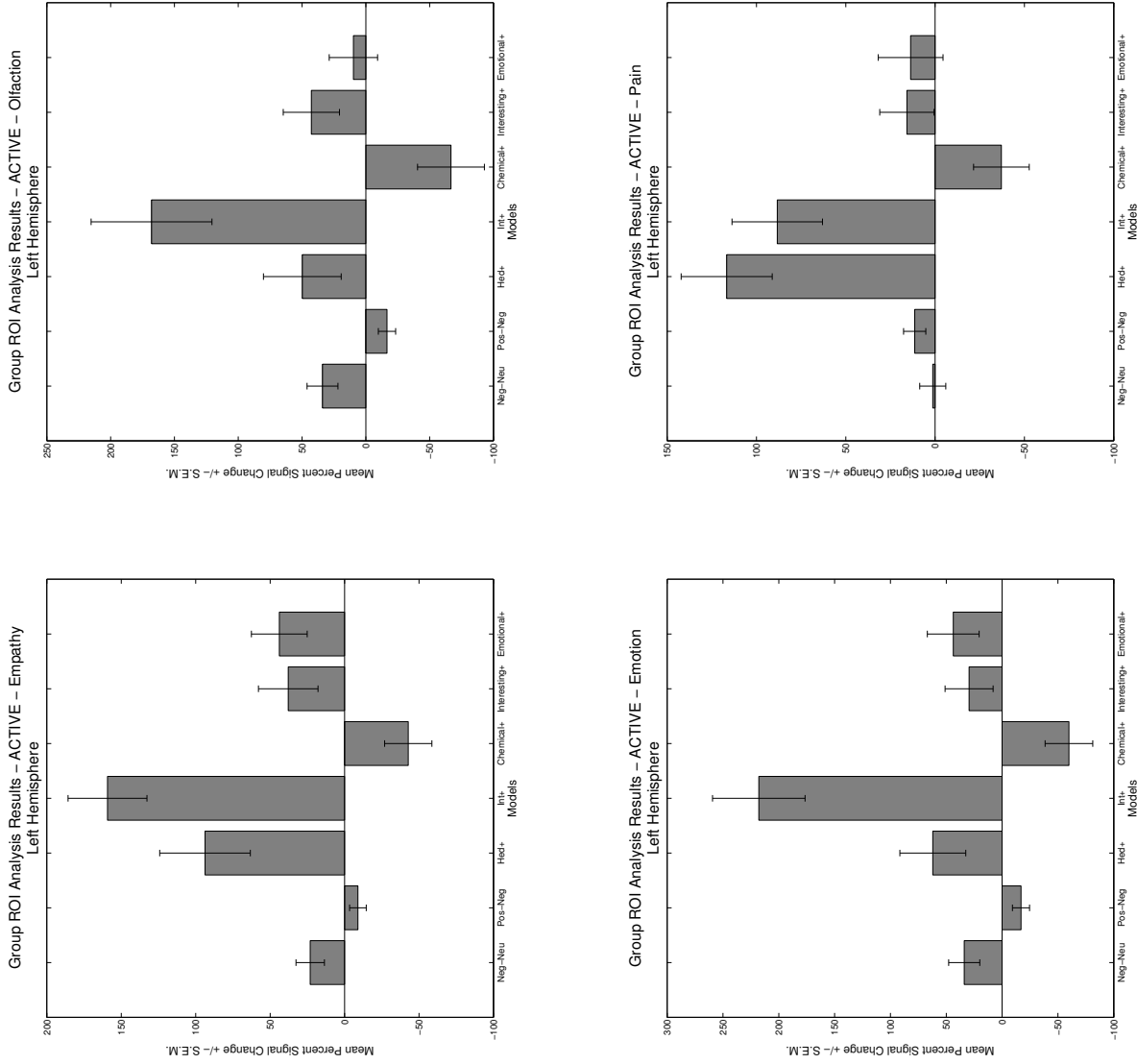
Figure 5.10: Revised ROI Analysis Results for the Functional Insular Regions, for Left-Hemisphere-Only Active Runs Models: Neg-Neu = [Negative - Positive]; Pos-Neg = [Positive - Negative]; Hed+ = Effect of Increasing Hedonic Value; Int+ = Effect of Increasing Intensity Value; Interesting+ = Effect of Increasing Interesting-ness; Emotional+ = Effect of Increasing Emotional Intensity; Chemical+ = Effect of Increasing Chemical-like Quality.
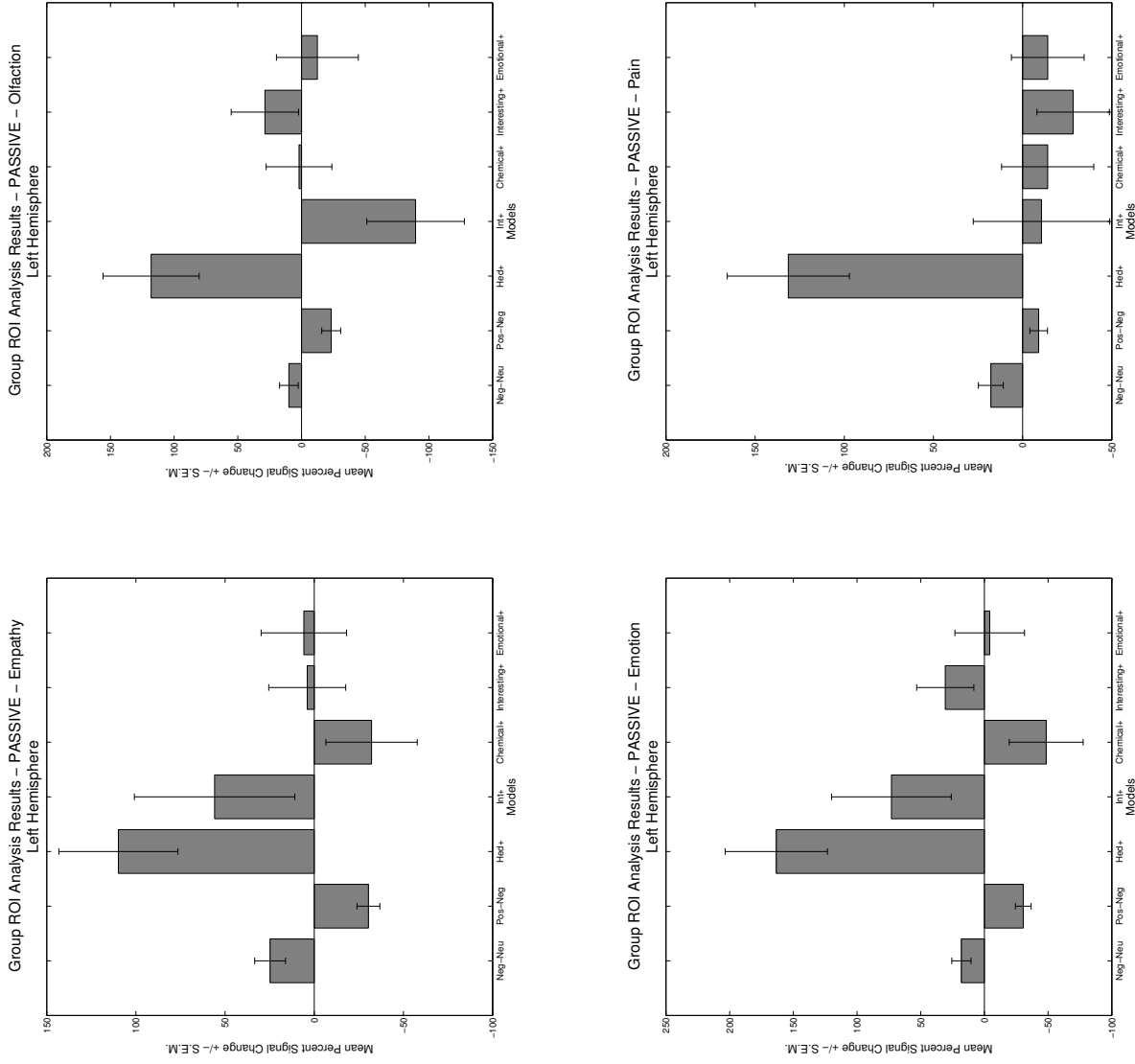
Figure 5.11: Revised ROI Analysis Results for the Functional Insular Regions, for Left-Hemisphere-Only Passive Runs Models: Neg-Neu = [Negative - Positive]; Pos-Neg = [Positive - Negative]; Hed+ = Effect of Increasing Hedonic Value; Int+ = Effect of Increasing Intensity Value; Interesting+ = Effect of Increasing Interesting-ness; Emotional+ = Effect of Increasing Emotional Intensity; Chemical+ = Effect of Increasing Chemical-like Quality.
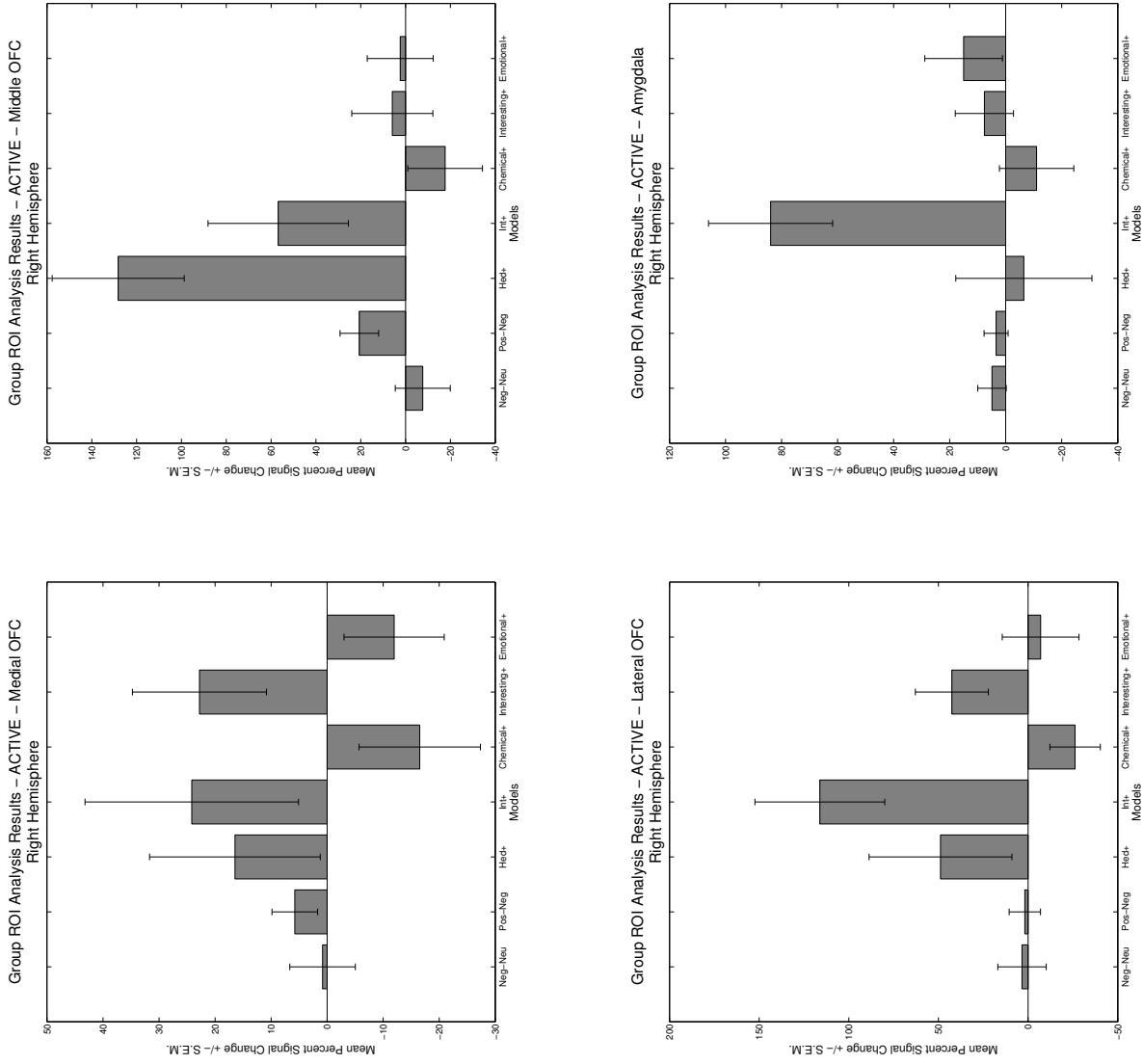
Figure 5.12: Revised ROI Analysis Results for the OFC and Amygdala, for Right-Hemisphere-Only Active Runs Models: Neg-Neu = [Negative - Positive]; Pos-Neg = [Positive - Negative]; Hed+ = Effect of Increasing Hedonic Value; Int+ = Effect of Increasing Intensity Value; Interesting+ = Effect of Increasing Interesting-ness; Emotional+ = Effect of Increasing Emotional Intensity; Chemical+ = Effect of Increasing Chemical-like Quality.
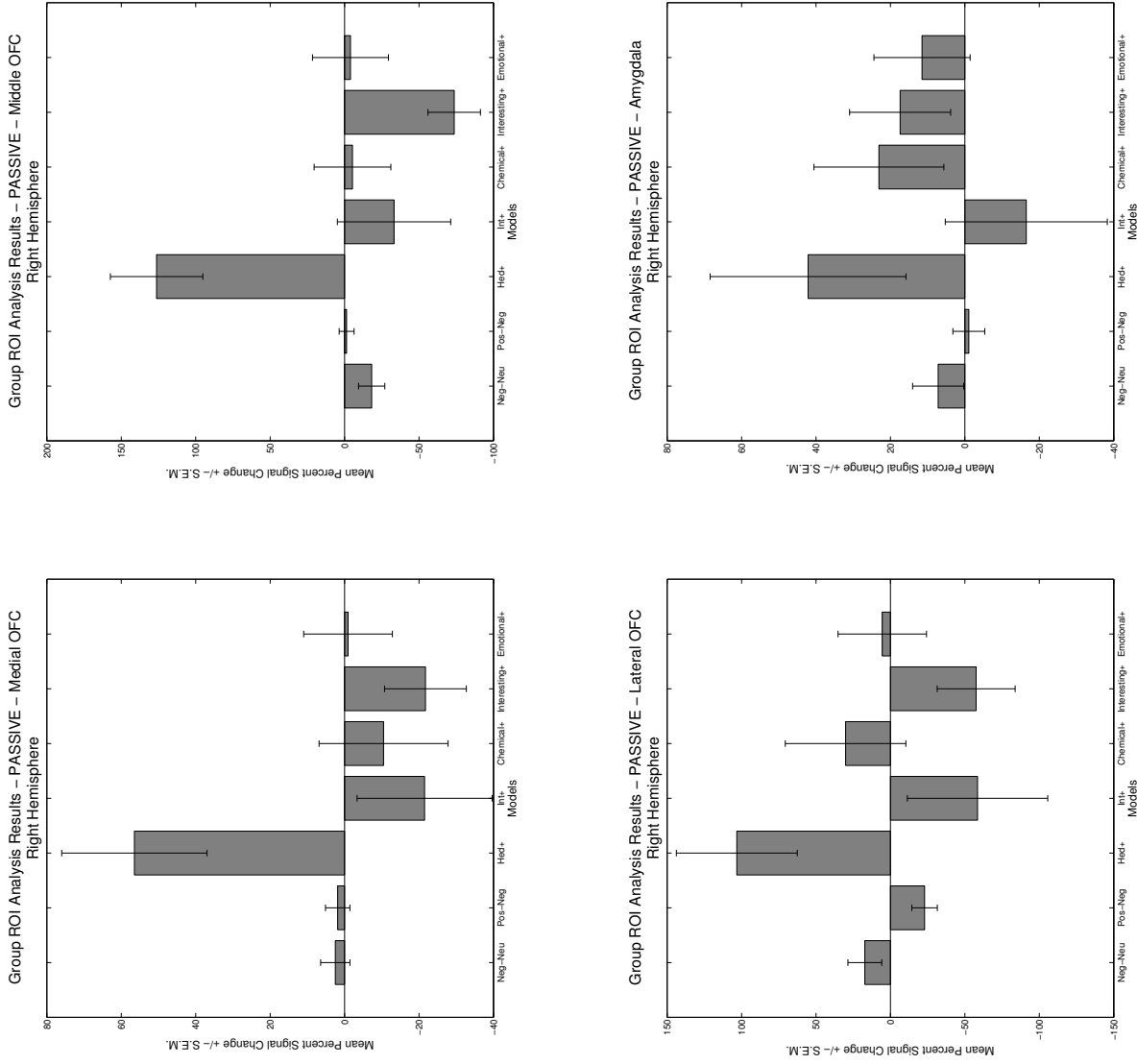
Figure 5.13: Revised ROI Analysis Results for the OFC and Amygdala, for Right-Hemisphere-Only Passive Runs Models: Neg-Neu = [Negative - Neutral]; Pos-Neg = [Positive - Negative]; Hed+ = Effect of Increasing Hedonic Value; Int+ = Effect of Increasing Intensity Value; Interesting+ = Effect of Increasing Interesting-ness; Emotional+ = Effect of Increasing Emotional Intensity; Chemical+ = Effect of Increasing Chemical-like Quality.
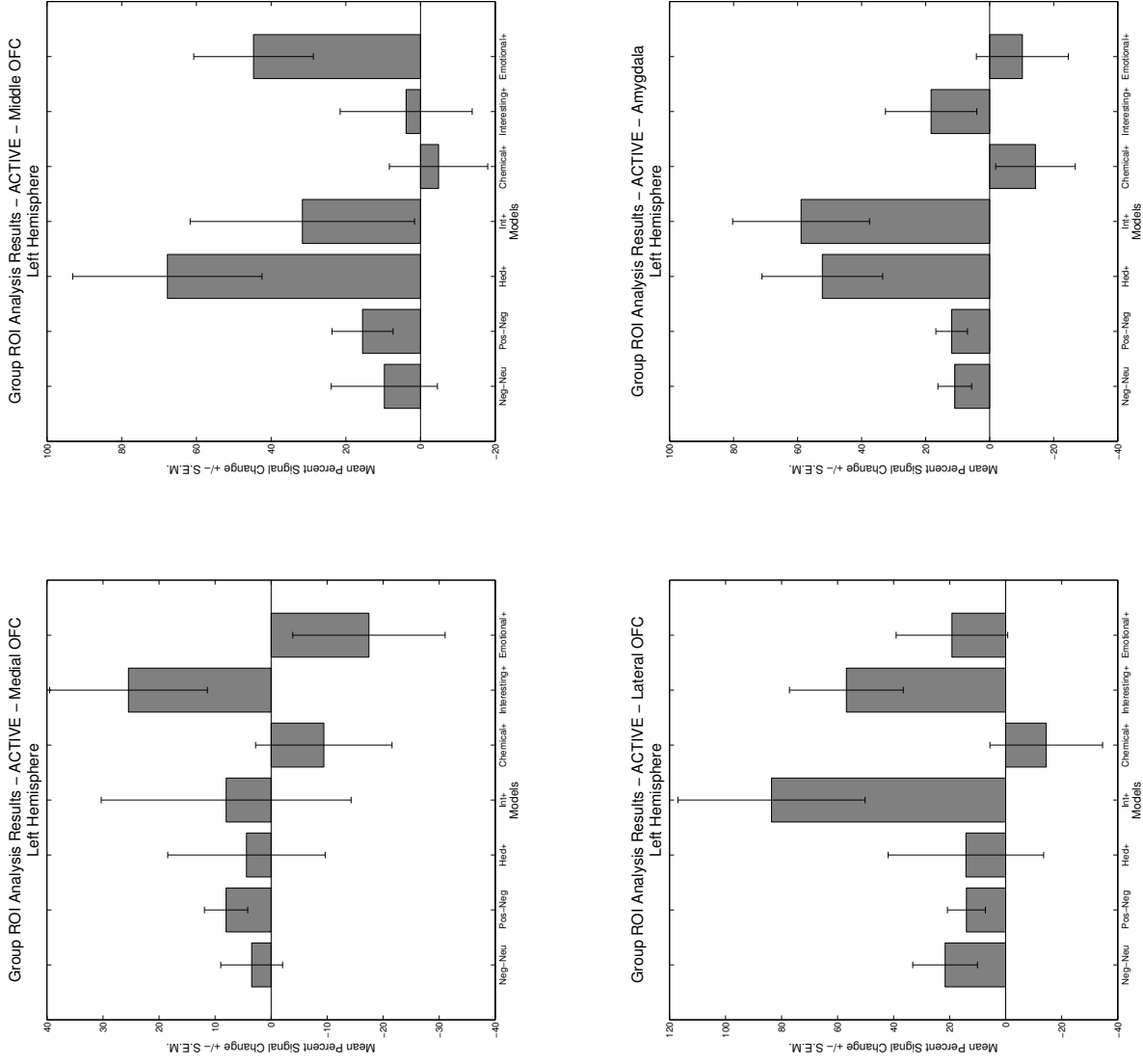
Figure 5.14: Revised ROI Analysis Results for the OFC and Amygdala, for Left-Hemisphere-Only Active Runs Models: Neg-Neu = [Negative - Neutral]; Pos-Neg = [Positive - Negative]; Hed+ = Effect of Increasing Hedonic Value; Int+ = Effect of Increasing Intensity Value; Interesting+ = Effect of Increasing Interesting-ness; Emotional+ = Effect of Increasing Emotional Intensity; Chemical+ = Effect of Increasing Chemical-like Quality.

Figure 5.15: Revised ROI Analysis Results for the OFC and Amygdala, for Left-Hemisphere-Only Passive Runs Models: Neg-Neu = [Negative - Neutral]; Pos-Neg = [Positive - Negative]; Hed+ = Effect of Increasing Hedonic Value; Int+ = Effect of Increasing Intensity Value; Interesting+ = Effect of Increasing Interesting-ness; Emotional+ = Effect of Increasing Emotional Intensity; Chemical+ = Effect of Increasing Chemical-like Quality.

Run Type	Active Runs							Passive Runs						
Model	[Neg - Neu]	[Pos - Neg]	Hedonic+	Intensity+	Chemical+	Interesting+	Emotional+	[Neg - Neu]	[Pos - Neg]	Hedonic+	Intensity+	Chemical+	Interesting+	Emotional+
Bilateral	0.616	0.674	0.051	0.957	0.127	0.458	0.039	0.238	0.020	0.808	0.926	0.940	0.781	0.078
Right Medial Fi vs. Right Lateral FI	0.659	0.979	0.103	0.606	0.434	0.917	0.079	0.589	0.066	0.468	0.586	0.840	0.831	0.302
Left Medial Fi vs. Left Lateral FI	0.320	0.503	0.157	0.698	0.160	0.252	0.214	0.158	0.016	0.700	0.760	0.731	0.795	0.139

Figure 5.16: All p-Values from Two-Tailed, Paired t-Tests, Comparing the Raw Signal Changes in the Medial and Lateral FI ROIs.

The p-values lower than 0.05 are highlighted in red.

Models: Neg-Neu = [Negative - Positive]; Pos-Neg = [Positive - Negative]; Hed+ = Effect of Increasing Hedonic Value; Int+ = Effect of Increasing Intensity Value; Interesting+ = Effect of Increasing Interesting-ness; Emotional+ = Effect of Increasing Emotional Intensity; Chemical+ = Effect of Increasing Chemical-like Quality.

ROI	[Neg - Neu]		[Pos - Neg]		Hedonic+		Intensity+		Chemical+		Interesting+		Emotional+	
	p	F(1,1)	p	F(1,1)	p	F(1,1)	p	F(1,1)	p	F(1,1)	p	F(1,1)	p	F(1,1)
Passive/Active														
Whole Insula	0.6363	0.4132	0.11917	27.87425	0.21766	7.89584	0.14052	19.86119	0.13176	22.68047	0.10618	35.2842	0.1564	15.90528
FI	0.45523	1.32607	0.13347	22.08589	0.34712	2.71776	0.0676	88.02043	0.41569	1.70918	0.28271	4.41754	0.14009	19.98797
Medial FI	0.61375	0.48169	0.24045	6.35295	0.34518	2.75533	0.05865	117.15457	0.65028	0.37479	0.4352	1.50679	0.05172	150.85781
Lateral FI	0.31982	3.31312	0.08691	52.99661	0.37312	2.26874	0.07684	67.97926	0.23118	6.92534	0.11928	27.82359	0.21944	7.7578
Non-FI Insula	0.972	0.00194	0.13258	22.39173	0.09469	44.53891	0.20778	8.72856	0.12803	24.06017	0.20631	8.86255	0.05998	111.96974
Empathy	0.54721	0.7425	0.37223	2.28251	0.76696	0.14694	0.06347	99.94089	0.06467	96.25093	0.08939	50.06003	0.0131	2,359.89
Olfaction	0.0005	1.63456E+11	0.23154	6.90193	0.26737	5.01481	0.15952	15.26539	0.28999	4.16689	0.31991	3.31099	0.19965	9.50739
Emotion	0.09051	48.80361	0.3804	2.15929	0.23995	6.38189	0.14998	17.35437	0.08463	55.92307	0.51421	0.91457	0.00967	4,336.29
Pain	0.68085	0.30033	0.40445	1.83966	0.41217	1.74886	0.12825	23.97751	0.92149	0.01536	0.36539	2.39205	0.2828	4.41464
Amygdala	0.12019	27.39091	0.35789	2.51977	0.88377	0.03409	0.22764	7.16338	0.07313	75.11074	0.13709	20.90103	0.46455	1.25005
Lateral OFC	0.00612	10,833.68	0.13708	20.90402	0.19147	10.39461	0.1167	29.09399	0.31764	3.36747	0.12913	23.64305	0.602	0.52094
Middle OFC	0.49968	1.002	0.09644	42.91137	0.5174	0.89637	0.17854	12.05331	0.99431	0.00008	0.323	3.2358	0.45566	1.32251
Medial OFC	0.38581	2.0821	0.28303	4.40626	0.03367	356.89006	0.20988	8.54157	0.07468	72.0125	0.13175	22.68352	0.57394	0.62573
Left/Right														
Whole Insula	0.44838	1.38514	0.88252	0.03484	0.08088	61.28643	0.47285	1.18628	0.25619	5.51936	0.11215	31.55864	0.99138	0.00018
FI	0.92617	0.01357	0.54596	0.74844	0.47697	1.15581	0.18624	11.02422	0.45871	1.29712	0.92059	0.01572	0.757	0.16112
Medial FI	0.63125	0.4278	0.43892	1.47127	0.51969	0.88356	0.30759	3.63309	0.52235	0.8689	0.81195	0.09259	0.46937	1.21256
Lateral FI	0.60304	0.51734	0.8293	0.07549	0.62446	0.44811	0.14125	19.65011	0.36171	2.45363	0.33795	2.90151	0.87916	0.03691
Non-FI Insula	0.33471	2.97021	0.72178	0.21823	0.03068	429.90828	0.71931	0.22269	0.47953	1.13733	0.18173	11.61067	0.68927	0.2819
Empathy	0.64248	0.39585	0.50116	0.99276	0.76599	0.14829	0.15599	15.99295	0.04101	240.31724	0.14106	19.70493	0.05127	153.53886
Olfaction	0.00099	413,290.96	0.08289	58.32054	0.71242	0.2354	0.24638	6.02026	0.32517	3.1845	0.687	0.28678	0.11598	29.46385
Emotion	0.49863	1.00868	0.71475	0.23104	0.3164	3.39902	0.95312	0.00544	0.0191	1,110.49	0.85479	0.05389	0.0404	247.64722
Pain	0.57754	0.61133	0.70863	0.24262	0.82113	0.08329	0.12323	26.02294	0.99238	0.00014	0.53741	0.79012	0.39636	1.94065
Amygdala	0.05251	146.3202	0.93454	0.01065	0.74051	0.18644	0.94673	0.00704	0.3053	3.69734	0.12821	23.99102	0.04444	204.58347
Lateral OFC	0.00465	18,770.53	0.58567	0.5799	0.74781	0.17494	0.87962	0.03663	0.7527	0.16749	0.31682	3.38828	0.74836	0.17408
Middle OFC	0.14579	18.40361	0.26215	5.24253	0.63294	0.42286	0.84308	0.06331	0.98171	0.00083	0.52405	0.85963	0.99925	1.40E-06
Medial OFC	0.33849	2.89027	0.77644	0.13422	0.14262	19.26239	0.76533	0.14921	0.06257	102.84002	0.40697	1.8095	0.30949	3.58088

Figure 5.17: All p-Values and F-ratios from the ANOVA, Examining the Effect of the Passive/Active (Top) and Left/Right (Bottom) Variables

Models: Neg-Neu = [Negative - Positive]; Pos-Neg = [Positive - Negative]; Hed+ = Effect of Increasing Hedonic Value; Int+ = Effect of Increasing Intensity Value; Interesting+ = Effect of Increasing Interesting-ness; Emotional+ = Effect of Increasing Emotional Intensity; Chemical+ = Effect of Increasing Chemical-like Quality.

	Active Runs							Passive Runs						
Run Type														
Model	[Neg - Neu]	[Pos - Neg]	Hedonic+	Intensity+	Chemical+	Interesting+	Emotional+	[Neg - Neu]	[Pos - Neg]	Hedonic+	Intensity+	Chemical+	Interesting+	Emotional+
Whole Insula - Bilateral														
Perceiving MSCEIT Pearson	-0.3570664	0.06003241	0.06487407	-0.1271905	0.2661426	-0.3823851	-0.094635	0.13451736	0.16847474	-0.0550564	-0.2083099	0.14051665	-0.163366	0.13060164
Perceiving MSCEIT Spearman	-0.2778853	0.0294986	0.04469736	-0.0792846	0.06239856	-0.3815074	-0.1339948	0.17931528	0.07419344	0.00712432	-0.1266428	0.2294235	-0.2305081	0.00585773
Overall MSCEIT Pearson	-0.4015048	0.15015637	0.07476485	-0.0534167	0.17071554	-0.3564079	-0.1607844	-0.0961192	0.38152469	-0.0829408	-0.2278104	0.27531335	-0.1768275	0.13360518
Overall MSCEIT Spearman	-0.3445778	0.15178369	-0.0043821	-0.0375186	0.00615197	-0.3152512	-0.1574393	-0.0429445	0.11817316	-0.0983156	-0.128465	0.34360986	-0.2516456	0.08538089
SNI Pearson	-0.1123599	0.1836458	0.19903262	0.03235504	-0.2516642	0.04878032	0.32504714	-0.0308167	0.08887279	-0.1371145	0.08807176	0.53984406	-0.0102865	-0.4117695
SNI Spearman	0.09862712	0.05776971	0.04521108	0.05643012	-0.1339587	0.15371766	0.31932415	0.07133303	0.08991981	0.05375095	0.08472891	0.02612195	0.11955818	-0.358326
Positive PANAS Pearson	0.05087109	0.10654133	0.17648224	-0.2474387	0.08994917	-0.0095672	0.11661299	0.23472262	0.05541529	-0.1299129	-0.0826227	0.24508454	-0.2035805	0.1055731
Positive PANAS Spearman	0.14050353	0.01672661	0.02458812	-0.2333362	0.08162586	-0.0481726	0.12695498	0.05988127	0.16492438	-0.0117086	-0.147696	0.22564198	-0.1757967	0.0996906
Negative PANAS Pearson	-0.0484139	0.13757094	0.14818763	0.03307245	0.02825177	-0.4157972	0.12616351	0.09744442	0.01239182	-0.0658753	-0.145775	0.01281678	-0.249959	0.24340637
Negative PANAS Spearman	0.0369595	0.09641608	0.32495789	0.21515069	-0.2651442	-0.0765972	0.02196144	0.02910337	0.02606805	-0.0196403	0.01678354	0.09230947	-0.3019252	0.20622328
Whole Insula - Right														
Perceiving MSCEIT Pearson	-0.3273121	0.02186224	0.08865414	-0.0977545	0.33670873	-0.4388324	-0.1865223	0.16329574	0.11904431	0.02703718	-0.3169027	0.06748316	-0.1006523	0.15885538
Perceiving MSCEIT Spearman	-0.2614855	-0.0127422	0.1217944	-0.0438009	0.22400895	-0.3818177	-0.1076919	0.23926233	-0.0312864	0.25404549	-0.2669521	0.13724718	-0.0446439	0.07848414
Overall MSCEIT Pearson	-0.4121849	0.17413077	0.13373753	-0.014684	0.26843208	-0.4294333	-0.2916586	-0.0532821	0.35741433	-0.0111537	-0.277262	0.21460666	-0.1494411	0.16093542
Overall MSCEIT Spearman	-0.3617064	0.16210863	0.10459577	-0.0391527	0.19618394	-0.365487	-0.2305081	0.08290922	0.0788417	0.10530105	-0.1904198	0.27431908	-0.1700111	0.11745805
SNI Pearson	-0.0899669	0.13877547	0.08541669	0.01582832	-0.2515694	0.00046601	0.27958282	0.14826965	-0.0542931	-0.1407742	0.08439068	0.5084908	-0.0249007	-0.3748957
SNI Spearman	0.032485	0.07669138	0.11604176	-0.004856	-0.118386	0.17732789	0.298728	0.20679881	-0.0031815	0.14785696	-0.0577697	0.01121904	0.03600141	-0.3399203
Positive PANAS Pearson	0.12464978	0.05386177	0.13562838	-0.3272551	0.1139772	0.02726164	0.05628704	0.22738039	0.06540024	-0.1256749	-0.1669919	0.25043727	-0.1957088	0.0793888
Positive PANAS Spearman	0.14251072	0.01572301	0.10621398	-0.2037301	0.1386636	-0.0230827	0.09651254	0.10437405	0.18633444	0.05787407	-0.2507319	0.24604844	-0.1241115	-0.0210755
Negative PANAS Pearson	-0.0738837	0.17242933	0.10669704	-0.0672095	-0.0045971	-0.3014401	0.06254232	0.07379268	0.03162823	-0.0726541	-0.1606822	0.00052739	-0.2160415	0.23022887
Negative PANAS Spearman	-0.0976659	0.13855347	0.18211926	0.12730493	-0.3997696	-0.0258895	0.06784835	0.06017077	0.00535645	-0.0203545	0.062849	0.10409365	-0.3215655	0.1826549
Whole Insula - Left														
Perceiving MSCEIT Pearson	-0.3709584	0.09223744	0.03006691	-0.1410946	0.18027927	-0.301464	-0.0120335	0.10273191	0.20740124	-0.1306084	-0.0978232	0.20424563	-0.2159499	0.09448353
Perceiving MSCEIT Spearman	-0.3083179	0.09475346	-0.003681	-0.0645826	-0.0443468	-0.3380213	-0.0060557	0.10493505	0.16385937	-0.1603651	-0.0519327	0.27642248	-0.2972006	0.00281772
Overall MSCEIT Pearson	-0.3794179	0.11711495	-0.002355	-0.0818743	0.06126052	-0.2625778	-0.0411309	-0.1329757	0.38754656	-0.1476714	-0.1715514	0.32152455	-0.1914943	0.09817445
Overall MSCEIT Spearman	-0.2987112	0.12111345	-0.0548638	-0.0112318	-0.1085006	-0.2973171	0.02137296	-0.1105597	0.15958478	-0.2118536	-0.1055053	0.33216272	-0.2075484	0.1310241
SNI Pearson	-0.128356	0.21391611	0.31090609	0.04372832	-0.2367601	0.0888054	0.3378618	0.0298375	-0.0075497	-0.1285073	0.08779774	0.54680725	0.00336142	-0.4179144
SNI Spearman	0.12191264	0.11118576	0.00971201	0.0643002	-0.1428335	0.18486307	0.25217733	0.02411257	0.16175518	0.06212337	0.13261916	0	0.14634993	-0.3930015
Positive PANAS Pearson	-0.0188577	0.14949963	0.20535136	-0.1566139	0.05972391	-0.0421321	0.15899256	0.23312439	0.04387775	-0.1290057	-0.0005355	0.22963139	-0.1995302	0.12310108
Positive PANAS Spearman	0.05051859	0.08814924	0.08196039	-0.1856654	0.04716904	-0.0066906	0.17880747	0.0710881	0.12160246	0.0187338	-0.059714	0.14602331	-0.1940287	0.16893877
Negative PANAS Pearson	-0.0230941	0.09525827	0.18092685	0.11660328	0.06032995	-0.4873796	0.17037877	0.11635157	-0.0061384	-0.0570026	-0.1257877	0.02403089	-0.2668252	0.2387922
Negative PANAS Spearman	0.09856689	0.06713416	0.4185172	0.24086165	-0.2206857	-0.1119498	0.02696079	0.02374692	0.0266037	0.02696079	0.02249708	0.07963254	-0.2426471	0.18622587

Figure 5.18: Correlation Coefficients between ROI Signal Changes and Individual Behavioral Measures - Whole Insula Models: Neg-Neu = [Negative - Neutral]; Pos-Neg = [Positive - Negative]; Hed+ = Effect of Increasing Hedonic Value; Int+ = Effect of Increasing Intensity Value; Interesting+ = Effect of Increasing Interesting-ness; Emotional+ = Effect of Increasing Emotional Intensity; Chemical+ = Effect of Increasing Chemical-like Quality.

Run Type	Active Runs							Passive Runs						
Model	[Neg - Neu]	[Pos - Neg]	Hedonic+	Intensity+	Chemical+	Interesting+	Emotional+	[Neg - Neu]	[Pos - Neg]	Hedonic+	Intensity+	Chemical+	Interesting+	Emotional+
FI - Bilateral														
Perceiving MSCEIT Pearson	-0.1952065	-0.0701988	0.06129356	-0.0320626	0.16961755	-0.2919428	-0.0780108	0.25525604	0.03480668	-0.0561837	-0.1548588	0.08213531	-0.099986	0.07593886
Perceiving MSCEIT Spearman	-0.1321094	-0.1139891	0.04984094	-0.0232806	0.04553444	-0.3104132	-0.0916566	0.20411178	-0.0138283	-0.0692961	-0.1579846	0.19587183	-0.1004031	0.0067681
Overall MSCEIT Pearson	-0.3116021	0.08534683	0.13206103	0.0614111	0.00216764	-0.2669253	-0.1815964	-0.0106755	0.2386463	-0.0427058	-0.1932231	0.15085943	-0.0427702	0.12628218
Overall MSCEIT Spearman	-0.3183381	0.06091294	0.15724464	0.05233751	-0.059545	-0.270771	-0.1711045	-0.1307313	0.05933919	-0.0883255	-0.2520101	0.23998237	-0.0417284	0.15637883
SNI Pearson	0.00173997	0.13151971	0.15830438	0.04524487	-0.2317017	0.10259378	0.12512446	0.06842735	-0.0445408	-0.1665138	0.02480864	0.46928751	0.01193788	-0.4736205
SNI Spearman	0.1009714	0.01021435	0.0769138	0.05743481	-0.1289353	0.16209008	0.16627629	0.06061633	0.07451455	0.0316475	-0.0090422	-0.0477228	0.30324911	-0.3436042
Positive PANAS Pearson	0.03289374	0.14289223	0.28356952	-0.2065047	0.01060662	-0.0794395	0.08630653	0.26093218	-0.119252	-0.189138	-0.0644736	0.15604421	-0.2071443	0.1010747
Positive PANAS Spearman	0.07961867	0.0409802	0.28017073	-0.2467175	0.08731291	-0.0381367	0.10086146	0.1885089	-0.0951744	-0.1456888	-0.0832985	0.18733804	-0.1778039	0.09701434
Negative PANAS Pearson	-0.0103918	0.13933505	0.22152773	-0.0447872	0.05459466	-0.4194781	0.07794866	0.06907052	-0.0111943	-0.0954035	-0.0860787	0.04477925	-0.1896647	0.11505984
Negative PANAS Spearman	0.0887385	0.16087201	0.31620902	0.06874109	-0.1646215	-0.0965946	0.0349947	-0.0748117	0.01196274	-0.1108785	-0.0571355	0.21068698	-0.3454909	0.07570448
FI - Right														
Perceiving MSCEIT Pearson	-0.2098333	-0.1041747	0.03794992	0.01981126	0.16990337	-0.2811806	-0.1685687	0.38695855	-0.0680456	0.00254067	-0.2681208	0.04947057	-0.0041273	0.12842885
Perceiving MSCEIT Spearman	-0.1506958	-0.1127089	0.02171055	0.00474581	0.07827133	-0.3307302	-0.207184	0.30782042	-0.100365	0.05853161	-0.2675111	0.15856058	-0.0135257	0.00035622
Overall MSCEIT Pearson	-0.3500627	0.04435066	0.11788461	0.08502769	0.12264162	-0.3136636	-0.2866056	0.09472487	0.16551186	0.052896	-0.2449725	0.10143453	-0.0419395	0.17040544
Overall MSCEIT Spearman	-0.3981504	0.0528323	0.16609453	0.02865061	0.08002629	-0.3300258	-0.264401	-0.0428241	-0.0409545	0.06134394	-0.1895776	0.25586707	-0.1231742	0.12574425
SNI Pearson	-0.0583306	0.13433865	0.13640933	0.01101412	-0.2436485	0.04186846	0.05006724	0.1018336	-0.0060652	-0.1295466	0.02988545	0.39190483	0.03346479	-0.4622941
SNI Spearman	-0.0639653	0.06731427	0.14048923	0.00853987	-0.1344611	0.07200282	0.09226408	0.16594139	0.03365713	-0.0028466	-0.0053583	-0.0842266	0.30291421	-0.4055601
Positive PANAS Pearson	0.06094784	0.06898756	0.22444934	-0.1938469	0.03273369	-0.0398408	-0.0066259	0.28303144	-0.0586965	-0.1945874	-0.0550273	0.15268885	-0.1382959	-0.0505633
Positive PANAS Spearman	0.11491182	-0.049009	0.19570135	-0.210588	0.080455	-0.0807895	-0.0155557	0.23433982	-0.0143849	-0.280338	-0.1000251	0.1702769	-0.0199047	-0.0985197
Negative PANAS Pearson	-0.0228616	0.17119234	0.18217262	-0.0672919	0.0563201	-0.3223106	0.01332174	0.04550802	0.05695113	-0.1034422	-0.1251568	0.01665805	-0.2181494	0.15581749
Negative PANAS Spearman	0.0839177	0.23229133	0.27603566	-0.0248182	-0.2005097	0.01481951	-0.0455298	-0.0546358	0.11480655	-0.1649786	-0.0740975	0.17015652	-0.4281588	0.09677317
FI - Left														
Perceiving MSCEIT Pearson	-0.1721937	-0.0288814	0.08096509	-0.082632	0.14660687	-0.2733722	0.01048762	0.08539836	0.11869544	-0.0988164	-0.0536751	0.10339449	-0.1666022	0.02463355
Perceiving MSCEIT Spearman	-0.1022253	-0.0308109	0.03133249	-0.0317264	0.02232542	-0.2815311	0.05120378	0.01292569	0.14545977	-0.0910732	-0.0529223	0.18649261	-0.2530119	-0.0071243
Overall MSCEIT Pearson	-0.2599527	0.1195682	0.13616994	0.03087213	-0.1054903	-0.2012194	-0.0685353	-0.1303343	0.27717702	-0.1166964	-0.1382176	0.18091681	-0.039141	0.07618268
Overall MSCEIT Spearman	-0.2928273	0.10874435	0.09609797	0.07098992	-0.1098769	-0.237757	-0.0329818	-0.2484605	0.18186848	-0.1343554	-0.1903026	0.20793662	-0.1112817	0.11755129
SNI Pearson	0.06157306	0.1164831	0.16769579	0.07617582	-0.1887473	0.14516406	0.17862497	0.0254785	-0.0728258	-0.1804546	0.0190885	0.49657884	-0.0062173	-0.4303374
SNI Spearman	0.19457507	-0.0606163	0.09912947	0.11704645	-0.112023	0.19072376	0.14568013	-0.0569325	0.12441418	0.07250517	-0.0293035	-0.0728401	0.18921672	-0.3144681
Positive PANAS Pearson	0.00391815	0.20410359	0.32193625	-0.1986859	-0.0104907	-0.1060452	0.15981763	0.21521415	-0.1589086	-0.1668173	-0.0675651	0.14605452	-0.2413849	0.21356312
Positive PANAS Spearman	0.03980933	0.1386636	0.31195129	-0.2020575	0.0883165	-0.06975	0.1682697	0.13297656	-0.1142428	-0.0782805	-0.093	0.14585605	-0.2694657	0.20858084
Negative PANAS Pearson	0.00246598	0.09427511	0.24420568	-0.0168834	0.04543731	-0.4635748	0.1271997	0.08992032	-0.0679741	-0.0799215	-0.0491123	0.06503548	-0.1488447	0.06908799
Negative PANAS Spearman	0.11873461	0.08766721	0.33138563	0.11569929	-0.1431957	-0.2399689	0.0469582	-0.0203545	-0.0824893	-0.1506948	0.02963902	0.24407551	-0.296047	0.07374044

Figure 5.19: Correlation Coefficients between ROI Signal Changes and Individual Behavioral Measures - FI Models: Neg-Neu = [Negative - Positive]; Pos-Neg = [Positive - Negative]; Hed+ = Effect of Increasing Hedonic Value; Int+ = Effect of Increasing Intensity Value; Interesting+ = Effect of Increasing Interesting-ness; Emotional+ = Effect of Increasing Emotional Intensity; Chemical+ = Effect of Increasing Chemical-like Quality.

Run Type	Active Runs							Passive Runs						
Model	[Neg - Neu]	[Pos - Neg]	Hedonic+	Intensity+	Chemical+	Interesting+	Emotional+	[Neg - Neu]	[Pos - Neg]	Hedonic+	Intensity+	Chemical+	Interesting+	Emotional+
Non-FI - Bilateral														
Perceiving MSCEIT Pearson	-0.3914334	0.08814817	0.09032263	-0.1572027	0.24851303	-0.3843218	-0.1023759	0.11278364	0.18144807	-0.0719991	-0.2076708	0.1402637	-0.148773	0.12238119
Perceiving MSCEIT Spearman	-0.3489511	0.05130968	0.05545682	-0.0461402	0.04106612	-0.3845544	-0.1134588	0.1847349	0.08653031	0.0021373	-0.1302872	0.24183383	-0.1816732	0.0076328
Overall MSCEIT Pearson	-0.4212516	0.17000502	0.10021579	-0.0978175	0.1550537	-0.364663	-0.146442	-0.1066581	0.39118854	-0.1043173	-0.2300805	0.29927589	-0.178876	0.10925927
Overall MSCEIT Spearman	-0.3824795	0.16108021	-0.0179006	-0.0366304	-0.000702	-0.3670341	-0.1339245	-0.0138859	0.13177022	-0.110427	-0.1000387	0.33414486	-0.2184816	0.08112072
SNI Pearson	-0.1379127	0.21899548	0.18755943	0.05316268	-0.2316752	0.02136853	0.35863067	0.07577882	-0.0248621	-0.1565247	0.08792622	0.60315988	-0.0617664	-0.3986086
SNI Spearman	0.12508398	0.08121249	0.06798406	0.03549907	-0.1510385	0.14685227	0.32903616	0.0743471	0.11302769	0.06697937	0.06195592	0.03097796	0.04755535	-0.3382458
Positive PANAS Pearson	0.06741072	0.10483414	0.14833793	-0.2648266	0.10784822	-0.0188758	0.14009315	0.20088557	0.09180844	-0.1313204	-0.0889325	0.25609829	-0.1914276	0.12832453
Positive PANAS Spearman	0.17245136	0.00117086	-0.0168939	-0.2457139	0.09617801	-0.0459982	0.17479308	0.01120683	0.18466178	0.03178056	-0.1796438	0.23952507	-0.1707787	0.12762404
Negative PANAS Pearson	-0.0586748	0.14661127	0.13033844	0.05539543	0.01942759	-0.412297	0.14436987	0.11088805	0.00652035	-0.0614419	-0.1429226	0.01458467	-0.2707647	0.2624295
Negative PANAS Spearman	-0.0385664	0.114628	0.27532147	0.2617518	-0.2758571	-0.071955	0.06213481	0.01624789	-0.0069634	-0.0235684	0.05927803	0.13212574	-0.3603105	0.22693488
Non-FI - Right														
Perceiving MSCEIT Pearson	-0.3455554	0.03950309	0.11286368	-0.1368089	0.33342584	-0.4197601	-0.1945089	0.13981521	0.15211387	0.00182329	-0.2981767	0.06419895	-0.0823867	0.12656656
Perceiving MSCEIT Spearman	-0.2512812	0.01328474	0.11667214	-0.03808	0.18016003	-0.3627433	-0.1631165	0.23613145	0.02585138	0.18309503	-0.2675111	0.12110594	-0.0315359	-0.0205596
Overall MSCEIT Pearson	-0.4285085	0.22085132	0.16813711	-0.0623793	0.23140603	-0.4145515	-0.2821359	-0.062328	0.37773066	-0.0636141	-0.269188	0.25458689	-0.1497398	0.11828449
Overall MSCEIT Spearman	-0.3511377	0.2333805	0.10784671	-0.0294986	0.14299538	-0.3513015	-0.2700485	0.10555023	0.12063976	0.07231185	-0.1736285	0.26769862	-0.1315807	0.04201315
SNI Pearson	-0.1054501	0.16033134	0.06872526	0.027618	-0.2576017	-0.0005385	0.32166107	0.14324224	-0.0810794	-0.1578269	0.09850968	0.59077636	-0.0856839	-0.3851707
SNI Spearman	0.10666465	0.02310788	0.032485	-0.0584395	-0.1121904	0.21014778	0.31597519	0.21065012	-0.0133959	0.15388511	-0.0915943	0.03918293	-0.0031815	-0.2975559
Positive PANAS Pearson	0.15595412	0.05598037	0.1083158	-0.3590231	0.12807395	0.0231356	0.08562878	0.19475791	0.09516047	-0.1130172	-0.1752729	0.25812389	-0.1970686	0.12326741
Positive PANAS Spearman	0.20389738	-0.0173957	0.00418165	-0.2462157	0.14769597	-0.0312788	0.07828054	0.07443342	0.18415998	0.06841184	-0.3007445	0.22965637	-0.1679352	0.0508489
Negative PANAS Pearson	-0.0833692	0.18521931	0.09130267	-0.0457336	-0.0237308	-0.3002677	0.08791774	0.08331244	0.0161177	-0.0752396	-0.1473591	0.01178486	-0.2399329	0.24194925
Negative PANAS Spearman	-0.1106999	0.1467667	0.15944362	0.17176346	-0.3408487	-0.0840962	0.12623364	0.06570577	-0.0244611	-0.0635632	0.10623623	0.13801783	-0.3490619	0.27264324
Non-FI - Left														
Perceiving MSCEIT Pearson	-0.4176615	0.12549505	0.05448058	-0.1582717	0.14852086	-0.3161627	-0.0139742	0.08404414	0.20035543	-0.1400754	-0.110467	0.20927851	-0.2012446	0.11033614
Perceiving MSCEIT Spearman	-0.3915244	0.18487611	-0.0063399	-0.0940373	-0.057477	-0.3553648	-0.023154	0.07893062	0.1323457	-0.1709393	-0.049746	0.29177065	-0.3126833	0.03486932
Overall MSCEIT Pearson	-0.4035718	0.11011408	0.01155516	-0.1179857	0.068629	-0.2850101	0.01709837	-0.1429446	0.3889525	-0.1396767	-0.1812796	0.3333215	-0.1965334	0.09339926
Overall MSCEIT Spearman	-0.3565379	0.15032316	0.30075545	-0.0539616	-0.1059897	-0.333066	0.03965564	-0.1122018	0.14962368	-0.2337768	-0.0373551	0.35131568	-0.2866569	0.10883454
SNI Pearson	-0.1608668	0.25551331	0.30077356	0.06977356	-0.1902736	0.03965564	0.35720207	0.01171057	0.02449592	-0.1499514	0.07393572	0.59677497	-0.037044	-0.3847148
SNI Spearman	0.08757553	0.16309477	0.07183538	0.12391184	-0.1615877	0.13647047	0.266243	0.01507036	0.1842924	0.0100469	0.12960508	0.03064306	0.07602159	-0.3559954
Positive PANAS Pearson	-0.012595	0.1412584	0.17647938	-0.1558206	0.08008121	-0.05598	0.17477421	0.19874546	0.08573522	-0.1443618	-0.0031841	0.24632039	-0.1778308	0.12466582
Positive PANAS Spearman	0.13230749	0.04031113	0.0493435	-0.1781384	0.06289206	-0.0669064	0.18549811	0.01421762	0.17004021	0.00752697	-0.0822949	0.16576071	-0.2043992	0.21627508
Negative PANAS Pearson	-0.034771	0.09985859	0.15953013	0.13707483	0.06277399	-0.4781395	0.18037467	0.13168278	-0.0019925	-0.0461956	-0.121932	0.01680518	-0.286019	0.26469788
Negative PANAS Spearman	0.04624401	0.06874109	0.37155899	0.28460598	-0.2317557	-0.1028438	0.02213999	0.02285418	0.00705325	0.03820933	0.0473153	0.11623494	-0.2871057	0.19229651

Figure 5.20: Correlation Coefficients between ROI Signal Changes and Individual Behavioral Measures - Non-FI Insula Models: Neg-Neu = [Negative - Positive]; Pos-Neg = [Positive - Negative]; Hed+ = Effect of Increasing Hedonic Value; Int+ = Effect of Increasing Intensity Value; Interesting+ = Effect of Increasing Interesting-ness; Emotional+ = Effect of Increasing Emotional Intensity; Chemical+ = Effect of Increasing Chemical-like Quality.

| Run Type | Active Runs | | | | | | | Passive Runs | | | | | | |
Model	[Neg - Neu]	[Pos - Neg]	Hedonic+	Intensity+	Chemical+	Interesting+	Emotional+	[Neg - Neu]	[Pos - Neg]	Hedonic+	Intensity+	Chemical+	Interesting+	Emotional+
Medial FI - Bilateral														
Perceiving MSCEIT Pearson	-0.1400793	-0.2138983	0.06306522	0.02669842	0.09002328	-0.2882231	-0.1122844	0.27802876	-0.0284572	-0.1784244	-0.1363198	0.10918785	-0.0585448	0.05387077
Perceiving MSCEIT Spearman	-0.1134566	-0.1528564	0.04703937	0.12305442	-0.0063179	-0.2479263	-0.1130941	0.26210425	0.01837939	-0.0943972	-0.1927865	0.20989352	-0.037331	0.01651616
Overall MSCEIT Pearson	-0.2588637	-0.0127049	0.13847343	0.09251178	-0.0577218	-0.2557919	-0.1776756	0.07380575	0.10942806	-0.1467602	-0.2132656	0.20335234	-0.0208959	0.11287873
Overall MSCEIT Spearman	-0.3990918	0.06918762	0.15638372	0.18536931	-0.139695	-0.253982	-0.1584043	-0.0653465	0.08104437	-0.0723119	-0.2768263	0.23762192	-0.0831381	0.15905778
SNI Pearson	0.03417763	0.10528394	0.07897032	0.06142974	-0.1779519	0.14115147	0.0357128	0.02818759	-0.0153655	-0.186272	-0.0011888	0.51814008	-0.1138651	-0.4236138
SNI Spearman	0.04537852	-0.0016745	0.12943764	-0.0092097	-0.0684864	0.15689918	0.08389166	0.08489635	0.09360367	0.0655398	-0.1063298	-0.0234428	0.16744843	-0.2429677
Positive PANAS Pearson	0.0661002	0.15907199	0.30087614	-0.203424	-0.009012	-0.2157563	0.11069302	0.18144987	-0.163808	-0.2059119	-0.0566625	0.1175147	-0.2540793	0.11182387
Positive PANAS Spearman	0.06941543	0.06991723	0.30191532	-0.2554153	0.06506652	-0.1622481	0.13832907	0.16141179	-0.1197625	-0.1246133	-0.129464	0.12795857	-0.2507319	0.12327512
Negative PANAS Pearson	0.01321254	0.12521801	0.20822963	-0.0552479	0.04991486	-0.4063452	0.05611091	0.09106151	-0.058498	-0.1297548	-0.0276657	0.04570359	-0.1215068	0.05365814
Negative PANAS Spearman	0.09480914	0.20104538	0.35691804	-0.003571	-0.1412317	-0.1733704	0.05374304	-0.078398	-0.0023211	-0.2028309	-0.0157122	0.2585393	-0.3192443	-0.0180334
Medial FI - Right														
Perceiving MSCEIT Pearson	-0.1170525	-0.2696608	0.00477471	0.11185798	0.0349118	-0.2268997	-0.1743703	0.4585263	-0.1484938	-0.1565121	-0.2353016	0.1120936	0.0718909	0.02708634
Perceiving MSCEIT Spearman	-0.0757586	-0.134194	0.00637108	0.14535993	-0.0249351	-0.2502419	-0.242246	0.44003577	-0.1078816	-0.013032	-0.242246	0.17359477	0.1233674	-0.0045447
Overall MSCEIT Pearson	-0.3141698	-0.0266358	0.07893595	0.1646382	0.00919905	-0.2627387	-0.2773389	0.19984186	-0.0073472	-0.0875217	-0.2544303	0.19890904	0.03690432	0.05006852
Overall MSCEIT Spearman	-0.3806052	0.07678294	0.12883743	0.15271549	-0.0783675	-0.2343142	-0.2948072	0.05913036	-0.0339757	0.03627818	-0.2776444	0.20827797	-0.0161531	0.07339955
SNI Pearson	-0.0903978	0.11396208	0.13704256	0.00048116	-0.2171458	0.11718629	-0.0015015	0.05662006	0.0005521	-0.1214627	0.05132713	0.49439915	-0.1087591	-0.5167221
SNI Spearman	-0.116879	-0.0016745	0.14015434	-0.0105493	-0.1311121	0.16510415	0.08154738	0.25267968	-0.0051909	-0.029136	0.05576033	-0.0740122	0.2295718	-0.3909921
Positive PANAS Pearson	0.06235971	0.03341478	0.25393665	-0.1352884	-0.0416853	-0.1704809	0.01772345	0.23380968	-0.1150005	-0.1849288	0.0132768	0.12221242	-0.1506184	-0.1432791
Positive PANAS Spearman	0.10353772	-0.0319478	0.25190276	-0.1313039	0.03211509	-0.0946726	-0.0734298	0.28468691	-0.1180899	-0.2405287	-0.0137158	0.08731291	-0.047169	-0.1262859
Negative PANAS Pearson	0.01197261	0.13285019	0.19670588	-0.0027258	0.06475054	-0.3714809	0.0277022	0.06914938	0.038802	-0.1726341	-0.0614664	0.05342103	-0.1627415	0.10137106
Negative PANAS Spearman	0.10516494	0.20068828	0.30388919	-0.0085703	-0.1180204	-0.085703	-0.0267822	-0.0858817	0.11873461	-0.3210298	-0.0160693	0.28639146	-0.4533341	0.0780256
Medial FI - Left														
Perceiving MSCEIT Pearson	-0.1487948	-0.1347617	0.10226291	-0.069819	0.11837998	-0.3000734	-0.0263712	0.03473169	0.06745851	-0.1740188	-0.0511856	0.10125044	-0.1625282	0.061583
Perceiving MSCEIT Spearman	-0.073799	-0.1588821	-0.0200763	0.04813706	-0.0001753	-0.1816702	0.00419106	0.03697308	0.18493986	-0.1425416	-0.0960575	0.19164191	-0.1568915	0.08999608
Overall MSCEIT Pearson	-0.1744565	0.00242792	0.16888949	-0.0051171	-0.1027118	-0.2149861	-0.0404231	-0.0796217	0.18553993	-0.1730018	-0.1611908	0.19569644	-0.0676147	0.13387568
Overall MSCEIT Spearman	-0.2447213	0.03985578	0.05424116	0.09061094	-0.1372472	-0.1930691	-0.0340751	-0.1859528	0.23292615	-0.1425416	-0.2106016	0.25587353	-0.1202346	0.17200434
SNI Pearson	0.15078975	0.0848419	0.02161209	0.11188236	-0.1057877	0.14190585	0.05992704	-0.0070159	-0.0257476	-0.2156301	-0.0380318	0.50472286	-0.1037167	-0.2647122
SNI Spearman	0.19072376	-0.0413598	0.11537197	0.01691229	-0.0164099	0.1615773	0.04152721	-0.0396853	0.1545549	0.07719373	-0.1553921	0.00569325	0.191561	-0.0862359
Positive PANAS Pearson	0.06363366	0.26166085	0.30033745	-0.2287992	0.02102342	-0.2244416	0.16586419	0.09841474	-0.1808928	-0.1977938	-0.0999611	0.10697529	-0.3082102	0.27556867
Positive PANAS Spearman	0.05402695	0.17429128	0.27381462	-0.3219873	0.12628591	-0.2149369	0.14602331	0.00836331	-0.1073848	-0.0883165	-0.1868362	0.09885427	-0.2758218	0.28953763
Negative PANAS Pearson	0.01320182	0.10347708	0.19083777	-0.0982084	0.02628946	-0.3802013	0.06744118	0.10234146	-0.1261723	-0.0843598	-0.0009345	0.03719286	-0.0716977	0.0071482
Negative PANAS Spearman	-0.007499	0.23889761	0.31674467	-0.0007142	-0.1067719	-0.2487178	0.03749514	-0.053743	-0.057314	-0.145874	0.05160046	0.19744441	-0.201581	-0.0139268

Figure 5.21: Correlation Coefficients between ROI Signal Changes and Individual Behavioral Measures - Medial FI Models: Neg-Neu = [Negative - Positive]; Pos-Neg = [Positive - Negative]; Hed+ = Effect of Increasing Hedonic Value; Int+ = Effect of Increasing Intensity Value; Interesting+ = Effect of Increasing Interesting-ness; Emotional+ = Effect of Increasing Emotional Intensity; Chemical+ = Effect of Increasing Chemical-like Quality.

Run Type	Active Runs							Passive Runs						
Model	[Neg - Neu]	[Pos - Neg]	Hedonic+	Intensity+	Chemical+	Interesting+	Emotional+	[Neg - Neu]	[Pos - Neg]	Hedonic+	Intensity+	Chemical+	Interesting+	Emotional+
Lateral FI - Bilateral														
Perceiving MSCEIT Pearson	-0.2253762	0.05062816	0.05326523	-0.0754523	0.24095352	-0.2681333	-0.0387776	0.20440268	0.08404425	0.04815352	-0.1611857	0.05431426	-0.1263578	0.08873353
Perceiving MSCEIT Spearman	-0.1146163	-0.0205596	0.05394079	-0.0533878	0.09875176	-0.2775418	-0.0417284	0.15373472	0.06907785	0.03235907	-0.1485092	0.14184687	-0.1703661	0.01107355
Overall MSCEIT Pearson	-0.3327514	0.15068646	0.11232894	0.03082916	0.06953585	-0.2510925	-0.1650493	-0.1009229	0.31560565	0.04567012	-0.1572137	0.09734299	-0.0581712	0.12805989
Overall MSCEIT Spearman	-0.2498234	0.11602781	0.12049112	0.00822697	0.00672503	-0.232193	-0.1215407	-0.1632115	0.12040286	-0.041298	-0.152518	0.17348558	0.00797459	0.12883985
SNI Pearson	-0.0235842	0.13535628	0.21585352	0.02808591	-0.2606617	0.06376007	0.19120025	0.10539889	-0.0631624	-0.1339131	0.04893231	0.40321374	0.13508569	-0.4795556
SNI Spearman	0.09594795	0.11219045	0.04989963	0.07568669	-0.1774953	0.11855349	0.22622283	0.06965855	0.10348313	0.0217683	0.05073687	-0.0709981	0.33690624	-0.4328542
Positive PANAS Pearson	0.00541309	0.11220485	0.2374186	-0.1887956	0.03131855	0.03226856	0.05594526	0.32032666	-0.0642213	-0.1588946	-0.0673359	0.1824542	-0.131207	0.08479986
Positive PANAS Spearman	0.03127876	0.04466005	0.17362222	-0.1754621	0.06222299	0.04164926	0.09550895	0.23517615	0.02224639	-0.1383291	-0.0821277	0.19871214	-0.1090575	0.08731291
Negative PANAS Pearson	-0.0282254	0.13273786	0.21069388	-0.0321734	0.0530074	-0.3914738	0.0892602	0.03740548	0.03086813	-0.0591938	-0.1378849	0.04176114	-0.2304591	0.15672926
Negative PANAS Spearman	0.0632061	0.11641349	0.25960922	0.08606028	-0.1867615	-0.0487437	-0.0098202	-0.0348169	0.01767628	-0.0669556	-0.0516005	0.14533831	-0.345848	0.10873591
Lateral FI - Right														
Perceiving MSCEIT Pearson	-0.2724472	0.03431652	0.06042395	-0.0643722	0.28200274	-0.2863792	-0.1315599	0.26606126	0.00566774	0.11378295	-0.2705534	0.0002665	-0.0833193	0.19081613
Perceiving MSCEIT Spearman	-0.2031752	-0.0792523	0.0061778	-0.0123275	0.15267988	-0.2889685	-0.1598068	0.25328503	-0.0220636	0.14706586	-0.2468497	0.13548311	-0.0666965	0.14776421
Overall MSCEIT Pearson	-0.3552918	0.09011947	0.13752719	0.00307121	0.22068361	-0.3122591	-0.2433353	-0.0363142	0.27535664	0.14442449	-0.2110644	0.02246333	-0.1168112	0.24230379
Overall MSCEIT Spearman	-0.3536888	-0.0058248	0.14773764	-0.032756	0.24164018	-0.3190913	-0.2490946	-0.0737945	0.07431009	0.11477455	-0.1518796	0.23797292	-0.085908	0.25153219
SNI Pearson	-0.0294193	0.12901265	0.12502901	0.01879069	-0.2213144	-0.0199744	0.09019122	0.14406727	-0.0102985	-0.1181534	0.00774089	0.27917464	0.17529167	-0.3619039
SNI Spearman	-0.0281313	0.12022797	0.13010743	0.0691562	-0.1141998	0.05659757	0.14166137	0.15103848	0.03164775	0.00602814	-0.0574348	-0.0066979	0.27712715	-0.3658748
Positive PANAS Pearson	0.05610207	0.08477506	0.18384812	-0.2196969	0.10640563	0.06320497	-0.0287061	0.3117697	-0.0053904	-0.1757342	-0.1101445	0.15935092	-0.0993784	0.02856103
Positive PANAS Spearman	0.1001924	-0.0590449	0.16676431	-0.1833237	0.13983447	-0.0354604	0.0789496	0.21426788	0.08580751	-0.223133	-0.1468596	0.220624	0.02141006	-0.0311115
Negative PANAS Pearson	-0.0488781	0.17353403	0.15641735	-0.1153663	0.03539588	-0.2447911	-0.0027909	0.0135792	0.06218171	-0.041198	-0.1689466	-0.0114083	-0.2347443	0.17904963
Negative PANAS Spearman	0.06195626	0.21300811	0.24711084	-0.0051779	-0.2813921	0.04338723	-0.0330314	-0.0596351	0.03820933	-0.1008798	-0.0892741	0.07659722	-0.3560253	0.0890956
Lateral FI - Left														
Perceiving MSCEIT Pearson	-0.1690364	0.06080374	0.03627898	-0.0787397	0.15453371	-0.214968	0.04278391	0.12550493	0.15007332	-0.0204488	-0.0494155	0.09963148	-0.1418617	-0.013678
Perceiving MSCEIT Spearman	-0.0982165	0.04923361	0.02029848	-0.075605	0.04813706	-0.1911324	0.02020207	0.06300292	0.17093335	-0.0179523	-0.047485	0.10431654	-0.245073	-0.0785767
Overall MSCEIT Pearson	-0.2919943	0.19376068	0.06449137	0.054602	-0.0898083	-0.1628015	-0.0816769	-0.1628619	0.32356373	-0.0543982	-0.0943299	0.15648493	-0.0059377	0.01069399
Overall MSCEIT Spearman	-0.2100995	0.14481533	0.03406615	0.03045203	-0.1129097	-0.1401638	-0.0337893	-0.2003351	0.17900618	-0.0599608	-0.1681913	0.07784026	-0.0041479	0.05309235
SNI Pearson	-0.016385	0.12331975	0.28943433	0.03423281	-0.254767	0.12802354	0.25894144	0.05724019	-0.1072175	-0.1331232	0.0807338	0.4606704	0.0869361	-0.5229791
SNI Spearman	0.0902547	-0.008205	0.01992636	0.03265244	-0.176993	0.2295718	0.28148081	-0.0341595	0.13881475	0.11805114	0.13261916	-0.1155394	0.25167499	-0.4633298
Positive PANAS Pearson	-0.0440725	0.12524882	0.26292178	-0.1400331	-0.0465863	0.00085807	0.12471672	0.30755532	-0.1138081	-0.1244365	-0.0227652	0.17538124	-0.1381585	0.12372463
Positive PANAS Spearman	-0.0374676	0.14585605	0.20122113	-0.1406708	0.02458812	0.12394419	0.14987043	0.24103046	-0.0040144	-0.0640629	-0.0061888	0.10571218	-0.2161078	0.13565281
Negative PANAS Pearson	-0.0063735	0.07182778	0.24140848	0.05168086	0.06032712	-0.4652968	0.16074022	0.06012348	-0.0017923	-0.0692367	-0.0969325	0.0881169	-0.197077	0.11731336
Negative PANAS Spearman	0.13730364	0.06641996	0.34102724	0.1571225	-0.1153422	-0.1999741	0.06731271	0.02213999	-0.0223185	-0.1444456	-0.0267822	0.3028179	-0.334421	0.14873073

Figure 5.22: Correlation Coefficients between ROI Signal Changes and Individual Behavioral Measures - Lateral FI Models: Neg-Neu = [Negative - Neutral]; Pos-Neg = [Positive - Negative]; Hed+ = Effect of Increasing Hedonic Value; Int+ = Effect of Increasing Intensity Value; Interesting+ = Effect of Increasing Interesting-ness; Emotional+ = Effect of Increasing Emotional Intensity; Chemical+ = Effect of Increasing Chemical-like Quality.

Run Type / Model	Active Runs [Neg - Neu]	[Pos - Neg]	Hedonic+	Intensity+	Chemical+	Interesting+	Emotional+	Passive Runs [Neg - Neu]	[Pos - Neg]	Hedonic+	Intensity+	Chemical+	Interesting+	Emotional+
Empathy - Bilateral														
Perceiving MSCEIT Pearson	-0.4200593	0.15874941	0.17521569	-0.2231004	0.22535697	-0.2751039	-0.1456668	0.09806735	0.16119734	0.09307487	-0.0860819	0.04851012	-0.3197137	0.06608289
Perceiving MSCEIT Spearman	-0.4309901	0.19137201	0.18244754	-0.1931719	0.03745399	-0.2583362	-0.0986683	0.12924774	0.12067608	0.06213698	-0.1025898	0.12139119	-0.4010554	-0.0111314
Overall MSCEIT Pearson	-0.3658692	0.29829009	0.20867959	-0.088783	0.0725802	-0.3018933	-0.1530482	-0.1177512	0.38192446	0.02879505	-0.1304216	0.14833902	-0.2645901	0.06205502
Overall MSCEIT Spearman	-0.4567263	0.34145362	0.13877284	-0.1211059	-0.0946113	-0.2597664	-0.0485398	-0.1085821	0.18789712	-0.1065986	-0.080359	0.22329544	-0.3285279	0.04811652
SNI Pearson	-0.107357	0.25903523	0.15414037	-0.0313414	-0.2027014	0.13332378	0.29632994	0.00544328	0.00220041	-0.1592447	0.11510607	0.40804266	0.02695203	-0.3488367
SNI Spearman	-0.0641327	0.149364	0.12407929	-0.1309447	-0.0798729	0.15606194	0.19691935	0.01306098	0.14182882	0.10766934	0.03968528	-0.0326524	-0.0363363	-0.2764805
Positive PANAS Pearson	-0.0220406	0.16103329	0.1326164	-0.3815628	0.06382789	-0.0848407	0.29599418	0.10813306	0.159329	-0.0918213	-0.0687981	0.23360385	-0.2872911	0.14635685
Positive PANAS Spearman	0.0893201	0.12494778	0.07276076	-0.3748433	0.08463665	-0.0806223	0.28535598	0.01622481	0.24103046	0.02341726	-0.1321402	0.20657364	-0.2739819	0.17857149
Negative PANAS Pearson	0.01705581	0.18563903	0.16107321	0.02472694	0.0010911	-0.4472296	0.2023523	0.08580157	0.01946951	0.00594926	-0.1564973	-0.0021126	-0.2043435	0.20467041
Negative PANAS Spearman	0.06891964	0.17676281	0.16444298	0.14855218	-0.2692508	0.0314245	0.18890409	0.00892741	0.01999741	-0.018569	-0.1244482	0.18801135	-0.2112226	0.16883152
Empathy - Right														
Perceiving MSCEIT Pearson	-0.3551074	0.22019746	0.15873437	-0.1026849	0.26455411	-0.2779159	-0.2929952	0.06890089	0.24581045	0.17341681	-0.227946	-0.146366	-0.1384761	0.05095891
Perceiving MSCEIT Spearman	-0.2399625	0.23724023	0.09051934	-0.1125643	0.03212878	-0.1734244	-0.2014705	0.15372385	0.20112679	0.3074049	-0.1214312	-0.0852778	-0.2180213	-0.0288819
Overall MSCEIT Pearson	-0.3065947	0.36182998	0.26778732	-0.014647	0.11181811	-0.3385937	-0.265389	-0.1257702	0.44637458	0.13279335	-0.1919778	-0.0064147	-0.1714649	0.04931623
Overall MSCEIT Spearman	-0.2073392	0.40529284	0.16941558	-0.0587756	0.00124255	-0.213541	-0.1578038	0.0226116	0.31697583	0.15834907	-0.0717713	0.09850743	-0.1968884	0.00612646
SNI Pearson	-0.0641577	0.13426388	0.07749668	-0.1051763	-0.2201997	-0.0052757	0.28548671	0.02614442	-0.034518	-0.0503942	0.09802405	0.25568894	0.16880839	-0.2407657
SNI Spearman	-0.0840591	0.12458163	0.11620021	-0.1870399	0.06128613	0.11520452	0.23392546	0.05609522	0.02545216	0.1808443	0.05190901	-0.0035164	0.02478237	-0.2791365
Positive PANAS Pearson	0.07929794	0.03754095	0.01181454	-0.4436151	0.16010944	0.03429585	0.32913716	0.10532101	0.18079774	-0.0349057	-0.2106101	0.24941368	-0.1385105	0.13066308
Positive PANAS Spearman	0.23668154	0.01672661	-0.052187	-0.45948	0.25056463	0.01672661	0.31864193	-0.0115414	0.23082723	0.1209334	-0.2617715	0.20941717	-0.1113992	0.08446938
Negative PANAS Pearson	-0.0274151	0.17942178	0.09636499	0.01715728	-0.0277725	-0.2581968	0.06989457	0.14963547	-0.0152601	-0.056496	-0.1446704	-0.0068786	-0.0939518	0.17681555
Negative PANAS Spearman	0.07106222	0.13266138	-0.0157122	0.13533961	-0.343884	0.11623494	0.19836715	0.08231076	-0.099987	-0.1983672	-0.0610635	0.18390474	-0.0899883	0.23157713
Empathy - Left														
Perceiving MSCEIT Pearson	-0.4561372	0.06569504	0.17337779	-0.2804805	0.15437911	-0.2203579	0.01606205	0.10917403	0.04056962	-0.004627	0.04097704	0.1926611	-0.3960745	0.06929067
Perceiving MSCEIT Spearman	-0.412866	0.1048417	0.15267988	-0.1729377	-0.0332712	-0.1882547	0.02562245	0.09660645	0.11434534	-0.0690613	0.05320115	0.26705741	-0.4768694	0.0849415
Overall MSCEIT Pearson	-0.4000697	0.17657341	0.12826647	-0.1377866	0.02689644	-0.2153995	-0.0196392	-0.0960496	0.21909524	-0.0853584	-0.057288	0.2513449	-0.2763305	0.06381759
Overall MSCEIT Spearman	-0.4567263	0.17485585	0.08454759	-0.0820662	-0.1674179	-0.153929	0.04457605	-0.1918128	0.16136586	-0.2152017	-0.0178539	0.32354014	-0.4171013	0.10622196
SNI Pearson	-0.1447756	0.33875647	0.21418128	0.05179834	-0.156006	0.21759162	0.23441118	-0.0120908	0.0349425	-0.2537225	0.1068658	0.48369901	-0.1061884	-0.3847322
SNI Spearman	0.00787008	0.11821859	0.09209664	-0.066477	-0.1205629	0.15673173	0.19597291	0.01507036	0.2004377	0.04956454	-0.0576023	-0.0301407	-0.0830544	-0.2541867
Positive PANAS Pearson	-0.1262709	0.25735071	0.23875929	-0.2102826	-0.0290881	-0.1629253	0.22664558	0.09654327	0.09678663	-0.1401711	0.05575283	0.19664701	-0.3420445	0.13670762
Positive PANAS Spearman	-0.0475036	0.21309702	0.19603588	-0.2848542	0.04683451	-0.1900143	0.26844806	0.02107553	0.26160419	-0.0642302	0.06055033	0.15222216	-0.2845196	0.28067253
Negative PANAS Pearson	0.06224852	0.15809911	0.20861122	0.02529664	0.02567147	-0.5122325	0.17426313	0.0456702	0.02279399	0.07102176	-0.1361625	0.00187083	-0.2472789	0.19616657
Negative PANAS Spearman	0.07034803	0.22318536	0.28014227	0.08623882	-0.1674783	-0.1210557	0.17426313	-0.0489222	0.13533961	0.11355671	-0.029639	0.13283993	-0.2546099	0.05999223

Figure 5.23: Correlation Coefficients between ROI Signal Changes and Individual Behavioral Measures - Empathy Functional Areas

Models: Neg-Neu = [Negative - Neutral]; Pos-Neg = [Positive - Negative]; Hed+ = Effect of Increasing Hedonic Value; Int+ = Effect of Increasing Intensity Value; Interesting+ = Effect of Increasing Interesting-ness; Emotional+ = Effect of Increasing Emotional Intensity; Chemical+ = Effect of Increasing Chemical-like Quality.

Run Type		Active Runs							Passive Runs						
Model	[Neg - Neu]	[Pos - Neg]	Hedonic+	Intensity+	Chemical+	Interesting+	Emotional+	[Neg - Neu]	[Pos - Neg]	Hedonic+	Intensity+	Chemical+	Interesting+	Emotional+
Olfaction - Bilateral														
Perceiving MSCEIT Pearson	-0.4905951	0.17891123	0.28728476	-0.1301641	0.12484733	-0.2336564	-0.0320159	0.19635636	0.07471974	-0.0481332	-0.1271177	0.06042828	0.06197267	0.08629609
Perceiving MSCEIT Spearman	-0.4349774	0.12063976	0.19968436	-0.0402524	0.05600374	-0.2361917	-0.0146078	0.26378806	-0.000541	-0.1816031	-0.1056727	0.15678951	0.16573511	0.07364788
Overall MSCEIT Pearson	-0.3824206	0.14681977	0.23667975	-0.0348949	0.03895612	-0.2901917	0.08626039	-0.0758295	0.19716817	-0.0077924	-0.0939392	0.19996883	-0.0604254	0.12398088
Overall MSCEIT Spearman	-0.3062966	0.16336635	0.21332033	0.01317999	0.1018568	-0.343422	0.06005418	0.00787688	-0.0629397	-0.1138191	-0.1216233	0.20649017	0.01821463	0.1625878
SNI Pearson	-0.0716434	0.18568801	0.20470726	-0.1210821	-0.1680646	-0.0047078	0.47864963	-0.0474405	-0.0460939	-0.1012041	0.00799306	0.45909677	0.12864932	-0.2870099
SNI Spearman	-0.1723044	0.18134665	0.31413325	-0.2243809	-0.0426993	0.13715172	0.18050941	0.03750845	0.13764261	0.16142029	0.11069266	-0.1699602	0.21667827	-0.2970535
Positive PANAS Pearson	0.08760164	0.10479685	0.14096137	-0.2034278	0.15956822	-0.0047883	0.02923341	0.09870762	0.1802837	-0.0922747	-0.1537312	0.07862199	-0.0003509	0.09843942
Positive PANAS Spearman	0.18466178	0.01271222	0.13933267	-0.2196204	0.21644234	-0.0678321	0.02609351	0.02492265	0.23584521	-0.0262608	-0.2103547	-0.0250899	0.04482732	0.07610608
Negative PANAS Pearson	-0.0328093	0.17207363	0.1930797	-0.1355299	-0.0649385	-0.3362202	0.25266441	0.06643019	-0.0906444	-0.1194053	-0.0734441	-0.0768967	-0.2024714	0.21534583
Negative PANAS Spearman	0.01089145	0.15908653	0.1308759	-0.1149851	-0.2553241	0.01419578	0.15605121	-0.0832035	-0.1598007	-0.0860603	-0.0246417	-0.0565998	-0.1822978	0.15997927
Olfaction - Right														
Perceiving MSCEIT Pearson	-0.3872086	0.25162996	0.33920794	-0.0212558	-0.0873896	-0.2679391	-0.1140092	0.0944481	0.00380972	0.09727801	-0.1133345	0.00403354	0.00237205	0.08613964
Perceiving MSCEIT Spearman	-0.3407323	0.12245282	0.27110502	0.03168257	-0.0271768	-0.1670653	-0.0345044	0.14618093	-0.0871056	-0.077571	-0.0986476	0.10959176	0.0828958	0.10192708
Overall MSCEIT Pearson	-0.344138	0.23858126	0.40185447	0.0961794	-0.1452439	-0.3092475	-0.0758097	-0.1826451	0.22704949	0.15888605	-0.0313572	0.15016285	-0.1000538	0.12302823
Overall MSCEIT Spearman	-0.3523317	0.30243501	0.27846059	0.06844136	0.02342214	-0.2603939	-0.0087602	-0.1302532	-0.0203787	-0.0079746	-0.0362489	0.22508323	-0.0225434	0.16217264
SNI Pearson	-0.1622547	0.23074139	0.26376084	-0.0824511	-0.19452	0.0032916	0.31283168	-0.0580194	-0.000516	-0.0247923	0.03963809	0.35707706	0.13977069	-0.1905673
SNI Spearman	-0.1791698	0.24179553	0.29186261	-0.1240793	0.02319355	0.06212337	0.09209664	-0.0147365	0.01992636	0.14534524	0.10013416	0.0155727	0.09377112	-0.2541867
Positive PANAS Pearson	0.02348317	0.16939196	0.1621597	-0.1782442	0.1822454	0.02072239	-0.1579267	0.19158617	0.16598386	-0.0226296	-0.1632572	0.11471234	-0.1158948	0.10397798
Positive PANAS Spearman	0.10621398	0.05151796	0.20239199	-0.2922139	0.30419884	-0.0209083	-0.1435143	0.07928413	0.27598908	0.05486328	-0.153383	0.05185249	-0.1222715	0.08865104
Negative PANAS Pearson	-0.0800916	0.2025988	0.12521408	-0.1921711	-0.1042547	-0.1996117	0.11134362	-0.0067277	-0.0798518	-0.1415402	-0.1153165	-0.0748672	-0.1357283	0.19056706
Negative PANAS Spearman	-0.024104	0.17158491	0.10284382	-0.2397904	-0.1857057	0.20872295	-0.0932022	-0.1144495	-0.0717764	-0.1212343	-0.0028568	-0.0203545	-0.2074731	0.22693488
Olfaction - Left														
Perceiving MSCEIT Pearson	-0.5421576	0.005723	0.05795432	-0.2060989	0.24261123	-0.0975642	0.09007394	0.27277179	0.13451561	-0.2102903	-0.1071232	0.10795643	0.10750961	0.06894489
Perceiving MSCEIT Spearman	-0.5263628	0.1179075	-0.0403641	-0.0488304	0.05846085	-0.1450097	0.0112631	0.24238766	0.08699719	-0.2804156	-0.1367969	0.22099628	-0.0028724	-0.0085889
Overall MSCEIT Pearson	-0.3707336	-0.0487829	-0.1283532	-0.1595969	0.18538948	-0.1494339	0.22821305	0.09619046	0.10162296	-0.2034657	-0.1536648	0.21546797	-0.0026056	0.09976104
Overall MSCEIT Spearman	-0.3515069	-0.0053432	-0.1309202	0.04021325	-0.0434434	-0.1919452	0.21006576	0.07856946	0.10006576	-0.3346317	-0.1870634	0.22561147	-0.0710913	0.08921943
SNI Pearson	0.05072819	0.05736747	0.01008455	-0.1272891	-0.0334438	-0.0124774	0.3764963	-0.0171424	-0.0857586	-0.1716024	-0.0395115	0.48397248	0.08330177	-0.32168
SNI Spearman	-0.0360014	-0.0428668	0.18837948	-0.2886811	-0.1296051	0.12776315	0.22722752	0.06932365	0.17448126	0.1123579	0.05442074	-0.2242134	0.21483633	-0.2319161
Positive PANAS Pearson	0.15407055	-0.0329536	0.03489075	-0.1735163	0.03408039	-0.0338145	0.24138921	-0.0623508	0.14199616	-0.1564369	-0.0951324	0.02675889	0.12009152	0.07311911
Positive PANAS Spearman	0.20222472	-0.013214	0.00150539	-0.236347	0.09701434	-0.1165845	0.17546215	-0.0269298	0.09366902	-0.059714	-0.1410053	-0.0752697	0.10219959	0.14435065
Negative PANAS Pearson	0.03036165	0.07188698	0.1867133	-0.041069	0.0142041	-0.3660571	0.26504831	0.14536756	-0.0756166	-0.069063	0.00787205	-0.0653081	-0.2188523	0.19550535
Negative PANAS Spearman	0.06731271	0.17087072	0.22693488	0.06517013	-0.0414232	-0.2867486	0.25514551	0.03910208	-0.1651572	0.10909301	-0.0258895	-0.0873101	-0.1305188	0.10212962

Figure 5.24: Correlation Coefficients between ROI Signal Changes and Individual Behavioral Measures - Olfaction Functional Areas

Models: Neg-Neu = [Negative - Positive]; Pos-Neg = [Positive - Negative]; Hed+ = Effect of Increasing Hedonic Value; Int+ = Effect of Increasing Intensity Value; Interesting+ = Effect of Increasing Interesting-ness; Emotional+ = Effect of Increasing Emotional Intensity; Chemical+ = Effect of Increasing Chemical-like Quality.

Run Type	Active Runs							Passive Runs						
Model	[Neg - Neu]	[Pos - Neg]	Hedonic+	Intensity+	Chemical+	Interesting+	Emotional+	[Neg - Neu]	[Pos - Neg]	Hedonic+	Intensity+	Chemical+	Interesting+	Emotional+
Emotion - Bilateral														
Perceiving MSCEIT Pearson	-0.3775175	0.04857127	0.14794676	-0.1294462	0.10464834	-0.3125781	-0.0514599	0.31162128	0.00405661	-0.0137865	-0.168653	-0.0198785	-0.0131718	0.06425912
Perceiving MSCEIT Spearman	-0.2631613	0.02806836	0.18676965	-0.1123567	0.04457605	-0.2951565	-0.0310637	0.32004522	-0.071486	-0.0091576	-0.0147598	0.02843039	0.01002209	-0.0101179
Overall MSCEIT Pearson	-0.3279077	0.11497661	0.1432157	-0.0245401	-0.0149489	-0.2561597	-0.1460246	0.04278145	0.27634978	0.00913558	-0.2241418	0.09983172	-0.072815	0.15165574
Overall MSCEIT Spearman	-0.2859976	0.17180698	0.10555023	-0.0281772	0.01719863	-0.2528906	-0.1070368	0.05768979	0.04853985	-0.0355737	-0.0584926	0.14846983	-0.0872833	0.17874961
SNI Pearson	-0.0228765	0.12880996	0.12669996	-0.0712989	-0.048816	-0.0835845	0.17688096	0.03658147	-0.0384496	-0.0551646	0.03535917	0.4575331	0.0068372	-0.3328126
SNI Spearman	-0.1006365	0.02411257	0.21383164	-0.0679841	0.08271952	0.01841933	0.18754224	0.07786352	-0.0733424	0.18938417	0.15924346	-0.1249165	-0.0239451	-0.290523
Positive PANAS Pearson	0.00789191	0.0786768	0.18524391	-0.2426463	0.13258457	-0.0993696	0.1345093	0.19288944	0.04898979	-0.1477427	-0.1073615	0.20258513	-0.155787	0.05083467
Positive PANAS Spearman	0.13147116	0.0085305	0.14786324	-0.2555826	0.18098193	-0.1694406	0.19101789	0.0503471	0.05252156	-0.0757715	-0.0946726	0.18867617	-0.1247805	0.00133813
Negative PANAS Pearson	-0.0577897	0.19166212	0.21140224	-0.0257183	-0.0761989	-0.3421271	0.15717808	0.05676453	0.02115866	-0.1006008	-0.0970227	0.03308863	-0.2557446	0.1608778
Negative PANAS Spearman	0.01606935	0.10141543	0.24300422	0.01303403	-0.3456695	-0.0669556	0.20461634	-0.0373166	0.13069735	-0.1614077	-0.0339242	0.21211537	-0.326029	0.0939164
Emotion - Right														
Perceiving MSCEIT Pearson	-0.3315045	0.06325875	0.19066328	-0.0099194	-0.0199361	-0.4506641	-0.0443422	0.21173225	0.03456316	0.07312744	-0.0829791	0.0091531	-0.1542657	0.1058056
Perceiving MSCEIT Spearman	-0.1939274	0.0436747	0.16715784	0.03308291	-0.0751124	-0.3737678	0.05142344	0.24725187	0.01033026	0.0559415	0.04792383	0.07856946	-0.1260395	0.05524283
Overall MSCEIT Pearson	-0.3462032	0.16030154	0.22968095	0.11230342	-0.0376017	-0.4310379	-0.2339047	-0.0856609	0.35348527	0.13465407	-0.1026273	0.11020001	-0.150662	0.11932112
Overall MSCEIT Spearman	-0.3012218	0.22365674	0.13727684	0.13950835	-0.0126357	-0.3701774	-0.0778396	-0.0498794	0.21693555	0.13101609	0.1403093	0.14992924	-0.1650134	0.14034181
SNI Pearson	-0.088619	0.08559808	0.14993166	-0.0854538	-0.114525	-0.1480188	0.12164357	0.00540112	-0.0210938	-0.0453515	0.04949179	0.3259814	0.000985	-0.2519194
SNI Spearman	-0.1212327	-0.00016745	0.18770969	-0.1339587	0.07652393	-0.0204287	0.32233823	0.07183538	-0.0964503	0.05726736	0.1496989	0.00368387	0.01925657	-0.3169799
Positive PANAS Pearson	0.01484345	0.06721661	0.18313462	-0.3142946	0.13148771	-0.0497645	0.12154146	0.22059181	-0.0088981	-0.0718393	-0.1643322	0.20618673	-0.1385043	-0.029788
Positive PANAS Spearman	0.07393162	0.01154136	0.19954847	-0.3141257	0.18349092	-0.1388309	0.18834164	0.09818521	0.00769424	-0.0635611	-0.2038974	0.19235602	-0.0742662	-0.1077194
Negative PANAS Pearson	-0.055765	0.20323508	0.20561322	-0.1403074	-0.1060939	-0.2296343	0.05571392	0.0851046	-0.0278887	-0.1212604	-0.1085567	-0.05985	-0.1251599	0.1432028
Negative PANAS Spearman	0.02713934	0.21015134	0.2296131	-0.1717635	-0.3667382	0.05749255	0.05642126	-0.0439229	0.03374563	-0.1285548	-0.0524932	0.09552334	-0.2246138	0.12087719
Emotion - Left														
Perceiving MSCEIT Pearson	-0.3702286	0.01869797	0.03764358	-0.2559457	0.18999175	-0.0640369	-0.0407215	0.42980061	-0.043668	-0.1295211	-0.2507278	-0.0506496	0.18626472	-0.0008544
Perceiving MSCEIT Spearman	-0.4077913	0.01745458	0.06599078	-0.199339	0.06620006	-0.1265553	-0.0832989	0.39591954	-0.0318145	-0.1166221	-0.206452	-0.0320516	0.27059651	-0.1311063
Overall MSCEIT Pearson	-0.2482682	0.0283017	-0.0366766	-0.1998467	0.0133459	0.01947838	-0.0068667	0.26624993	0.08529463	-0.163425	-0.3423897	0.06551338	0.05377776	0.16537635
Overall MSCEIT Spearman	-0.2707734	0.00748054	-0.0369338	-0.1181732	-0.0504381	-0.0894464	-0.0179523	0.19409885	0.02161978	-0.2497524	-0.2261996	0.08241839	0.07489237	0.13775793
SNI Pearson	0.06515763	-0.0618162	0.05383266	-0.0350834	0.03572057	0.01649112	0.17072299	0.08597101	-0.054515	-0.0571464	0.01350525	0.52328975	0.01322911	-0.3755144
SNI Spearman	0.0159076	-0.0539184	0.03047561	0.02160085	-0.0236102	0.09377112	0.04135976	0.10013416	-0.0266243	0.16627629	0.07049579	-0.1806769	0.03164775	-0.2704292
Positive PANAS Pearson	-0.0023467	0.08397773	0.13724538	-0.088572	0.08364189	-0.1298524	0.10110224	0.10429466	0.12451781	-0.2217933	-0.0234653	0.15789235	-0.1417964	0.14598688
Positive PANAS Spearman	0.17211682	0.01421762	0.06740824	-0.1410053	0.18232006	-0.158401	0.15355029	0.1105629	0.04583091	-0.1488668	-0.0498453	0.16308445	-0.1145773	0.14050353
Negative PANAS Pearson	-0.0509512	0.14470983	0.16212286	0.13056526	-0.0174464	-0.3779611	0.20321769	-0.0060439	0.09082455	-0.0508088	-0.0707366	0.13755746	-0.3728503	0.15361614
Negative PANAS Spearman	0.08177512	0.03124595	0.21872166	0.17587007	-0.23122	-0.2340768	0.20229521	-0.0460655	0.15747959	-0.0721335	0.01231983	0.29888984	-0.2808565	0.08677447

Figure 5.25: Correlation Coefficients between ROI Signal Changes and Individual Behavioral Measures - Emotion Functional Areas

Models: Neg-Neu = [Negative - Positive]; Pos-Neg = [Positive - Negative]; Hed+ = Effect of Increasing Hedonic Value; Int+ = Effect of Increasing Intensity Value; Interesting+ = Effect of Increasing Interesting-ness; Emotional+ = Effect of Increasing Emotional Intensity; Chemical+ = Effect of Increasing Chemical-like Quality.

Run Type	Active Runs							Passive Runs						
Model	[Neg - Neu]	[Pos - Neg]	Hedonic+	Intensity+	Chemical+	Interesting+	Emotional+	[Neg - Neu]	[Pos - Neg]	Hedonic+	Intensity+	Chemical+	Interesting+	Emotional+
Pain - Bilateral														
Perceiving MSCEIT Pearson	-0.3676607	0.11931456	0.12298421	-0.2855748	0.15932339	-0.400258	0.09356687	-0.0663454	0.4008184	-0.0084804	-0.2520409	0.08379468	-0.222632	0.22877762
Perceiving MSCEIT Spearman	-0.2707734	0.15039595	0.14950273	-0.0646797	0.06905024	-0.3391445	0.10459577	-0.1013679	0.34987123	0.12221872	-0.1853176	0.1148222	-0.2125687	0.24098149
Overall MSCEIT Pearson	-0.4105135	0.18919964	0.13364009	-0.2294029	0.1145217	-0.3433359	0.01570911	0.0287864	0.3694945	-0.1258726	-0.1950029	0.32359037	-0.2510125	0.06710987
Overall MSCEIT Spearman	-0.3548691	0.18808299	0.2194001	-0.0005259	-0.087156	-0.3234119	0.0747614	0.02806836	0.17574012	0.01444083	0.00163998	0.27120581	-0.3420049	0.10352888
SNI Pearson	-0.2379128	0.31748755	0.14485818	0.10005966	-0.1900835	-0.0308477	0.48104794	0.16271534	-0.0830185	-0.1490566	0.03385956	0.69724411	-0.1908985	-0.3124428
SNI Spearman	0.10532506	0.03600141	-0.0637979	0.18000706	-0.1744813	0.10365058	0.45679931	0.03750845	0.22722752	0.10113885	-0.0375084	0.15438745	0.00334897	-0.158077
Positive PANAS Pearson	0.04820623	0.06532048	0.07908668	-0.0570851	-0.0081908	0.09546126	0.26461345	0.17493879	0.0312472	-0.0788203	-0.1781463	0.24871719	-0.0161711	0.15351622
Positive PANAS Spearman	0.05954673	-0.0528561	0.05419422	-0.0819604	0.0503471	0.14050353	0.28234519	0.07526975	0.13548555	0.01823201	-0.2120934	0.24554665	-0.0245881	0.24738657
Negative PANAS Pearson	-0.1432706	0.03955166	0.03229823	0.19783394	0.04819901	-0.2802611	0.03801581	0.14643589	-0.142313	-0.1311859	-0.093483	0.04123056	-0.3146499	0.35805503
Negative PANAS Spearman	-0.0474938	0.13480396	0.2199715	0.30192516	-0.1401604	-0.168371	-0.020176	0.03499547	-0.3026394	-0.1437314	0.03963772	0.10248672	-0.394333	0.26800099
Pain - Right														
Perceiving MSCEIT Pearson	-0.1837638	-0.0121436	0.07406299	-0.1223783	0.35703689	-0.5417729	0.107554	0.05889901	0.35327291	-0.0910968	-0.1853078	0.03181906	-0.0866937	0.14110178
Perceiving MSCEIT Spearman	-0.187182	-0.0633542	0.14299943	-0.0264313	0.16812715	-0.533739	0.13153273	0.06689636	0.3466532	-0.0339791	-0.1004334	-0.0035395	-0.0797007	0.11459053
Overall MSCEIT Pearson	-0.3289964	0.24901415	-0.0259054	-0.1206554	0.39345302	-0.3410848	-0.0787663	0.12697646	0.21694782	-0.154568	-0.1786804	0.1516837	-0.1412015	0.1270404
Overall MSCEIT Spearman	-0.3552346	0.21526436	0.09756365	-0.0393844	0.06760112	-0.3255019	-0.0055027	0.19113245	0.0581033	-0.104061	0.0785463	0.0874254	-0.2121209	0.12788409
SNI Pearson	0.19045818	0.0522058	-0.2312645	0.29819585	-0.1169701	-0.1784729	0.34581813	0.30924857	-0.0878898	-0.0806918	0.15929218	0.45711792	-0.2726112	-0.1644992
SNI Spearman	0.43419378	-0.1619226	-0.2417955	0.27361073	-0.0689888	-0.107167	0.40154133	0.26557321	0.08355677	0.18352348	-0.0545882	-0.1800071	0.15254552	-0.1176424
Positive PANAS Pearson	0.37010807	-0.2594885	-0.13242	0.10378429	0.02656788	-0.0252843	0.03702716	0.27541562	0.0165434	-0.17583	0.0123678	0.21237842	-0.0331559	0.20673484
Positive PANAS Spearman	0.30258439	-0.3378775	-0.1354855	0.04432552	0.05436148	-0.1110647	0.03529315	0.20473372	0.07777874	-0.075437	-0.0195701	0.12210426	-0.0068579	0.22658088
Negative PANAS Pearson	-0.2386925	0.06119645	0.00575573	0.16168862	-0.0340532	0.05057982	-0.2524753	0.07856186	0.0018392	-0.0105072	-0.1673381	0.05363545	-0.3086663	0.30217758
Negative PANAS Spearman	-0.1215914	0.10123688	0.04963643	0.31085258	-0.1455169	-0.0698124	-0.3490619	0.05624271	-0.0908811	-0.0824893	0.04231595	0.27674985	-0.3015681	0.13186893
Pain - Left														
Perceiving MSCEIT Pearson	-0.3430551	0.1554524	0.12429947	-0.3171181	-0.014546	-0.2284741	0.06740903	-0.1227013	0.33204392	0.03447496	-0.2477031	0.10202032	-0.266387	0.23109059
Perceiving MSCEIT Spearman	-0.2357291	0.19295017	0.10739584	-0.0796241	-0.0635513	-0.1331906	0.09012078	-0.1441359	0.26655054	0.13450061	-0.1372116	0.10982881	-0.1615711	0.18181412
Overall MSCEIT Pearson	-0.3235389	0.10776372	0.18485303	-0.2423247	-0.0976388	-0.2626941	0.06046197	-0.0235857	0.35495736	-0.094516	-0.1739794	0.37851619	-0.2764085	0.02471936
Overall MSCEIT Spearman	-0.2674722	0.1258525	0.18930494	0.0388453	-0.2700033	-0.2411734	0.13356545	-0.0045555	0.19099847	0.01203427	0.00419106	0.32191204	-0.2717985	0.00245695
SNI Pearson	-0.3733302	0.36929687	0.29576301	-0.0301801	-0.1792357	0.05482531	0.44490829	0.07135122	-0.0625648	-0.1627978	0.7363148	0.7363148	-0.1205725	-0.3300576
SNI Spearman	0.01934191	0.14300096	0.04119231	0.0477228	-0.0967852	0.17883492	0.37910324	-0.0219357	0.19383775	0.06111868	0.00318152	0.33841328	-0.0282988	-0.3519766
Positive PANAS Pearson	-0.1202666	0.21489625	0.16434328	-0.1342956	-0.0276388	0.13719217	0.3223649	0.10418352	0.03099031	-0.0185721	-0.2419911	0.23641316	-0.0046855	0.09839031
Positive PANAS Spearman	-0.1111576	0.14635784	0.15656108	-0.1338129	-0.0247554	0.22631104	0.35962213	0.06389565	0.07653064	0.12478052	-0.2032283	0.2082463	-0.0118759	0.18031286
Negative PANAS Pearson	-0.0554403	0.01786363	0.03908825	0.1769581	0.08555884	-0.3901802	0.17687194	0.16073897	-0.176377	-0.1739704	-0.0451605	0.02938408	-0.2752212	0.32063539
Negative PANAS Spearman	-0.1221372	0.13319703	0.23871907	0.16140766	-0.1512304	-0.1240911	0.10909301	0.05302884	-0.3327525	-0.1842618	0.005535	0.03231724	-0.1860473	0.31888725

Figure 5.26: Correlation Coefficients between ROI Signal Changes and Individual Behavioral Measures - Pain Functional Areas Models: Neg-Neu = [Negative - Positive]; Pos-Neg = [Positive - Negative]; Hed+ = Effect of Increasing Hedonic Value; Int+ = Effect of Increasing Intensity Value; Interesting+ = Effect of Increasing Interesting-ness; Emotional+ = Effect of Increasing Emotional Intensity; Chemical+ = Effect of Increasing Chemical-like Quality.

Run Type	Active Runs							Passive Runs						
Model	[Neg - Neu]	[Pos - Neg]	Hedonic+	Intensity+	Chemical+	Interesting+	Emotional+	[Neg - Neu]	[Pos - Neg]	Hedonic+	Intensity+	Chemical+	Interesting+	Emotional+
Amygdala - Bilateral														
Perceiving MSCEIT Pearson	-0.023017	0.10300456	0.16124262	0.11454761	0.1319909	-0.5629403	-0.1740863	0.04597659	0.03585516	-0.1449311	-0.145451	0.27714882	-0.1956542	0.1042683
Perceiving MSCEIT Spearman	0.00466761	-0.0192394	0.18564039	0.20595841	-0.020883	-0.5851449	-0.0732212	0.05096865	0.03378308	0.03372412	-0.1957634	0.27855784	-0.2728947	0.09636208
Overall MSCEIT Pearson	-0.087897	0.04539965	0.10231004	0.04421102	-0.0102602	-0.4153393	-0.0389494	-0.038524	0.08182812	-0.0935278	-0.0362258	0.29179517	-0.191259	0.20322313
Overall MSCEIT Spearman	-0.0671418	0.00017651	0.16847741	0.13093697	-0.1518441	-0.4306795	0.03117338	0.00495529	-0.0806943	0.02037875	-0.0509521	0.20422856	-0.2714789	0.1828913
SNI Pearson	-0.1591357	0.31668607	0.2426234	-0.1028524	0.02562015	-0.0349411	0.21326099	0.12150857	0.15492464	-0.2897009	0.14547344	0.57531983	-0.1633326	-0.2014895
SNI Spearman	-0.12994	0.22689262	0.07451455	-0.2051243	0.29454179	-0.0306431	0.33992031	0.11537197	0.28784385	-0.0440389	0.02578706	0.13529833	0.16376456	-0.0348293
Positive PANAS Pearson	0.11995412	0.20573622	0.21811801	0.00284245	-0.0719337	-0.0132373	0.10429997	0.2840135	-0.0866167	-0.1749021	-0.0378285	-0.0330437	-0.1119662	0.41014885
Positive PANAS Spearman	0.18114919	0.1396672	0.12310786	0.00635611	0.07694241	-0.0633939	0.09701434	0.26862937	-0.0162248	-0.1756294	-0.0628921	-0.0287698	-0.0791169	0.42519045
Negative PANAS Pearson	-0.0983069	0.04980388	0.1368849	-0.1531735	0.02803618	-0.1418765	-0.0092946	0.22665333	-0.0579702	-0.153491	-0.0745704	-0.0334446	-0.028402	0.1184272
Negative PANAS Spearman	-0.0899883	0.04320869	0.23104149	-0.0548143	-0.1548014	-0.0253539	-0.1733704	0.06588432	-0.0116056	-0.1376607	-0.2130081	0.1046293	-0.1180204	0.01178419
Amygdala - Right														
Perceiving MSCEIT Pearson	-0.0431911	0.08047454	0.11117912	0.10792721	0.08548324	-0.5464052	-0.1697067	0.1068272	0.04120426	-0.0915141	-0.1187333	0.16556535	-0.1071442	-0.0158171
Perceiving MSCEIT Spearman	-0.0804265	0.05545682	0.16171079	0.20498932	0.01474169	-0.5440256	-0.0861437	0.05413965	0.08147574	0.09457478	-0.1029464	0.12246634	-0.2151584	-0.0501105
Overall MSCEIT Pearson	-0.05282	0.00736261	0.12235314	0.02571978	-0.0433588	-0.4285832	-0.0220229	0.04287238	0.07169948	-0.0928894	0.0644659	0.2424155	-0.2069915	0.00981492
Overall MSCEIT Spearman	-0.0815036	0.05580781	0.2562171	0.13489847	-0.1081057	-0.439976	0.00366569	-0.0062127	0.01828323	0.04105572	0.09974048	0.15149016	-0.2758801	-0.0085643
SNI Pearson	-0.1462109	0.33649926	0.24570758	-0.0901135	-0.0362829	0.04097663	0.03715387	0.14263272	0.05512302	-0.3239192	0.19256319	0.61717987	-0.2370825	-0.4411685
SNI Spearman	-0.2263903	0.26540576	0.16359712	-0.2463166	0.20847329	-0.1041529	0.1870399	0.13496343	0.12290715	-0.0648025	0.0107167	0.15572704	0.16945781	-0.1925657
Positive PANAS Pearson	-0.0082064	0.21349571	0.19035901	0.02609229	-0.0776915	-0.0839535	-0.0100433	0.19724464	-0.0484343	-0.1102345	0.00259959	-0.1257565	0.0808389	0.1176214
Positive PANAS Spearman	-0.0175629	0.20005026	0.13648914	0.05770681	0.01883927	-0.1597391	0.05569961	0.1905161	-0.0945054	-0.0627248	-0.0357949	-0.2087481	0.07192443	0.14501972
Negative PANAS Pearson	-0.0790897	0.1198507	0.12018926	-0.1632949	0.10577635	-0.2233493	-0.0027151	0.18288691	-0.0641342	-0.1147766	-0.0807034	-0.0517546	-0.1301858	0.11739333
Negative PANAS Spearman	-0.0392806	0.08516754	0.13908912	-0.0976659	-0.094452	0.06588432	-0.1155993	0.05231465	-0.0207116	-0.1337327	-0.2278276	0.08713157	-0.2496105	0.0235637
Amygdala - Left														
Perceiving MSCEIT Pearson	0.00400715	0.11459825	0.19842053	0.11055932	0.16457874	-0.4992184	-0.1513822	-0.0271114	0.02681225	-0.183295	-0.1420882	0.38482942	-0.2381684	0.16429382
Perceiving MSCEIT Spearman	0.03410946	-0.0448736	0.18637702	0.18306221	-0.0726004	-0.5603898	-0.0768118	-0.0338298	0.03406615	-0.0655001	-0.1482081	0.37493195	-0.2746644	0.1768121
Overall MSCEIT Pearson	-0.10665	0.07789823	0.05130476	0.06098599	0.03108078	-0.3478408	-0.050097	-0.1278856	0.07834168	-0.0779462	-0.1203366	0.31026574	-0.1272842	0.28847125
Overall MSCEIT Spearman	-0.0872484	0.02091719	0.07792034	0.10780719	-0.1467983	-0.3353108	0.07927254	-0.0629269	-0.1071407	-0.0591098	-0.0577457	0.26380205	-0.2247576	0.32122039
SNI Pearson	-0.1396598	0.26591749	0.18564066	-0.1067329	0.09492658	-0.0915974	0.36666316	0.08698971	0.2099889	-0.1877775	0.07584444	0.41746704	-0.0471976	0.06932872
SNI Spearman	-0.0848964	0.22069703	-0.0629606	-0.1552247	0.22806476	-0.0572674	0.45998083	0.02126595	0.33841328	0.02762899	0.03566652	0.0532486	0.09946437	0.14752207
Positive PANAS Pearson	0.23287194	0.17769025	0.21070752	-0.0243848	-0.0525608	0.0458933	0.20961397	0.35885792	-0.1038371	-0.224775	-0.0674641	0.10232129	-0.2823815	0.50752741
Positive PANAS Spearman	0.29104303	0.09550895	0.14000173	-0.0431547	0.06004853	-0.0244209	0.17128049	0.32416172	-0.015723	-0.2478884	-0.0709208	0.10889024	-0.2202895	0.50430731
Negative PANAS Pearson	-0.098282	-0.0231745	0.13117565	-0.1253618	-0.0693919	-0.056476	-0.0147782	0.25726427	-0.0450825	-0.1736583	-0.0551162	-0.0020778	0.08325678	0.0771992
Negative PANAS Spearman	-0.1569439	-0.0701695	0.32549354	0.00267822	-0.1190917	-0.0064277	-0.1278406	0.11587784	0.05106481	-0.1897968	-0.0832035	0.19176087	0.02446112	-0.0078561

Figure 5.27: Correlation Coefficients between ROI Signal Changes and Individual Behavioral Measures - Amygdala Models: Neg-Neu = [Negative - Neutral]; Pos-Neg = [Positive - Negative]; Hed+ = Effect of Increasing Hedonic Value; Int+ = Effect of Increasing Intensity Value; Interesting+ = Effect of Increasing Interesting-ness; Emotional+ = Effect of Increasing Emotional Intensity; Chemical+ = Effect of Increasing Chemical-like Quality.

Run Type	Active Runs							Passive Runs						
Model	[Neg - Neu]	[Pos - Neg]	Hedonic+	Intensity+	Chemical+	Interesting+	Emotional+	[Neg - Neu]	[Pos - Neg]	Hedonic+	Intensity+	Chemical+	Interesting+	Emotional+
Lateral OFC - Bilateral														
Perceiving MSCEIT Pearson	-0.1807903	0.15142012	0.02769732	-0.1473655	0.23599767	-0.2461048	-0.0064687	0.3009088	-0.081837	-0.1344732	-0.0022756	-0.0425966	0.02992826	-0.0106972
Perceiving MSCEIT Spearman	-0.0318915	0.14809066	0.02665279	-0.0653808	0.04938735	-0.3148403	-0.0766129	0.28658333	-0.1260931	-0.1599641	-0.0496599	0.0555697	0.07647699	-0.0479854
Overall MSCEIT Pearson	-0.3413725	0.23172127	0.14797675	-0.125805	-0.0055365	-0.1882871	-0.0524498	0.06602873	0.02727864	-0.1330873	-0.0298686	0.02493016	0.11468166	0.042013
Overall MSCEIT Spearman	-0.2987537	0.21657597	0.14985574	-0.1095523	-0.1117345	-0.2421848	0.04068915	-0.0316439	-0.0746697	-0.0921552	-0.029361	0.0623378	0.07683604	0.10212272
SNI Pearson	0.04670279	0.10342914	0.0840192	0.21466399	-0.2513403	-0.0593358	0.14723098	-0.0283686	-0.0267181	-0.2958836	0.06194545	0.5861725	-0.1409741	-0.51964
SNI Spearman	0.2558612	-0.1203954	0.01054925	0.2396187	-0.1939053	-0.1004691	0.2188551	0.0643002	0.13563323	0.04789025	0.01121904	-0.1466848	0.18352348	-0.0046886
Positive PANAS Pearson	0.18289692	-0.0445444	0.17444465	-0.0072669	-0.0097057	0.00721423	0.1776749	0.1772788	-0.1426045	-0.2088216	0.03170547	0.05963137	-0.1033476	0.22334629
Positive PANAS Spearman	0.19519955	-0.074768	0.13147116	0.03529315	0.07175716	-0.0043237	0.0898219	0.19034883	-0.1465251	-0.1853308	-0.0607176	0.08848377	-0.0505144	0.37099623
Negative PANAS Pearson	-0.0540817	0.17378069	0.26419957	-0.0062162	0.01545738	-0.2470609	0.13965414	0.05050326	0.13826504	0.05903219	-0.1453348	0.09138185	-0.2304751	0.08016503
Negative PANAS Spearman	0.03517401	0.09605898	0.31888725	0.19086812	-0.0933808	-0.1174848	-0.0080347	0.00357097	0.04856514	0.00196403	-0.0224971	0.27442872	-0.5279673	-0.0092845
Lateral OFC - Right														
Perceiving MSCEIT Pearson	-0.2288948	0.16278762	0.13689568	-0.1213782	0.08804719	-0.1456877	-0.0547857	0.36405864	-0.0194516	-0.0639092	0.00790219	-0.1075613	0.08547206	-0.0361148
Perceiving MSCEIT Spearman	-0.0498534	0.10784671	0.08736535	-0.0602288	0.02513328	-0.1632115	-0.1279326	0.35072245	-0.0202985	-0.0800675	-0.0398962	0.05413965	0.08101742	-0.0720481
Overall MSCEIT Pearson	-0.3863864	0.24434367	0.27325522	-0.1763077	-0.001158	-0.1658122	-0.1561651	0.10552413	0.09600264	-0.0691411	-0.0242104	-0.0222076	0.05081787	0.0222365
Overall MSCEIT Spearman	-0.3438416	0.23987509	0.23449774	-0.1986494	-0.0355456	-0.1263573	-0.0744135	0.10970797	0.08242948	-0.1360788	0.00712432	0.14573329	0.00688383	0.14570519
SNI Pearson	-0.0364284	0.09960479	-0.0126699	0.14606318	-0.3488076	-0.0313262	0.10277644	0.02524505	0.06202591	-0.2149793	0.06509809	0.54796606	-0.1572895	-0.5551819
SNI Spearman	0.13077722	-0.1115207	-0.0818891	0.25485651	-0.2310788	0.00267917	0.07652393	0.15689918	0.08757553	0.04789025	-0.0219357	-0.1438382	0.1701276	-0.0351642
Positive PANAS Pearson	0.17880969	-0.0023292	0.07424385	-0.045416	0.10974245	0.04541637	0.14589859	0.12535279	-0.0240029	-0.1943034	0.05999259	0.05089536	-0.1180076	0.22936886
Positive PANAS Spearman	0.14033626	-0.1082212	-0.0030947	0.00585431	0.08028773	-0.0254244	0.08530571	0.15789921	-0.0304424	-0.1572301	-0.0493435	0.0710881	-0.062223	0.34389912
Negative PANAS Pearson	-0.0761011	0.20348226	0.17313157	-0.0633859	0.06784873	-0.1136637	0.04227021	-0.0252931	0.26455802	0.10611391	-0.1970387	0.08183591	-0.2165333	0.07096269
Negative PANAS Spearman	0.04838659	0.1567654	0.1611533	0.0417803	-0.1049864	0.04030014	-0.0469582	-0.083833	0.1726562	0.07481173	-0.0940949	0.20800876	-0.5186828	-0.0378522
Lateral OFC - Left														
Perceiving MSCEIT Pearson	-0.1102223	0.11038015	-0.1375246	-0.1458294	0.29856791	-0.2989649	0.04265139	0.19576588	-0.1209432	-0.1865956	-0.0128936	0.02983999	-0.0291059	0.01304699
Perceiving MSCEIT Spearman	0.01576246	0.17169612	-0.0986476	-0.0890436	0.07765509	-0.3488274	0.05697976	0.20180368	-0.117689	-0.1841301	-0.0830082	0.10959176	0.06053435	-0.0120779
Overall MSCEIT Pearson	-0.259541	0.17511797	-0.0677788	-0.0448336	-0.0076264	-0.1746915	0.06130283	0.01437935	-0.027155	-0.1791937	-0.0335751	0.0743956	0.16984629	0.05746388
Overall MSCEIT Spearman	-0.1865836	0.14889829	0.0088368	0.00861713	-0.1421302	-0.2387359	0.21247595	-0.0651038	-0.1120848	-0.0715961	-0.076846	0.06275156	0.19718975	0.11500249
SNI Pearson	0.13992457	0.09049818	0.20169606	0.14606608	-0.1389797	-0.0758718	0.16135281	-0.0837457	-0.0916671	-0.3414533	0.05387696	0.59391236	-0.1126021	-0.4543664
SNI Spearman	0.31513794	-0.1811792	0.1227397	0.21768296	-0.131447	-0.0716739	0.2935371	-0.0864034	0.17565534	0.00870732	0.00267917	-0.0118888	0.12089777	-0.0266243
Positive PANAS Pearson	0.1745396	-0.0910876	0.27545026	0.03546124	-0.0908993	-0.0321499	0.17135823	0.21380317	-0.2185615	-0.2017503	0.00024533	0.06560311	-0.0799296	0.20367824
Positive PANAS Spearman	0.17981107	-0.0712554	0.23801967	-0.0378021	-0.0480054	-0.0812145	0.15907007	0.1988794	-0.1617463	-0.1978758	-0.075437	0.09667981	-0.1165845	0.32081639
Negative PANAS Pearson	-0.024577	0.10593603	0.33057689	0.05671227	-0.0237476	-0.3326033	0.21202607	0.12754158	0.02758074	0.00983281	-0.081012	0.09637881	-0.2244305	0.08354132
Negative PANAS Spearman	0.03267434	0.06588432	0.39102076	0.23961181	-0.1476594	-0.2876653	0.07463319	0.04160175	-0.0623134	-0.0569569	-0.0565998	0.20604473	-0.5211825	0.01410532

Figure 5.28: Correlation Coefficients between ROI Signal Changes and Individual Behavioral Measures - Lateral OFC Models: Neg-Neu = [Negative - Neutral]; Pos-Neg = [Positive - Negative]; Hed+ = Effect of Increasing Hedonic Value; Int+ = Effect of Increasing Intensity Value; Interesting+ = Effect of Increasing Interesting-ness; Emotional+ = Effect of Increasing Emotional Intensity; Chemical+ = Effect of Increasing Chemical-like Quality.

Run Type	Active Runs							Passive Runs						
Model	[Neg - Neu]	[Pos - Neg]	Hedonic+	Intensity+	Chemical+	Interesting+	Emotional+	[Neg - Neu]	[Pos - Neg]	Hedonic+	Intensity+	Chemical+	Interesting+	Emotional+
Middle OFC - Bilateral														
Perceiving MSCEIT Pearson	-0.1828493	-0.0257854	-0.0576043	-0.1054103	-0.0068591	-0.1745575	0.09046767	0.43943905	-0.0694919	-0.212481	-0.2090429	0.12170488	-0.0866748	0.10882019
Perceiving MSCEIT Spearman	-0.0934788	0.0355826	-0.0968592	0.01366033	0.00389344	-0.2705014	0.19520638	0.36753632	-0.0631091	-0.1578605	-0.0810878	0.24663396	-0.1359304	0.08400561
Overall MSCEIT Pearson	-0.1791469	-0.0301773	-0.0169391	-0.0547733	-0.0151002	-0.199076	0.0208588	0.259039951	-0.3223061	-0.261363	-0.2573928	0.15416136	-0.1500701	0.20266983
Overall MSCEIT Spearman	-0.25857	0.06958765	-0.0577633	-0.0406307	0.00778688	-0.2081593	0.21871663	0.12216057	-0.1038708	-0.1774618	-0.1084208	0.2179271	-0.1613041	0.27966866
SNI Pearson	0.05735917	-0.0176264	0.09131827	0.06882783	-0.4989319	0.04120813	0.3868986	-0.0150205	-0.1378219	-0.2638036	0.05149697	0.60384083	-0.1827271	-0.5127483
SNI Spearman	0.2769597	-0.123242	0.10934382	-0.107167	-0.4504363	0.1068321	0.3568326	0.06614213	0.04454128	0.28315529	-0.004856	-0.038848	0.20763605	-0.223762
Positive PANAS Pearson	0.00988301	0.01254601	0.19085465	0.16146187	-0.0948508	0.04195704	0.06150813	0.18690128	-0.0934117	-0.0922084	0.15786557	0.0967072	-0.2382452	0.0838261
Positive PANAS Spearman	0.15889201	0.01103956	0.07577155	0.1189262	-0.0337878	-0.0685791	0.02475538	0.23383802	-0.0650665	-0.0677428	0.14351432	0.09651254	-0.2070754	0.24002686
Negative PANAS Pearson	-0.1886423	0.15467963	0.16608347	0.01862256	0.06661662	-0.0581566	-0.0726829	0.06174435	0.07228595	-0.0822254	-0.1374309	0.0975296	-0.2810226	0.13086339
Negative PANAS Spearman	-0.1890826	0.2196144	0.18086942	0.14944492	0.01481951	-0.078561	-0.0915953	0.04106611	0.01089145	-0.1653357	0.02213999	0.19747441	-0.4656539	0.10891446
Middle OFC - Right														
Perceiving MSCEIT Pearson	-0.1220807	0.01744117	-0.0367768	-0.1372862	0.06803005	-0.1038008	-0.0007838	0.48528016	-0.1255084	-0.1970714	-0.1753517	0.10426042	-0.053536	0.0636733
Perceiving MSCEIT Spearman	-0.0220486	0.04253517	-0.0007124	0.09231103	0.0704269	-0.0527384	-0.0699088	0.45419435	-0.1616569	-0.2119103	-0.1047764	0.23972788	-0.0549342	-0.0197797
Overall MSCEIT Pearson	-0.0973449	-0.0422984	0.08742734	-0.156081	0.05096247	-0.13596	0.03651106	0.33464935	-0.1107649	-0.1923243	-0.172255	0.0754407	-0.1916218	0.19657652
Overall MSCEIT Spearman	-0.1951575	0.08734588	0.07053077	-0.0400131	0.09337301	-0.0722056	0.05792957	0.1981939	-0.1752199	-0.293522	-0.0442794	0.1589996	-0.2348167	0.23823195
SNI Pearson	-0.0521476	0.06244151	0.07981068	-0.0167148	-0.5256769	0.08272541	0.49526548	0.02670437	0.13558857	-0.1148457	0.04687644	0.51821194	-0.1884525	-0.4565767
SNI Spearman	0.10030161	-0.0497322	0.06128613	-0.175486	-0.3888153	0.1220699	0.28393254	0.06212337	0.17330912	0.27612246	-0.0641327	-0.0574348	0.23174863	-0.2165108
Positive PANAS Pearson	-0.0007146	0.12044466	0.11925078	0.09749395	0.00575981	0.04748932	0.07773759	0.11544436	0.17389536	-0.0214093	0.08587181	0.08268778	-0.2574238	0.1172371
Positive PANAS Spearman	0.10303592	0.10554491	-0.0262608	0.07142263	0.0488417	0.01722841	-0.0163934	0.13849634	0.13799454	0.0093669	0.02810071	0.15104129	-0.2204567	0.18449452
Negative PANAS Pearson	-0.1686104	0.16648484	0.09547698	0.025233215	0.16094647	-0.0637376	-0.0860411	0.08826201	0.12678587	-0.09912	-0.1926556	0.05119494	-0.2241743	0.19009614
Negative PANAS Spearman	-0.1737275	0.2669297	0.07070512	0.08106092	0.03731659	0.13230428	-0.0769607	0.00446371	0.17961958	-0.2026523	-0.0103558	0.26675115	-0.3869141	0.09570188
Middle OFC - Left														
Perceiving MSCEIT Pearson	-0.2223999	-0.0727102	-0.0778698	-0.0506068	-0.1079546	-0.2249083	0.15988439	0.27687966	-0.0120271	-0.2007822	-0.2059152	0.12759117	-0.1190813	0.14700835
Perceiving MSCEIT Spearman	-0.1178064	-0.0226527	-0.1838891	0.01471113	-0.0848953	-0.3115208	0.29515645	0.20696151	-0.0547548	-0.141099	-0.1935079	0.2250656	-0.1231672	0.1426591
Overall MSCEIT Pearson	-0.2376129	-0.0129528	-0.1458534	0.0696611	-0.1024528	-0.236975	0.00051662	0.09840815	0.0312612	-0.2926074	-0.3197679	0.21999072	-0.0647386	0.1948401
Overall MSCEIT Spearman	-0.1950149	-0.0056632	0.09085944	0.06760112	-0.1370578	-0.2072138	0.26697922	-0.0017811	-0.1196884	-0.0898541	-0.3125342	0.20428489	-0.061217	0.25538605
SNI Pearson	0.15546398	-0.1074877	0.09613625	0.15347742	-0.3601211	-0.0116158	0.18955209	-0.0674545	-0.3077143	-0.3674183	0.04576786	0.63094141	-0.1441098	-0.5340088
SNI Spearman	0.44357089	-0.2886811	0.15589449	-0.0316478	-0.493638	0.09176174	0.30073738	0.05559288	-0.078031	0.15237807	0.14484289	0.0850638	0.10331568	-0.241963
Positive PANAS Pearson	0.01899658	-0.1124838	0.26128279	0.20511403	-0.2137337	0.02905042	0.03113581	0.23598553	-0.2711418	-0.1455016	0.23070007	0.10129072	-0.1715234	0.0442001
Positive PANAS Spearman	0.16693158	-0.0692482	0.21594054	0.12344239	-0.1480305	-0.1314712	0.07928413	0.23082723	-0.1774693	-0.1717823	0.24203406	0.14451792	-0.1645898	0.24604844
Negative PANAS Pearson	-0.1921401	0.12467595	0.23792712	0.00780614	-0.0766117	-0.0425446	-0.0425541	0.01038335	0.01003366	-0.0568815	-0.0165582	0.13548129	-0.312543	0.06188837
Negative PANAS Spearman	-0.1906896	0.17354894	0.35941771	0.18569022	-0.062849	-0.1753344	-0.0673127	0.02285418	-0.0789183	-0.2378263	0.05088626	0.14926637	-0.380933	0.10605769

Figure 5.29: Correlation Coefficients between ROI Signal Changes and Individual Behavioral Measures - Middle OFC Models: Neg-Neu = [Negative - Neutral]; Pos-Neg = [Positive - Negative]; Hed+ = Effect of Increasing Hedonic Value; Int+ = Effect of Increasing Intensity Value; Interesting+ = Effect of Increasing Interesting-ness; Emotional+ = Effect of Increasing Emotional Intensity; Chemical+ = Effect of Increasing Chemical-like Quality.

| Run Type | Active Runs | | | | | | | Passive Runs | | | | | | |
Model	[Neg - Neu]	[Pos - Neg]	Hedonic+	Intensity+	Chemical+	Interesting+	Emotional+	[Neg - Neu]	[Pos - Neg]	Hedonic+	Intensity+	Chemical+	Interesting+	Emotional+
Medial OFC - Bilateral														
Perceiving MSCEIT Pearson	-0.1631301	-0.0766451	0.08822337	-0.0538582	0.15966922	-0.3482667	-0.0941619	0.2182835	-0.0860976	-0.2376747	-0.2429243	0.09468106	-0.0803979	0.09131115
Perceiving MSCEIT Spearman	-0.1814516	0.04574906	0.14069937	-0.0573397	0.11137688	-0.27939	-0.1307486	0.22543988	-0.1063412	-0.2155169	-0.1357982	0.21292623	0.01282378	0.11342701
Overall MSCEIT Pearson	-0.3143255	0.02903634	0.10840304	0.04045056	0.11574051	-0.3427552	-0.1736814	0.20999831	-0.0207449	-0.1288082	-0.2537247	0.06418725	0.11419636	0.15732989
Overall MSCEIT Spearman	-0.4420821	0.16318918	0.12889993	-0.076453	0.05842432	-0.2414828	-0.1159605	0.08174487	-0.083491	-0.0548942	-0.1906224	0.14534763	0.11577021	0.25862778
SNI Pearson	-0.1474698	0.16809777	0.00808419	-0.1321573	0.20127877	-0.1809479	-0.0977307	-0.0093562	0.13107116	-0.1750941	0.04619946	0.55088045	-0.2131732	-0.3389636
SNI Spearman	-0.0637979	-0.0164099	-0.0693236	-0.1249165	0.02361023	-0.1033157	0.01222374	0.00117214	0.29186261	0.02545216	-0.1215676	0.07334241	0.08724063	-0.1210652
Positive PANAS Pearson	0.04473325	-0.0868224	0.26903132	-0.193263	-0.0699575	-0.100949	0.05019088	0.09119704	-0.1701288	-0.1061511	-0.2304834	0.21464409	-0.2947521	0.19655901
Positive PANAS Spearman	0.00903237	-0.0150539	0.23768514	-0.1398345	-0.0112068	0.00752697	-0.0351259	0.08430212	-0.0680773	-0.0237518	-0.1619136	0.25207002	-0.2386887	0.25240456
Negative PANAS Pearson	-0.115782	0.0886996	0.17652476	-0.151591	0.03070273	-0.124662	0.16219122	0.18792297	0.11053463	-0.2234101	0.02320279	0.23202279	-0.184758	0.10566984
Negative PANAS Spearman	0.08641737	0.21818601	0.34138433	-0.0951662	-0.0823108	-0.1460525	0.16265749	-0.1590865	0.15855088	-0.0366024	0.01946176	0.14712379	-0.5570707	0.00821322
Medial OFC - Right														
Perceiving MSCEIT Pearson	-0.1649405	-0.0209333	0.10952628	-0.0800367	0.15828543	-0.3270483	-0.0970981	0.23180661	-0.0819874	-0.215745	-0.2827855	0.12725106	-0.0688924	0.0666832
Perceiving MSCEIT Spearman	-0.1400293	0.10758824	0.17033073	-0.0542536	0.0701985	-0.136253	-0.1758422	0.27766057	-0.1044149	-0.2007677	-0.1893274	0.2443914	-0.0337893	0.06194636
Overall MSCEIT Pearson	-0.2621154	0.03599923	0.18814583	-0.0439418	0.1831731	-0.3720386	-0.1117559	0.23415724	-0.0587639	-0.131782	-0.3148314	0.07835607	0.12163878	0.16003366
Overall MSCEIT Spearman	-0.3918622	0.23027043	0.20704451	-0.1305587	0.0905607	-0.1894933	-0.1197185	0.08300819	-0.0966281	-0.0905561	-0.1503535	0.16394068	0.01912939	0.2622986
SNI Pearson	-0.1478329	0.1429296	0.04645906	-0.2024722	0.12584995	-0.103854	-0.1661714	-0.0256838	0.19536247	-0.1286527	0.05919186	0.52698433	-0.1999679	-0.4783782
SNI Spearman	-0.0643002	0.00301432	-0.0192566	-0.1791698	0.03717355	-0.1995985	-0.0493973	0.03482927	0.35432088	0.07803097	-0.150871	0.02612195	0.06446765	-0.0940302
Positive PANAS Pearson	0.03595321	0.02108182	0.25555999	-0.1668365	0.01162626	-0.1338234	0.01435748	-0.0154498	-0.0386468	-0.0968429	-0.1716413	0.2088218	-0.3402689	0.14027305
Positive PANAS Spearman	0.00234173	0.05436603	0.22162759	-0.1214352	0.07309529	-0.0981852	-0.0491762	0.0197374	0.05937947	-0.0178975	-0.1821528	0.2580916	-0.3064315	0.18760462
Negative PANAS Pearson	-0.1234805	0.11731391	0.1442153	-0.1075011	0.0625542	-0.0683295	0.11872316	-0.0946139	0.26274212	0.12953154	-0.2997328	0.01168658	-0.0993157	0.07665007
Negative PANAS Spearman	0.07070512	0.16588522	0.21675763	-0.0940949	-0.0271393	0.0939164	0.01285548	-0.155337	0.18622587	-0.0046423	0.0473153	0.19676022	-0.4520843	-0.0110709
Medial OFC - Left														
Perceiving MSCEIT Pearson	-0.1485365	-0.1251343	0.05622027	-0.0282744	0.14257056	-0.3382968	-0.0878439	0.17186807	-0.0823669	-0.2463779	-0.1715232	0.05047489	-0.0852805	0.10516928
Perceiving MSCEIT Spearman	-0.087358	-0.0831852	0.0527799	-0.0253835	0.15113621	-0.2879438	-0.1149071	0.13269795	-0.1192029	-0.242809	-0.0786356	0.16068551	0.02010663	0.1308227
Overall MSCEIT Pearson	-0.340577	0.01934561	0.0131026	0.10632525	0.04521213	-0.292353	-0.2029098	0.15524043	0.00598642	-0.1198815	-0.1615049	0.04380656	0.09784308	0.14368435
Overall MSCEIT Spearman	-0.3545066	0.01754963	0.01400283	-0.0026626	0.02690012	-0.1804681	-0.1445605	-0.0153959	-0.1002707	-0.1549637	-0.0491989	0.10405784	0.17018824	0.22170631
SNI Pearson	-0.1361726	0.17726099	-0.0323489	-0.0645678	0.24197482	-0.2290404	-0.049914	0.00646705	0.07834292	-0.2091088	0.02766531	0.55122457	-0.2091415	-0.1988411
SNI Spearman	0.02947092	-0.0041862	-0.1379775	0.01155394	0.05073687	-0.0462158	0.03482927	-0.0835568	0.28167179	-0.051909	-0.0760216	0.11855349	0.12960508	-0.1800071
Positive PANAS Pearson	0.05036385	-0.186495	0.25295785	-0.1995519	-0.1309712	-0.0665062	0.06988636	0.17356718	-0.244376	-0.1095913	-0.2508545	0.21055534	-0.2275259	0.22927214
Positive PANAS Spearman	0.09065823	-0.1644226	0.21159163	-0.1706114	-0.0874802	0.00518525	-0.0240863	0.16425532	-0.154985	-0.0523543	-0.1895125	0.22631104	-0.130133	0.28937037
Negative PANAS Pearson	-0.0993687	0.05159801	0.1902494	-0.1755086	0.00020002	-0.1604224	0.18068895	-0.0062449	0.12376118	0.08775365	-0.1216025	0.03589023	-0.2219493	0.12221947
Negative PANAS Spearman	0.02856773	0.15051621	0.37941512	-0.1490878	-0.153373	-0.2565739	0.26942937	-0.1474809	0.11865525	0.00124984	0.01374822	0.18801135	-0.5104696	0.05856384

Figure 5.30: Correlation Coefficients between ROI Signal Changes and Individual Behavioral Measures - Medial OFC Models: Neg-Neu = [Negative - Neutral]; Pos-Neg = [Positive - Negative]; Hed+ = Effect of Increasing Hedonic Value; Int+ = Effect of Increasing Intensity Value; Interesting+ = Effect of Increasing Interesting-ness; Emotional+ = Effect of Increasing Emotional Intensity; Chemical+ = Effect of Increasing Chemical-like Quality.

Bibliography

[1] Adolphs, R., Tranel, D., & Damasio, A. R. (2003). Dissociable neural systems for recognizing emotions. Brain and Cognition, 52(1), 61–69. http://doi.org/10.1016/S0278-2626(03)00009-5

[2] Afif, A., & Mertens, P. (2009). Description of sulcal organization of the insular cortex. Surgical and Radiologic Anatomy, 32(5), 491–498. http://doi.org/10.1007/s00276-009-0598-4

[3] Albrecht, J., Kopietz, R., Frasnelli, J., Wiesmann, M., Hummel, T., & Lundström, J. N. (2010). The neuronal correlates of intranasal trigeminal function—an ALE meta-analysis of human functional brain imaging data. Brain Research Reviews, 62(2), 183–196. http://doi.org/10.1016/j.brainresrev.2009.11.001

[4] Allen, G. V., Saper, C. B., Hurley, K. M., and Cechetto, D. F. (1991). Organization of visceral and limbic connections in the insular cortex of the rat. J. Comp. Neurol. 311, 1–16.

[5] Allen Mouse Brain Atlas. (2004). Allen Institute for Brain Science. Available at: http://www.brain-map.org

[6] Allman, J. M. (1977). "Evolution of the visual system in the early primates," in Progress in Psychobiology and Physiological Psychology, Vol. 7, eds J. M. Sprague and A. N. Epstein (New York, NY: Academic Press), 1–53.

[7] Allman, J. M. Evolving Brains (Scientific American Library, New York, 2000).

[8] Allman, J.M., Tetreault, N.A., Hakeem, A.Y., Manaye, K.F., Semendeferi, K., Erwin, J.M., Park, S., Goubert, V., and Hof, P.R. (2010). The von Economo neurons in frontoinsular and anterior cingulate cortex in great apes and humans. Brain Structure & Function 214, 495-517.

[9] Amaral, D.G., and Insausti, R. (1992). Retrograde transport of D-[H3]-aspartate injected into the monkey amygdaloid complex. Experimental Brain Research 88, 375-388.

[10] An, X., Bandler, R., Öngür, D., and Price, J.L. (1998). Prefrontal cortical projections to longitudinal columns in the midbrain periaqueductal gray in macaque monkeys. Journal of Comparative Neurology 401, 455-479.

[11] Anderson, A. K., Christoff, K., Stappen, I., Panitz, D., Ghahremani, D. G., Glover, G., Gabrieli, J. D., and Sobel, N. (2003). Dissociated neural representations of intensity and valence in human olfaction. Nat. Neurosci. 6, 196-202.

[12] Arikuni, T., and Kubota, K. (1985). Claustral and amygdaloid afferents to the head of the caudate nucleus in macaque monkeys. Neuroscience research 2, 239-254.

[13] Atanasova, B., Graux, J., El-Hage, W., Hommet, C., Camus, V., and Belzung, C. (2008). Olfaction: a potential cognitive marker of psychiatric disorders. Neurosci. Biobehav. Rev. 32, 1315-1325.

[14] Atanasova, B., El-Hage, W., Chabanet, C., Gaillard, P., Belzung, C., and Camus, V. (2010). Olfactory anhedonia and negative olfactory alliesthesia in depressed patients. Psychiatry Res. 176, 190-196.

[15] Bamiou, D.-E., Musiek, F. E., & Luxon, L. M. (2003). The insula (Island of Reil) and its role in auditory processing. Brain Research Reviews, 42(2), 143–154. http://doi.org/10.1016/S0165-0173(03)00172-3

[16] Bartels, A., & Zeki, S. (2004). The neural correlates of maternal and romantic love. NeuroImage 21(3), 1155–1166. http://doi.org/10.1016/j.neuroimage.2003.11.003

[17] Bauernfeind, A. L., de Sousa, A. A., Avasthi, T., Dobson, S. D., Raghanti, M. A., Lewandowski, A. H., et al. (2013). A volumetric comparison of the insular cortex and its subregions in primates. Journal of Human Evolution 64(4), 263–279. http://doi.org/10.1016/j.jhevol.2012.12.003

[18] Baxter, M. G., Murry, E. A. (2002). The amygdala and reward. Nature Reviews Neuroscience 3, 563-573.

[19] Bayer, S.A., and Altman, J. (1991a). Development of the endopiriform nucleus and the claustrum in the rat-brain. Neuroscience 45, 391-412.

[20] Bayer, S.A., and Altman, J. (1991b). Neocortical Development. New York: Raven Press.

[21] Beck, A. T., Steer, R. A., & Brown, G. K. (1996). Manual for the beck depression inventory-II.

[22] Beckstead, R.M., Morse, J.R., and Norgren, R. (1980). The nucleus of the solitary tract in the monkey - projections to the thalamus and brainstem nuclei. Journal of Comparative Neurology 190, 259-282.

[23] Behan, M., and Haberly, L.B. (1999). Intrinsic and efferent connections of the endopiriform nucleus in rat. Journal of Comparative Neurology 408, 532-548.

[24] Behrens, T.E.J., Berg, H.J., Jbabdi, S., Rushworth, M.F.S., and Woolrich, M.W. (2007). Probabilistic diffusion tractography with multiple fibre orientations: What can we gain? Neuroimage 34, 144-155.

[25] Behrens, T.E.J., Johansen-Berg, H., Woolrich, M.W., Smith, S.M., Wheeler-Kingshott, C.a.M., Boulby, P.A., Barker, G.J., Sillery, E.L., Sheehan, K., Ciccarelli, O., Thompson, A.J., Brady, J.M., and Matthews, P.M. (2003). Non-

invasive mapping of connections between human thalamus and cortex using diffusion imaging. Nature Neuroscience 6, 750-757.

[26] Behrens, T.E.J., Woolrich, M.W., Jenkinson, M., Johansen-Berg, H., Nunes, R.G., Clare, S., Matthews, P.M., Brady, J.M., and Smith, S.M. (2003). Characterization and propagation of uncertainty in diffusion-weighted MR imaging. Magnetic Resonance in Medicine 50, 1077-1088.

[27] Bengtsson, S., Berglund, H., Gulyas, B., Cohen, E., and Savic, I. (2001). Brain activation during odor perception in males and females. Neuroreport. 12(9), 2027 - 2033.

[28] Bermpohl, F., Pascual-Leone, A., Amedi, A., Merabet, L. B., Fregni, F., Gaab, N., et al. (2006). Dissociable networks for the expectancy and perception of emotional stimuli in the human brain. NeuroImage, 30(2), 588–600. http://doi.org/10.1016/j.neuroimage.2005.09.040

[29] Bernhardt, B. C., & Singer, T. (2012). The Neural Basis of Empathy. Annual Review of Neuroscience, 35(1), 1–23. http://doi.org/10.1146/annurev-neuro-062111-150536

[30] Bernhardt, B. C., Valk, S. L., Silani, G., Bird, G., Frith, U., & Singer, T. (2014). Selective Disruption of Sociocognitive Structural Brain Networks in Autism and Alexithymia. Cerebral Cortex, 24(12), 3258–3267. http://doi.org/10.1093/cercor/bht182

[31] Berns, G. S., McClure, S. M., Pagnoni, G., Montague, P. R. (2001). Predictability modulates human brain response to reward. J Neurosci. 21(8):2793-8.

[32] Bohland, J. W., & Guenther, F. H. (2006). An fMRI investigation of syllable sequence production. NeuroImage, 32(2), 821–841. http://doi.org/10.1016/j.neuroimage.2006.04.173

[33] Botvinick, M., Jha, A. P., Bylsma, L. M., Fabian, S. A., Solomon, P. E., & Prkachin, K. M. (2005). Viewing facial expressions of pain engages cortical

areas involved in the direct experience of pain. NeuroImage, 25(1), 312–319. http://doi.org/10.1016/j.neuroimage.2004.11.043

[34] Brillat-Savarin, J. A. The Physiology of Taste: Or Meditations on Transcendental Gastronomy (Vintage, New York, 2011).

[35] Britton, J. C., Taylor, S. F., Sudheimer, K. D., & Liberzon, I. (2006). Facial expressions and complex IAPS pictures: Common and differential networks. NeuroImage, 31(2), 906–919. http://doi.org/10.1016/j.neuroimage.2005.12.050

[36] Brodmann, K. (1909). Vergleichende Lokalisationlehre der Großhirnrinde in ihren Prinziprien dargestellt auf Grund des Zellenbaues. Leipzig: Johann Ambrosius Barth.

[37] Brown, S., Martinez, M. J., & Parsons, L. M. (2006). Music and language side by side in the brain: a PET study of the generation of melodies and sentences. European Journal of Neuroscience, 23(10), 2791–2803. http://doi.org/10.1111/j.1460-9568.2006.04785.x

[38] Buck, L. B. (2005). Unraveling the sense of smell (Nobel Lecture). Angew. Chem. Int. Ed. 44, 6128-6140.

[39] Butler, T., Pan, H., Tuescher, O., Engelien, A., Goldstein, M., Epstein, J., et al. (2007). Human fear-related motor neurocircuitry. Neuroscience, 150(1), 1–7. http://doi.org/10.1016/j.neuroscience.2007.09.048

[40] Butti, C., Sherwood, C. C., Hakeem, A. Y., Allman, J. M., & Hof, P. R. (2009). Total number and volume of Von Economo neurons in the cerebral cortex of cetaceans. The Journal of Comparative Neurology, 515(2), 243–259. http://doi.org/10.1002/cne.22055

[41] Calder, A. J., Keane, J., Manes, F., Antoun, N., and Young, A. W. (2000). Impaired recognition and experience of disgust following brain injury. Nature Neuroscience 3, 1077 - 1078.

[42] Carey, R.G., Fitzpatrick, D., and Diamond, I.T. (1979). Layer-I of striate cortex of Tupaia glis and Galago senegalensis - projections from thalamus and claustrum revealed by retrograde transport of horseradish peroxidase. Journal of Comparative Neurology 186, 393-437.

[43] Carey, R.G., and Neal, T.L. (1985). The rat claustrum - afferent and efferent connections with visual-cortex. Brain Research 329, 185-193.

[44] Caruana, F., Jezzini, A., Sbriscia-Fioretti, B., Rizzolatti, G., & Gallese, V. (2011). Emotional and Social Behaviors Elicited by Electrical Stimulation of the Insula in the Macaque Monkey. Current Biology, 21(3), 195–199. http://doi.org/10.1016/j.cub.2010.12.042

[45] Cauda, F., Costa, T., Torta, D. M. E., Sacco, K., D'Agata, F., Duca, S., et al. (2012). Meta-analytic clustering of the insular cortex. NeuroImage, 62(1), 343–355. http://doi.org/10.1016/j.neuroimage.2012.04.012

[46] Cauda, F., D'Agata, F., Sacco, K., Duca, S., Geminiani, G., & Vercelli, A. (2011). Functional connectivity of the insula in the resting brain. NeuroImage, 55(1), 8–23. http://doi.org/10.1016/j.neuroimage.2010.11.049

[47] Cerliani, L., Thomas, R.M., Jbabdi, S., Siero, J.C.W., Nanetti, L., Crippa, A., Gazzola, V., D'Arceuil, H., and Keysers, C. (2011). Probabilistic tractography recovers a rostrocaudal trajectory of connectivity variability in the human insula cortex. Human Brain Mapping doi: 10.1002/hbm.21338

[48] Chang, L. J., Yarkoni, T., Khaw, M. W., & Sanfey, A. G. (2013). Decoding the Role of the Insula in Human Cognition: Functional Parcellation and Large-Scale Reverse Inference. Cerebral Cortex, 23(3), 739–749. http://doi.org/10.1093/cercor/bhs065

[49] Cheng, Y., Lin, C.-P., Liu, H.-L., Hsu, Y.-Y., Lim, K.-E., Hung, D., & Decety, J. (2007). Expertise Modulates the Perception of Pain in Others. Current Biology, 17(19), 1708–1713. http://doi.org/10.1016/j.cub.2007.09.020

[50] Chikama, M., Mcfarland, N.R., Amaral, D.G., and Haber, S.N. (1997). Insular cortical projections to functional regions of the striatum correlate with cortical cytoarchitectonic organization in the primate. Journal of Neuroscience 17, 9686-9705.

[51] Chklovskii, D. B. and Koulahkov, A. A. (2004). Maps in the brain: What can we learn from them? Annu. Rev. Neurosci. 27,369-392.

[52] Ciumas, C., Lindström, P., Aoun, B., & Savic, I. (2008). Imaging of odor perception delineates functional disintegration of the limbic circuits in mesial temporal lobe epilepsy. NeuroImage, 39(2), 578–592. http://doi.org/10.1016/j.neuroimage.2007.09.004

[53] Cohen, S., Doyle, W. J., Skoner, D. P., Rabin, B. S., & Gwaltney, J. M. (1997). Social Ties and Susceptibility to the Common Cold. Jama, 277(24), 1940–1944. http://doi.org/10.1001/jama.1997.03540480040036

[54] Craig, A.D. (2002). How do you feel? Interoception: the sense of the physiological condition of the body. Nature Reviews Neuroscience 3, 655-666.

[55] Craig, A. D. B. (2010). The sentient self. Brain Structure and Function, 214(5-6), 563–577. http://doi.org/10.1007/s00429-010-0248-y

[56] Cloutman, L. L., Binney, R. J., Drakesmith, M., Parker, G. J. M., & Ralph, M. A. L. (2012). The variation of function across the human insula mirrors its patterns of structural connectivity: Evidence from in vivo probabilistic tractography. NeuroImage, 59(4), 3514–3521. http://doi.org/10.1016/j.neuroimage.2011.11.016

[57] Damasio, A. R., Grabowski, T. J., Bechara, A., Damasio, H., Ponto, L. L. B., Parvizi, J., & Hichwa, R. D. (2000). Subcortical and cortical brain activity during the feeling of self-generated emotions. Nature Neuroscience, 3(10), 1049–1056. http://doi.org/10.1038/79871

[58] D'Arceuil, H., Liu, C., Levitt, P., Thompson, B., Kosofsky, B., and De Crespigny, A. (2008). Three-dimensional high-resolution diffusion tensor imaging and tractography of the developing rabbit brain. Developmental Neuroscience 30, 262-275.

[59] D'Arceuil, H.E., Westmoreland, S., and De Crespigny, A.J. (2007). An approach to high resolution diffusion tensor imaging in fixed primate brain. Neuroimage 35, 553-565.

[60] de Araujo, I. E. (2004). Representation in the Human Brain of Food Texture and Oral Fat. Journal of Neuroscience, 24(12), 3086–3093. http://doi.org/10.1523/JNEUROSCI.0130-04.2004

[61] de Araujo, I. E. T. (2003). Human Cortical Responses to Water in the Mouth, and the Effects of Thirst. Journal of Neurophysiology, 90(3), 1865–1876. http://doi.org/10.1152/jn.00297.2003

[62] de Araujo, I. E. T., Rolls, E. T., Kringelbach, M. L., McGlone, F., & Phillips, N. (2003). Taste-olfactory convergence, and the representation of the pleasantness of flavour, in the human brain. European Journal of Neuroscience, 18(7), 2059–2068. http://doi.org/10.1046/j.1460-9568.2003.02915.x

[63] de Araujo, I. E., Rolls, E. T., Velazco, M. I., Margot, C., & Cayeux, I. (2005). Cognitive Modulation of Olfactory Processing. Neuron, 46(4), 671–679. http://doi.org/10.1016/j.neuron.2005.04.021

[64] Deen, B., Pitskel, N.B., and Pelphrey, K.A. (2011). Three systems of insular functional connectivity identified with cluster analysis. Cerebral Cortex 21, 1498-1506.

[65] Di Martino, A., Ross, K., Uddin, L. Q., Sklar, A. B., Castellanos, F. X., & Milham, M. P. (2009). Functional Brain Correlates of Social and Nonsocial Processes in Autism Spectrum Disorders: An Activation

Likelihood Estimation Meta-Analysis. Biological Psychiatry, 65(1), 63–74. http://doi.org/10.1016/j.biopsych.2008.09.022

[66] Dinopoulos, A., Papadopoulos, G.C., Michaloudi, H., Parnavelas, J.G., Uylings, H.B.M., and Karamanlidis, A.N. (1992). Claustrum in the hedgehog (Erinaceus europaeus) brain - cytoarchitecture and connections with cortical and subcortical structures. Journal of Comparative Neurology 316, 187-205.

[67] Doeller, C.F., Barry, C., and Burgess, N. (2010). Evidence for grid cells in a human memory network. Nature 463, 657-687.

[68] Dravnieks, A. (1985). Atlas of odor character profiles. ASTM Committee on sensory evaluation of materials

[69] Dyrby, T.B., Baaré, W.F.C., Alexander, D.C., Jelsing, J., Garde, E., and Søgaard, L.V. (2011). An Ex Vivo Imaging Pipeline for Producing High-Quality and High-Resolution Diffusion-Weighted Imaging Datasets. Human Brain Mapping 32, 544-563.

[70] Dyrby, T.B., Søgaard, L.V., Parker, G.J., Alexander, D.C., Lind, N.M., Baaré, W.F.C., Hay-Schmidt, A., Eriksen, N., Pakkenberg, B., Paulson, O.B., and Jelsing, J. (2007). Validation of in vitro probabilistic tractography. Neuroimage 37, 1267-1277.

[71] Edelstein, L.R., and Denaro, F.J. (2004). The claustrum: A historical review of its anatomy, physiology, cytochemistry and functional significance. Cellular and Molecular Biology 50, 675-702.

[72] Elliott, R., Newman, J. L., Longe, O. A., Deakin, J. F. W. (2003). Differential response patterns in the striatum and orbitofrontal cortex to financial reward in humans: a parametric functional magnetic resonance imaging study. J. Neurosci. 23(1), 303-307.

[73] Escobedo, J. R., & Adolphs, R. (2010). Becoming a better person: Temporal remoteness biases autobiographical memories for moral events. Emotion, 10(4), 511–518. http://doi.org/10.1037/a0018723

[74] Evrard, H. C., Forro, T., & Logothetis, N. K. (2012). Von Economo Neurons in the Anterior Insula of the Macaque Monkey. Neuron, 74(3), 482–489. http://doi.org/10.1016/j.neuron.2012.03.003

[75] Evrard, H. C., Logothetis, N. K., & Bud Craig, A. D. (2013). Modular architectonic organization of the insula in the macaque monkey. The Journal of Comparative Neurology, 522(1), 64–97. http://doi.org/10.1002/cne.23436

[76] Fajardo, C., Escobar, M. I., Buriticá, E., Arteaga, G., Umbarila, J., Casanova, M. F., & Pimienta, H. (2008). Von Economo neurons are present in the dorsolateral (dysgranular) prefrontal cortex of humans. Neuroscience Letters, 435(3), 215–218. http://doi.org/10.1016/j.neulet.2008.02.048

[77] Fan, J., Gu, X., Liu, X., Guise, K. G., Park, Y., Martin, L., et al. (2011). Involvement of the anterior cingulate and frontoinsular cortices in rapid processing of salient facial emotional information. NeuroImage, 54(3), 2539–2546. http://doi.org/10.1016/j.neuroimage.2010.10.007

[78] Fernandez-Miranda, J.C., Rhoton, A.L., Jr., Kakizawa, Y., Choi, C., and Alvarez-Linera, J. (2008). The claustrum and its projection system in the human brain: a microsurgical and tractographic anatomical study. Journal of neurosurgery 108, 764-774.

[79] Filimonoff, I.N. (1966). The claustrum, its origin and development. Journal für Hirnforschung 8, 503-528.

[80] Francis, S., Rolls, E. T., Bowtell, R., McGlone, F., O'Doherty, J., Browning, A., et al. (1999). The representation of pleasant touch in the brain and its relationship with taste and olfactory areas. NeuroReport, 10(3), 453.

[81] Frank, L.M., Brown, E.N., and Wilson, M. (2000). Trajectory encoding in the hippocampus and entorhinal cortex. Neuron 27, 169-178.

[82] Frot, M., Faillenot, I., & Mauguière, F. (2014). Processing of nociceptive input from posterior to anterior insula in humans. Human Brain Mapping, 35(11), 5486–5499. http://doi.org/10.1002/hbm.22565

[83] Fulbright, R. K., Skudlarski, P., Lacadie, C. M., Warrenburg, S., Bowers, A. A., Core, J. C., and Wexler, B. E. (1998). Functional MR imaging of regional brain responses to pleasant and unpleasant odors. Am. J. Neuroradiol. 19, 1721-1726.

[84] Fuster, J.M. (2008). The Prefrontal Cortex. London: Academic Press.

[85] Gallyas, F. (1979). Silver staining of myelin by means of physical development. Neurological research 1, 203-209.

[86] Gottfried, J. A., O'Doherty, J., and Dolan, R. J. (2003) Encoding predictive reward value in human amygdala and orbitofrontal cortex. Science 301, 1104-1107.

[87] Garrett, A. S., & Maddock, R. J. (2006). Separating subjective emotion from the perception of emotion-inducing stimuli: An fMRI study. NeuroImage, 33(1), 263–274. http://doi.org/10.1016/j.neuroimage.2006.05.024

[88] Grabenhorst, F., Rolls, E. T., Margot, C., da Silva, A. A. P., and Velazco, M. I. (2007). How pleasant and unpleasant stimuli combine in different brain regions: odor mixtures. J. Neuro. 27, 13532-13540.

[89] Grabenhorst, F., & Rolls, E. T. (2009). Different representations of relative and absolute subjective value in the human brain. NeuroImage, 48(1), 258–268. http://doi.org/10.1016/j.neuroimage.2009.06.045

[90] Griffanti, L., Salimi-Khorshidi, G., Beckmann, C. F., Auerbach, E. J., Douaud, G., Sexton, C. E., et al. (2014). ICA-based artefact removal and accelerated

fMRI acquisition for improved resting state network imaging. NeuroImage, 95, 232–247. http://doi.org/10.1016/j.neuroimage.2014.03.034

[91] Gu, X., & Han, S. (2007). Attention and reality constraints on the neural processes of empathy for pain. NeuroImage, 36(1), 256–267. http://doi.org/10.1016/j.neuroimage.2007.02.025

[92] Gu, X., Liu, X., Guise, K. G., Naidich, T. P., Hof, P. R., & Fan, J. (2010). Functional Dissociation of the Frontoinsular and Anterior Cingulate Cortices in Empathy for Pain. Journal of Neuroscience, 30(10), 3739–3744. http://doi.org/10.1523/JNEUROSCI.4844-09.2010

[93] Guilfoyle, D.N., Helpern, J.A., and Lim, K.O. (2003). Diffusion tensor imaging in fixed brain tissue at 7.0 T. Nmr in Biomedicine 16, 77-81.

[94] Haase, L., Cerf-Ducastel, B., Buracas, G., & Murphy, C. (2007). On-line psychophysical data acquisition and event-related fMRI protocol optimized for the investigation of brain activation in response to gustatory stimuli. Journal of Neuroscience Methods, 159(1), 98–107. http://doi.org/10.1016/j.jneumeth.2006.07.009

[95] Habib, M., Daquin, G., Milandre, L., Royere, M. L., Rey, M., Lanteri, A., et al. (1995). Mutism and auditory agnosia due to bilateral insular damage—Role of the insula in human communication. Neuropsychologia, 33(3), 327–339. http://doi.org/10.1016/0028-3932(94)00108-2

[96] Hayes, C. J., Stevenson, R. J., and Coltheart, M. (2007). Disgust and Huntington's disease. Neuropsychologia 45, 1135-1151

[97] Hof, P. R., and van der Gucht, E. (2007). Structure of the cerebral cortex of the humpback whale, Megaptera novaeangliae (Cetacea, Mysticeti, Balaenopteridae). Anat Rec (Hoboken). 290(1):1-31.

[98] Hafting, T., Fyhn, M., Molden, S., Moser, M.B., and Moser, E.I. (2005). Microstructure of a spatial map in the entorhinal cortex. Nature 436, 801-806.

[99] Husted, D. S., Shapira, N. A., and Goodman, W. K. (2006). The neurocircuitry of obsessive-compulsive disorder and disgust. Prog. Neuropsychopharmacol. Biol. Psychiatry 30, 389-399

[100] Iachini, I., Iavarone, A., Senese, V.P., Ruotolo, F., and Ruggiero, G. (2009). Visuospatial memory in healthy elderly, AD and MCI: a review. Current aging science 2, 43-59.

[101] Iaria, G., Committeri, G., Pastorelli, C., Pizzamiglio, L., Watkins, K. E., & Carota, A. (2008). Neural activity of the anterior insula in emotional processing depends on the individuals' emotional susceptibility. Human Brain Mappin.g, 29(3), 363–373. http://doi.org/10.1002/hbm.20393

[102] Ibañez, A., Gleichgerrcht, E., & Manes, F. (2010). Clinical effects of insular damage in humans. Brain Structure and Function, 214(5-6), 397–410. http://doi.org/10.1007/s00429-010-0256-y

[103] Ibañez, A., & Manes, F. (2012). Contextual social cognition and the behavioral variant of frontotemporal dementia. Neurology, 78(17), 1354–1362. http://doi.org/10.1212/WNL.0b013e3182518375

[104] Ilg, R., Vogeley, K., Goschke, T., Bolte, A., Shah, J. N., Pöppel, E., & Fink, G. R. (2007). Neural processes underlying intuitive coherence judgments as revealed by fMRI on a semantic judgment task. NeuroImage, 38(1), 228–238. http://doi.org/10.1016/j.neuroimage.2007.07.014

[105] Insausti, R., Amaral, D.G., and Cowan, W.M. (1987). The entorhinal cortex of the monkey: 3. Subcortical afferents. Journal of Comparative Neurology 264, 396-408.

[106] Iwabuchi, S. J., Liddle, P. F., & Palaniyappan, L. (2014). Structural connectivity of the salience-executive loop in schizophrenia. European Archives of Psychiatry and Clinical Neuroscience, 265(2), 163–166. http://doi.org/10.1007/s00406-014-0547-z

[107] Jabbi, M., Swart, M., & Keysers, C. (2007). Empathy for positive and negative emotions in the gustatory cortex. NeuroImage, 34(4), 1744–1753. http://doi.org/10.1016/j.neuroimage.2006.10.032

[108] Jacobs, J., Kahana, M.J., Ekstrom, A.D., Mollison, M.V., and Fried, I. (2010). A sense of direction in human entorhinal cortex. Proceedings of the National Academy of Sciences of the United States of America 107, 6487-6492.

[109] Jacobs, M., Snow, J., Geraci, M., Vythilingam, M., Blair, R. J. R., Charney, D. S., Pine, D. S., Blair, K. S. (2008). Association between level of emotional intelligence and severity of anxiety in generalized social phobia. Journal of Anxiety Disorders 22(8), 1487-1495.

[110] Jakab, A., Molnár, P. P., Bogner, P., Béres, M., & Berényi, E. L. (2011). Connectivity-based parcellation reveals interhemispheric differences in the insula. Brain Topography, 25(3), 264–271. http://doi.org/10.1007/s10548-011-0205-y

[111] Jardri, R., Pins, D., Bubrovszky, M., Despretz, P., Pruvo, J.-P., Steinling, M., & Thomas, P. (2007). Self awareness and speech processing: An fMRI study. NeuroImage, 35(4), 1645–1653. http://doi.org/10.1016/j.neuroimage.2007.02.002

[112] Jenkinson, M. and Smith, S. M. (2001).A global optimisation method for robust affine registration of brain images. Medical Image Analysis, 5(2), 143-156.

[113] Jenkinson, M., Bannister, P. R., Brady, J. M., and Smith, S. M. (2002). Improved optimisation for the robust and accurate linear registration and motion correction of brain images. NeuroImage, 17(2), 825-841.

[114] Jenkinson, M., Beckmann, C. F., Behrens, T. E.,Woolrich, M . W., Smith, S. M. (2012). FSL. NeuroImage, 62:782-90.

[115] Jiménez-Castellanos, J., and Reinoso-Suárez, F. (1985). Topographical organization of the afferent connections of the principal ventromedial thalamic nucleus in the cat. Journal of Comparative Neurology 236, 297-314.

[116] Jürgens, U. (1983). Afferent fibers to the cingular vocalization region in the squirrel monkey. Experimental Neurology 80, 395-409.

[117] Katata, K., Sakai, N., Doi, K., Kawamitsu, H., Fujii, M., Sugimura, K., and Nibu, K-I. (2009). Functional MRI of regional brain reponses to 'pleasant' and 'unpleasant' odors. Acta Otolaryngol. 129, 85-90.

[118] Katzir, T., Misra, M., & Poldrack, R. A. (2005). Imaging phonology without print: Assessing the neural correlates of phonemic awareness using fMRI. NeuroImage, 27(1), 106–115. http://doi.org/10.1016/j.neuroimage.2005.04.013

[119] Kaufman, J. A., Paul, L. K., Manaye, K. F., Granstedt, A. E., Hof, P. R., Hakeem, A. Y., & Allman, J. M. (2008). Selective reduction of Von Economo neuron number in agenesis of the corpus callosum. Acta Neuropathologica, 116(5), 479–489. http://doi.org/10.1007/s00401-008-0434-7

[120] Kelly, C., Toro, R., Di Martino, A., Cox, C. L., Bellec, P., Castellanos, F. X., & Milham, M. P. (2012). A convergent functional architecture of the insula emerges across imaging modalities. NeuroImage, 61(4), 1129–1142. http://doi.org/10.1016/j.neuroimage.2012.03.021

[121] Kennedy, D. P., Semendeferi, K., & Courchesne, E. (2007). No reduction of spindle neuron number in frontoinsular cortex in autism. Brain and Cognition, 64(2), 124–129. http://doi.org/10.1016/j.bandc.2007.01.007

[122] Khokhryakova, I. M. (1978). Structural organization of the prefrontal cortex in cats and its differences from that in monkeys. Neurosci. Behav. Physiol. 9, 103–109.

[123] Knutson, K. M., Krueger, F., Koenigs, M., Hawley, A., Escobedo, J. R., Vasudeva, V., et al. (2010). Behavioral norms for condensed moral vignettes. Social Cognitive and Affective Neuroscience, 5(4), 378–384. http://doi.org/10.1093/scan/nsq005

[124] Kobayashi, M., Takeda, M., Hattori, N., Fukunaga, M., Sasabe, T., Inoue, N., et al. (2004). Functional imaging of gustatory perception and imagery: "top-down" processing of gustatory signals. NeuroImage, 23(4), 1271–1282. http://doi.org/10.1016/j.neuroimage.2004.08.002

[125] Koppelstaetter, F., Poeppel, T. D., Siedentopf, C. M., Ischebeck, A., Verius, M., Haala, I., et al. (2008). Does caffeine modulate verbal working memory processes? An fMRI study. NeuroImage, 39(1), 492–499. http://doi.org/10.1016/j.neuroimage.2007.08.037

[126] Koulakov, A. A., Kolterman, B. E., Enikolopov, A. G., and Rinberg, D. (2011). In search of the structure of human olfactory space. Front. Syst. Neurosci. 5, 65.

[127] Kowianski, P., Dziewiatkowski, J., Berdel, B., Lipowska, M., and Morys, J. (1998). The corticoclaustral con- nections in the rat studied by means of the fluorescent retrograde axonal transport method. Folia Morphol. (Warsz) 57, 85–92.

[128] Kringelbach, M. L. (2005). The human orbitofrontal cortex: linking reward to hedonic experience. Nature Reviews Neuroscience, 6(9), 691–702. http://doi.org/10.1038/nrn1747

[129] Kroenke, C. D., Bretthorst, G. L., Inder, T. E., and Neil, J. J. (2005). Diffusion MR imaging characteristics of the developing primate brain. Neuroimage 25, 1205–1213.

[130] Krolak Salmon, P., Hénaff, M. A., Isnard, J., Tallon Baudry, C., Guénot, M., Vighetto, A., et al. (2003). An attention modulated response to disgust in human ventral anterior insula. Annals of Neurology, 53(4), 446–453. http://doi.org/10.1002/ana.10502

[131] Kurth, F., Eickhoff, S. B., Schleicher, A., Hoemke, L., Zilles, K., & Amunts, K. (2010a). Cytoarchitecture and Probabilistic Maps of the

Human Posterior Insular Cortex. Cerebral Cortex, 20(6), 1448–1461. http://doi.org/10.1093/cercor/bhp208

[132] Kurth, F., Zilles, K., Fox, P. T., Laird, A. R., & Eickhoff, S. B. (2010b). A link between the systems: functional differentiation and integration within the human insula revealed by meta-analysis. Brain Structure and Function, 214(5-6), 519–534. http://doi.org/10.1007/s00429-010-0255-z

[133] Kühn, S., & Gallinat, J. (2012). The neural correlates of subjective pleasantness. NeuroImage, 61(1), 289–294. http://doi.org/10.1016/j.neuroimage.2012.02.065

[134] Landau, E. (1919). The comparative anatomy of the nucleus amygdalae, the claustrum and the insular cortex. J. Anat. 53, 351–360.

[135] Le Gros Clark,W.E.(1931).Thebrainof Microcebus murinus. Proc. Zool. Soc. Lond. 101, 463–485.

[136] LeVay, S., and Sherk, H. (1981). The visual claustrum of the cat: 1. Struc- ture and connections. J. Neurosci. 1, 956–980.

[137] Lipowska, M., Kowianski, P., Majak, K., Jagalska-Majewska, H., and Morys, J. (2000). The connections of the endopiriform nucleus with the insular claustrum in the rat and rabbit. Folia Morphol. (Warsz) 59, 77–83.

[138] Lundström, J. N., Boesveldt, S., & Albrecht, J. (2011). Central Processing of the Chemical Senses: An Overview. ACS Chemical Neuroscience, 2(1), 5–16. http://doi.org/10.1021/cn1000843

[139] Lutkenhoff, E. S., Rosenberg, M., Chiang, J., Zhang, K., Pickard, J.D., Owen, A.M., and Monti M. M (2014). Optimized Brain Extraction for Pathological Brains (optiBET). PLoS ONE 9(12): e115551. doi:10.1371/journal.pone.0115551

[140] Mak, Y. E., Simmons, K. B., Gitelman, D. R., and Small, D. M. (2005). Taste and olfactory intensity perception changes following left insular stroke. Behav. Neurosci. 119, 1693-1700.

[141] Manes, F., Paradiso, S., Springer, J. A., & Lamberty, G. (1999). Neglect after right insular cortex infarction. Stroke. 30:946-948

[142] Manes, F., Springer, J., Jorge, R., & Robinson, R. G. (1999b). Verbal memory impairment after left insular cortex infarction. Journal of Neurology, Neurosurgery & Psychiatry, 67(4), 532–534. http://doi.org/10.1136/jnnp.67.4.532

[143] Maltby, N., Tolin, D. F., Worhunsky, P., O'Keefe, T. M., & Kiehl, K. A. (2005). Dysfunctional action monitoring hyperactivates frontal–striatal circuits in obsessive–compulsive disorder: an event-related fMRI study. NeuroImage, 24(2), 495–503. http://doi.org/10.1016/j.neuroimage.2004.08.041

[144] Martin, R. D. (1990). Primate Origins and Evolution. Princeton: Princeton University Press.

[145] Mathur, B. N., Caprioli, R. M., and Deutch, A. Y. (2009). Proteomic analysis illuminates a novel structural definition of the claustrum and insula. Cereb. Cortex 19, 2372–2379.

[146] Mayer, J. D. (2002). Mayer: Mayer-Salovey-Caruso emotional intelligence Test (MSCEIT).

[147] Mayer, J. S., Bittner, R. A., NikoliÄ, D., Bledowski, C., Goebel, R., & Linden, D. E. J. (2007). Common neural substrates for visual working memory and attention. NeuroImage, 36(2), 441–453. http://doi.org/10.1016/j.neuroimage.2007.03.007

[148] McGeorge, A. J., and Faull, R. L. M. (1989). The organization of the projection from the cerebral-cortex to the striatum in the rat. Neuroscience 29, 503–537.

[149] Menon, V., and Uddin, L. Q. (2010). Saliency, switching, attention and control: a network model of insula function. Brain Struct. Funct. 214, 655–667.

[150] Mesulam, M. M., and Mufson, E. J. (1982a). Insula of the old-world monkey: 1. Architectonics in the insulo-orbito-temporal component of the paralimbic brain. J. Comp. Neurol. 212, 1–22.

[151] Mesulam, M. M., and Mufson, E. J. (1982b). Insula of the old- world monkey: 3. Efferent cortical output and comments on function. J. Comp. Neurol. 212, 38–52.

[152] Meynert, T. (1868). Neue Untersuchungen über den Bau der Grosshirn- rinde und ihre örtliche Verschiedenheiten. Alleg. Wien. Medizin. Ztg. 13, 419–428.

[153] Miller, K. L., Stagg, C. J., Douaud, G., Jbabdi, S., Smith, S. M., Behrens, T. E. J., Jenkinson, M., Chance, S. A., Esiri, M. M., Voets, N. L., Jenkinson, N., Aziz, T. Z., Turner, M. R., Johansen- Berg, H., and McNab, J. A. (2011). Diffusion imaging of whole, post-mortem human brains on a clinical MRI scanner. Neuroimage 57, 167–181.

[154] Mori, S., Itoh, R., Zhang, J. Y., Kauf- mann, W. E., Van Zijl, P. C. M., Solaiyappan, M., and Yarowsky, P. (2001). Diffusion tensor imaging of the developing mouse brain. Magn. Reson. Med. 46, 18–23.

[155] Morrison, S. E., and Salzman, C. D. (2010). Re-valuing the amygdala. Current Opinion in Neurobiology 20(2), 221-230.

[156] Morys, J., Bobinski, M., Wegiel, J., Wisniewski, H. M., and Narkiewicz, O. (1996). Alzheimer's disease severely affects areas of the claustrum connected with the entorhinal cortex. J. Brain Res. 37, 173–180.

[157] Mouse Connectome Project. (2011). Laboratory of Neuro Imaging. Available at: http://www.mouseconnectome.org/

[158] Mufson, E. J., and Mesulam, M. M. (1982). Insula of the old-world monkey: 2. Afferent cortical input and comments on the claustrum. J. Comp. Neurol. 212, 23–37.

[159] Mufson, E. J., and Mesulam, M. M. (1984). Thalamic connections of the insula in the rhesus monkey and comments on the paralimbic connectivity of the medial pulvinar nucleus. J. Comp. Neurol. 227, 109–120.

[160] Mufson, E. J., Mesulam, M. M., and Pandya, D. N. (1981). Insular interconnections with the amygdala in the rhesus monkey. Neuroscience 6, 1231–1248.

[161] Naidich, T. P., Kang, E., Fatterpekar, G. M., Delman, B. N., Gultekin, S. H., Ortiz, O., Yousry, I., Weismann, M., and Yousry, T. A. (2004) The Insula: Anatomic Study and MR Imaging Display at 1.5 T. Am J Neuroradiol. 25:222–232

[162] Najib, A., Lorberbaum, J. P., Kose, S., Bohning, D. E., & George, M. S. (2004). Regional Brain Activity in Women Grieving a Romantic Relationship Breakup. American Journal of Psychiatry, 161(12), 2245–2256. http://doi.org/10.1176/appi.ajp.161.12.2245

[163] Nanetti, L., Cerliani, L., Gazzola, V., Renken, R., & Keysers, C. (2009). Group analyses of connectivity-based cortical parcellation using repeated k-means clustering. NeuroImage, 47(4), 1666–1677. http://doi.org/10.1016/j.neuroimage.2009.06.014

[164] Nelson, S. M., Dosenbach, N. U. F., Cohen, A. L., Wheeler, M. E., Schlaggar, B. L., & Petersen, S. E. (2010). Role of the anterior insula in task-level control and focal attention. Brain Structure and Function, 214(5-6), 669–680. http://doi.org/10.1007/s00429-010-0260-2

[165] Ng, L., Bernard, A., Lau, C., Overly, C. C., Dong, H.-W., Kuan, C., Pathak, S., Sunkin, S. M., Dang, C., Boh- land, J. W., Bokil, H., Mitra, P. P., Puelles, L., Hohmann, J., Anderson, D. J., Lein, E. S., Jones, A. R., and Hawrylycz,

M. (2009). An anatomic gene expression atlas of the adult mouse brain. Nat. Neurosci. 12, 356–362.

[166] Nimchinsky, E. A., Vogt, B. A., Morrison, J. H. & Hof, P. R. (1995) Spindle neurons of the human anterior cingulate cortex. J. Comp. Neurol. 355, 27–37.

[167] Nimchinsky, E. A., Gilissen, E., Allman, J. M., Perl, D. P., Erwin, J. M., & Hof, P. R. (1999). A neuronal morphologic type unique to humans and great apes. Proceedings of the National Academy of Sciences, 96(9), 5268–5273. http://doi.org/10.1073/pnas.96.9.5268

[168] Norita, M. (1977). Demonstration of bilateral claustro-cortical connections in cat with method of retrograde axonal transport of horseradish-peroxidase. Arch. Histol. Jpn. 40, 1–10.

[169] O'Doherty, J. (2004). Reward representations and reward-related learning in the human brain: insights from neuroimaging. Current Opinion in Neurobiology 14(6), 769-776.

[170] O'Doherty, J., Kringelbach, M. L., Rolls, E. T., Hornak, J., and Andrews, C. (2001). Abstract reward and punishment representations in the human orbitofrontal cortex. Nat. Neurosci. 4, 95-102.

[171] O'Doherty, J., Winston, J., Critchley, H., Perrett, D., Burt, D. M., and Dolan, R. J. (2003). Beauty in a smile: the role of medial orbitofrontal cortex in facial attractiveness. Neuropsychologia 41, 147-155.

[172] Olson, C. R., and Graybiel, A. M. (1980). Sensory maps in the claustrum of the cat. Nature 288, 479–481.

[173] Öngür, D., An, X., and Price, J. L. (1998). Prefrontal cortical projections to the hypothalamus in macaque monkeys. J. Comp. Neurol. 401, 480–505.

[174] Paul, L. K., Brown, W. S., Adolphs, R., Tyszka, J. M., Richards, L. J., Mukherjee, P., & Sherr, E. H. (2007). Agenesis of the corpus callosum: genetic, devel-

opmental and functional aspects of connectivity. Nature Reviews Neuroscience, 8(4), 287–299. http://doi.org/10.1038/nrn2107

[175] Park, S., Tyszka, J. M., and Allman, J. M. (2012). The claustrum and insula in *Microcebus murinus*: a high resolution diffusion imaging study. Front. Neuroanat. 6(21), doi: 10.3389/fnana.2012.00021

[176] Pearson, R. C. A., Brodal, P., Gatter, K. C., and Powell, T. P. S. (1982). The organization of the connections between the cortex and the claustrum in the monkey. Brain Res. 234, 435–441.

[177] Phan, K. L., Filtzgerald, P. J., Nathan, P. J., Tancer, M. E. (2006). Association between amygdala hyperactivity to harsh faces and severity of social anxiety in generalized social phobia. Biological Psychiatry 59(5), 424-429.

[178] Plailly, J., d'Amato, T., Saoud, M., and Royet, J.-P. (2006). Left temporo-limbic and orbital dysfunction in schizophrenia during odor familiarity and hedonicity judgments. Neuroimage 29, 302-313.

[179] Poellinger, A., Thomas, R., Lio, P., Lee, A., Makris, N., Rosen, B. R., & Kwong, K. K. (2001). Activation and Habituation in Olfaction—An fMRI Study. NeuroImage, 13(4), 547–560. http://doi.org/10.1006/nimg.2000.0713

[180] Puelles, L., Kuwana, E., Puelles, E., Bulfone, A., Shimamura, K., Keleher, J., Smiga, S., and Rubenstein, J. L. R. (2000). Pallial and subpallial derivatives in the embryonic chick and mouse telencephalon, traced by the expression of the genes Dlx-2, Emx-1, Nkx-2.1, Pax- 6, and Tbr-1. J. Comp. Neurol. 424, 409–438.

[181] Radinsky, L. (1975). Primate brain evolution. Am. Sci. 63, 656–663.

[182] Ramón Y Cajal, S. (1900). Studien über die Hirnrinde des Menschen. Leipzig: Verlag von Johann Ambrosius Barth.

[183] Riecker, A., Kassubek, J., Gröschel, K., Grodd, W., & Ackermann, H. (2006). The cerebral control of speech tempo: Opposite relationship between speaking rate and BOLD signal changes at striatal and cerebellar structures. NeuroImage, 29(1), 46–53. http://doi.org/10.1016/j.neuroimage.2005.03.046

[184] Roebroeck, A., Galuske, R., Formisano, E., Chiry, O., Bratzke, H., Ronen, I., Kim, D. S., and Goebel, R. (2008). High-resolution diffusion tensor imaging and tractography of the human optic chiasm at 9.4 T. Neuroimage 39, 157–168.

[185] Rolls, E. T., Kringelbach, M. L., & de Araujo, I. E. T. (2003). Different representations of pleasant and unpleasant odours in the human brain. European Journal of Neuroscience, 18(3), 695–703. http://doi.org/10.1046/j.1460-9568.2003.02779.x

[186] Rozenkrantz, L., Zachor, D., Heller, I., Plotkin, A., Weissbrod, A., Snitz, K., et al. (2015). A Mechanistic Link between Olfaction and Autism Spectrum Disorder. Current Biology. http://doi.org/10.1016/j.cub.2015.05.048

[187] Rose, M. (1928). The ontogenesis of the insular lobe – a contribution to the histogenetic cortex arrangement. J. Psychol. Neurol. 36, 182–209.

[188] Royet, J.-P., Plailly, J., Delon-Martin, C., Kareken, D. A., & Segebarth, C. (2003). fMRI of emotional responses to odors:influence of hedonic valence and judgment, handedness, and gender. NeuroImage, 20(2), 713–728. http://doi.org/10.1016/S1053-8119(03)00388-4

[189] Rubia, K., Smith, A. B., Woolley, J., Nosarti, C., Heyman, I., Taylor, E., & Brammer, M. (2006). Progressive increase of frontostriatal brain activation from childhood to adulthood during event-related tasks of cognitive control. Human Brain Mapping, 27(12), 973–993. http://doi.org/10.1002/hbm.20237

[190] Saarela, M. V., Hlushchuk, Y., Williams, A. C. D. C., Schurmann, M., Kalso, E., & Hari, R. (2006). The Compassionate Brain: Humans Detect

Intensity of Pain from Another's Face. Cerebral Cortex, 17(1), 230–237. http://doi.org/10.1093/cercor/bhj141

[191] Salimi-Khorshidi, G., Douaud, G., & Beckmann, C. F. (2014). Automatic denoising of functional MRI data: Combining independent component analysis and hierarchical fusion of classifiers. NeuroImage 90(15), 449-468.

[192] Santos, M., Uppal, N., Butti, C., Wicinski, B., Schmeidler, J., Giannakopoulos, P., et al. (2011). von Economo neurons in autism: A stereologic study of the frontoinsular cortex in children. Brain Research, 1380, 206–217. http://doi.org/10.1016/j.brainres.2010.08.067

[193] Savic, I., Gulyas, B., Larsson, M., Roland, P. (2000). Olfactory functions are mediated by parallel and hierarchical processing. Neuron, 26(3):735-45.

[194] Schoenfeld, M. A., Neuer, G., Tempelmann, C., Schüßler, K., Noesselt, T., Hopf, J. M., & Heinze, H. J. (2004). Functional magnetic resonance tomography correlates of taste perception in the human primary taste cortex. Neuroscience, 127(2), 347–353. http://doi.org/10.1016/j.neuroscience.2004.05.024

[195] Seeley, W. W., Carlin, D. A., Allman, J. M., Macedo, M. N., Bush, C., Miller, B. L., & DeArmond, S. J. (2006). Early frontotemporal dementia targets neurons unique to apes and humans. Annals of Neurology, 60(6), 660–667. http://doi.org/10.1002/ana.21055

[196] Seeley, W. W., Menon, V., Schatzberg, A. F., Keller, J., Glover, G. H., Kenna, H., et al. (2007). Dissociable Intrinsic Connectivity Networks for Salience Processing and Executive Control. Journal of Neuroscience, 27(9), 2349–2356. http://doi.org/10.1523/JNEUROSCI.5587-06.2007

[197] Seeley, W. W. (2008). Selective functional, regional, and neuronal vulnerability in frontotemporal dementia. Current Opinion in Neurology, 21(6), 701–707. http://doi.org/10.1097/WCO.0b013e3283168e2d

[198] Senatorov, V. V., Damadzic, R., Mann, C. L., Schwandt, M. L., George, D. T., Hommer, D. W., et al. (2015). Reduced anterior insula, enlarged amygdala in alcoholism and associated depleted von Economo neurons. Brain, 138(1), 69–79. http://doi.org/10.1093/brain/awu305

[199] Seubert, J., Freiherr, J., Djordjevic, J., and Lundström, J. N. (2013). Statistical localization of human olfactory cortex. Neuroimage 66, 333-342.

[200] Shankman, S. A., Gorka, S. M., Nelson, B. D., Fitzgerald, D. A., Phan, L., & O'Daly, O. (2014). Anterior insula responds to temporally unpredictable aversiveness. NeuroReport, 1–5. http://doi.org/10.1097/WNR.0000000000000144

[201] Sheline, Y. I., Barch, D. M., Donnelly, J. M., Ollinger, J. M., Snyder, A. Z., Mintun, M. A. (2001). Increased amygdala response to masked emotional faces in depressed subjects resolves with antidepressant treatment: an fMRI study. Biological Psychiatry 50(9), 651-658.

[202] Shepherd, G. Neurogastronomy: How the Brain Creates Flavor and Why It Matters (Columbia University Press, New York, 2011).

[203] Sherwood, C. C., Lee, P. W. H., Rivara, C.-B. E. N. E. D., Holloway, R. L., Gilissen, E. P. E., Simmons, R. M. T., et al. (2003). Evolution of specialized pyramidal neurons in primate visual and motor cortex. Brain, Behavior and Evolution, 61(1), 28–44. http://doi.org/10.1159/000068879

[204] Shuren, J. (1993). Insula and aphasia. Journal of Neurology, 240(4), 216–218. http://doi.org/10.1007/BF00818707

[205] Shi, C. J., and Cassell, M. D. (1998). Cortical, thalamic, and amygdaloid connections of the anterior and posterior insular cortices. J. Comp. Neurol. 399, 440–468.

[206] Siegle, G. J., Thompson, W., Carter, C. S., Steinhauer, S. R., Thase, M. E. (2007). Increased amygdala and decreased dorsolateral prefrontal BOLD re-

sponses in unipolar depression: related and independent features. Biological Psychiatry 61(2), 198-209.

[207] Simms, M. L., Kemper, T. L., Timbie, C. M., Bauman, M. L., & Blatt, G. J. (2009). The anterior cingulate cortex in autism: heterogeneity of qualitative and quantitative cytoarchitectonic features suggests possible subgroups. Acta Neuropathologica, 118(5), 673–684. http://doi.org/10.1007/s00401-009-0568-2

[208] Singer, T. (2004). Empathy for Pain Involves the Affective but not Sensory Components of Pain. Science, 303(5661), 1157–1162. http://doi.org/10.1126/science.1093535

[209] Singer, T., Critchley, H. D., Preuschoff, K. (2009). A common role of insula in feelings, empathy and uncertainty. Trends in Cognitive Sciences 13(8), 334-340.

[210] Small, D. M., Zatorre, R. J., Dagher, A., Evans, A. C., and Jones-Gotman, M. (2001). Changes in brain activity related to eating chocolate: from pleasure to aversion. Brain 124, 1720-1733.

[211] Small, D. M., Gregory, M. D., Mak, Y. E., Gitelman, D., Mesulam, M. M., & Parrish, T. (2003). Dissociation of neural representation of intensity and affective valuation in human gustation. Neuron, 39(4), 701–711. http://doi.org/10.1016/S0896-6273(03)00467-7

[212] Small, D. M. (2010). Taste representation in the human insula. Brain Structure and Function, 214(5-6), 551–561. http://doi.org/10.1007/s00429-010-0266-9

[213] Smith, J. B., and Alloway, K. D. (2010). Functional specificity of claustrum connections in the rat: interhemispheric communication between specific parts of motor cortex. J. Neurosci. 30, 16832–16844.

[214] Smith, S. M., Jenkinson, M., Woolrich, M. W., Beckmann, C. F., Behrens, T. E. J., Johansen-Berg, H., Bannister, P. R., De Luca, M., Drobnjak, I., Flitney, D. E., Niazy, R. K., Saunders, J., Vickers, J., Zhang, Y. Y., De Stefano, N., Brady,

J. M., and Matthews, P. M. (2004). Advances in functional and structural MR image analysis and imple- mentation as FSL. Neuroimage 23, S208–S219.

[215] Sobel, N., Prabhakaran, V. Zhao, Z., Desmond, J. E., Glover, G. H., Sullivan, E. V., Gabrieli, J. D. E. (2000). Time Course of Odorant-Induced Activation in the Human Primary Olfactory Cortex. Journal of Neurophysiology, 83 (1) 537-551.

[216] Solstad, T., Boccara, C. N., Kropff, E., Moser, M.-B., and Moser, E. I. (2008). Representation of geometric borders in the entorhinal cortex. Science 322, 1865–1868.

[217] Sosulski, D. L., Bloom, M. L., Cutforth, T., Axel, R., and Datta, S. R. (2011). Distinct representations of olfactory information in different cortical centres. Nature 472, 213-216.

[218] Spielberger, C. D., Gorsuch, R. L., Lushene, R., Vagg, P. R., & Jacobs, G. A. (1983). Manual for the State-Trait Anxiety Inventory. Palo Alto, CA: Consulting Psychologists Press.

[219] Stein, M. B., Goldin, P. R., Sareen, J., Zorrilla, L. T., Brown, G. G. (2002). Increased amygdala activation to angry and contemptuous faces in generalized social phobia. Archives of General Psychiatry 59(11), 1027-1034.

[220] Straube, T., Kolassa, I. T., Glauer, M., Mentzel, H. J., Miltner, W. H. (2004). Effect of task conditions on brain responses to threatening faces in social phobics: an event-related functional magnetic resonance imaging study. Biological Psychiatry 56(12), 921-930.

[221] Striedter, G. F. (1997). The telencephalon of tetrapods in evolution. Brain Behav. Evol. 49, 179–213.

[222] Sun, S. W., Neil, J. J., and Song, S. K. (2003). Relative indices of water diffusion anisotropy are equivalent in live and formalin-fixed mouse brains. Magn. Reson. Med. 50, 743–748.

[223] Suslow, T., Konrad, C., Kugel, H., Rumstadt, D., Zwitserlood, P., Schön-ing, S., Ohrmann, P., Bauer, J., Pyka, M., Kersting, A., Arolt, V., Heindel, W., Dannlowski, U. (2010). Automatic mood-congruent amygdala responses to masked facial expressions in major depression. Biological Psychiatry 67(2), 155-160.

[224] Suzuki, Y., Critchley, H. D., Suckling, J., Fukuda, R., Williams, S. C., Andrew, C., Howard, R., Ouldred, E., Bryant, C., Swift, C.G., Jackson, S.H. (2001). Functional magnetic resonance imaging of odor identification: the effect of ag-ing. J Gerontol A Biol Sci Med Sci. 56(12), 756-60.

[225] Takahashi, E., Dai, G., Rosen, G. D., Wang, R., Ohki, K., Folkerth, R. D., Galaburda, A. M., Wedeen, V. J., and Grant, P. E. (2011). Developing neocortex organization and connectivity in cats revealed by direct correlation of diffusion tractography and histology. Cereb. Cortex 21, 200–211.

[226] Takahashi, E., Dai, G., Wang, R., Ohki, K., Rosen, G. D., Galaburda, A. M., Grant, P. E., and Wedeen, V. J. (2010). Development of cerebral fiber pathways in cats revealed by diffusion spectrum imaging. Neuroimage 49, 1231–1240.

[227] Takahashi, E., Folkerth, R. D., Gal- aburda, A. M., and Grant, P. E. (2012). Emerging cerebral connec- tivity in the human fetal brain: an MR Tractography Study. Cereb. Cor tex 22, 455–464.

[228] Tanné-Gariépy, J., Boussaoud, D., and Rouiller, E. M. (2002). Projections of the claustrum to the primary motor, premotor, and prefrontal cortices in the macaque monkey. J. Comp. Neurol. 454, 140–157.

[229] Taylor, K. S., Seminowicz, D. A., and Davis, K. D. (2009). Two sys- tems of resting state connectiv- ity between the insula and cingu- late cortex. Hum. Brain Mapp. 30, 2731–2745.

[230] Touroutoglou, A., Hollenbeck, M., Dickerson, B. C., & Barrett, L. F. (2012). Dissociable large-scale networks anchored in the right anterior insula

subserve affective experience and attention. NeuroImage, 60(4), 1947–1958. http://doi.org/10.1016/j.neuroimage.2012.02.012

[231] Uddin, L. Q., & Menon, V. (2009). The anterior insula in autism: Underconnected and under-examined. Neuroscience & Biobehavioral Reviews, 33(8), 1198–1203. http://doi.org/10.1016/j.neubiorev.2009.06.002

[232] Uddin LQ, Supekar K, Amin H, Rykhlevskaia E, Nguyen DA, Greicius MD, Menon V. (2010). Dissociable Connectivity within Human Angular Gyrus and Intraparietal Sulcus: Evidence from Functional and Structural Connectivity. Cerebral Cortex 20:2636-2646.

[233] Uddin, L. Q., Supekar, K., Lynch, C. J., Khouzam, A., Phillips, J., Feinstein, C., et al. (2013). Salience Network–Based Classification and Prediction of Symptom Severity in Children With Autism. JAMA Psychiatry, 70(8), 869–11. http://doi.org/10.1001/jamapsychiatry.2013.104

[234] van de Werd, H. J. J. M., Rajkowska, G., Evers, P., and Uylings, H. B. M. (2010). Cytoarchitectonic and chemoarchitectonic characterization of the prefrontal cortical areas in the mouse. Brain Struct. Funct. 214, 339–353.

[235] van den Heuvel, M. P., Mandl, R. C. W., Kahn, R. S., & Hulshoff Pol, H. E. (2009). Functionally linked resting-state networks reflect the underlying structural connectivity architecture of the human brain. Human Brain Mapping, 30(10), 3127–3141. http://doi.org/10.1002/hbm.20737

[236] van Turennout, M., Bielamowicz, L., & Martin, A. (2003). Modulation of neural activity during object naming: effects of time and practice. Cereb. Cortex.13(4), 381-391.

[237] von Economo, C., and Koskinas, G. N. (1925). Atlas of Cytoarchitectonics of the Adult Human Cerebral Cortex. S. Karger AG (Switzerland).

[238] Watson, D., Clark, L. A., & Tellegen, A. (1988). Development and validation of brief measures of positive and negative affect: The PANAS

scales. Journal of Personality and Social Psychology, 54(6), 1063–1070. http://doi.org/10.1037/0022-3514.54.6.1063

[239] Watson, K. K., Jones, T. K., & Allman, J. M. (2006a). Dendritic architecture of the von Economo neurons. Neuroscience, 141(3), 1107–1112. http://doi.org/10.1016/j.neuroscience.2006.04.084

[240] Watson, K. K., Matthews, B. J., & Allman, J. M. (2006b). Brain Activation during Sight Gags and Language-Dependent Humor. Cerebral Cortex, 17(2), 314–324. http://doi.org/10.1093/cercor/bhj149

[241] Whitwell, J. L., Sampson, E. L., Loy, C. T., Warren, J. E., Rossor, M. N., Fox, N. C., and Warren, J. D. (2007). VBM signatures of abnormal eating behaviours in frontotemporal lobar degeneration. Neuroimage 35, 207-213.

[242] Wicker, B., Keysers, C., Plailly, J., Royet, J.-P., Gallese, V., & Rizzolatti, G. (2003). Both of Us Disgusted in My Insula. Neuron, 40(3), 655–664. http://doi.org/10.1016/S0896-6273(03)00679-2

[243] Wiech, K., Jbabdi, S., Lin, C. S., Andersson, J., & Tracey, I. (2014). Differential structural and resting state connectivity between insular subdivisions and other pain-related brain regions. Pain, 155(10), 2047–2055. http://doi.org/10.1016/j.pain.2014.07.009

[244] Wildes, J. E., Zucker, N. L., & Marcus, M. D. (2012). Picky eating in adults: Results of a web-based survey. International Journal of Eating Disorders, 45(4), 575–582. http://doi.org/10.1002/eat.20975

[245] Wilson, R. S., Arnold, S. E., Schneider, J. A., Boyle, P. A., Buchman, A. S., and Bennett, D. A. (2009). Olfactory impairment in presymptomatic Alzheimer's disease. Ann. NY Acad. Sci. 1170, 730-735.

[246] Wilson, R. S., Yu, L., and Bennett, D. A. (2011a). Olfactory identification and mortality in old age. Chem. Senses 36, 63-67.

[247] Wilson, R. S., Yu, L., Schneider, J. A., Arnold, S. E., Buchman, A. S., and Bennett, D.A. (2011b). Lewy bodies and olfactory dysfunction in old age. Chem. Senses 36, 367-73.

[248] Witter, M. P., Room, P., Groenewegen, H. J., and Lohman, A. H. M. (1988). Reciprocal connections of the insular and piriform claustrum with limbic cortex – an anatomical study in the cat. Neuroscience 24, 519–539.

[249] Woolley, J. D., Gorno-Tempini, M.-L., Seeley, W. W., Rankin, K., Lee, S. S., Matthews, B. R., and Miller, B. L. (2007). Binge eating is associated with right orbitofrontal-insular-striatal atrophy in frontotemporal dementia. Neurology 69,1424-1433.

[250] Woolrich, M. W., Jbabdi, S., Patenaude, B., Chappell, M., Makni, S., Behrens, T., Beckmann, C., Jenkinson, M., and Smith, S. M. (2009). Bayesian analysis of neuroimaging data in FSL. Neuroimage 45, S173–S186.

[251] Yeung, N. and Sanfey, A. G. (2004). Independent coding of reward magnitude and valence in the human brain. J. Neurosci. 24(28), 6258-6264.

[252] Zald, D. H., Hagen, M.C., Pardo, J.V. (2002). Neural correlates of tasting concentrated quinine and sugar solutions. J Neurophysiol, 87(2):1068-75.

[253] Zatorre, R. J., Jones-Gotman, M. Evans, A. C., and Meyer, E. (1992). Functional localization and lateralization of human olfactory cortex. Nature, 360(6402):339-40.

[254] Zhang, J. Y., Miller, M. I., Plachez, C., Richards, L. J., Yarowsky, P., Van Zijl, P., and Mori, S. (2005). Mapping postnatal mouse brain development with diffusion tensor microimaging. Neuroimage 26, 1042–1051.

[255] Zhang, J. Y., Richards, L. J., Yarowsky, P., Huang, H., Van Zijl, P. C. M., and Mori, S. (2003). Three-dimensional anatomical characterization of the developing mouse brain by diffusion tensor microimaging. Neuroimage 20, 1639–1648.